ENERGY ABSORPTION THROUGH THE LATERAL COLLAPSE OF THIN-WALLED SINGLE AND NESTED TUBES

A thesis submitted for the degree of

Doctor of Philosophy

by

Ahmad Baroutaji

(B.ENG.)

School of Mechanical and Manufacturing Engineering

Faculty of Engineering and Computing

Dublin City University

July 2014

Supervisor

Prof. Abdul-Ghani Olabi

Declaration

I hereby certify that this material, which I now submit for assessment on the programme of study leading to the award of Doctor of Philosophy is entirely my own work, and that I have exercised reasonable care to ensure that the work is original, and does not to the best of my knowledge breach any law of copyright, and has not been taken from the work of others save and to the extent that such work has been cited and acknowledged within the text of my work.

…….....

(AHMAD BAROUTAJI)

ID No. 56116691

Date:

Acknowledgements

I would like to thank the following people who have supported and assisted me in the undertaking and completion of this thesis.

Firstly, I would like to express my sincere thanks to my supervisor, Prof. Abdul Ghani Olabi for his inspiration, advices and invaluable supports and help throughout the different stages of this research.

I would also like to express my special appreciation towards Prof. Michael D Gilchrist and Dr. Edmund Morris for their assistance.

Also I would like to thank the technician Chris who has assisted me with the technical issues during the testing of my work.

I would also like to thank my wife for her understanding, patience and encouragement, my thanks also goes to my little daughter (Leen) who provides me with the happiness and joy.

I am also most thankful to my family in Syria (Mam-Dad-Brother and Sister) for their continuous support, pray and unconditional love.

Another big thank-you goes to my friends and colleagues (Mustafa-Shadi-Hussam-Abed-Abdulaleam) who have supported me in many ways during my research.

Finally, I would like to gratefully acknowledge the financial support of the University of Aleppo.

Contents

Declaration ..... *II*

Acknowledgements ..... *III*

Contents ..... *IV*

Abstract ..... *X*

Nomenclature ..... *XI*

Thesis Abbreviations ..... *XIII*

List of Figures ..... *XIV*

List of Tables ..... *XXV*

1 Introduction *1*

1.1 Importance of energy absorption systems *1*

1.2 Design of energy absorption systems *3*

1.2.1 Irreversible energy conversion *4*

1.2.2 Restricted and constant reactive force *4*

1.2.3 Long stroke *4*

1.2.4 Stable and repeatable deformation mode *4*

1.2.5 Light weight and high specific energy-absorption capacity *5*

1.2.6 Low cost and easy installation *5*

1.3 Thin walled components as energy absorber *5*

1.4 Aims of this Thesis *6*

1.5 Thesis outline *7*

2 Literature review 11

2.1 Impact mechanics 11

2.1.1 Inertia effects 11

2.1.2 Strain rate effects 13

2.2 Structural crashworthiness 15

2.3 Energy absorber characteristics 20

2.3.1 Energy absorption capacity (E) 20

2.3.2 Specific energy absorption (SEA) 20

2.3.3 Stroke efficiency (e_g) 20

2.3.4 Energy efficiency (e_E) 21

2.3.5 Work effectiveness (W_{eff}) 21

2.3.6 Energy absorbed per unit crush length (E_{cl}) 21

2.3.7 Dynamic amplification factor (DAF) 22

2.4 Energy absorbing structures 22

2.4.1 Empty thin-walled energy tubes 23

2.4.2 Nested tube energy absorbers 48

2.4.3 Foam-filled energy absorber 51

2.5 Analysis of energy absorbers 58

2.5.1 Analytical modeling 58

2.5.2 Empirical modeling 59

2.5.3 Factorial analysis 60

2.6 Advantages and disadvantages of various types of energy absorbing structures .. 61

2.7 Summary of literature review and knowledge gaps 62

3 Theoretical Background 65

3.1 Finite element method (FEM) 65

3.1.1 Linearity and nonlinearity 66

3.1.2 Static and dynamic analysis 66

3.1.3 Material models 67

3.1.4 Contact Capabilities within ANSYS and ANSYS/LS-DYNA 69

3.2 Design of Experiment (DOE) 71

3.3 Response surface methodology (RSM) 72

3.4 Response Surfaces Based Optimization 81

3.4.1 Desirability approach 82

3.4.2 Optimization approach in Design-expert V8 software 83

3.5 Summary 85

4 Material & Methods 87

4.1 Experimental Set-Up 87

4.1.1 Quasi-Static Loading 87

4.1.2 Dynamic Loading 90

4.2 Material Properties & Samples 91

4.2.1 Material Properties 91

4.2.2 Samples 93

4.3 Summary 96

5 Development & Validation of Finite Element (FE) models 98

5.1 Development of finite element models 99

5.1.1 Quasi - Static loading case 99

5.1.2 Dynamic Loading case 100

5.2 Validation of FE models for various tubes 101

5.2.1 Circular tubes 101

5.2.2 Oblong tube 106

5.2.3 Nested tube 109

5.3 Summary 111

6 Responses Of Single Tubes Under Lateral Loading 113

6.1 Circular tubes 113

6.1.1 Effect of cross section shape 113

6.1.2 Development and validation of Response Surface (RS) models for a CTFIU system 119

6.1.3 Parametric study 127

6.1.4 Multi-objective optimization design (MOD) of the CTFIU system 132

6.1.5 Responses of circular tube under a lateral oblique load 135

6.1.6 Dynamic response of a single circular tube 138

6.2 Oblong tube 142

6.2.1 Oblong Tube Specimen Preparation 142

6.2.2 Experimental results comparison of oblong and circular tubes under lateral loading 143

6.2.3 Responses of oblong tube compressed by different indenters and exposed to external constraints 145

6.2.4 Energy absorption characteristics (OT) 155

6.2.5 Development and validation of response surface (RS) models for an OTFIU system 156

6.2.6 Parametric study 161

6.2.7 Multi-objective optimization design (MOD) of OTFIU system 166

6.3 Elliptical tube 169

6.3.1 Effect of elliptical ratio on the responses of laterally crushed elliptical tubes (ET) 169

6.4 Summary 172

7 Responses Of Nested Tubes Under Lateral Loading 174

7.1 Introduction: 174

7.2 Responses of nested systems under quasi-static loading conditions 174

7.2.1 Analysis of the NTCO system 174

7.2.2 Analysis of the NTDC system 177

7.2.3 Analysis of the NTSC system 178

7.3 Responses of nested systems under dynamic loading conditions 180

7.3.1 Evaluation of the NTCO 180

7.3.2 Evaluation of the NTDC 182

7.3.3 Evaluation of the NTSC 184

7.4 Summary 188

8 Discussion & Conclusion 190

8.1 Discussion 190

8.2 Conclusion *198*

8.3 Future work *199*

9 References *202*

10 Appendices ..... *I*

Appendices A ..... *I*

Certificate of calibration of Instron 4204 ..... *I*

Appendices B ..... *VI*

Material properties from company catalogue ..... *VI*

Appendices C ..... *VIII*

VFPS Application ..... *VIII*

Appendices D ..... *X*

Sandwich tube systems with external constraints ..... *X*

Appendices E ..... *XI*

Various configurations of sandwich tube systems ..... *XI*

Appendices F ..... *XII*

Publication ..... *XII*

Abstract

Over the last several decades increasing attention has been paid to minimising injuries to people inside a structure that experiences an impact, as well as alleviating the effect of an impact on a structure. This has led to significant research being carried out into the design and development of energy absorbers in order to mitigate the adverse effects of an impact and to increase the safety of a structure. Energy absorbers have found common application in the automobile, nuclear, spacecraft, and aircraft industries.

This work presents the energy absorption response and crashworthiness optimisation of thin walled single and nested tubes under quasi-static and dynamic lateral loading. The primary aim of this study was to conduct investigations into the above systems and thus, where applicable, employ them in crashworthiness applications and energy absorption systems. Two different configurations of energy absorbing mechanisms were studied in this thesis. The first type was a single tube, the geometrical profile of which was varied in order to study its absorption characteristics. In an attempt to enhance the energy absorption capacity of a single tube, internally nested tubes were also examined as energy absorbers. This nested system formed the second configuration. Due to strain localisation around the plastic hinges, external constraints were employed to increase the number of plastic hinges and thereby increase the volume of material reaching plasticity. Various indicators that described the effectiveness of an energy absorbing mechanism were used as markers to compare the various systems.

Detailed finite element models, validated against experiments and existing experimental and numerical results, were developed using both the implicit code (ANSYS) and explicit code (ANSYS-LSDYNA) to assess the energy absorption responses and deformation modes. Response surface methodology (RSM) was employed in parallel with the finite element models to perform both parametric studies and multi-objective optimization in order to establish the optimal configurations for the various mechanisms proposed in this study. Major findings show that the energy absorption response can be effectively controlled by varying geometric parameters such as diameter, thickness, and width.

Nomenclature

Symbol	Definition	Units
σ_y	*Yield stress*	N/m^2
σ_d	*Dynamic Flow Stress*	N/m^2
σ_s	*Static Flow Stress*	N/m^2
ε	*Uniaxial Plastic Strain Rate*	*1/s*
D, q	*Material Constants*	-
SEA	*Specific Energy Absorbed Capacity*	*J/Kg*
E	*Energy Absorbing Capacity*	*J*
F	*Crush Force*	*N*
W_{eff}	*Weight Effectiveness*	*J/Kg*
e_g	*Crush Efficiency*	-
e_E	*Energy Efficiency*	-
DAF	*Dynamic Amplification Factor*	
F_{max}	*Peak Load*	*N*

Symbol	Definition	Unit
δ	*displacement*	*m*
E_{cl}	*Energy absorbed per unit*	*J/m*
I	*area moment of inertia*	m^4
ρ	*Density*	Kg/m^3
$\sigma_1, \sigma_2, \sigma_3$	*Principle Stresses*	N/m^2
V	*Velocity*	m/sec^2
D	*Diameter*	*m*
t	*thickness*	*m*
w	*width*	*m*

Thesis Abbreviations

Acronym	Definition
FE	*Finite Element (standard)*
RS	*Response Surface (Standard)*
MOD	*Multi-objective optimization design*
CTS	*Circular tube systems*
OTS	*Oblong tube systems*
CTFIU	*Circular tube flat indenter unconstrained*
OTFIU	*Oblong tube flat plate indenter unconstrained*
OTFIIC	*Oblong tube flat plate indenter incline constrain*
OTFISC	*Oblong tube flat plate indenter side constrain*
OTCIU	*Oblong tube cylindrical indenter unconstrained*
OTCIIC	*Oblong tube cylindrical indenter incline constrain*
OTCISC	*Oblong tube flat cylindrical indenter side constrain*
OTPIU	*Oblong tube point indenter unconstrained*
OTPIIC	*Oblong tube point indenter incline constrain*
OTPISC	*Oblong tube point indenter side constrain*
ETS	*Elliptical tube systems*
NTS	*Nested tubes systems*
NTCO	*Nested tubes circular and oblong system*
NTSC	*Nested tubes similar circular tubes*
NTDC	*Nested tubes different circular tubes*

List of Figures

Figure 1-1: Road Deaths by Road User Type in Ireland in 2011(http://www.rsa.ie [Accessed April 2013]). 3

Figure 1-2: Crash management system (www.constellium.com [Accessed April 2013]). 6

Figure 1-3: A Vehicle Frontal Protection (VFPS) system consisting of a single circular tube crushed laterally. 7

Figure 2-1: Two classes of structures [4]. 12

Figure 2-2: Fundamental concept of crash energy management for cars [16]. 15

Figure 2-3: Energy absorption system used for cars manufactured by the Honda company (www.honda.com). 16

Figure 2-4: A typical helicopter subfloor structure [17]. 17

Figure 2-5: Metallic cylindrical shells as energy absorbers in train structures [19]. . 18

Figure 2-6: Partial schematics (left) and a photo (right) of the SWRC flexible crashworthy device [20]. 18

Figure 2-7: Bulldozer with ROPS and FE model of the assembly of ROPS& energy absorber [21]. 19

Figure 2-8: A general view of the shock absorber model: (a) 1 and 4 are the top and bottom rings, 2 are the working rings, 3 are the cuts [23]. 19

Figure 2-9: Sketch of the gas gun used for the experiments [30]. 24

Figure 2-10: Mild steel samples: Deformation states at velocities of 385 m/s, 277 m/s, 227 m/s, 173m/s and 0 /ms respectively [30]. 25

Figure 2-11: Schematic view of the impact rig for testing lateral impact on axially pre-loaded tubes [32].....26

Figure 2-12: One quarter finite element model including trigger position [33]. 27

Figure 2-13: The axial deformation stages for a 2.5 mm thick tube with the trigger at the mid-section under impact loading [33]. 27

Figure 2-14: Final post-buckling deformation of an LS-DYNA hexagonal section model [34].....28

Figure 2-15: Tube mesh, geometry, and loading arrangement used in the FE model [35]. 29

Figure 2-16: Collapse sequence of straight and tapered rectangular tubes under a quasi-static axial load [36]. 30

Figure 2-17: Various configurations of multi-cell columns [40]. 31

Figure 2-18: Comparison between ABAQUS and experimental deformed shape [44]. 33

Figure 2-19: Experimental results and ABAQUS solutions for quasi-static internal inversion of mild-steel tubes [44]. 33

Figure 2-20: Set-up for dynamic tests [10]. 34

Figure 2-21: Schematic diagram of dynamic test arrangement for a tube inversion process [45]. 34

Figure 2-22: Sketch of the experimental set-up [50]. 36

Figure 2-23: Photographs of typical specimens after tests [50]. 36

Figure 2-24: Typical mild steel specimens in their final deformed stages [51].....37

Figure 2-25: Final deformation of the N234S(top), N486S(second), K234S(third) and K486S(bottom) tubes subjected to static loading [53]. 38

Figure 2-26: Final stages of deformation of rings support with (a) 90" arc, (b) 60" arc [58]. 40

Figure 2-27: Modified split Hopkinson pressure bar test apparatus and recording system [61]. 41

Figure 2-28: Sketch of the Finite element model [61]. 41

Figure 2-29: Deformed profiles of aluminium tubes at different stages of lateral compression [70]. 44

Figure 2-30: Symmetric and asymmetric deformations for 0^0 bracing [80]. 47

Figure 2-31: Finite element mesh and two deformation stages for a 200 braced elliptical tube [80]. 48

Figure 2-32: Final stage of deformed profile of nested tubes [88]. 50

Figure 2-33: Schematic of (a) standard design. (b) Optimised design [13]. 51

Figure 2-34: Typical foam-filled tubular sections a) Foam-filled circular tubes (Al/polystyrene) [92]; -b) Foam-filled frusta [[102]; -c) Foam-filled rectangle tube [95]. 52

Figure 2-35: Deformation modes of foam-filled circular tubes [6]. 53

Figure 2-36: Concertina and diamond deformation modes foam-filled tubes and empty tubes, of three different lengths [111] 54

Figure 2-37: Axially crushed circular tubes: (a) filled, (b) empty [112]. 55

Figure 2-38: (a) Global bending and formation of plastic hinges during global collapse for each tube (b) Load vs deflection curve of the empty and filled conical tubes under oblique loading [102]. 57

Figure 2-39: Collapse mechanisms proposed by: (a) DeRuntz and Hodge [66] (b) Burton and Craig [119], and (c) also showing the forces on a deforming segment [15]. 59

Figure 3-1: Yield surface in principle stress space [132].....68

Figure 3-2: The Isotropic Hardening Rule [132]. 68

Figure 3-3: Illustration of a contact pair. 69

Figure 3-4: contact pairs used in FE models of circular tube under lateral loading. .70

Figure 3-5: Illustration of the surface to surface contact algorithm in ANSYS/LS-DYNA (www.dynasupport.com). 71

Figure 3-6: A schematic diagram for BBD for three factors [136].....73

Figure 3-7: Flow charts of performing MOD study.....84

Figure 4-1: Instron Model 4204 with the control unit. 88

Figure 4-2: Schematic of a nested tubes sample tube under quasi-static load. 89

Figure 4-3: Experimental Set-up of oblique loading.....89

Figure 4-4: Zwick Roell 5HV series used to conduct the impact experiments.....91

Figure 4-5: The tensile test carried out to indicate the mechanical properties of the steel tubes. 93

Figure 4-6: True stress–strain curves obtained from three tensile tests. 93

Figure 5-1: FE model of (a) a Circular Tube, (b) an Oblong Tube, (c) Nested Tubes. 100

Figure 5-2: Convergence of crushing force versus mesh density for OTFIU system 100

Figure 5-3: Comparison of FE & experimental results for a circular tube. 102

Figure 5-4: Comparison of (a) the experimental and (b) the numerical deformation mode of a circular tube.....103

Figure 5-5: Comparison of FE & experimental results for a circular tube with L cross section. 104

Figure 5-6: Comparison of (a) the experimental and (b) the numerical deformation mode of a circular tube with L cross section.....104

Figure 5-7: Comparison of FE & experimental results for a circular tube with T cross section. 105

Figure 5-8: Comparison of (a) the experimental and (b) the numerical deformation mode of a circular tube with T cross section.....105

Figure 5-9: Comparison of FE & experimental results for a circular tube with U cross section. 105

Figure 5-10: Comparison of (a) the experimental and (b) the numerical deformation mode of a circular tube with U cross section. 106

Figure 5-11: Comparison of FE & experimental results for a circular tube system under dynamic loading (V=4.5 m/sec).....106

Figure 5-12: (a) Initial and (b) final deformed shape of the FE model.....107

Figure 5-13: Comparison of FE & experimental results for an oblong tub 108

Figure 5-14: Comparison of (a) the experimental, and (b) the numerical deformation mode of an oblong tube. 108

Figure 5-15: Comparison of FE & experimental results for a nested tube system under quasi-static loading. 109

Figure 5-16: Comparison of FE & experimental results for a nested tube system under dynamic loading (V=4.5 m/sec). 110

Figure 5-17: Comparison of (a) the experimental and (b) the numerical deformation mode of nested tubes. 110

Figure 6-1: Section of a circular tube. 114

Figure 6-2: The experimental force- deflection responses of L, T, and U cross section circular tubes. 116

Figure 6-3: The experimental energy- deflection responses of L, T, and U cross section circular tubes. 116

Figure 6-4: Initial and final stages of deflection for circular tubes with different cross sectional shapes under quasi-static loading condition. 117

Figure 6-5: The numerical force-deflection responses of L, T, U, I, and R cross sectional circular tubes. 118

Figure 6-6: Flow chart showing the steps of creating the RS models. 120

Figure 6-7: Scatter diagram of SEA (CTFIU). 126

Figure 6-8: Scatter diagram of F (CTFIU). 126

Figure 6-9: Perturbation plot of SEA (CTFIU) 128

Figure 6-10: Effect of D on SEA (CTFIU) 128

Figure 6-11: Effect of t on SEA (CTFIU). 129

Figure 6-12: Variation of SEA with D & t (CTFIU). 129

Figure 6-13: Interaction effects of D and t on F (CTFIU). 130

Figure 6-14: Interaction effect D and W on F (CTFIU)..... 131

Figure 6-15: Interaction effect of t and W on F (CTFIU). 131

Figure 6-16: Variation of F with W and t (CTFIU). 132

Figure 6-17: Effect of load angle on the Force-Displacement response. 136

Figure 6-18: Deformation history of a circular tube under quasi-static loading. 136

Figure 6-19: Deformation history of a circular tube under quasi-static oblique loading where $\alpha=10^{o}$ 137

Figure 6-20: Deformation history of a circular tube under quasi static oblique load where $\alpha=20^{o}$ 137

Figure 6-21: Comparison of experimental responses for a circular tube under static and dynamic loading (v=4.5 m/sec). 139

Figure 6-22: Initial and final stages of deflection for a circular tube under dynamic loading (v=4.5 m/sec). 139

Figure 6-23: Effect of impact velocity on the *DAF*. 140

Figure 6-24: Deformed profiles of a circular tube under two different compression velocities a: v=10m/sec, and b: v=100 m/sec. 141

Figure 6-25: Elongation procedure of an oblong tube. 143

Figure 6-26: Tensile force–deflection response of the test piece during the tensile loading phase. 143

Figure 6-27: Comparison of load-deflection responses of circular and oblong tubes. 144

Figure 6-28: Experimental responses of an OTFIU system. 146

Figure 6-29: (a) Initial and (b) final stages of an OTFIU system 146

Figure 6-30: Experimental responses of an OTFIIC system. 147

Figure 6-31: (a) Initial and (b) final stages of an OTFIIC system. 147

Figure 6-32: Experimental responses of an OTFISC system. 148

Figure 6-33: (a) Initial and (b) final stages of OTFISC system. 148

Figure 6-34: Experimental responses of an OTCIU system. 149

Figure 6-35: Initial and final stages of OTCIU system. 149

Figure 6-36: Experimental responses of an OTCIIC system. 150

Figure 6-37: Initial and final stages of an OTCIIC system. 151

Figure 6-38: Experimental responses of an OTCISC system 151

Figure 6-39: Initial and final stages of an OTCISC system. 151

Figure 6-40: Experimental responses of an OTPIU system. 152

Figure 6-41: (a) Initial and (b) final stages of an OTPIU system. 152

Figure 6-42: Experimental responses of an OTPIIC system. 153

Figure 6-43: Initial and final stages of an OTPIIC system. 153

Figure 6-44: Experimental responses of an OTPISC system. 154

Figure 6-45: Initial and final stages of an OTPISC system. 154

Figure 6-46: The final collapse profile of specimen with a point load application. 154

Figure 6-47: Comparison of effectiveness indicators for OT systems.....155

Figure 6-48: Scatter diagram of SEA (OTFIU). 160

Figure 6-49: Scatter diagram of F (OTFIU).....161

Figure 6-50: Perturbation plot of SEA (OTFIU) 162

Figure 6-51: Effect of Diameter on SEA (OTFIU).....163

Figure 6-52: Effect of thickness on SEA (OTFIU).....163

Figure 6-53: Variation of SEA with diameter and thickness (OTFIU).....164

Figure 6-54: Effect of diameter on F (OTFIU). 165

Figure 6-55: Interaction effect of Thickness and width on F (OTFIU) 165

Figure 6-56: Variation of F with thickness and width (OTFIU).....166

Figure 6-57: Elliptical tube. 169

Figure 6-58: Load-displacement responses for elliptical tubes with various elliptical ratios.....171

Figure 6-59: Energy-displacement response for elliptical tubes with various elliptical ratios.....171

Figure 7-1: Experimental force and energy responses of a NTCO system.....176

Figure 7-2: Deformation history of a NTCO system. 176

Figure 7-3: Experimental force and energy responses of the NTDC system.....178

Figure 7-4: Deformation history of the NTDC system. 178

Figure 7-5: Experimental force and energy responses of the NTSC system. 179

Figure 7-6: Deformation history of the NTSC system. 180

Figure 7-7: Comparison of load-displacement curves of the NTCO system for quasi-static and dynamic crushing (v=4.5 m/sec). 181

Figure 7-8: a- initial, and b- final stages of NTCO under dynamic loading. 181

Figure 7-9: Deformed profiles of the NCOT system under two different compression velocity a: v=10m/sec, and b: v=100 m/sec. 182

Figure 7-10: Comparison of load-displacement curves for the NTDC system for quasi-static and dynamic crushing (v=4.5 m/sec) 183

Figure 7-11: a- initial, and b- final stages of the NTDC under dynamic loading 183

Figure 7-12: Deformation profiles of the NTDC system under two different compression velocity a- v=10m/sec, and b- v=100 m/sec 184

Figure 7-13: Comparison of the quasi-static and dynamic crushing load-displacement curves for the NTSC system (v=4.5 m/sec). 185

Figure 7-14: a- initial, and b- final stages of NTSC under dynamic loading. 185

Figure 7-15: Energy-deflection responses of the NTSC system under different impact velocities. 186

Figure 7-16: Deformation profiles of the NTSC system under two different impact velocity, a: v=10 m/sec, and b: v=100 m/sec. 187

Figure 7-17: Energy-displacement responses for each component of the NTSC system under an impact velocity of 100 m/sec where e_1 is the energy absorbed by

main tube, e_2 is energy absorbed by upper tube and e_3 is the energy absorbed by the lower tube. 187

Figure A-1: Application of lateral crushed thin walled tubes in VFPS system [Car photo www.automobiles.honda.com [Accessed April 2013]]. VIII

Figure A-2: A VFPS system consisting of single circular tube crushed laterally..... IX

Figure A-3: a- Initial and b- final stages of VFPS system IX

List of Tables

Table 2-1: D and q values for various metals [11]. 14

Table 3-1: Design matrix for BBD, coded values 74

Table 3-2: ANOVA table for full model 77

Table 4-1: Chemical Composition of steel tubes [from company catalogue as seen in Appendices B] 92

Table 4-2: Material properties of empty and nested tubes 92

Table 4-3: Configurations and dimensions of samples used in this work 93

Table 4-4: The geometrical and mass properties of circular tubes with various longitudinal cross sections 95

Table 5-1: Comparison of the FEA results with the Experimental results for a circular tube 103

Table 5-2: Comparison of FE & experimental results for an oblong tube 108

Table 6-1: Comparison of effectiveness indicators for CT with various longitudinal cross sections. 118

Table 6-2: Independent variables and experimental design levels that were used (CTFIU) 122

Table 6-3: The design matrix (CTFIU). 122

Table 6-4: Analysis of variance (ANOVA) table for SEA – Reduced Linear Model (CTFIU) 123

Table 6-5: Analysis of variance (ANOVA) table for F–Quadratic model (CTFIU) 125

Table 6-6: Confirmation experiment (CTFIU). 127

Table 6-7: The criterion of numerical optimization (CTFIU).....133

Table 6-8: Optimal solutions as obtained by Design-Expert (CTFIU). 134

Table 6-9: Confirmation experiment of optimal solution (CTFIU). 134

Table 6-10: Comparison of effectiveness indicators for circular tubes compressed under various load angles (CT). 138

Table 6-11: Comparison of E and SEA for circular and oblong tubes 144

Table 6-12: Independent variables and experimental design levels used (OTFIU). 156

Table 6-13: The design matrix (OTFIU).....157

Table 6-14: Analysis of variance (ANOVA) table for SEA – Linear model (OTFIU). 158

Table 6-15: Analysis of variance (ANOVA) table for F – Quadratic model (OTFIU). 160

Table 6-16: Confirmation experiment.....161

Table 6-17: The criterion of numerical optimization (OTFIU). 167

Table 6-18: Optimal solutions as obtained by Design-Expert (OTFIU).....167

Table 6-19: Confirmation experiment of optimal solution (OTFIU).....168

Table 6-20: Comparison of effectiveness indicators for ET systems. 171

Table 8-1: The various performance characteristics of the main systems analysed in this thesis.....197

1

Chapter 1

INTRODUCTION

1.1 Importance of energy absorption systems

The demand for advanced transportation in modern society is increasing on a daily basis. This has led to continuously increasing numbers of vehicles on the roads. Inevitably, vehicular crash accidents have also increased, and have become a major worldwide health problem. In addition, these vehicular accidents also cause huge economic loss to society in general. Some very stark and tragic statics on vehicular road crashes were reported by the Association for Safe International Road Travel (ASIRT). For example, annual global road crash statistics are as follow (www.asirt.org [Accessed April 2013]):

- Nearly 1.3 million people die in road crashes each year, on average 3,287 deaths a day.
- An additional 20-50 million are injured or disabled.
- More than half of all road traffic deaths occur among young adults ages 15-44.
- Road traffic crashes rank as the 9th leading cause of death and account for 2.2% of all deaths globally.

- Road crashes are the leading cause of death among young people ages 15-29, and the second leading cause of death worldwide among young people ages 5-14.
- Each year nearly 400,000 people under 25 die on the world's roads, on average over 1,000 a day.
- Over 90% of all road fatalities occur in low and middle-income countries, which have less than half of the world's vehicles.
- Road crashes cost USD $518 billion globally, costing individual countries from 1-2% of their annual GDP.
- Road crashes cost low and middle-income counties USD $65 billion annually, exceeding the total amount received in developmental assistance.
- Unless action is taken, road traffic injuries are predicted to become the fifth leading cause of death by 2030.

It is clear from these statistics that vehicle accidents have a serious effect on health and safety, and cause very significant economic loss to society. Thus, the demand on engineers and researchers in the field of structures has increased for components and systems that dissipate the energy during an impact event. To this end, over the past several decades, continuous efforts have been made to design and develop energy absorbers to mitigate the detrimental effects of impact events and to increase the safety aspects of structures. This is particularly in cars, which gave rise to the greatest number of road casualties, as illustrated in Figure 1-1.

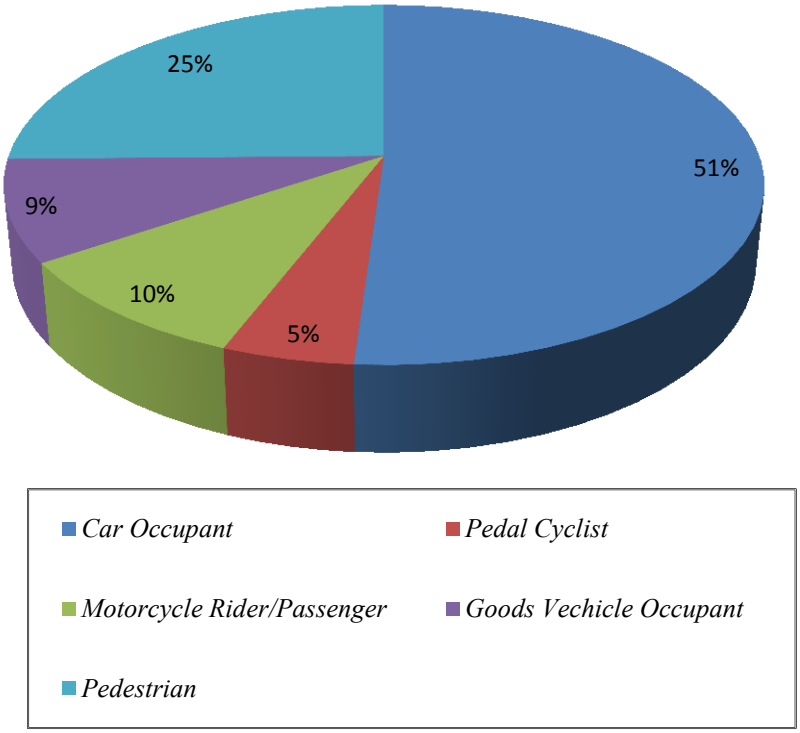

Figure 1-1: Road Deaths by Road User Type in Ireland in 2011(http://www.rsa.ie [Accessed April 2013]).

1.2 Design of energy absorption systems

Engineers and researchers who are involved in the design and development of energy absorption systems are required to have a thorough knowledge of a range of topics, such as mechanics of materials, structural mechanics, theory of plasticity, and impact dynamics.

In general, energy absorption systems should be designed to sustain impact and dynamic loads, and their collapsing behaviour should involve strain-hardening effects, strain rate effects, and large deformation changes. In addition, the deformation mode of the energy absorbers is a combination of different deformation modes such as bending and stretching. The main principles of the designing and selection of energy absorber components are addressed below.

1.2.1 Irreversible energy conversion

The energy absorption device should be able to convert kinetic energy into non-recoverable energy (inelastic) during the impact event. Inelastic forms of dissipating kinetic energy include plastic deformation, viscous energy dissipation, and energy dissipated by friction or fracture.

1.2.2 Restricted and constant reactive force

The reaction force offered by the energy absorption components under the impact load should be kept below a certain threshold, and ideally should remain constant during the deformation process. A higher reactive force causes higher deceleration, particular at the beginning of impact. This high deceleration is unacceptable as it causes serious damage to the occupants of the vehicle, as is clear from biomechanics studies. Keeping the reactive force and the deceleration constant during deformation, minimizes injures and damage to the occupants.

1.2.3 Long stroke

The energy absorbed by a structure is given by

$$E = F * L \qquad (1\text{-}1)$$

Where E is the energy absorbed, F is the reactive force, and L is the displacement experienced along the acting line of the force. It is clear that the energy absorbed (E) can be maximize by increasing the stroke length (L), as the reactive force needs to be restricted and almost constant, as pointed out in last section. Therefore, the energy absorber should be able to provide a sufficient stroke length to absorb a larger amount of kinetic energy.

1.2.4 Stable and repeatable deformation mode

To ensure the reliability of the energy absorption structure, the deformation mode and specific energy absorbing capacity should be stable and repeatable. The energy absorbers are designed to work under dynamic loads that are variable with respect to their load magnitude, pulse shape, direction, and distribution. Therefore, the

responses and behaviour of energy absorbers should be insensitive to the variability of these factors.

1.2.5 Light weight and high specific energy-absorption capacity

The energy absorption components should be light, and should also have a high specific energy absorption capacity. The energy absorber weight and specific energy absorption capacity are very important parameters, particularly in the case of moving vehicles such as aircraft and cars, because any increase in weight results in increased fuel consumption and air pollution.

1.2.6 Low cost and easy installation

Energy absorbing components are normally used a single time. Once they are deformed and destroyed, they need to be replaced with new components. Therefore, the manufacture, installation, and maintenance of these components should be easy and cost-effective.

1.3 Thin walled components as energy absorber

Thin walled tubes have been extensively employed in crashworthiness applications, to absorb kinetic energy through plastic deformation. The widespread use of thin walled tubes as energy absorbers is due to their good performance under dynamic loading, and their availability, low manufacturing cost, and efficiency. The most important application of thin walled components as impact energy absorbers is in crash boxes behind a car bumper. Figure 1-2 shows a vehicle crash management system that consists of a car bumper beam and two crash boxes. The crash boxes should be deformed before the other components of the vehicle, thus preventing the load transmitting to the other parts and reducing the cost of repair. The function of this system is to protect the integrity of the whole automobile structure as well as the passengers.

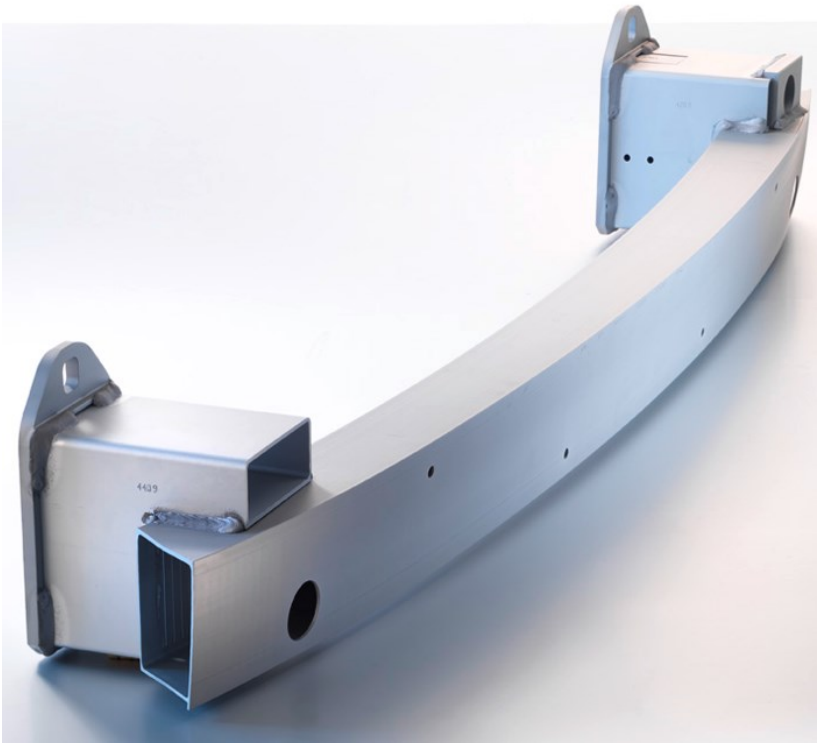

Figure 1-2: Crash management system (www.constellium.com [Accessed April 2013]).

1.4 Aims of this Thesis

The main aim of this thesis is to generate design information on the behaviour and energy absorption capability of thin walled, single and nested tubes under lateral loading, to employ them in crashworthiness applications and energy absorption systems. The second aim of this thesis is to examine multi-objective optimization designs of various tubes, in order to establish the optimal configurations of the various components used in this work.

The other aims of this thesis are:

1. To develop finite elements (FE) models for single and nested tubes and to validate these models with experiments and existing theoretical and numerical models.
2. Construct Response Surface (RS) models of various tubes by using statistical software, Design-expert V8 (DOE).

3. To investigate the influence of the geometric parameters on the energy absorption responses by performing parametric studies on the various tubes.

The main outcome of this thesis was design guidelines for the use of laterally crushed thin-walled tubes as energy absorbing structures in impact applications.

Figure 1-3 shows one potential application for the use of laterally crushed tubes as energy absorption devices in a car bumper.

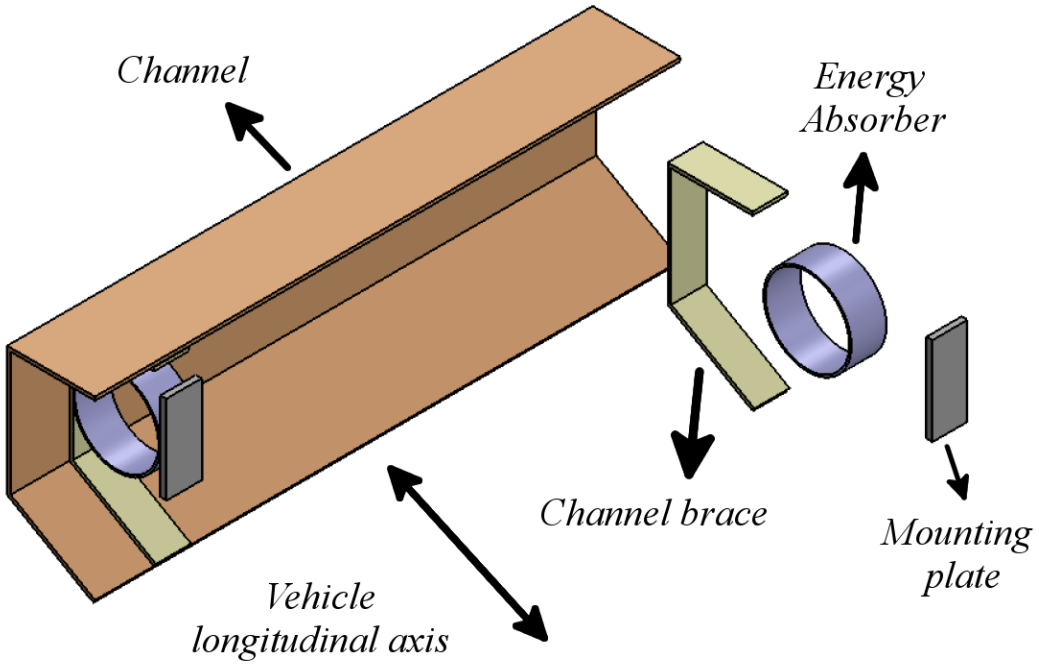

Figure 1-3: A Vehicle Frontal Protection (VFPS) system consisting of a single circular tube crushed laterally.

1.5 Thesis outline

Chapter 2- Chapter 2 provides a detailed review of previous studies and research relating to the aims and scope of this thesis. At the beginning of this chapter, the fundamental concepts of impact mechanics and structural crashworthiness, with their applications, are introduced. Then, a detailed review of the various structures used as energy absorbing components are presented and discussed. Areas where further investigations are required are highlighted. Finally in this chapter, the techniques and analysis methods of energy absorption systems are presented.

Chapter 3- Chapter 3 outlines important theory that is used to assist in the analysis and solution of the various aims of this thesis. This chapter is divided into three sections. The first section provides a brief description of the principles involved in finite element modelling of energy absorbing structures. Section 2 and section 3 of this chapter deal with the response surface method and optimisation approach used by design expert software.

Chapter 4- Chapter 4 introduces the various instruments used to carry out the experimental work on the various systems analysed in this thesis. Features, and the setup, of various machines that were used to perform the quasi-static and dynamic tests are discussed. In addition, this chapter describe the material properties and geometrical dimension for various configurations of energy absorbing systems developed in this thesis.

Chapter 5- Chapter 5 describes the development and validation of finite element models used for the simulation of single and nested tube systems under lateral loading. The procedure used to simulate the quasi-static and dynamic loading conditions is introduced. The development of appropriate material models to represent the material behaviour of various systems under lateral loading is also discussed. This is followed by confirmation of the validity of the developed FE models by comparing the results offered by FE models with the experimental results. The validated FE models developed in this chapter serve as a basis for the parametric studies conducted in subsequent chapters on the response of various systems under lateral loading.

Chapter 6- Chapter 6 investigates the experimental response of single tubes under quasi-static and dynamic lateral loading. The crush behaviour of three different configurations of thin-walled single tubes, namely circular, oblong, and elliptical tubes, is examined. This chapter also provides a parametric study of the energy absorption response of various single tubes under quasi-static lateral loading. Finite element techniques using ANSYS, along with Response Surface Methodology (RSM) for Design of Experiment (DOE), were employed to construct the RS models and to perform the parametric studies. Parametric study examines the relative effect of various geometry parameters on the quantified energy absorption and deformation response of the various tubes. In addition, Multi-objective Optimization Design (MOD) of the

various single tubes is carried out by adopting a desirability approach to find the optimum configuration of the energy absorbing structure.

Chapter 7- Chapter 7 presents responses of nested tube systems under quasi-static and dynamic loading conditions. Nested systems in the form of internally stacked tubes are proposed as energy absorbing structures for applications that have limited crush zones. Three configurations of nested tube systems are analysed in this thesis. The crush behaviour and energy absorbing responses of these systems are presented and discussed. Since the dynamic loading instrument has a limited velocity of 4.5 m/sec, the validated FE models were employed to investigate the responses of nested tube systems under higher velocities. The inertia effect of these systems under high impact velocity is presented and discussed.

Chapter 9- This chapter presents a clear and concise discussion of the results, summarizes the main conclusions of this thesis, and provides suggestions for future research in the area relating to this work.

2

Chapter 2

LITERATURE REVIEW

2.1 Impact mechanics

In general, energy absorbing systems are designed to work under dynamic loading conditions. The responses of these systems under dynamic impact loads are different from their responses under quasi-static loads. This difference is due to inertia and strain rate effects, which play an important role in the energy absorption response of a structure under a dynamic load.

2.1.1 Inertia effects

Inertia effects have been studied by Calladine and English [1]. The authors tested two types of structures termed as Type I and Type II structures. The Type I was modelled as lateral compression of a circular tube and had a relatively "flat-topped" load-displacement curve, while the Type II structure was modelled as an axial compression of a column with two separate steel sheets fixed and clamped together at either end. The force-displacement curve of the Type II structure had an initial peak load followed by a steep decline. Figure 2-1 shows the models of Type I and Type II structures with their corresponding force-deflection curves. The authors

reported that the Type II structure had more sensitive impact velocity and inertial effects; hence the parameters of inertia should be handled carefully in the Type II structures scale modelling. By using theoretical techniques, Zhang and Yu [2] discussed the velocity sensitivity of a Type II structure. The authors endeavoured to quantify the effects of both strain-rate and inertia of a Type II structure and to validate their theoretical model by comparing the results with the results obtained by Calladine [1]. Another study on the response of Type II structures were carried out by Tam and Callidine [3].

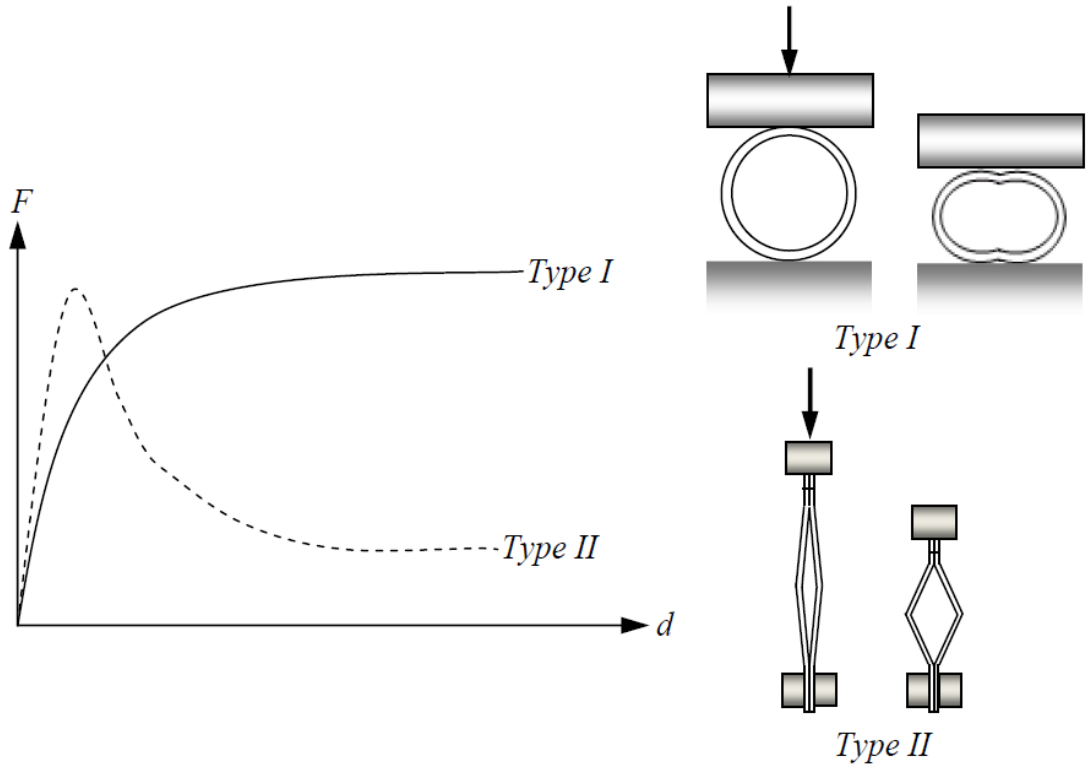

Figure 2-1: Two classes of structures [4].

In this study an attempt was made by the authors to remove the various limitations of previous studies [1]. Dimensional analysis with variables such as material type and specimen size were performed, and a thorough theoretical analysis of the response of Type II structures was presented. It was observed that the deformation of Type II structures consisted of two phases: plastic compression and sole rotation of the plastic hinges. It was reported that the first deformation phase is dominated by lateral inertia, while the second phase is more sensitive to strain-rate. Theoretical analysis of the inertia and elasticity effects on the responses of Type II structures was

performed by Su et al. [5]. The peak load was predicted by employing an elastic-perfectly plastic material model. The mathematical model proposed in this study consisted of four compressible elastic-plastic rods connected by four elastic-plastic hinges. A comparison between the quasi-static and the dynamic responses of a Type II structure was carried out. It was found that the dynamic response of a Type II structure under dynamic conditions is significantly different from its behaviour under quasi-static conditions, even if the strain-rate effect was ignored. This difference is due to inertia effects which play an important role in the dynamic behaviour of a Type II structure.

In most cases, the inertia effects cause an increase in the load required to crush the structural component, such as reported in [6], [7] , and [8].

The strengthening of structural components under a dynamic load due to inertia effects or strain-rate effects is an undesirable feature in energy absorbing devices, as this strengthening increase the possibility that the absorbing structure could transmit the forces and decelerations to the occupants.

Nagel [9] has reported that tapered rectangular tubes are less affected by the inertia effects than straight tubes, so tapered rectangular tubes are more suitable for use as energy absorbing devices. Harrigan et al. [10] noted that in some applications the inertia effects tended to decrease the crush force of energy absorbers. These authors investigated the dynamic behaviour of a metal tube inverted onto a die. It was reported that inertia effects assist in the inversion process, and thus the dynamic collapse load is much lower than its quasi-static counterpart.

Overall, it can be concluded that the inertia effects on the responses of thin-walled tubes rely significantly upon the type of energy absorber.

2.1.2 Strain rate effects

The mechanical properties of many materials are sensitive to loading rate. These materials are classed as strain rate dependent, or visco-plasticity materials. The responses of visco-plasticity materials under dynamic loading are different to the corresponding responses under quasi-static loading. In general, the yield stress and ultimate stress increases as the strain rate increases. Many researchers have tried to establish constitutive equations for describing the strain-rate behaviour of visco-

plasticity materials. The most popular equation used by engineers and designers in the field of structural impact is the Cowper-Symonds relationship, which considers the strain-rate effects. This relationship displays good agreement with the available experimental data for various metals, and it is defined as.

$$\sigma_d = \sigma_s \left(1 + \left(\frac{\varepsilon}{D} \right)^{\frac{1}{q}} \right) \qquad (2\text{-}1)$$

Where σ_d is the dynamic flow stress, σ_s is the static yield stress, ε is the strain rate, the constants D and q are parameters of the material. Table 2-1 shows the D and q constants for certain materials.

Table 2-1: D and q values for various metals [11].

Material	*D (s^{-1})*	*Q*
Mild steel	40.4	5
Aluminium alloy	6500	4
α-Titanium (Ti 50A)	120	9
Stainless steel 304	100	10
High tensile steel	3200	5

It is worth noting that the values of D and q for mild steel in Table 2-1 are only applicable in the case of small strains (e.g. 2-4 %). The researchers in the field of crashworthiness applications that involved large strains have adopted the values of *D* = 6844 S and q = 3.91. These values of D and q were employed by [8] , [12], [13], and [14] to investigate the crushing behaviour of mild steel tubes under dynamic load.

Su et al. [12] employed the Cowper-Symonds relationship to study the effect of strain-rate on the dynamic behaviour of Type II structures. Due to the combined effects of inertia and strain-rate, the dynamic peak load of a Type II structure is

much higher than the corresponding quasi-static load. The authors found that the elastic strain energy stored in a structure made of rate-dependant material was greater than that noticed in a structure that was made of a rate-independent material. Therefore the elasticity has a significant effect on the dynamic response of a structure which is made of rate-dependant material.

2.2 Structural crashworthiness

In general, crashworthiness is the ability of a structure to protect itself and its occupants from serious injury or death when it is subjected to an impact load. According to Lu and Yu [15]

The term 'crashworthiness' refers to: *"the quality of response of a vehicle when it is involved in or undergoes an impact. The less damaged the vehicle and/or its occupants and contents after the given event, the higher the crashworthiness of the vehicle or the better its crashworthy performance."*

The term 'structural crashworthiness' refers to the performance of a structure under impact or dynamic load. Jones [11] defined structural crashworthiness as:

"The term 'structural crashworthiness' is used to describe the impact performance of a structure when it collides with another object."

In the last few decades, there has been a continuous focus on crashworthiness as a primary requirement in the design of occupant-carrying structures. As shown in Figure 2-2, the crashworthiness requirement of the structure of the vehicle is to protect the passenger compartment or the survival space. The crushable body parts are designed to deform and absorb crush energy.

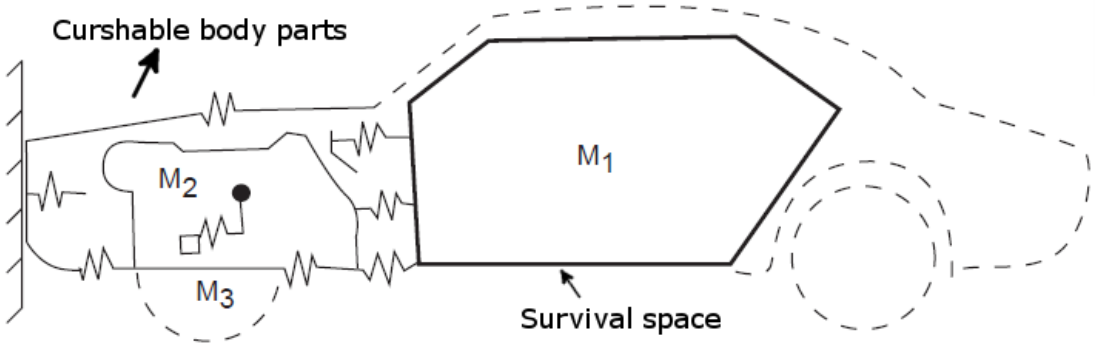

Figure 2-2: Fundamental concept of crash energy management for cars [16].

The thin walled energy absorbing components are used to absorb the energy of an impact, and thus enhance the crashworthiness of the structure. The most common example of using thin walled tubes for maintaining the crashworthiness of a vehicle is the front chassis rails of a vehicle which deform to absorb energy in the event of frontal impact, which is the most common type of crash occurrence. Different energy absorbing devices are employed for absorbing energy of different types of impact. Side impact on vehicles can be absorbed by reinforcing the doors and side-pillars. Figure 2-3 shows one example of an energy absorption system used by the Honda Company to maintain the crashworthiness of a vehicle. The structure uses the engine compartment to efficiently absorb and dissipate impact energy during a frontal vehicle-to-vehicle collision. This system consist of a highly efficient energy-absorbing main frame (Green structure), and an ACE (advanced compatibility engineering) frame (Red structure), which consist of an upper frame that absorbs the upper part of the impact energy, and a lower member that prevents misalignment of the impact-absorbing member of the oncoming vehicle. This design dissipates the impact energy over a larger frontal area, which enhances energy absorption by the engine bay, reduces the chance of deformation of the survival space, and results in more occupant protection. At the same time, the structure reduces the chance of vertical or lateral misalignment between the vehicle and other vehicle's safety structures.

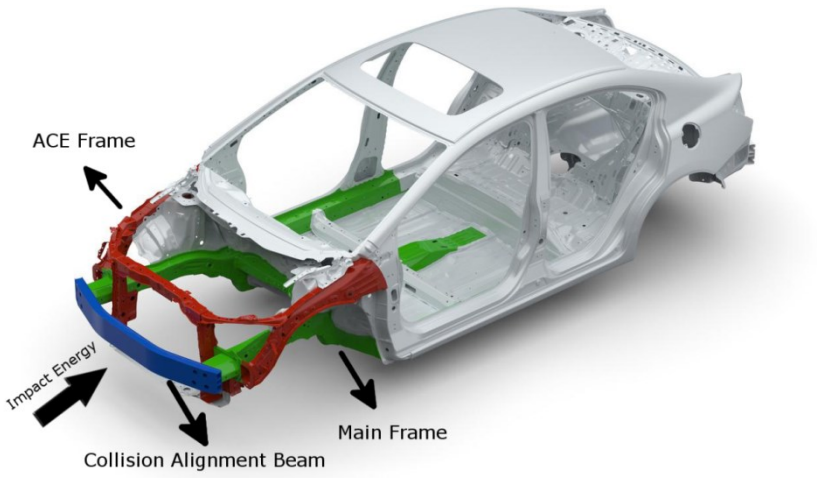

Figure 2-3: Energy absorption system used for cars manufactured by the Honda company (www.honda.com).

Many other applications employ energy absorbers to enhance the crashworthiness of structure such as:

- Aircraft sub floor structures that deform to reduce impact decelerations transmitted to the occupants and to provide a post-crash structural integrity of the cabin floor in the event of crash landings [17] and [18]. The Figure 2-4 shows a typical subfloor structure of a helicopter.

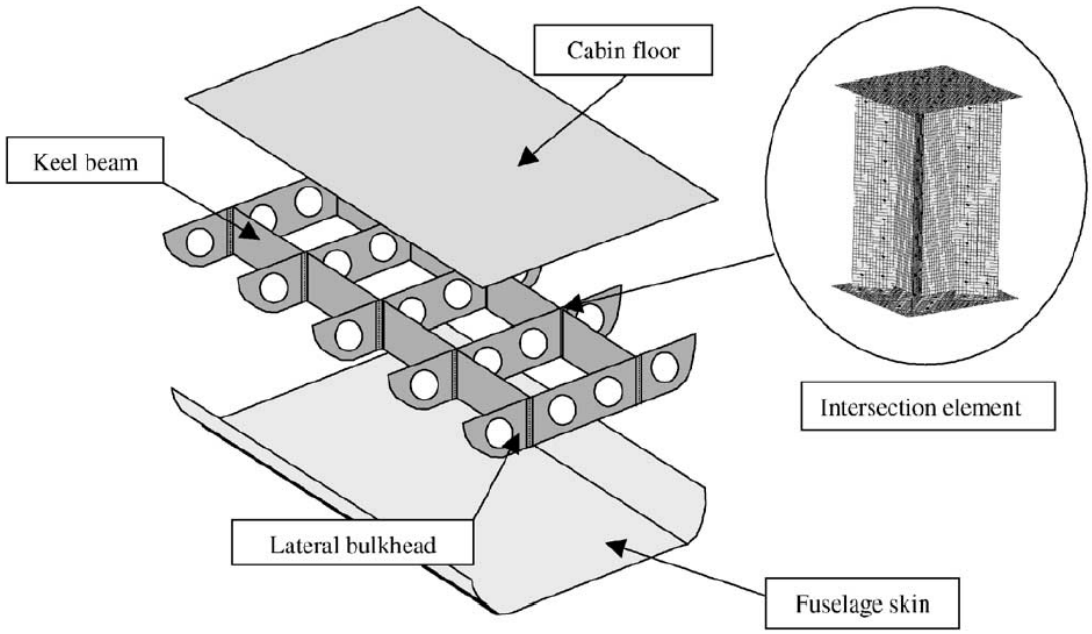

Figure 2-4: A typical helicopter subfloor structure [17].

- Energy absorption devices at the front of passenger trains (Figure 2-5). These components collapse during a frontal collision, reducing impact forces transmitted down the length of the train, and thus localise deformation towards the front of the train.

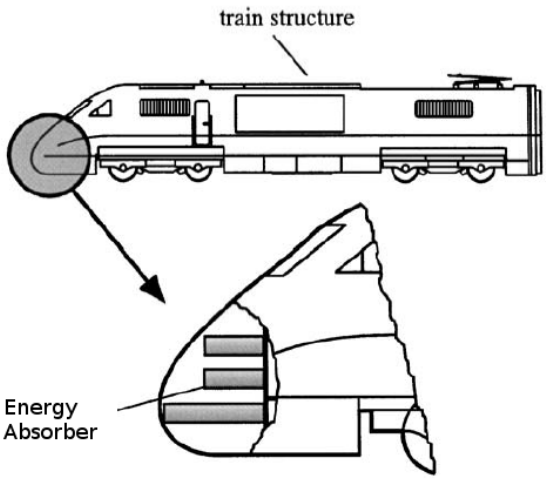

Figure 2-5: Metallic cylindrical shells as energy absorbers in train structures [19].

- Thin-walled tubes at the base of lift shafts to provide controllable stopping of the lift in the event of a cable-breakage or over-wind.
- Energy-dissipating crashworthy device used in a ship–bridge collision [20]. This device consists of hundreds of Steel Wire Rope Coils (SWRC) connected in parallel and series as shown in Figure 2-6. This device enables the ship to have enough time to change direction, and with the result that a large percentage of the initial kinetic energy of the ship is dissipated by the turning away of the ship.

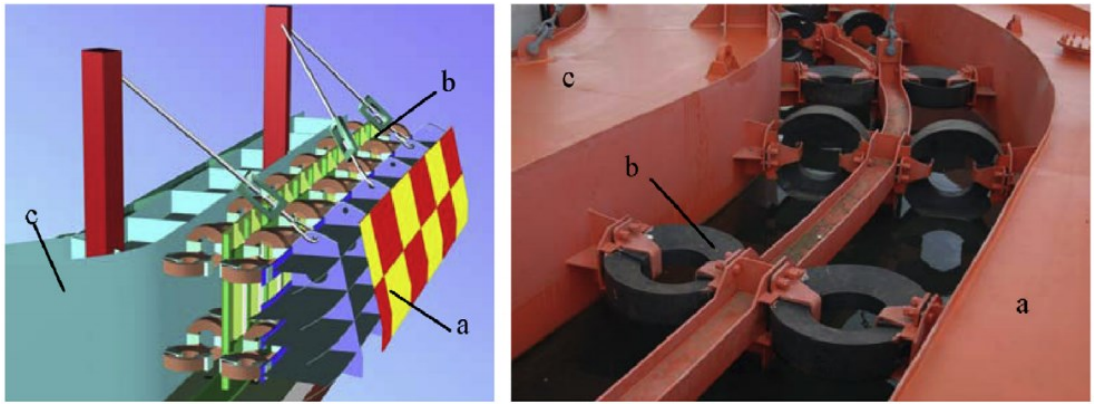

Figure 2-6: Partial schematics (left) and a photo (right) of the SWRC flexible crashworthy device [20].

- Thin walled energy absorbers are used to enhance the performance of Rollover Protective Structures (ROPS) of heavy vehicles, such as bulldozers

and tractors. [21] and [22] reported that structural responses of ROPS under rollover impact can be reinforced by inclusion of thin-walled frusta in a ROPS as shown in Figure 2-7.

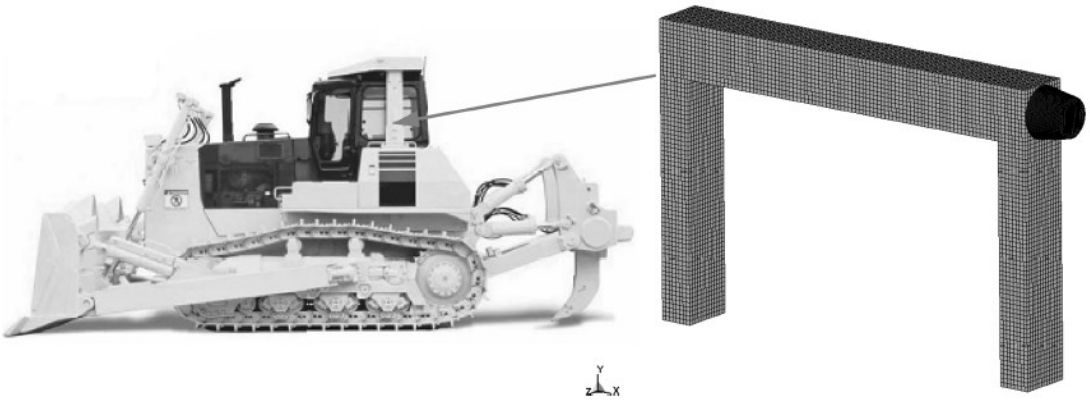

Figure 2-7: Bulldozer with ROPS and FE model of the assembly of ROPS& energy absorber [21].

- Energy absorber components (Figure 2-8) used in the container of nuclear fuel assemblies [23]. The function of this absorber is to avoid failure of fuel assemblies in case of hypothetical spent fuel assemblies dropping accidentally during uploading or unloading of spent fuel assemblies to and from the container.

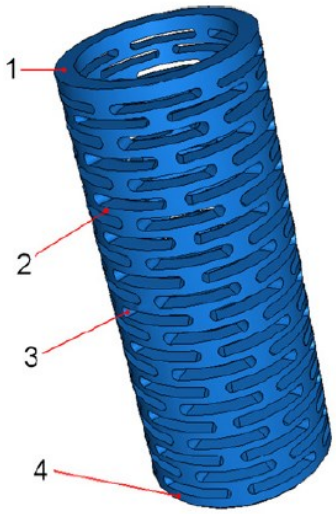

Figure 2-8: A general view of the shock absorber model: (a) 1 and 4 are the top and bottom rings, 2 are the working rings, 3 are the cuts [23].

2.3 Energy absorber characteristics

The performance of energy absorbing systems can be evaluated by means of several criteria. Such criteria are used in the initial design stages of energy absorbing devices. Some useful indicators were proposed by Thornton et al. [24], such as crush efficiency, energy efficiency, specific energy absorption capacity, and weight effectiveness. This section discusses indicators used to describe the effectiveness of energy absorbing structures.

2.3.1 Energy absorption capacity (E)

Energy absorption capacity (E) can be measured by calculating the area under the force-deflection response of an energy absorbing device. It can be defined as the integration of a load-displacement curve as follow.

$$E = \int_0^{\delta} F(\delta) \, . \, d\delta \qquad (2\text{-}2)$$

Where E is the energy absorption capacity, δ is the displacement, and F (δ) is the load-displacement response.

2.3.2 Specific energy absorption (SEA)

The specific energy absorption capacity is the most important characteristic of energy absorbers. SEA is defined by energy absorbed per unit mass, and is given by:

$$\text{SEA} = \frac{E}{m} \qquad (2\text{-}3)$$

Where m is the mass of the energy absorber. SEA is a very important energy absorption indictor, particularly in structures where weight is of critical importance.

2.3.3 Stroke efficiency (e_g)

The stroke efficiency is defined as the stroke length divided by the characteristic length of a structure, such as the outer diameter or the original length. The stroke efficiency for lateral collapse of a circular tube can be defined by the equation

$$e_g = \frac{\delta}{D} \qquad (2\text{-}4)$$

Where D is the outer diameter of the tube, e_g is considered as a good indicator for describing the amount of material that can be used during collapse. This indicator is very useful in applications that have restrictions on energy absorber space.

2.3.4 Energy efficiency (e_E)

The energy efficiency indictor is given by

$$e_E = \frac{E}{F_{max} * L_o} \qquad (2\text{-}5)$$

Where F_{max} is the maximum load observed in the force-displacement response, and L_o is the original length of the absorber. It is recommended to maximize the energy efficiency of the energy absorber. Ideally, to achieve the maximum value of e_E, the force-displacement response of the energy absorber should be a rectangle response.

2.3.5 Work effectiveness (W_{eff})

The work effectiveness is a combination of the specific energy absorption capacity and the crush efficiency indicator, and it is defined as follow:

$$W_{eff} = SEA \times e_g \qquad (2\text{-}6)$$

This indicator is a very useful one, particularly in structures that are restricted in terms of both weight and space.

2.3.6 Energy absorbed per unit crush length (E_{cl})

The energy absorbed per unit crush length can be calculated by absorbed energy divided by either the undeformed length or the maximum crush distance of the energy absorber. This parameter is a very important one in applications that have a limited crush zone. Introducing the nested tubes system is expected to increase the

E_{cl} as the nested system has more than one tube deformed simultaneously in the same space.

2.3.7 Dynamic amplification factor (DAF)

The dynamic amplification factor can be defined as the ratio between the energy absorbed under dynamic loading and the energy absorbed under quasi-static loading up to a given crush distance, and is given by:

$$\mathrm{DAF} = \frac{E_d}{E_s} \qquad (2\text{-}7)$$

This parameter is used to assess the effect of dynamic loading on the energy absorption of the energy absorber structure.

2.4 Energy absorbing structures

The function of energy absorption structures is to minimise the injuries to human beings and to protect the vital structures from impact damage or any other kind of dynamic loads. The design and development of these systems require study and understanding of materials engineering, structural mechanics, impact mechanics, and the theory of plasticity. The behaviour and responses of these structures under dynamic loadings such as impact, is considered to be a very important field for design and research engineers who are involved in the automobile, aircraft, spacecraft, and nuclear industries. In general, passive energy absorbing structures can be classified into three major groups as follow:

- Empty thin walled tubes
- Nested thin walled tubes
- Foam-Filled tubes

Over the last four decades, a significant amount of research has been conducted on the energy dissipated by thin walled tubes. The main findings were outlined and presented in a review article by Olabi et al. [25], Alghamdi [26], and Abramowicz [27]. General information and discussion about energy absorption structures and materials can be found in books by Lu and Yu [15] and Jones [11].

2.4.1 Empty thin-walled energy tubes

The most popular form of collapsible energy absorption systems are thin-walled tubes. These structural elements can absorb kinetic energy as a result of many types of deformation, leading to various energy absorption responses. The most common materials used for thin-walled tubes are steel and aluminium alloy. The principle ways of destroying tubes include lateral compression, lateral indentation, axial crushing, tube splitting, and tube inversion.

2.4.1.1 Axial Loading/Buckling

There are a number of modes for axial deformation of tubes. These modes were investigated by Reid [28]. Importance was given to the modes of splitting and inversion buckling in order to study the generation of plastic deformation during the process of absorbing energy. Other research used thin-walled tubes filled with a honeycomb material similar to foam, to enhance the effectiveness of the energy absorption system.

An experimental investigation on the crushing of tapered sheet-metal tubes of rectangular cross-section under dynamic and static conditions was conducted by Reid and Reddy [8]. In addition to experimentation, a theoretical method was also used to get the mean crushing force of these tubes. It was found that these tapered tubes provide a solution for absorbing off-axis/oblique loads. The theoretical method gave good predictions for the magnitude of the crushing force in both static and dynamic cases. The authors reported that the tapered tubes are recommended more than straight tubes due to their ability to absorb the off-axis loads, as its shape enables it to avoid failure by global buckling.

Guillow et al. [29] performed an experimental examination on axial compression of a circular aluminium tube under quasi-static conditions. Series of tubes with different D/t ratios were used and a diagram which describes the various modes of deformation was created. A brief investigation was also described on the effect of filling the tubes with foam. A non-dimensional empirical formula was developed by using the average force.

Wang and Lu [30] found a new deformation mechanism called ‘Mushrooming’ which made the walls of the shell thicker. A cylindrical shell was studied and

exposed to axial impact with velocities values of up to 300 m/sec. A gas gun (Figure 2-9) was used to carry out the tests in this study. They found that high impact speeds produced a unique plastic deformation that needed the application of the finite element method, in addition to experiments, to investigate it. Figure 2-10 shows a typical cylindrical specimen subjected to high impact velocity. They reported that there are three modes of deformation depending on the velocity of impact.

The 3 deformation modes are:

- Dynamic progressive folding of thin tubes under low impact
- End mushrooming with folds formed away from the striking end at medium velocity
- Mushrooming and wrinkling of thick tubes at high velocity.

The authors reported that the material model that suits the dynamic failure in these tubes under high impact speed was not available, so the agreement between the numerical and experimental results at high speed impact could not be obtained. However the simulations related to low impact velocity provided good data for engineers and designers.

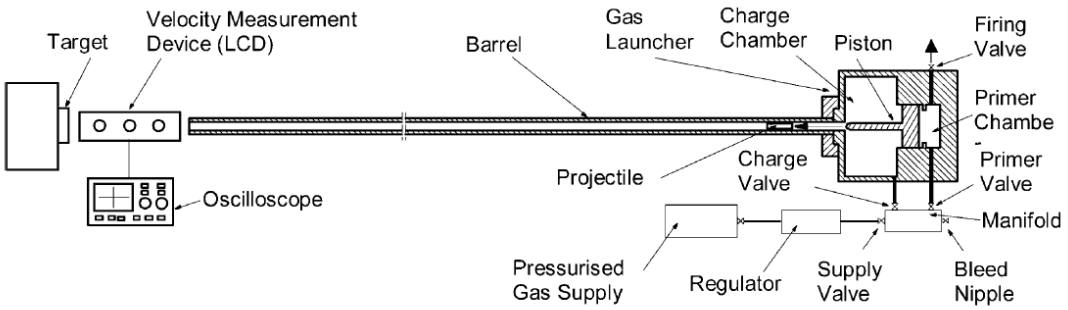

Figure 2-9: Sketch of the gas gun used for the experiments [30].

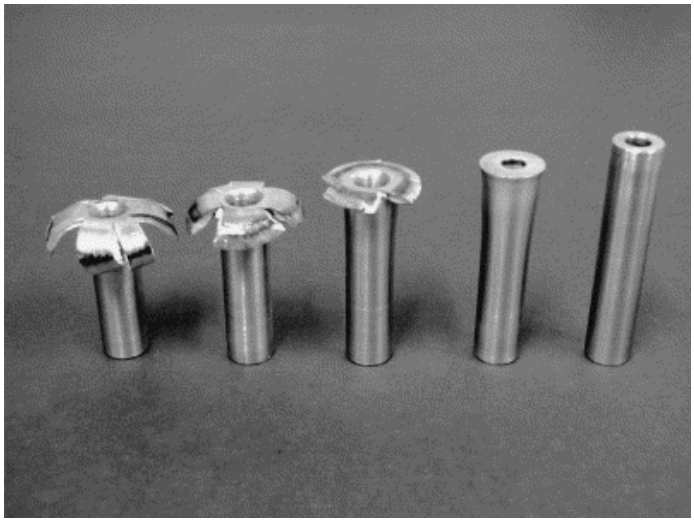

Figure 2-10: Mild steel samples: Deformation states at velocities of 385 m/s, 277 m/s, 227 m/s, 173m/s and 0 /ms respectively [30].

The response of circular stainless steel, mild steel, and aluminium alloy compressed axially under quasi-static and dynamic conditions was investigated by Hsu and Jones [31], the objective of this study was to examine the effects of strain rate, strain hardening, and inertia on the effectiveness of energy absorber systems and to compare the performance of these materials during the energy absorption process. It was found that aluminium tubes absorbed the smallest energy per unit volume but that was the most efficient, while the stainless steel tube absorbed the most energy per unit volume but it had the lowest energy absorbing efficiency.

Zeinoddini et al. [32] carried out an experimental investigation on the axially preloaded steel tubes subjected to lateral impacts. In some applications using tubular energy absorbers, the absorption system should be able to withstand normal workloads before an impact event happens, for example in collisions of supply ships with offshore oil rigs. A drop weight rig, as shown in Figure 2-11, has been used to apply a lateral impact load on axially preloaded tubes. It was possible to control axial preloading during the test. The other parameters such as indenter shape, impact location, orientation of indenter, and the residual stress level inherent within the tube were ignored so further work would provide a fuller understanding of the effect of these other parameters on the output response. It was reported by the authors that

pre-loading had an important influence on the amount of damage when integrated with impact loads.

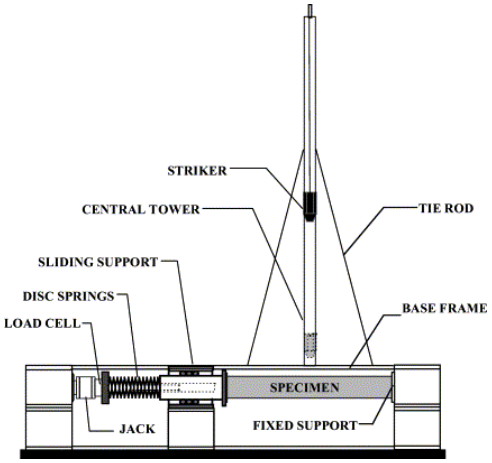

Figure 2-11: Schematic view of the impact rig for testing lateral impact on axially pre-loaded tubes [32].

Validated finite element simulations of square aluminium extrusions under axial loading were carried out by Langseth et al. [33]. Close agreement of the results from finite element simulations, and those from experiments was achieved. The author developed a finite element model using isotropic elasticity, the Von Mises yield criterion, the associated flow rule, and non-linear isotropic strain hardening. During the experiments the square aluminium extrusions were subjected to static and dynamic axial loads. A tensile test was carried out to obtain the yield stress and strain hardening characteristic of the tubes. A trigger mechanism (Figure 2-12) was used in the numerical model to obtain a symmetric folding mechanism. A parametric study was performed on the mean load to test the effect of the impact parameters. Figure 2-13 shows the axial deformation stages for a 2.5 mm thick tube with the trigger at the mid-section under impact loading. It was noted that mean load had a proportional correlation with respect to impact velocity, but it was not affected by the mass ratio of specimen to projectile.

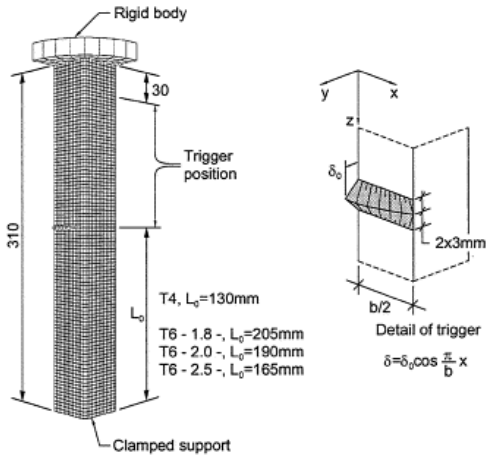

Figure 2-12: One quarter finite element model including trigger position [33].

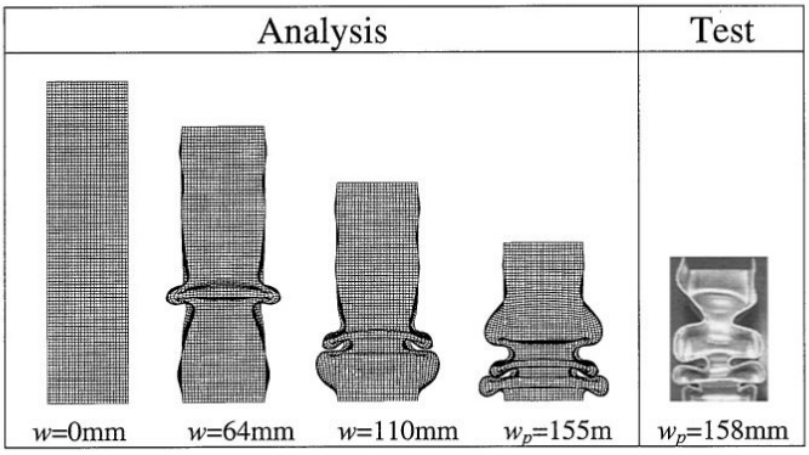

Figure 2-13: The axial deformation stages for a 2.5 mm thick tube with the trigger at the mid-section under impact loading [33].

In order to obtain a good understanding of the post-bulking behaviour of energy absorbers components under impact loads, Rossi et al. [34] studied the axial collapse of aluminium alloy extruded polygon sections. This study was conducted using the finite element code LS-DYNA. The authors performed two separate analyses during their investigation. Firstly, an attempt was made to validate the numerical results using LS-DYNA software with experimental data published by other researchers. Following the resultant validation attempt, the symmetric and asymmetric behaviour of post-buckling deformation was investigated. It was concluded that the finite element software (LS-DYNA) was able to predict these modes of deformation. In addition, the study was able to give an accurate value for mean dynamic crushing

force and permanent displacement with +/- 5% deviation from the real values. Figure 2-14 illustrates the final post-buckling deformation state of a hexagonal sectioned model.

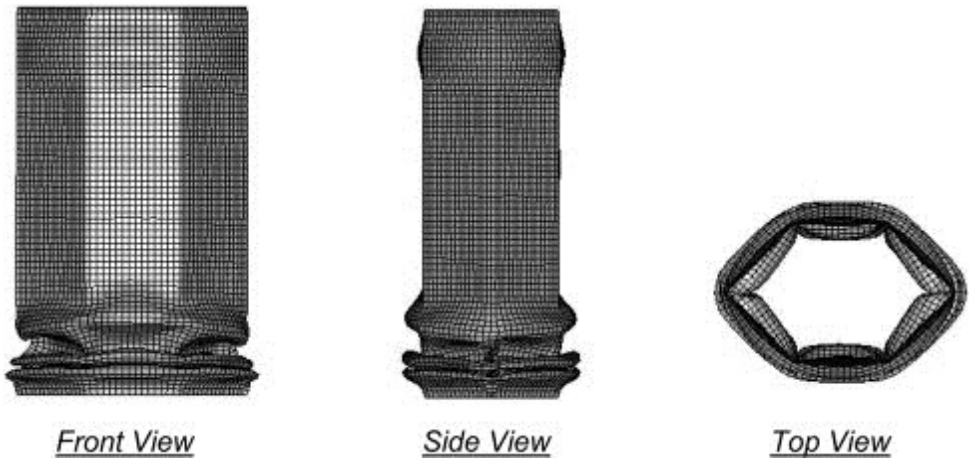

Figure 2-14: Final post-buckling deformation of an LS-DYNA hexagonal section model [34]

Numerical analysis of energy absorption responses of tapered thin-walled tubes subjected to an impact load was carried out by Nagel and Thambiratnam [35]. A comparison between straight tubes and tapered tubes (under both quasi-static and dynamic loading) was undertaken. The effect of parameters such as angle of taper, thickness, and impact velocity on the responses of these systems were illustrated. It was found that straight tubes were more affected by the lateral effects than tapered tubes. In addition to this the authors reported that the energy absorbing response was affected by the changes in the taper angle and wall thickness more than the other parameters. Figure 2-15 illustrates the finite element model of a straight and tapered energy absorber.

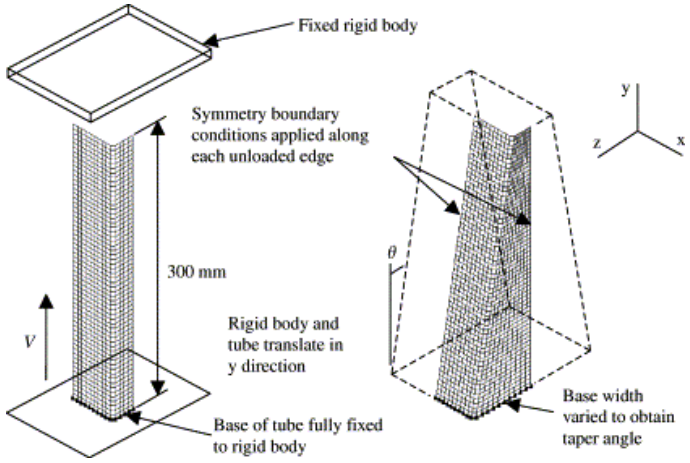

Figure 2-15: Tube mesh, geometry, and loading arrangement used in the FE model [35].

The previous work was further expanded on by the same authors [36]. Tapered tubes of either straight, double taper, triple taper, and frusta were used. Impact load was applied to these devises to investigate the dynamic energy absorption responses. The numerical results showed that frusta have the lowest energy absorption capacity and triple tapered tubes have the highest, whereas the capacity of straight tubes is intermediate, ranking between the frusta and triple tapered tubes. Figure 2-16 shows the collapse sequence for straight and tapered tubes of 300 mm in length under a quasi-static axial load. It was found that in applications where weight is important, the straight tubes represented the most effective structure for absorbing energy. The effectiveness of straight tubes was indicated by the results that showed that the specific energy absorption per unit mass was reduced by increasing the taper on the tubes.

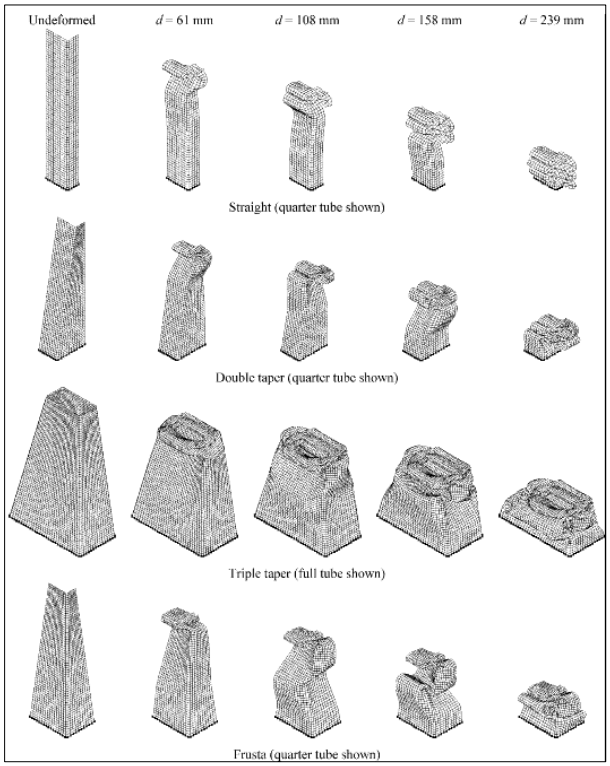

Figure 2-16: Collapse sequence of straight and tapered rectangular tubes under a quasi-static axial load [36].

In other work carried out by the same authors [37], the main aim was to provide valuable data that will enable engineers and designers to build an efficient energy absorption system by using tapered tubes.

Tapered wall tubes have been used by Nagel and Thambiratnam [38] to increase the energy absorption in the VFPS (Vehicle Frontal Protection Systems). The function of VFPS is to protect the vehicle structure and reduce damage caused from animal strikes. The tapered tubes, axial crushing of honeycomb, and recoverable semi-rigid foams are the three mechanisms suggested for filling the gap between the chassis rail of the vehicle and the VFPS. Papers published in the future on this area will concentrate on the effect of using each of these mechanisms on the energy absorbed by VFPS.

Gupta and Gupta [39] studied the effect of the presence of cut-outs in the aluminium tubes for the two conditions of ‘as-received’ and ‘annealed’. An Instron machine was used to compress the aluminium tubes statically; these tubes have different L/D and

D/t ratios. The cut-outs were holes. It was noticed that in tubes that had cut-out holes, the peak load was reduced. While for tubes without cut-outs, it was noticed that there was a correlation between the deformation mode, initial state of work hardening, and the ensuing annealing process. It was reported that using cut-outs provided the benefit of much longer crush displacements before the beginning of Euler buckling.

Multi-cell columns crushed axially were proposed as energy absorbing structures, and the energy absorption characteristics of these new columns were presented by Xiong and Hui [40]. These authors carried out experimental investigations and theoretical analyses of these structures. In addition, numerical simulations were performed to simulate the compression tests. Figure 2-17 shows the various multi-cell columns. It was observed that multi-cell metal columns are more efficient than single-cell columns, increases in absorbed specific energy of 120% and 220% were recorded for specimens S4 and S5.

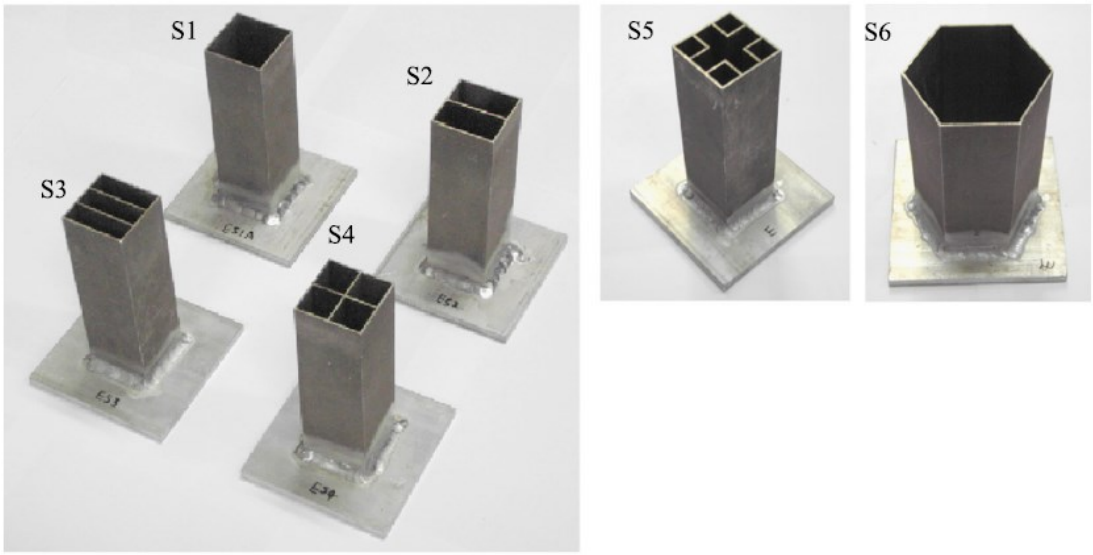

Figure 2-17: Various configurations of multi-cell columns [40].

2.4.1.2 Axial Inversion

The strain-rate and inertial effects in the free inversion of mild steel circular tubes was investigated by Colokoglu and Reddy [41]. It was found that the strain-rate sensitivity increased the resistance to inversion, while the inertial effects had two effects on resisting and assisting the force needed for the inversion process. In addition to experimental procedure, the Cowper-Symonds relation was used to predict the flow stress of the material. It was noticed that the theoretical results over-estimated the real value, because the empirical constants D and q were too small in inversion conditions.

Simulations using the finite element method on the dynamic and static axial inversion of tubes with circular and square cross section were carried out by Webb et al. [42]. This work emphasises the importance of using finite element techniques in the design of these energy absorbers, in order to predict as well as optimize the results from experiments.

A trial was carried out by Kinklead [43] to increase the convergence between the experimental and theoretical results for circular tube inversion. 'Engineering strain' was used instead of 'natural strain' to increase convergence. It was found that engineering strain gave a better theoretical approach to the experimental results than natural stress. The aim of this new theory was to enable researchers to design new energy absorption systems with a greater level of exactness.

Reid and Harrigan [44] studied the plastic deformation of mild steel circular tubes during quasi-static internal inversion. The nosing of circular tubes was investigated experimentally and numerically by using ABAQUS. Close agreement between the results coming from the experiments and those coming from the numerical code was obtained. Figure 2-18 shows the deformed shapes produced by ABAQUS and that of the experiment. Figure 2-19 shows the force-deflection response of the tube.

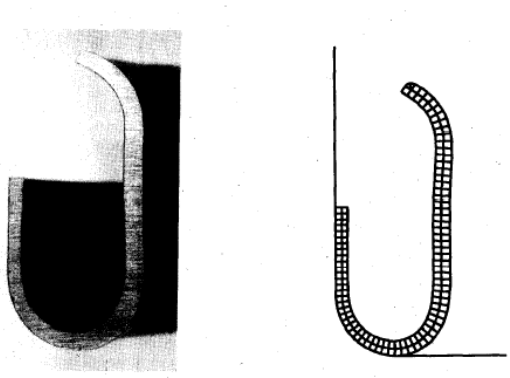

Figure 2-18: Comparison between ABAQUS and experimental deformed shape [44].

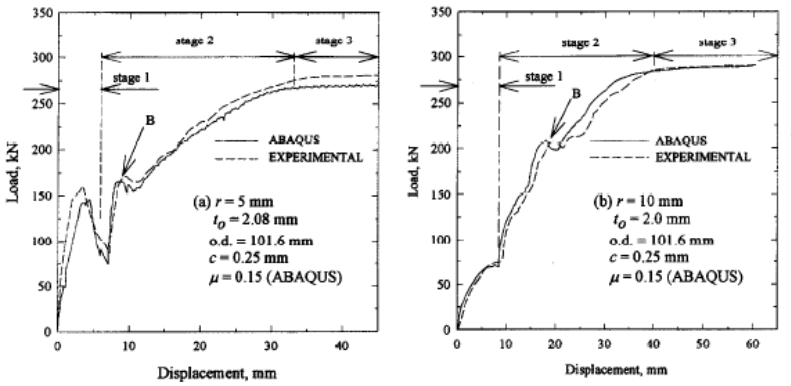

Figure 2-19: Experimental results and ABAQUS solutions for quasi-static internal inversion of mild-steel tubes [44].

Harrigan et al. [10] expanded on this previous work by investigating the inertial effects caused by dynamic loading in the internal inversion of tapered circular metal tubes and aluminium honeycomb material. It was noticed that the early peak load was generated by the inertial effects of impact loading. Figure 2-20 shows the apparatus used to apply dynamic inversion.

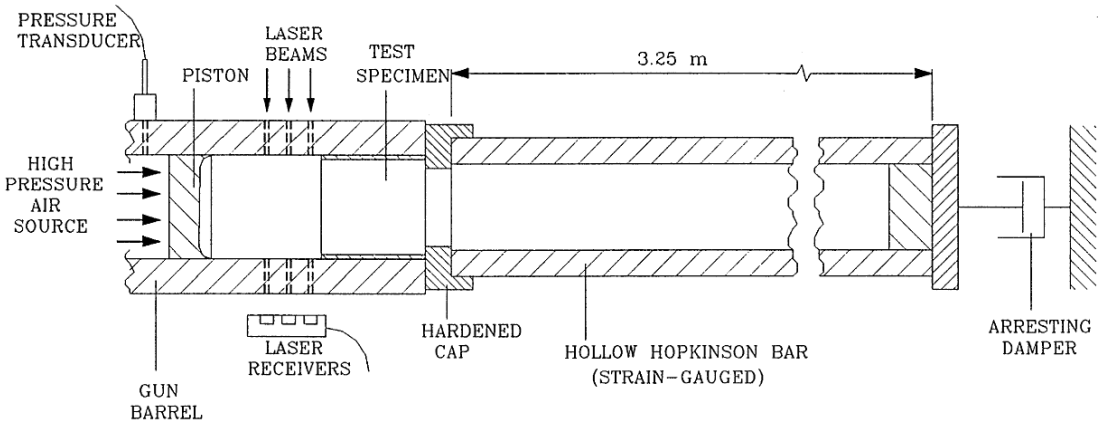

Figure 2-20: Set-up for dynamic tests [10].

Miscow and Al-Qureshi [45] carried out an investigation on external inversion by using copper and brass tubes experimentally and theoretically. The objective was to develop a method which predicted dynamic inversion loading based on quasi-static experimental data. A drop-hammer instrument (Figure 2-21) was used to carry out the dynamic test. It was reported that the theoretical results must not be taken as the absolute values, since other parameters inherent in the dynamic testing have an effect on the predicted values. However, close agreement between the theoretical and the experimental results was obtained.

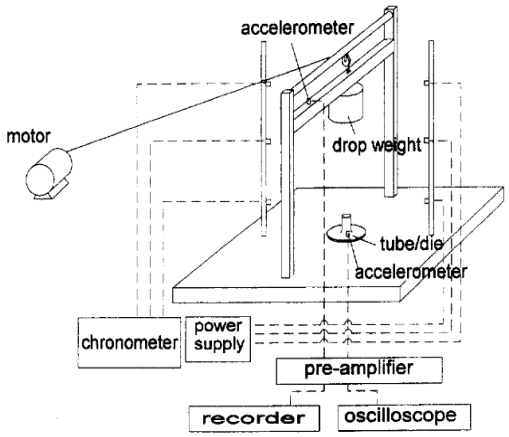

Figure 2-21: Schematic diagram of dynamic test arrangement for a tube inversion process [45].

2.4.1.3 Axial Splitting/Tearing

The deformation mode of axial splitting of a tube can be expressed as the intermediate between inversion and compression under axial load.

There are many parameters which have an effect on the splitting of tubes, such as die radius and frictional effects. The optimal force-deflection curve can be achieved by modifying these parameters. This conclusion was derived by Reddy and Reid [46]. In their study, a number of static and dynamic experiments were carried out to inspect the deformation mode and the corresponding force-deflection curve for splitting of circular metallic tubes. It was noted that the mean crushing force was lower, but 95% crush efficiency can be achieved.

Lu et al. [47] also performed a study on splitting square tubes. This investigation was to determine the energy associated with tube tearing. The authors determined the Rc (the tearing energy per unit torn area) experimentally for both steel and aluminium square tubes. It was reported that the ultimate tensile stress of the material and strain to fracture have a great influence on the tearing energy per unit torn area.

Jiang et al. [48] conducted a study to see the size effects in the axial tearing of circular tubes under static and dynamic conditions. The Buckingham Pi theorem was used, and recognized 11 input and 8 output parameters. During this investigation a new scaling law was developed to include the effects of strain hardening under dynamic or impact loading. It was found that the material strain hardening effects did not follow geometric scaling laws. A correction factor was used, which reconciled the difference between the dynamic yield stress of the prototype and the model. It was reported by the authors that this new scaling mass is important for the design and safety assessment of larger scale energy absorbing devices.

Stronge et al. [49] subjected a square tube to an axial force using a die causing the corners to split and curl outwards as deformation proceeds. For this mode of deformation, the energy absorbing mechanisms are fracture energies due to splitting, plastic deformation as large deformations ensue, and frictional energy as the tube is passed over the mandrel. The advantage of using a square tube over any other cross section, such as circular tubes, stems from the observation that the specific energy dissipation processes can be separated analytically. This helps to accurately analyse

the contribution and influence of each mechanism when a square is subjected to an axial splitting process.

Huang et al. [50] examined the energy absorption behaviour of axially splitting square metal tubes. They conducted this study theoretically and experimentally and they got good agreement between the results from the experiments and the theoretical results. It was observed that the energy was dissipated by means of three mechanisms: bending, tearing, and friction. It was concluded that the splitting and curling behaviour of a square metal tube can be considered as an efficient energy absorbing system. Figure 2-22 depicts a typical theoretical model of subjecting a square tube to a pyramidal die. Figure 2-23 shows the various samples after testing.

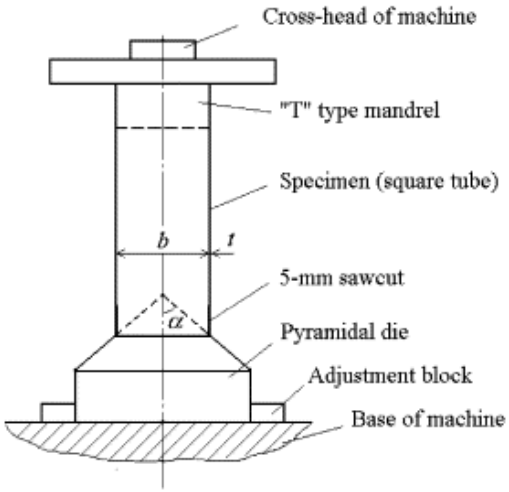

Figure 2-22: Sketch of the experimental set-up [50].

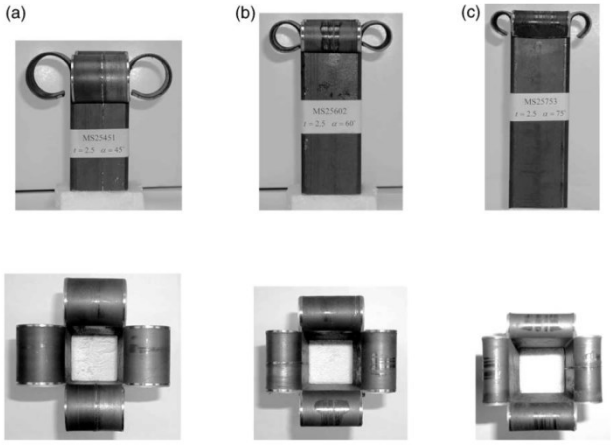

Figure 2-23: Photographs of typical specimens after tests [50].

Huang et al. [51] expanded on previous work by providing more details on axial splitting and curling of circular metal tubes by using experimental and theoretical techniques. Various dies with different semi-angles were used to compress the mild steel and aluminium tubes axially. Figure 2-24 shows photographs of typical mild steel specimens after testing. It was found in previous work that energy during the splitting process was dissipated by three mechanisms: bending, tearing, and friction. The role played by each mechanism was explained, which may be useful to the designer.

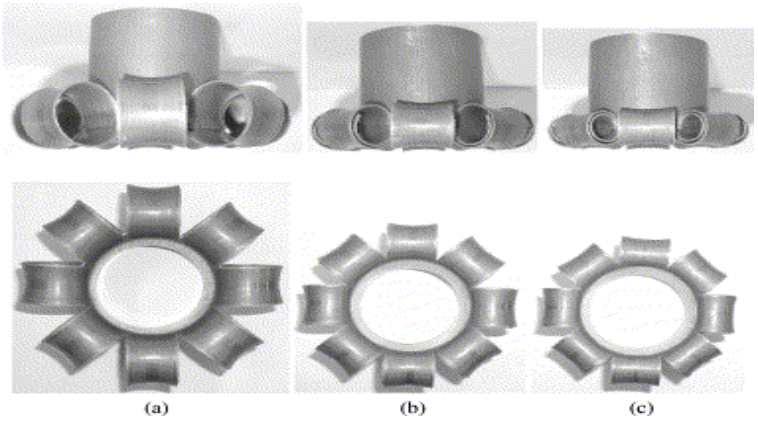

Figure 2-24: Typical mild steel specimens in their final deformed stages [51].

2.4.1.4 Lateral Indentation

A diametric circular tube compression was investigated theoretically and experimentally by Sowerby et al. [52]. Compression by point loads was studied. The theory of slip-line field was used to estimate the collapse load. This theory can be used to establish theoretical solutions for cases which have velocity irregularities and large deformations. The assumptions of rigid-perfectly plastic material model, plain strain deformation, and quasi-static loading should be included in this theory. It was found that the theoretical value of collapse load was in good agreement with the value measured experimentally.

Jing and Barton [53] examined the quasi-static and dynamic responses for ‘square’ cross-sectioned tubes loaded laterally. Two types of constraints were used during the tests, ie: one fully clamped and the second simply supported. Tubes used in the experiments had various thicknesses. The main aim of this study was to investigate

the collapse mechanism of the tube to derive the correlation between energy absorption and tube deflection. Finite element software, DYNA3D, was employed to simulate the dynamic cases. The specimens were subjected to velocities up to 6 m/sec during the dynamic tests. It was noticed that in both quasi-static and dynamic cases that local buckling caused a 'wrinkle' and made the deformation style of tubes more complex (Figure 2-25). The numerical code gave under-predicted values for the deformation of fully clamped tube because in real conditions, the clamped constraint does not exist. However, the results coming from numerical analyses were very similar to the test values. The authors stated that the quasi-static tests would be sufficient to determine the efficiency of the absorption systems, since the tubes under quasi-static and dynamic conditions exhibited a negligible difference in terms of deformation mode. However, to get an accurate response of the systems, the strain rate sensitivity of the material should be considered in the study.

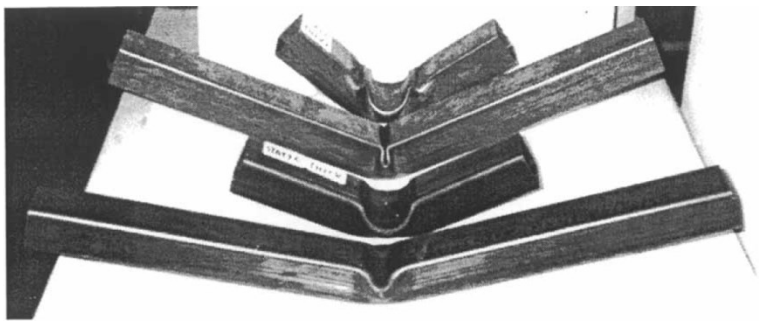

Figure 2-25: Final deformation of the N234S(top), N486S(second), K234S(third) and K486S(bottom) tubes subjected to static loading [53].

The collapse stages of tubes subjected to quasi-static load at mid-span were examined by Thomas et al. [54]. The tube's collapse started with a sharp increase in load. This increase remained until the deflection of tube was noted. This stage of deflection was defined as a pure crumpling phase. The second stage consisted of crumpling and bending where further crumpling occurred as well as bending between the support points. In the final stage of collapse, the high levels of rotation of the tube ends around the supports and caused tube destruction after the highest load was obtained.

Watson et al. [55] experimentally investigated the collapse of circular tubes by centrally opposed wedge shaped indenters. The main aim of this work was to make

energy absorbing capacity estimations easier in an impact event where the deformation speed is not enough to produce significant inertia forces. The authors described three modes of deformation during the experiments: 1) Ring mode for short lengths (L < 1.5D); 2) Transitional mode for medium lengths; 3) Reversing Ovality for moderate or long tubes.

1. Ring mode for short lengths (L < 1.5D): This mode comprises of hoop bending about the generators and is comparable to the mode of a compressed ring.
2. Transitional mode for medium lengths: The deformation commences as ring mode and then transforms to an *'increasing ovality'* mode as the deformation continues.
3. Reversing Ovality for moderate or long tubes: Membrane extending was noticed in the axial direction of the tube; this extending was greatest near the indenters, and it was accompanied by axial bending of the generators.

The third paper by Watson, Reid, and Johnson [56] studied the surface stresses created in simply supported tubes subjected to transverse loading. This investigation was carried out using the brittle lacquer method using strain gauges. It was found that simple plastic beam theory cannot be used to estimate the bending failure. The authors reported that the section of tube overhanging the supports has a great influence on the force-deflection response.

A study on the compression of a metallic thin walled ring under quasi-static conditions was conducted by Zhao et al. [57]. Arc shaped supports were used in this study. The authors performed a theoretical analysis by using 'Equivalent Structure Technique' (EST), which gives a higher bound solution and is utilized to calculate the load of collapse for tubes under point loading. It was found that tubes deform elastically followed by a soften stage. The results coming from EST analysis were in good agreement with experimental results, where the value of the collapse load and the positions of the plastic hinges were accurately estimated.

A study of metallic thin walled rings subjected to impact load was carried out by Zhao and Fang [58]. Two kinds of arc shaped supports were employed in this investigation: 1) 60° inflected support; 2) 90° inflected support. By inspection of the photos with a high-speed camera system, the authors discovered that the rebound of

the hammer had no effect on the last shape of the rings. The drop height and residual displacement had a linear relationship between each other. Also the authors found that the mechanism of deformation was similar in quasi-static and dynamic cases where the reduction of impact velocity made the strain rate effects smaller and could be neglected. It was noticed that the arc angle had a significant influence on the final deformation of the ring, and the deformation model was a five-hinge model. Figure 2-26 displays final shapes of the rings after impact.

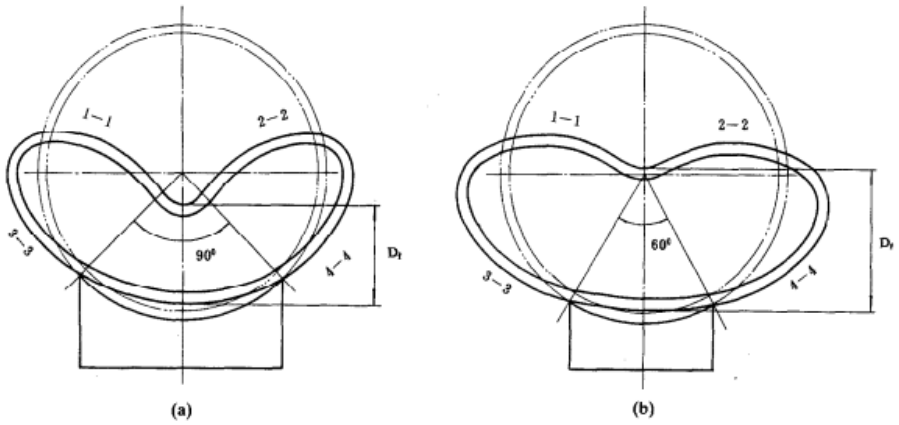

Figure 2-26: Final stages of deformation of rings support with (a) 90” arc, (b) 60” arc [58].

To investigate the role of strain hardening, Reid and Bell [59] carried out a study by using rings loaded by opposing point loads. They employed the ‘Plastica’ theory to investigate the plastic regions. It was found that the influence of strain hardening is important in the post-collapse response of tubes. By using the ‘Plastica’ theory the authors discovered that the earlier rigid perfectly theory had some limitations.

The destroying of mild steel tubes by two indenters was examined by Lu [60]. Tubes with four different diameters were used in this study. The purpose of this work was to derive empirical relations by conduction experiments using combinations of diameter D and length L of the tubes. The empirical relations derived were only applicable in cases which have the same loading conditions and the same range of tube parameters stated in this work.

Liu et al. [61] examined the dynamic behaviour of ring systems subjected to pulse loading. The Hopkinson pressure bar test system (SHPB) (Figure 2-27) was

employed to conduct the experiments. In addition to experimental procedures, a numerical technique using LS-DYNA was used to perform this study. Figure 2-28 depicts the finite element model of the system. It was concluded that the thickness of the rings had an important role in energy redistribution, whereas the influence of loading duration and the number of rings could be ignored.

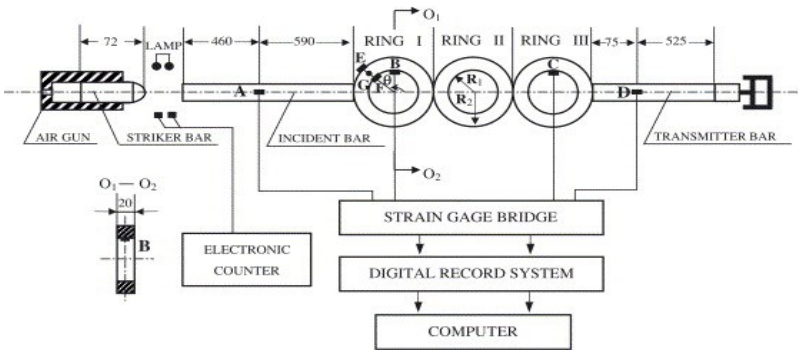

Figure 2-27: Modified split Hopkinson pressure bar test apparatus and recording system [61].

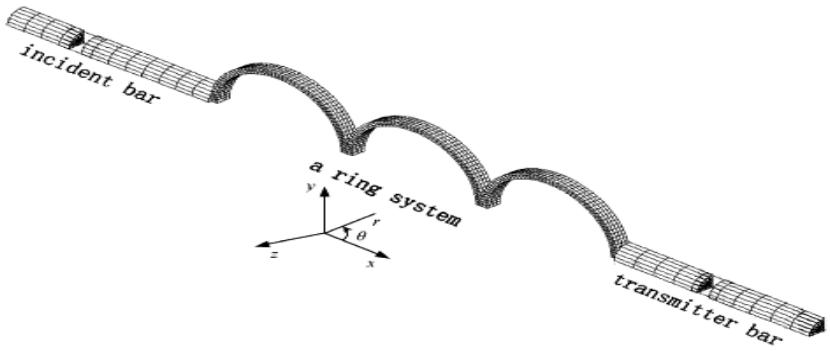

Figure 2-28: Sketch of the Finite element model [61].

Shim and Stronge [62] compressed ductile, thin walled tubes to investigate the post-collapse response of these tubes. Cylindrical indenters were used in this study. It was found that the radius of curvature and the degree of side constraints determined the behaviour of post-collapse response, which can be either stable (monotonically increasing) or unstable (monotonically decreasing). The stability of post-collapse can be increased by making the curvature of indenter smaller. It was reported that these systems are sensitive to load failure.

Kardaras and Lu [63] conducted an investigation on large deformations of thin cylindrical tubes subjected to point loads about its mid-span. They used a finite

element method to perform this study. The purpose of this work was to establish a detailed study on the effect of various parameters such as large deflections, change in curvature, stationary and travelling plastic hinges, rigid body rotations of the generators, and commanding strains on the response of energy absorber system. It was found, that using the finite element method made the process of getting detailed results on the parameters mentioned before easier than employing experimental or analytical methods.

Wierzbicki and Suh [64] used combined loading in the shape of bending moments, lateral indentation, and axially forces to investigate the indentation of tubes. It was concluded that the type of boundary conditions, such as rotationally and axially constrained or unconstrained tubes, play a key role in the resistance of the tube to local indentation. The difference between the theoretical results and experimental results was approximately 10% to 20%.

Ghosh et al. [65] subjected mild steel rings and short tubes to lateral loads by using opposed conically-headed cylindrical punchers to examine experimentally and theoretically the deflection response of these tubes. Tubes with different lengths and thicknesses were tested in their ‘as-received’ and ‘annealed’ conditions during this investigation. The objective of this paper was to obtain the collapse load as a function of ultimate tensile strength, yield stress, and strain to failure. It was noticed that short rings of L/D ratio of up to 1.5 displayed a ‘knee-shaped’ response in the plastic phases of deformation. The initial structural collapse load happened somewhere along this ‘knee-shaped’ area. Interrupted annealed testing was used to remove the strain-hardening of the short tubes. This removal provided the ability to calculate the collapse load as mildly deformed tubes. Finally it was concluded that the tubes with decreasing L/D ratios give more accurate predictions for the increase in the horizontal diameter. This accuracy was obtained by employing the assumption of rigid-perfectly plastic and the concept of plastic hinges.

2.4.1.5 Lateral Compression Flattening.

The compression of mild steel tubes under quasi-static conditions was investigated by DeRuntz and Hodge [66] . The material model used to predict the load deformation response was rigid-perfectly plastic model. This material model doesn’t consider the phenomenon of strain hardening and this resulted in the rate of strain

hardening to be under estimated. It was found that the tube's deformed contour comprised of four circular arcs which keep their original radius and plastic deformation occurring at the hinges only.

An attempt to include the effects of material strain hardening was performed by Redwood [67]. A rigid-linear hardening material model was used instead of the rigid-perfectly plastic model to predict the energy absorption and force response.

Reid and Reddy [68] performed further investigations on the strain hardening effects. They developed an accurate material model depending on a rigid-linear hardening material model. The localised hinges were replaced by arcs of variable lengths in the new material model. This replacement provided the ability to consider the geometric and material strain hardening effects. The authors developed a new dimensionless parameter *'mR'* which is a function of the mean radius R of the tube, the thickness t, yield stress in tension, and the strain hardening modulus E_p. The shape of the force-deflection curve can be managed by this parameter. The authors reported that energy absorbing capacity can be maximised by choosing appropriate tube dimensions and made the value of *'mR'* smaller.

Reddy and Reid [69] laterally compressed aluminium and mild steel tubes in an Instron machine. His objective was to study the phenomena associated with the crushing of metal tubes between rigid plates. It was found that the perfectly-plastic theory is suitable for the responses of fully annealed tubes where the process of annealing eliminates the strain-hardening effects. The strain hardening effects caused differences in the results between experiments and theoretical analysis in the case of 'as-received' tubes.

Gupta et al. [70] numerically and experimentally examined the lateral crushing of circular metallic tubes under quasi-static conditions. Aluminium and mild steel tubes with different ratios of diameter to thickness were used in this investigation. The authors found that the energy absorbing capacity and mean collapse load increased with an increase in thickness and a decrease in diameter. Moreover, this study created a detailed report on the responses of these systems and their deformation mechanism. The deformed profiles of aluminium tubes at different stages of lateral compression are displayed in Figure 2-29.

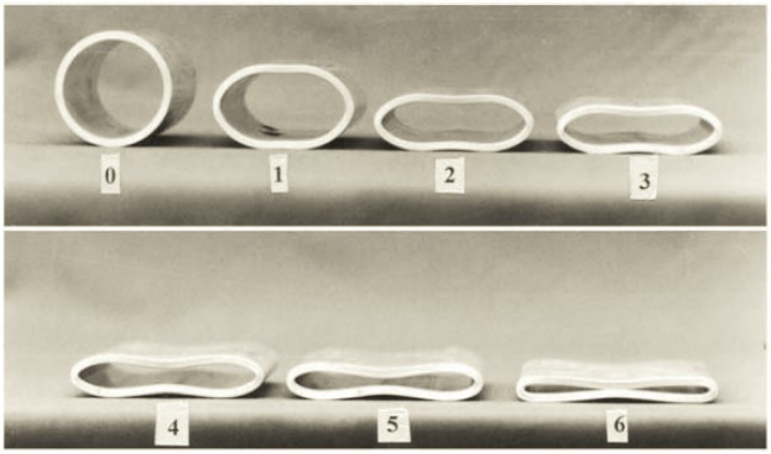

Figure 2-29: Deformed profiles of aluminium tubes at different stages of lateral compression [70].

Avallel and Goglio [71] compressed aluminium tubes laterally and studied the strain range created during this compression. They also tested the theoretical models suggested by the other authors such as [66]- [68], and concluded that the Reid and Reddy model [68] was more accurate due to this theory accounting for the main parameters that predict the deformation response. These parameters include material yield stress, strain hardening modulus, and geometrical parameters involving tube diameters and thicknesses.

In order to maximize the energy absorption, Reddy and Reid [72] built a tubular system with side constraints in which the horizontal diameter of the tube was prevented from becoming greater. The authors investigated the crushing of constrained systems experimentally and theoretically under quasi-static conditions. In addition to a former study, the authors investigated the relationship between a single tube and a system of tubes. It was found that side constraints increased the specific energy absorption capacity of the tube due to increasing the number of plastic hinges during the plastic deformation. It was reported that constrained systems offer an energy absorption capacity that is three times higher than the normal system. However, the constrained system has a maximum deflection that is less than systems without constraints. In general, it was concluded that building a constrained system will increase the efficiency of an energy absorbing system.

Reid and Reddy [73] carried out an experimental examination on the differences of responses of copper tubes with R/t ratios from 1.5 to 7.5 compressed between flat

plates. The authors discovered that their 'Plastica' theory did not predict the behaviour of the ring with an R/t ratio of less than 3.5. This shortfall in behaviour prediction was because 'Plastica' did not account for the shear effect, which in this case was a commanding mode of deformation. The rings with an R/t ratio of greater than 3.5 were in close agreement with the experiments.

A new way of obtaining more realistic force-deflection curves was suggested by Reddy and Reid [74]. The rigid-linear hardening material model was used. The authors subjected lateral loads on the tubes using rigid plates. It was proposed that the 'mR' parameter can be obtained by using an average value for the strain hardening modulus, and hence these two parameters would be constant over all of the deflection range. Also, it has been further suggested that if the strain hardening modulus has a known variation with strain, this variation can be employed to update 'mR' at each load step. Therefore, a more realistic load-deflection characteristic can be achieved. It was reported that material properties can be obtained from a ring compression test by using the method mentioned above.

Reid and Reddy [75] studied the effect of strain rate on tubes which were dynamically compressed by rigid plates. The authors developed a new modification on their old theory (quasi-static large deflection theory) to insert the effects of strain rate. It was found that the modified theory can be used to predict the dynamic responses of aluminium and mild steel tubes.

The collapse mechanism and energy absorbing capacity of braced metal tubes were analysed experimentally by Reid et al. [76]. Rigid plates were used to compress the braced tubes. The objective of this investigation was to build systems to deal with both 'trapping' and 'redirectional' occurrences in vehicles involved in side impacts. The word 'redirectional' means reverse displacement of the vehicle after the impact has happened. 'Trapping' means stopping the vehicles and preventing reverse displacement. The authors started the study with small scale components to examine the probability of obtaining the desired response by using tension members across the diameters of the mild steel tubes. Two types of systems were analysed; one with single braced tubes and the other with double braced tubes of different angles. It was reported that an important increase in the energy absorbing capacity can be obtained by systems with braced tubes but these systems are sensitive to the direction of loading. Full scale testing was also conducted on the double braced tubes.

An investigation on the lateral compression of aluminium tubes by using the finite element method was carried out by Leu [77]. The static explicit approach was employed in this study to prevent convergence related problems occurring. An elastic-plastic model was used to anticipate the responses of the aluminium tubes. A stress-strain curve of the aluminium tubes was constructed by using the power law relationship. The effects of parameters such as friction coefficient values, strain hardening exponent, thickness of tube, and elastic modulus were examined on the occurrence of punch and buckling load during the deformation process. It was concluded that this type of study would be useful in understanding the buckling mechanism of aluminium and clad tubes.

The collapse behaviour of thin walled empty and filled square tubes was analysed by Gupta and Ray [78]. The authors laterally compressed different sizes of tubes between rigid plates. The tubes were studied both in 'as-received' and annealed conditions. Kail wood and polyurethane foam were used as filler material in these systems. A theoretical analysis was used to predict the load-deflection and peak load responses. The theoretical results correlated well with the actual values. It was reported by authors that the use of filler material increases the specific energy absorbing capacity in the system. This was due to the increase in the stroke length and the post collapse load-deflection response.

Sherbourne and Lu [79] used the 'Moving Hinge Method' to conduct theoretical analyses on the compression of tubes by means of rigid plates. In spite of this theory using a rigid perfectly plastic material, the author endeavoured to insert the effects of strain hardening into the model. Close agreement between the theoretical results and the experimental data was achieved. It has been reported by authors that the moving hinge method has advantages in comparison to the other theories used to predict collapse load, such as 'Plastica Theory' by Reid and 'Limit Analysis' by DeRuntz [66]. The 'Moving Hinge Method' theory provides the ability of increased manoeuvrability without compromising the accuracy of the solution. Also, the 'Moving Hinge Method' can be used in other deformation modes, such as axial compression of tubes.

The initial collapse of braced elliptical tubes was investigated theoretically by Wu and Carney [80]. The elliptical tubes were compressed laterally. The crush efficiency in the elliptical tube is greater than in the circular tube. Increased crush efficiency

corresponds to an increased energy absorbing capacity for the elliptical tube. The specific energy absorbing capacity of circular or elliptical tube can be increased further by using either horizontal or angled metallic wires where these wires produce a greater collapse load and hence the specific energy absorbing capacity becomes bigger. The authors employed the finite element code, ABAQUS, to capture the initial collapse load and the deformation mechanisms. Three modes of collapse mechanism were noticed for elliptical braced tubes, as also reported by Reid [76]. These modes are as follows: tubes with small bracing angles, tubes with horizontal bracing, and tubes with big bracing angles. It was found that the ratio of the ellipse axes b/a, and the bracing angle have a great influence on the initial collapse load of braced elliptical tubes. Figure 2-30 shows the symmetric and asymmetric deformations for a 0^0 braced tube. Figure 2-31 shows the finite element model at two stages of displacement.

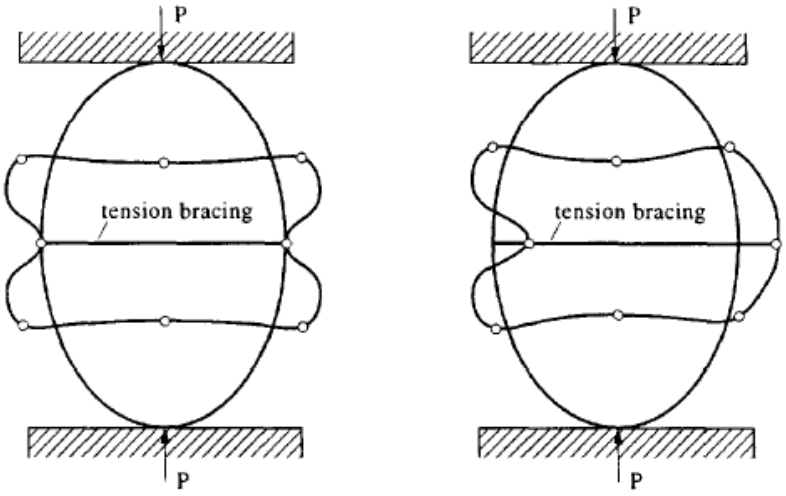

Figure 2-30: Symmetric and asymmetric deformations for 0^0 bracing [80].

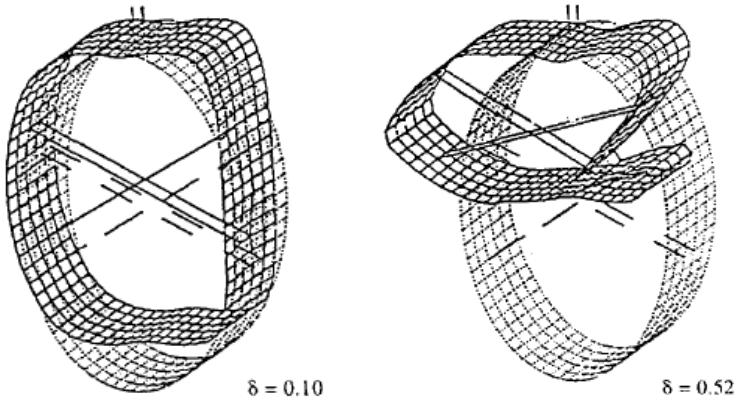

Figure 2-31: Finite element mesh and two deformation stages for a 200 braced elliptical tube [80].

Wu and Carney [81] expanded on their previous work where experimental compression on braced elliptical tubes was investigated. Rigid plates were used to compress the tubes. The objective of this work was to confirm the numerical and theoretical results presented in their previous paper. It was noticed that for a circular tube with a small braced angle, close agreement of the initial collapse load value was achieved in experimental and theoretical and finite elements results, whereas the theoretical predictions were higher than the experimental values in the large brace angles. The authors stated that this difference was because of the tubes becoming more sensitive to geometrical flaws. It was also reported that the results using ABAQUS were much lower than the theoretical results using EST (Equivalent Structure Technique) method. The difference in these results was mainly due to membrane stresses not being taken into account in the second case.

2.4.2 Nested tube energy absorbers

Shrive et al. [82] investigated a nested system comprised of two concentric rings with a layer of smaller tubes between them. The axes of these tubes were parallel. The rings were connected to concentric tubes by Tack welding. It was found that the level of welding had a great influence on the system responses, with the responses increasing as the level of welding increased. It was noticed from the dynamic impact test that full deformation did not happen, but that maximum forces were comparable to those of the quasi-static test.

Johnson et al. [83] built a nested system consisting of several layers. Within each layer, all circular tubes were parallel and tubes of the next layers were rotated 90 degree with respect to the first layer. The authors studied the quasi-static behaviour of these mild steel tubes used to build this system under lateral loading. It was concluded that nested tubes systems played a key role in creating a stable load-deflection response where the oscillations in the response caused by the failure of one member of the system did not produce catastrophic failure in the system as a whole.

Reid et al. [84] conducted a dynamic test on the nested system to investigate the effect of system inertia. The nested system was in the form of a line of rings. The authors tested many different rings systems with different parameters such as diameter to thickness ratios, materials, and number of rings. It was found that the time of deformation was affected by the inertia properties of the system. Also the authors reported that the time of deformation can be increased by inserting small plates between the rings.

Reid and Reddy [85] examined nested systems subjected to end impact loading. The systems were in the form of a line of rings. The main objective of this study was to identify the important parameters that dominate the deformation of such systems, and then suggest the form of a mathematical model of the system. It was found that in cases of low speed impact, the effects of inertia was incidental, and so the design of the energy absorbing systems could be obtained with only the material strain rate being considered.

Reddy et al. [86] carried out experiments on a one dimensional system with free distal ends. The systems were subjected to lateral impact by a rigid projectile. The elastic-plastic structural shock wave theory was employed to examine the deformation of typical ring chain systems. This theory uses the bilinear material model to predict the collapse behaviour of tubes.

New systems of elliptical/oblong shaped energy absorbers were proposed by Morris et al. [87]. The energy absorbing systems involved nested tubes of different diameters subjected to lateral deformation. A prescribed compression velocity of 5 mm/min was used to ensure that no dynamic effects occurred. Experimental and numerical studies were conducted on these systems to examine their responses. It

was found that these systems were well suited to applications where space or volume restrictions are an important design consideration.

In another study carried out by Morris et al. [88], the compression of nested systems by using two types of indenters was presented. Different variations of external constraints were incorporated. It was found that the external constraints subjected more material volume to plastic deformation and therefore absorbed more energy. The finite element code via ANSYS was employed to predict the responses of these tubes. Close agreements between the computational and experimental results were obtained. Figure 2-32 shows the experimental and predicted final stage of the deformed profile of nested tubes.

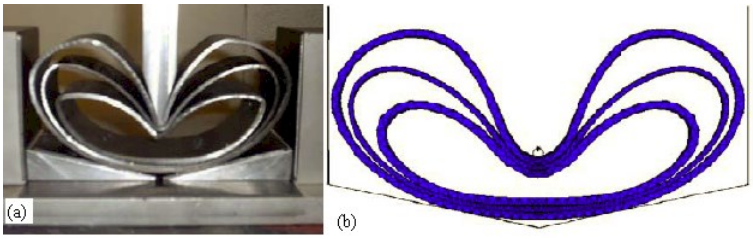

Figure 2-32: Final stage of deformed profile of nested tubes [88].

Olabi et al. [13] and [14] tested two groups of nested systems. One system was standard and the other was an optimized system. The responses of these two kinds were obtained and analyzed. The tests were conducted by using a fixed mass travelling at velocities ranging between 3 to 5 m/sec. In addition to the experimental work, a computational method using LS_DYNA was used to predict the loading and response of such systems. It was found that the optimized energy absorber displayed a more desirable force-deflection response than the standard system because of a simple design adaption with mild steel cylindrical dampers. Figure 2-33 shows a schematic representation of both the standard and the optimized nested oblong tubes. The main objective of these investigations was to show the effectiveness of a new form of nested tube systems as energy absorbing components, and also to optimize their responses by using a simple mechanism.

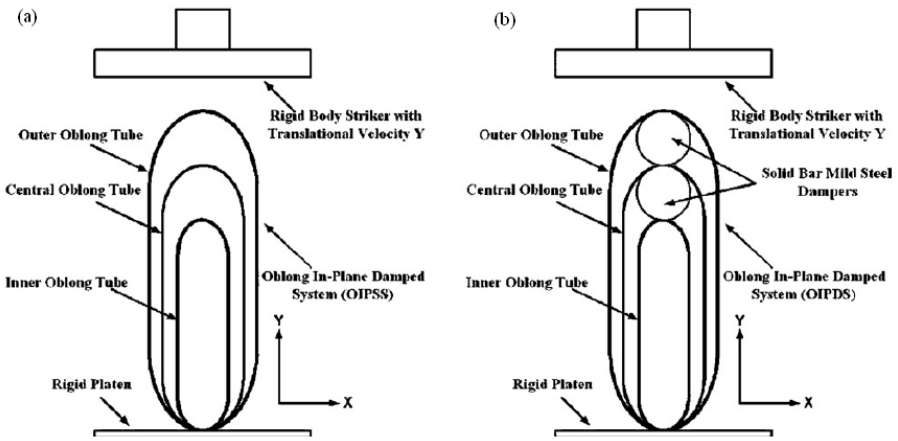

Figure 2-33: Schematic of (a) standard design. (b) Optimised design [13].

2.4.3 Foam-filled energy absorber

Of interest for thin-walled components used in crashworthiness application is to enhance their energy absorption performance by using filler material. A light material such as a honeycomb, cork, wood, foam, and rubber can be used as a filler material in thin-walled components. Using filler materials along with thin-walled component enhances the absorption of energy of the whole structure. The structural and weight efficiencies of these structures make them practical for engineering applications.

For example, Taher et al. [89] used polyurethane foams to reinforce and improve the crashworthiness performance of the keel beam system of a helicopter sub- floor.

Cheon and Meguid [90] numerically investigated the crush behaviour of aluminium foam to facilitate the design of car bumpers. Using foams as filler material in thin-walled tubes provides several potential benefits for energy absorption. Much research has been performed to investigate crush and energy absorption responses of foam-filled thin-walled tubes under axial loading. Examples include foam-filled circular tubes (Borvik et al. [91]; Kavi et al. [92]; Toksoy and Guden [93]; Yan et al. [94], foam-filled square tubes (Hanssen et al. [95]; Santosa et al. [96]; Seitzberger et al. [97]; Zarei and Kroger [98], foam-filled conical tubes (Gupta and Velmurugan [99], Ahmad [100]- [102], foam-filled tapered rectangular tubes (Mirfendereski et al. [103]; Reid et al. [8] and foam-filled hat sections (Chen [104]; Song et al. [105]). Figure 2-34 shows examples of foam filled tubes.

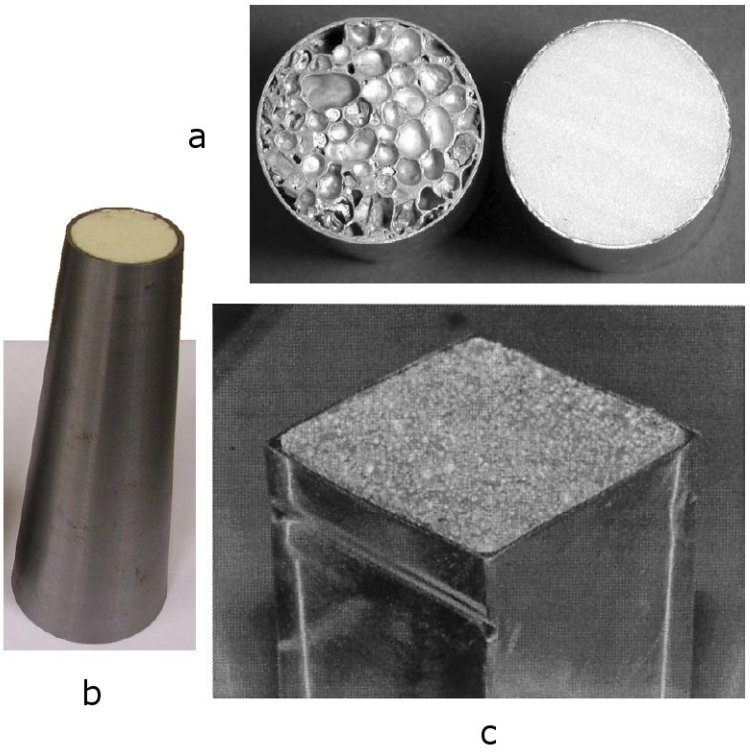

Figure 2-34: Typical foam-filled tubular sections a) Foam-filled circular tubes (Al/polystyrene) [92]; -b) Foam-filled frusta [[102]; -c) Foam-filled rectangle tube [95].

It was reported by the researchers that the use of foam as a filler material enhanced and stabilised the crush response of thin-walled tubes when subjected to impact loads.

Thornton [106] used polyurethane foam as a filler material. Many compression tests were performed in order to investigate the effect of polyurethane foam-filling on the collapse of metallic thin-walled structures. It was concluded that polyurethane foam-filling is not weight effective, unless relatively thin sections made of high density low strength alloy are used. The same author Thornton et al. [24], in a companion paper, reported that using a foam density of below 220kg/m^3 increases collapse load of the tube with more weight effectiveness.

Similar conclusions were reported by Lampinen and Jeryan [107]. They found that weight effectiveness tends to be reduced when the wall thickness of a section filled with polyurethane foam is reduced below a certain limit. So it was reported that using thicker columns is still more weight efficient than filling the tubes with polymer foams.

In contrast to above findings, Santosa et al. [96], Banhart [108] and Reyes et al. [109] reported that using aluminium foam as a filler material is more weight efficient and better than thickening the column wall in terms of the energy absorption capacity.

Furthermore, Hanssen et al. [110] found that using aluminium foam-filled tubes as impact energy absorbers reduced the length and volume of the tube by 32% and 68%, respectively. This is a very important feature in the design of energy absorbing systems. Foam-filling is preferable compared to thickening the tube wall, since increasing the thickness certainly increases the mass and decreases the weight efficiency of the energy absorber.

In general, using metallic foam such as aluminium foam is preferable. The researchers have reported that there are two significant changes that can be observed in the collapsing behaviour of foam filled tubes. Firstly, it increases the number of lobes, and secondly it shortens the fold length. Hanssen et al. [6] noticed that the number of lobes increased with increasing foam density as shown in Figure 2-35. The author reported that the presence of foam produced more resistance to inward bending and thus the plastic fold length reduced and number of lobs increased.

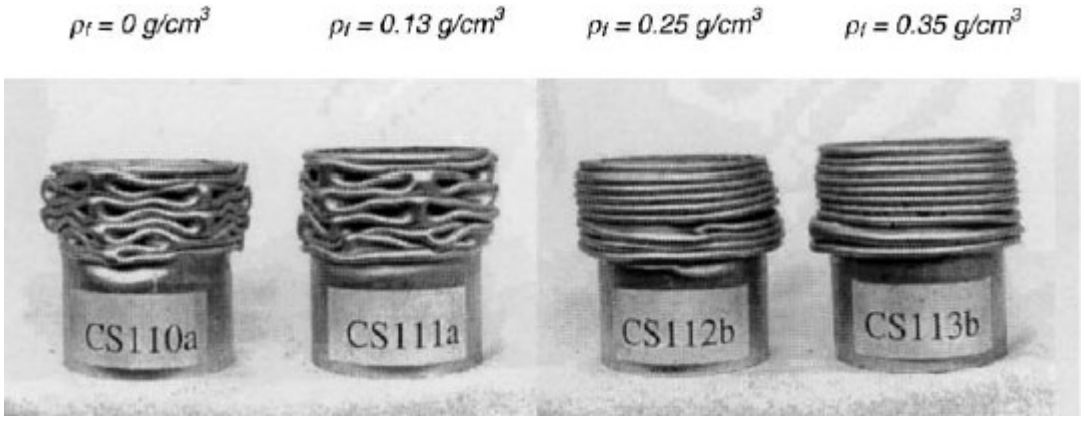

Figure 2-35: Deformation modes of foam-filled circular tubes [6].

In addition to this effect of using foam as filler material, it was also found that due to the interaction effect of both materials (the thin walled component and the foam filling), the diamond deformation mode of circular tubes changed to a concertina mode, regardless of the foam type and density used [6], [95], and [111] as shown in Figure 2-36. This change in deformation mode is due to the presence of foam filler,

which results in the initial buckling of the sidewalls occurring on an elastic foundation. This behaviour causes higher strain energy to be dissipated by the tube wall, particularly when using higher foam strengths (Lu and Yu [15]).

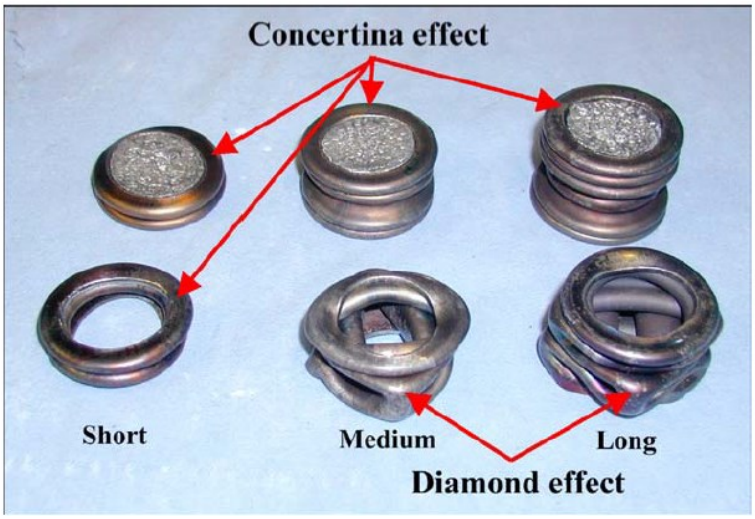

Figure 2-36: Concertina and diamond deformation modes foam-filled tubes and empty tubes, of three different lengths [111]

Another point worth noting that was reported by Asavavisithchai et al. [111] and Jones [11] is that the collapse mode of foam filling absorbers is compact mode.

Zarei and Kroger [98] have noticed that foam-filled tubes offer better crash stability than empty tubes.

The undesirable deformation mode known as global bending can occur in foam filled circular (Seitzberger et al. [112]) and square tubes (Reid et al. [113]). Reid et al. [113] found that using foam density of higher than 320kg/m^3 may cause global bending in foam-filled square tubes. Seitzberger et al. [112] noticed that using a foam density of 0.7 g/cm^3 in foam filled circular tubes can cause global bending, as shown in Figure 2-37. In order to avoid this undesirable feature, the author suggested that using foam density of lower than 0.6-0.7 g/cm^3 may prevent progressive buckling characteristics in foam-filled circular tubes.

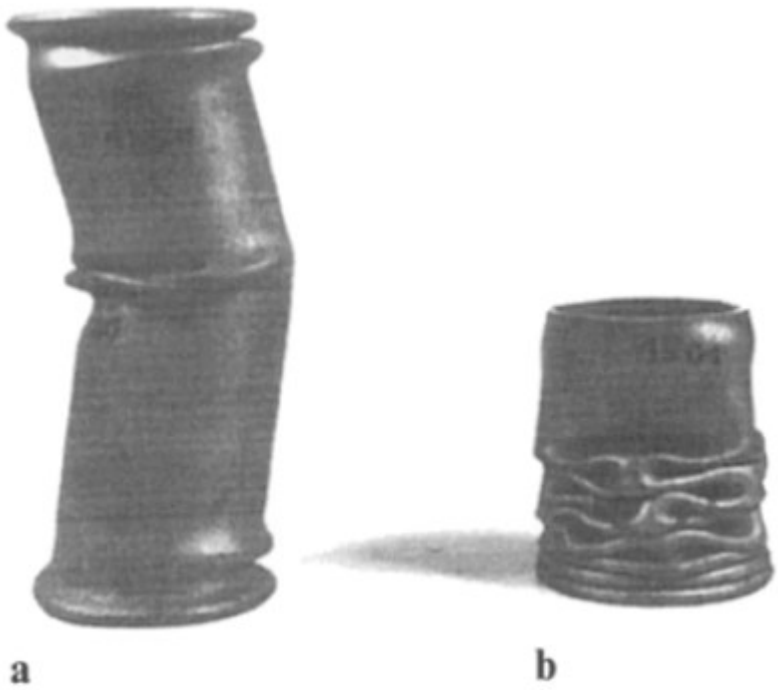

Figure 2-37: Axially crushed circular tubes: (a) filled, (b) empty [112].

Mirfendereski et al. [103] reported that a foam density of greater than 230 kg/m^3 is not practical as the crush force increases monotonically upon optimum performance (>100%) and the system then absorbs energy in an inefficient way. The level of the plateau stress and the locking strain plays an important role in this behaviour.

(Lu and Yu 2003 [15]; Zhang and Cheng [114]) both author have reported that tubes filled with higher foam densities were more subject to the global bending phenomena.

Asavavisithchai et al. [111] reported that the reason for the rapid increase in the crush force noticed at 50 – 60% strain, is a strain locking which is due to densification of the foams. The locking strain also provides a limit to the compression stroke achievable by the foam-filled tubes. This limit reduces the effective length of each fold, so mean force increases.

Borvik et al. [91] and Reyes et al. [115] have examined foam-filled circular and square tubes under oblique load. Both authors have reported that both initial peak load and mean load of foam-filled tubes decrease as the load angle increases.

The effects of foam density distribution and impactor inclination on the crashworthiness of metal foam-filled columns were investigated by Shahbeyk et al.

[116]. It was reported that medium- and high-density foam-filled columns experience global buckling under a slightly inclined impactor.

The tapered tubes can be considered as a solution for an unstable crush mode in the case of foam-filled tubes subjected to an oblique loading. Moreover, the tapered tubes offer an almost constant mean load-deflection response under impact loading, therefore foam-filled tapered tubes are preferable to foam-filled straight tubes. Experimental investigations on responses of tapered rectangular tubes filled with polyurethane foam under static and dynamic loading conditions have been carried out by Reid et al. [113] under static and dynamic loading conditions. It was noticed that the presence of foam prevents global bending and reduces the magnitude of the load amplitude. The author also found that mean load increased as the crush progressed under impact loading.

Mirfendereski et al. [103] examined the collapse and energy absorption response of empty and foam-filled tapered rectangular tubes under static and dynamic loading. By using validated finite element models the authors performed a series of parametric studies. It was found that the foam-filled tapered tubes had enhanced performance regarding energy absorption.

Gupta and Velmurugan [99] used conical tubes, made of composite materials filled with polyurethane foam as an energy absorber. These authors carried out quasi-static tests by using samples with a constant length and variation in both semi-apical angle and wall thickness. It was concluded that the crush response in the foam-filled tubes was more stable than empty tubes. It was also reported that the presence of foam material improved energy absorption efficiencies.

Ahmad and Thambiratnam [102] examined the crush response and energy absorption of empty and foam filled conical tubes under oblique impact loading. The authors found that foam-filled conical tubes were effective energy absorbing devices as they can absorb an oblique impact load as effectively as an axial impact load. It was also reported that undesirable global bending collapse can be avoided by: i) Increasing the semi-apical angle, and ii) Increasing the wall thickness, and/or iii) using a filled tube to minimise the reduction in absorbed energy as shown in Figure 2-38.

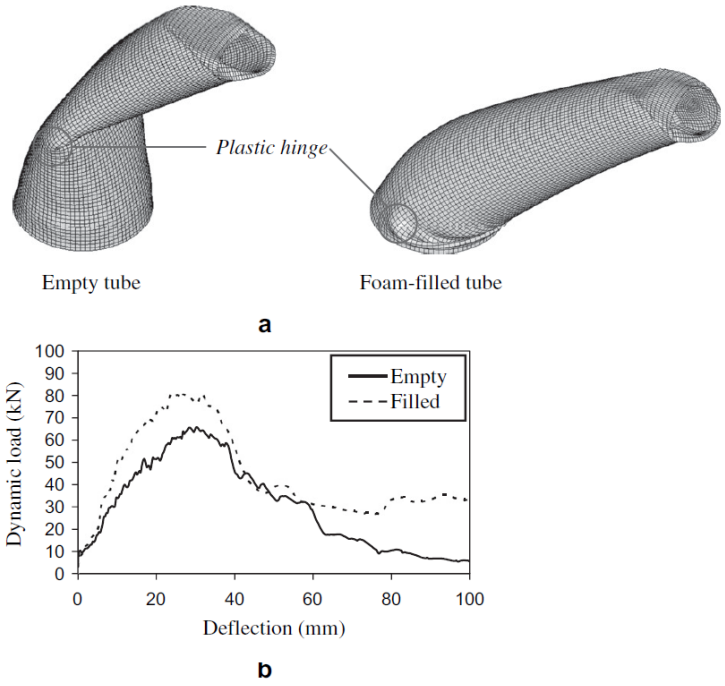

Figure 2-38: (a) Global bending and formation of plastic hinges during global collapse for each tube (b) Load vs deflection curve of the empty and filled conical tubes under oblique loading [102].

Overall, studies on the collapse behaviour and energy absorption response of foam-filled tubes (either rectangular or circular cross-section) under lateral loading have been less reported in the literature. Considering the importance of such structures, a few studies [117], [118], and [142] were performed to investigate the collapse behaviour and energy absorption response of foam-filled tubes under lateral loading. Fan et al. [117] carried out a set of experiments to investigate lateral collapsing behavior of sandwich tubes. Variation of sandwich tubes with different diameter to thickness ratios were employed in this study. Two types of bonding were used to assemble the foam core with solid tubes. In addition to experimental work, numerical investigations using ABAQUS/Explicit were carried out to validate the experimental results. Three types of collapse patterns were observed in a lateral collapse of sandwich tubes termed simultaneous collapse pattern, simultaneous collapse pattern with facture of the foam core, and sequential collapse pattern. The experimental and numerical results showed that using sandwich tubes as energy absorbers enhanced the crush strength and energy absorption.

In a companion paper, Fan et al. [118] experimentally and numerically examined the dynamic response of sandwich tubes under lateral loading. It was reported that the same collapse patterns in the quasi-static tests were observed in the dynamic crushing experiments on the sandwich tubes. Non-symmetric deformation pattern about the horizontal plane were observed in the case of high velocity impact. This behaviour is due to plastic deformation starting at the sections near the impact region. In addition, the critical velocity was identified for mode change and was related to t/D by means of dimensional analysis. A double-moving hinges mechanism was proposed for the propagation of plastic bending in the case of high velocity impact.

2.5 Analysis of energy absorbers

In the past, the study and analysis of energy absorbing devices was performed by several methods such as experimental, empirical, and analytical techniques. In recent times traditional techniques have been complemented with the finite element method (FEM), which is very powerful tool particularly for performing parametric studies. In addition to FEM, the factorial method is now employed by the researchers to conduct parametric studies. This section briefly describes the techniques and analysis methods of energy absorption systems.

2.5.1 Analytical modeling

With this method, the energy absorption responses of thin-walled tubes are predicted by the development of theoretical models. These models are established by simplifying the deformation mechanism and adopting some limited assumptions, and employing plastic analysis of the structure. The theoretical models are developed based on the experimental observations of the collapse mode during the test. Many researchers have tried to establish theoretical models for the responses of energy absorbers. Of relevance are investigations conducted on the lateral collapse of short length circular tubes [66] and [119], A simple rigid plastic analysis for the lateral compression of a circular tube by flat plates (Figure 2-39) was performed by [66] and [119], the flattening force (F) of the lateral collapse is given by:

$$F = \frac{2\sigma_y t^2 \times w}{D \times (1 - (\frac{\delta}{D})^2)^{1/2}} \qquad (2\text{-}8)$$

Where σ_y is the yield stress, h is thickness, w is the width, δ is the displacement and D is the outer diameter of the tube.

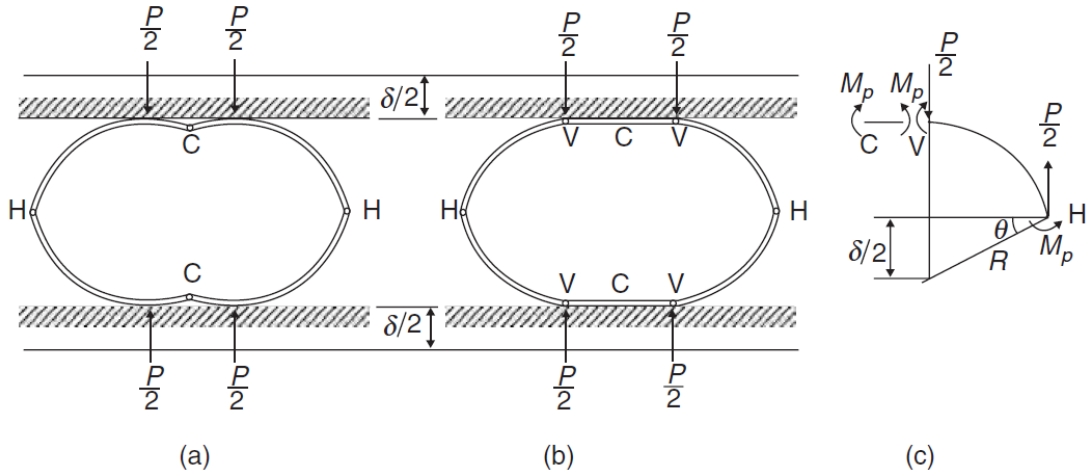

Figure 2-39: Collapse mechanisms proposed by: (a) DeRuntz and Hodge [66] (b) Burton and Craig [119], and (c) also showing the forces on a deforming segment [15].

2.5.2 Empirical modeling

The designers and researchers of impact attenuation devices commonly used the empirical technique to build up expressions for describing the responses of energy absorbers. The empirical expressions can be derived by employing linear or nonlinear multivariable regression analysis on experimental or FE results. These expressions can then be developed to relate the energy responses with the geometry parameters. Many researchers have used empirical modelling in their investigations. Of relevance are studies carried out on the quasi-static [70] and dynamic [118] lateral collapse of circular tubes. Gupta et al. [70] have empirically derived the relationship between the SEA and (D/t) and (δ/D) ratios of the lateral collapse of circular tube, which is given by:

$$\text{SEA} = \left(0.0106e^{4.0633(\delta/D)}\right) * \left({}^{D}/_{t}\right)^{-1.22} \qquad (2\text{-}8)$$

Fan et al. [118] also employed empirical modelling to study the effect of material properties and geometry of a circular tube on the critical velocity. The following equation was developed by the authors:

$$V_{cr} = \sqrt{0.3 \times \frac{t}{D} \times \frac{\sigma_Y}{\rho_s}} \qquad (2\text{-}9)$$

In general, empirical modelling is based on observations and experimentations rather than theory.

2.5.3 Factorial analysis

Factorial analysis is an alternative approach to investigate the responses of energy absorbing systems. Factorial analysis is considered as a very powerful tool for evaluating the main and interaction effects of the various parameters on the energy absorption responses. It is also used for conducting parametric studies, particularly if commercial software such as design experts (DOE) is employed.

The factorial analysis of energy absorbing structures can be performed by choosing a number of design variables (factors), which can pertain to material, geometry, or loading parameters. Then specific levels for each variable are chosen and the tests are run, either by experiments or simulations, using all the possible combinations and the corresponding design responses are calculated. The main and interaction effects can be specified accordingly. Main effects refer to changes in the system's response with change in one factor (variable). The interaction effect occurs when the response is affected by the settings of two factors. The response surface methodology (RSM) is considered as a common technique for performing factorial analysis of energy absorbing structures. In addition to factorial analysis, employing RSM in the field of energy absorbing systems provides the ability to find an optimal design and to perform multi-objective optimization design (MOD) of the energy absorbing structure. The optimization design can be achieved by using the RS

models in the optimization algorithm, such as the multi-objective particle swarm optimization (MOPSO) algorithm and desirability approach. Many studies have used RSM with the optimization algorithm to seek an optimal design for empty and foam-filled thin-walled tubes under pure axial [98], [120]-[126], lateral [127], [128], and oblique loads [129].

2.6 Advantages and disadvantages of various types of energy absorbing structures

Axial crushing of tubes has comparatively high energy absorbing capacity. This behaviour is due to the fact that under axial loading most of the tube's material deforms plastically and participates in the absorption of energy. The energy absorbing capacity of laterally flattened tubes was found to be greater than that of lateral indentation, but not as much as for axial crushing. The absorbed energy through the lateral collapse of the tubes can be effectively and easily increased by using internal bracing or external constraints. Constraining the tubes laterally induces more plastic hinges to be formed during collapse, thus increasing the volume of material reaching plasticity. The force-deflection response of axially loaded tubes consists of a high peak collapse load followed by large fluctuations of force about a mean load. In contrast, the force deflection response for the lateral collapse of tubes is smoother without any incidence of oscillations. The main advantage of the inversion process of the uniform tube is the constant inversion load. However, successful inversion of tubes requires a material with certain ductility and strain hardening properties. In addition to this, the global dimensions of the die radius must be within a compatible range in conjunction with suitable material properties in order to achieve the desired energy absorbing behaviour. Therefore, the tube inversion is considered to be a complex process. The axially loaded tubes might adopt an undesirable deformation mode termed global bending, particularly in tubes with large L/D ratios. This deformation mode is generally unstable and cause extreme reduction in the energy absorbing capacity. The deformation mode of a tube compressed laterally is plastic bending at plastic hinges. This deformation mode results in smooth force-deflection response as mentioned earlier in this section. For the tubes crushed axially, the successful loading occurred when the angle between the load application and the longitudinal axis of the tube is less than 15% [25]. This

feature is considered an undesirable behaviour for transport applications, since the line of action of the kinetic force may be outside of this range. However, it is possible to apply the load laterally with an angle of more than 15 % on the tubular structures since the tubes will deform for most of the deformation stroke before losing its symmetry [25]. Building the energy absorbing system using laterally loaded tubes is easier compared to axially split or inverted tubes. This is because the inversion and splitting processes require dies and mandrels which are manufactured to a high level of accuracy to ensure successful operation and to achieve the desired output response.

2.7 Summary of literature review and knowledge gaps

This chapter has provided a background of topics related to this thesis. The main topics presented were structural crashworthiness and impact, energy absorbing characteristic, energy absorbers, and analysis of energy absorbers.

The findings of the literature review show that axially loaded tubes have been widely used as energy absorbing structures and have received considerable attention by researchers due to the fact that these structures have high energy absorbing capacities and stroke length per unit mass. However, these structures have certain drawbacks, such as very large fluctuations of the collapse load about a mean load, and the unstable deformation mode (global bending mode). Laterally loaded tubes have a distinct advantage over tubes compressed axially due to fact that the bending collapse mode generated from lateral loading result in a smooth force-deflection response. Also, the laterally loaded tubes do not undergo any kind of unstable deformation mode even under the off-axis loading. In spite of these advantages of the laterally loaded structures, this type of energy absorbers has received relatively limited research attention in the literature. Few studies were carried out to investigate energy absorption responses of laterally loaded thin-walled tubes, and there still are a number of areas requiring further investigations. Considering the importance of the laterally loaded structures, it would be beneficial to formulate design instructions for the use of these structures in energy absorbing systems, such as in impact and crashworthiness applications. Providing such knowledge requires answering the following questions.

What are the responses of thin-walled single and nested metallic tube under quasi-static and dynamic lateral loading?

How do laterally loaded thin-walled tubes respond under oblique loading?

What are the effects of the geometrical factors on the responses of laterally loaded tubes?

What is the optimal configuration of the laterally loaded energy absorber?

How can the energy absorption capacity of these structures be enhanced?

Therefore, taking this into consideration an attempt is made, in this thesis, to answer these important questions and to fill the knowledge gaps.

3

Chapter 3

THEORETICAL BACKGROUND

3.1 Finite element method (FEM)

The finite element method is a numerical analysis technique used by engineers, scientists, and mathematicians to obtain solutions to differential equations that describe, or approximately describe, a wide variety of physical (and non-physical) problems. Physical problems range in diversity from solid, fluid, and soil mechanics, to electromagnetism and dynamics. With regard to energy absorbing systems, the FEM is a very powerful tool in the field of design and development of energy absorbers as it provides much more detailed information than other traditional methods. In fact, the deformation modes of energy absorbers are very complex, therefore the design of energy absorbing components requires several design iterations and design loops. The FEM is widely employed by researchers and engineers to conduct parametric studies, as it is more time and cost-effective than real testing. There are many commercial non-linear finite element (FE) codes, such as LS-DYNA3D, PAMCRASH, ADINA, ABAQUS, CRASH CAD, RADIOSS and ANSYS, that are used by researchers to investigate quasi-static and dynamic responses of energy absorbers. In this thesis, ANSYS & LS-DYNA are used in the quasi-static and dynamic simulations of energy absorbing components.

3.1.1 Linearity and nonlinearity

All structural problems in FE modelling can be categorized as linear or nonlinear. A linear analysis is used for structures that have a linear relationship between the applied load and responses of the structure. It assumes that the stiffness of the structure is constant during the whole period of loading. Nonlinear analysis is employed for structural problems where the stiffness of structure is not constant and changes as the structure deforms. In reality, the behaviour of all structures used in engineering applications is nonlinear, so using linear analysis for most structural problems is ineffective. FE simulations of mechanical behaviour of structural components include three sources of nonlinearity: material nonlinearity, boundary nonlinearity, and geometry nonlinearity. Material nonlinearity means that the stress-strain relationship is nonlinear. In general, the stress-strain response of metallic material exhibits nonlinear behaviour when it is loaded beyond the yield stress or when it is loaded dynamically, as noticed in impact loading scenarios. Boundary nonlinearity takes place when the boundary conditions change during the analysis, and geometry nonlinearity occurs whenever the magnitude of the displacements affects the response of the structure. Most of FE commercial codes employ the Newton-Raphson algorithm to obtain solutions of non-linear problems. In general, the solution of nonlinear analysis is obtained by dividing the simulations into a specific numbers of load increments and hence at the end of each load increment an approximate equilibrium solution is founded. The approximate final solution of the nonlinear analysis is the sum of all sub responses.

3.1.2 Static and dynamic analysis

The solution algorithms used by the finite element codes are either implicit or explicit. The implicit method updates the stiffness matrix throughout the solution process using the predictor-corrector method so it is computational cost to analyse the dynamic events by using implicit FE codes. In the explicit method, the equilibrium checking is not performed, i.e: there is no corrector step, thus decreasing the solution time. In general, the implicit FE code such as ANSYS is suitable for quasi-static analysis of energy absorbers while, the explicit FE code such as LS-DYNA is suited to simulate high-speed dynamic events such as impact events. The explicit FE codes can be used effectively to carry out FE modelling for quasi-static problems as reported by [130] . El-Hage et al. [130] and Meguid et al. [131] have

suggested a simple guide for simulating the quasi-static problems by using FE explicit packages as follow:

i. *The ratio of the total kinetic energy (KE) to the total initial energy (IE) is less than 5% over the period of the crushing process*
ii. *The crushing force-displacement response is independent of the loading velocity*

In this thesis, implicit FE code (ANSYS) was employed to perform the quasi-static analysis of single and nested tubes systems. In addition, the LS-DYNA package was used to perform the dynamic analysis of various systems presented in this thesis.

3.1.3 Material models

For getting an accurate prediction of the responses of the FE model, the material model should be selected carefully so it represents the mechanical behavior of the real material used. Nonlinear FE codes (ANSYS&LS-DYNA) provide a variety of material models such as elasticity, viscoelasticity, plasticity, visco-plasticity, cast iron plasticity, creep, hyper-elasticity, gaskets, and anisotropy which can simulate the behavior of wide range of materials such as metals, foams, plastic, bio tissues, glass, concrete, and rubber under various loading conditions. In the present thesis, a Bilinear Isotropic Hardening Material Model was used to simulate the responses of metallic tubes and layers under quasi-static conditions. This material model option employs the von Mises yield criteria, coupled with an isotropic work hardening assumption and is highly recommended for modeling large strain problems. Based on Von Mises yield criteria, the yield stress is given as:

$$\sigma_y = \frac{1}{\sqrt{2}}\sqrt{(\sigma_1 - \sigma_2)^2 + (\sigma_2 - \sigma_3)^2 + (\sigma_3 - \sigma_1)^2} \quad (3\text{-}1)$$

Where σ_y is the yield stress, σ_1, σ_2, σ_3 are the stresses defined in a three-dimensional principle stress space as shown in Figure 3-1.

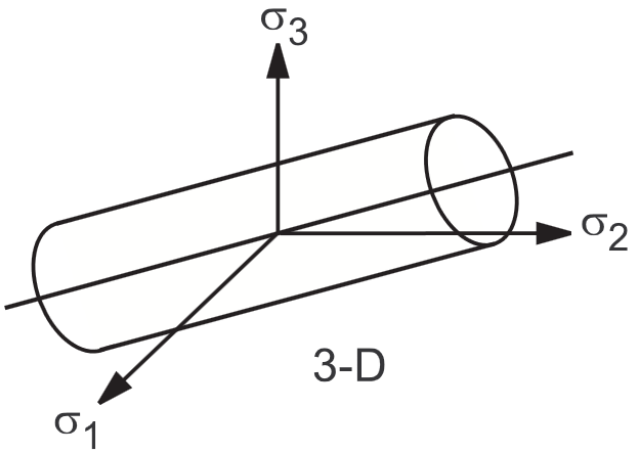

Figure 3-1: Yield surface in principle stress space [132].

The hardening rule describes the changing of the yield surface with progressive yielding, so that the conditions (i.e. stress states) for subsequent yielding can be established. Two hardening rules are available: work (or isotropic) hardening and kinematic hardening. In work hardening, the yield surface remains centred about its initial centreline and expands in size as the plastic strains develop. For materials with isotropic plastic behaviour this is termed isotropic hardening and is plotted Figure 3-2.

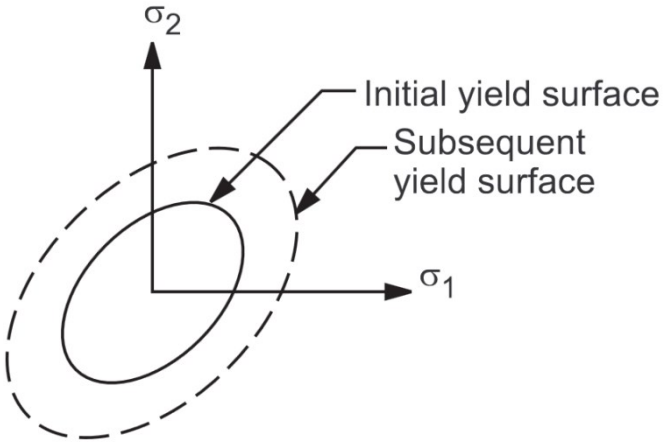

Figure 3-2: The Isotropic Hardening Rule [132].

For steel tubes subjected to impact dynamic loading, the '*PLASTIC KINEMATIC HARDENING'* material model was used. This material option accounts for material strain rate sensitivity phenomena by using the Cowper-Symonds constitutive equation (equation (2-1)).

3.1.4 Contact Capabilities within ANSYS and ANSYS/LS-DYNA

ANSYS offers a number of contact types such as node to node, node to surface and surface to surface models. In this thesis, a surface to surface contact type was employed to capture the deformation process of the various energy absorbers. Figure 3-3 demonstrates a surface to surface contact pair used to define the interaction between the two solid bodies. It can be seen that the contact surface usually consists of the deformable body, while the target surface may consist of either a deformable or rigid surface. Contact detection points are located at the integration points of the contact elements which are interior to the element surface. The contact element is constrained against penetration into the target surface at its integration points. However, the target surface can, in principle, penetrate through into the contact surface. An example of contact pairs used in FE models of energy absorbers studied in this thesis is displayed in Figure 3-4.

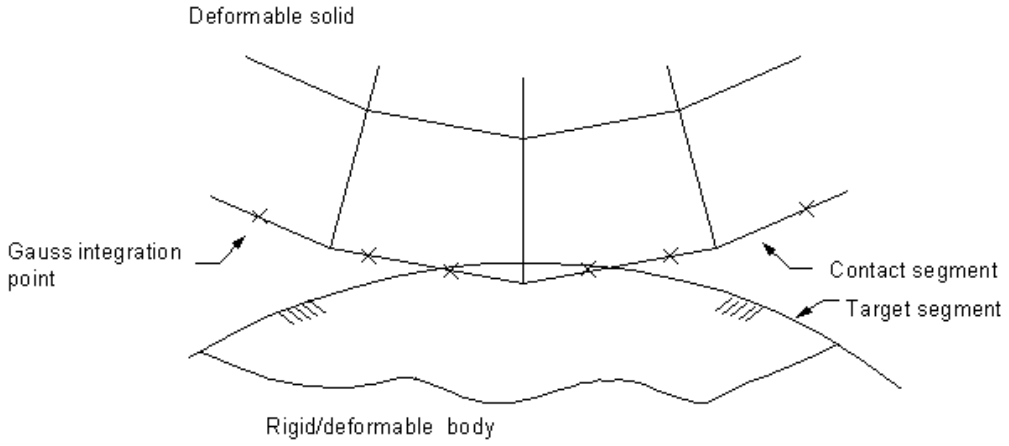

Figure 3-3: Illustration of a contact pair.

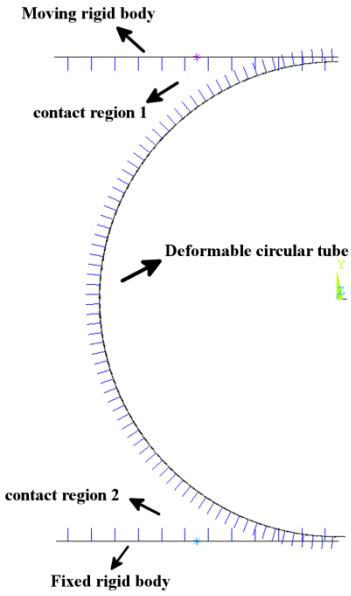

Figure 3-4: contact pairs used in FE models of circular tube under lateral loading.

In LS-DYNA, contact is defined by identifying (via parts, part sets, segment sets, and/or node sets) what locations are to be checked for potential penetration of a *slave* node through a *master* segment. LS-DYNA also uses the penalty method approach, in which, when a penetration is found, a force proportional to the penetration depth is applied to resist, and ultimately eliminate, the penetration. An AUTOMATIC SURFACE to SURFACE contact format, which is a two way contact, is used to simulate the contact interaction of the various energy absorbers subjected to dynamic impact as shown in Figure 3-5. This contact is typically used in impact analysis due to the fact that predetermination of where the contact will occur is almost impossible. In a two-way contact, nodes on the slave side are first checked for penetration through the master surface and then master nodes are checked for penetration through the slave surface.

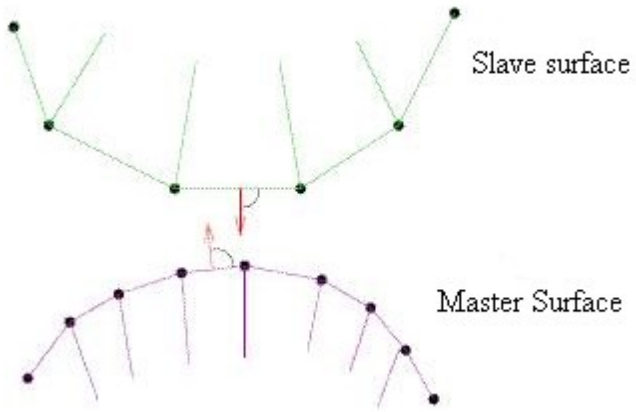

Figure 3-5: Illustration of the surface to surface contact algorithm in ANSYS/LS-DYNA (www.dynasupport.com).

3.2 Design of Experiment (DOE)

Whether it is in industry or research, experiments are carried out to understand, explore, confirm, and improve processes, methods, and product quality, or unveil phenomena and facts [144]. There are several approaches to experimental work. One conventional approach is what is called "one-variable-at-a-time" (OVAT). In this technique, the engineers vary one variable at one time and observe the effects of this variation on the process. This approach requires considerable resources to obtain just a limited amount of information about the process. This is because OVAT technique always carries the risk that the experimenter may find one input variable to have a significant effect on the response (output), while failing to discover that changing another variable may alter the effect of the first (i.e. due to a dependency or interaction that could occur) Thus, OVAT approach does not readily allow for establishing the relationship between the different process variables [144].

Nowadays, the statistical based approach Design of Experiments (DOE) is more commonly used in different fields such as biology, pharmacy, and engineering. DOE is a systematic approach to the investigation of a system that helps in planning, performing, analyzing, and understanding data collected from experiments, as well as allowing direct observation of the effect of many variables on the monitored responses. A well designed DOE experiment should help to identify which set of process variables causes the most significant effect on the process performance, thus allowing a more efficient process

optimisation [144]. Back in the early 1920s, DOE was first employed by Sir R. Fisher to determine the effect of various fertilisers on a range of land plots. Since then, the use of DOE has expanded to reach almost all research areas and industrial applications.

Recently, in the field of energy absorbing structures, DOE technique was utilized by researchers [120]-[129] to construct surrogate models, such as Response Surface (RS) models, which relate the crushing and energy absorption responses to design variables for analysis and optimization purposes. The design variables could be one or more of the following geometrical parameters, material parameters and loading parameters.

3.3 Response surface methodology (RSM)

The Response Surface Method (RSM) is a set of mathematical and statistical techniques that are useful for modelling the responses that are being studied as functions of the controllable input variables. If all independent variables are measurable and can be repeated with negligible error, the response surface can be expressed by

$$\mathrm{Y} = f\ (x_1, x_2, \ldots\ldots, x_k) \qquad (3\text{-}2)$$

Where: k is the number of independent variables

Usually, a second order polynomial (Equation (3-3)) is used in RSM to describe the true functional relationship between the independent variables and the response surface

$$\mathrm{y} = b_o + \sum b_i x_i + \sum b_{ij} x_i x_j + \sum b_{ii} x_{ii}^2 + \varepsilon \qquad (3\text{-}3)$$

One of the most popular DOE designs which used to creat RS models is the Box-Behnken design (BBD), which is based on three levels of each factor (coded as -1, 0, & +1). This design was developed by Box and Behnken in 1960 [134] by combining two-level factorial designs with incomplete block designs, with a specified number of centre points then added. Figure 3-6 displays a schematic diagram for BBD for

three factors. The advantages of the Box-Behnken designs include the fact that they are all spherical designs and require factors to run at only three levels. The designs are also rotatable, which indicates that the variance of the predicted values of y is a function of the distance of a point from the centre of the design and is not a function of the direction the point lies from the centre. Furthermore, when using BBD design type, the region of interest will be the same as the region of operability. An advantage of these designs is that there are no runs where all factors are at either the -1 or 1 levels (corner points). This would be advantageous when the corner represent runs that are expensive or inconvenient because they are positioned at the end of the range of the factor levels [135].

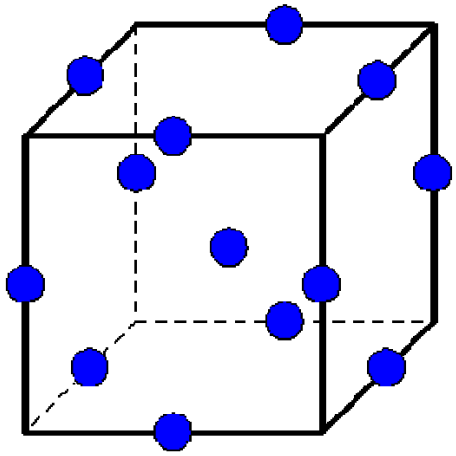

Figure 3-6: A schematic diagram for BBD for three factors [136].

In the present study, the RSM method with the BBD design type was applied to the data obtained from finite element models to investigate the effect of geometrical parameters on the energy absorbing responses of various thin walled tubes. The following steps were carried out to create a mathematical model of response Y as a function of three factors (x_1, x2, and x3) using an integration of finite element modelling and the DOE technique.

1. Identifying the factors which have a significant effect on the response

These factors can often be defined from the literature or by conducting a preliminary study (i.e. screening study). Subsequently, factor limits were selected based on trial and error experience.

2. Design matrix development

The matrix depends on the type of RSM design selected. For BBD design type, the design matrix in coded values (-1, 0, +1) are shown in (Table 3-1).

Table 3-1: Design matrix for BBD, coded values

Run no	X_1	X_2	X_3
1	-1	-1	0
2	1	-1	0
3	-1	1	0
4	1	1	0
5	-1	0	-1
6	1	0	-1
7	-1	0	1
8	1	0	1
9	0	-1	-1
10	0	1	-1
11	0	-1	1
12	0	1	1
13	0	0	0
14	0	0	0
15	0	0	0
16	0	0	0
17	0	0	0

3. Performing the experiments (numerical simulations)

Based on the validated finite element modelling, numerical simulations were conducted and responses were calculated for each case stated in (Table 3-1). The resultant values determine the response surface model.

4. Development of the mathematical model

To model the response (Y) as a function of three factors (X_1, X_2, and X_3), the following second order polynomial was used (Equation (3-4)).

$$\begin{aligned} Y = b_0 + b_1X_1 + b_2X_2 + b_3X_3 + b_{11}X_1^2 + b_{22}X_2^2 \\ + b_{33}X_3^2 + b_{12}X_1X_2 + b_{13}X_1X_3 \\ + b_{23}X_2X_3 \end{aligned} \quad (3\text{-}4)$$

5. Estimation of the coefficients in the model

A regression analysis was applied using the Design-expert V8 computer software to specify the values of the 10 coefficients in (Equation (3-4)). The following equations (Equations (3-5)-(3-8)) were used:

$$b_0 = \overline{y}_0 \quad (3\text{-}5)$$

$$b_i = A\sum_{u=1}^{N} x_{iu}y_u \quad (3\text{-}6)$$

$$b_{ii} = \mathrm{B}\sum_{u=1}^{N} x_{iu}^2y_u + C_1\sum_{u=1}^{N} x_{ii}^2y_u - (\frac{\overline{y}_o}{s}) \quad (3\text{-}7)$$

$$b_{ij} = D_1\sum_{u=1}^{N} x_{iu}x_{ju}y_u \quad (3\text{-}8)$$

Where N is number of the conducted experiments, i is the number of factors, and $\overline{y}_0$ is the average value of the observations made at the centre points. A, B, C1, and D1 are constants and for the three factors design they are equal to 1/8, 1/4, -1/16, and 1/4 respectively [134]. The sum of squares for each term of BBD was calculated using Equations (3-9) and (3-11) for designs with 3 factors.

$$SS_{b_i} = \mathrm{A}\sum_{u=1}^{N}(x_{iu}y_u)^2 \tag{3-9}$$

$$SS_{b_{ij}} = D_1\sum_{u=1}^{N}(x_{iu}x_{ju}y_u)^2 \tag{3-10}$$

$$SS_{ii} = b_0\sum_{u=1}^{N}y_u + b_{ii}\sum_{u=1}^{N}x_{iu}^2y_u - \sum_{u=1}^{N}(y_u)^2/N \tag{3-11}$$

6. Testing the adequacy of the developed models

An analysis of variance (ANOVA) was used to test the adequacy of the developed models (Table 3-2). The statistical significance of the developed model and each term in the regression equation were examined using the sequential F-test depending on the values of the Prob > F (p-values), which were computed by means of an ANOVA. If the Prob > F of the model and of each term in the model does not exceed the level of significance (α= 0.05), then the model may be considered adequate within the confidence interval of (1- Prob.> F).

Table 3-2: ANOVA table for full model

Source	*SS*	*Df*	*MS*	*Fcal-value*	*p-value or Prob>F*
Model	SSM	P	Each SS divided by its D_F	Each MS divided by M_{SR}	From table or software library
X_1	SS_1	1			
X_2	SS_2	1			
X_3	SS_3	1			
X_1X_2	SS_{12}	1			
X_1X_3	SS_{13}	1			
X_2X_3	SS_{23}	1			
X_1^2	SS_{11}	1			
X_2^2	SS_{22}	1			
X_3^2	SS_{33}	1			
Residual	SS_R	N-P-			-
Cor	SS_T	N-1	-	-	-

Other adequacy measures (R^2, Adjusted R^2, Predicted R^2, and Adequate Precision ratio) were checked in the ANOVA table to obtain the best fit. The proportion of variability in a data set that is accounted for by the proposed model can be determined by the value of R2. However, the variability of the model is defined as the sum of squares, and can be calculated in Equations (3-12) and (3-14). Adjusted R^2 is an important modification of R^2, and adjusts for the number of explanatory terms in a model. Unlike R^2, the adjusted $R2$ increases only if adding a new term improves the model more than would be expected by chance. The predicted R^2 can prevent over-fitting the model because it is calculated using observations not included in model estimation. However, the Predicted R^2 should be in reasonable agreement with the Adjusted R^2. The adequate precision ratio compares the range of the predicted value at the design points to the average prediction error. A ratio greater than 4 indicates that the suggested model can be used to navigate the design space.

Here follows statistical terminology and definitions used in the ANOVA analysis:

- Term: Each of the listed factors or factor interactions (A, B, AB, AB2, etc.) having an effect on the model.
- Residual: Terms not included in the model but which are used to estimate experimental error.
- Model: Terms estimating factor effects.
- Pure error: Amount of variation in the response in replicated design points.
- Lack of fit (LOF): Variation of the data around the fitted model. LOF is significant if the model does not fit the data properly.
- Curvature: The variable that compares the average of the actual centre points to the estimated value of the centre point calculated as an average from all factorial points. A strong curvature is undesirable as it can mask the effect of the factors. If curvature is found to be significant it indicates the requirement for reduction of the factor ranges.
- Term sum of squares (SS): The number of factorial experiments divided by 4 times the squared factor effect.
- Term degrees of freedom (DF): It is the number of levels for a factor minus 1.
- Term mean square (MS): Estimate term variance, which is calculated as term SS/DF.
- Term F value: It is calculated as term mean square divided by the residual mean square. The term is less likely to have an effect on the response if the term variance is close to the residual variance (ratio ≈ 1).
- Term Prob>F: Probability of observing the calculated F value if there is no factor effect. This probability corresponds to the area under the F-distribution beyond the calculated F value. If (Prob>F)<0.05 the individual term on the model has significant effect on the response.
- Model SS: Total of the sum of squares for the terms in the model.
- Model DF: It is the number of model terms (p) minus 1.
- Model MS: Estimate model variance, which is calculated as MSmodel=SS/DF=SS/p-1.

- Model F value and Prob>F: The same as for terms but with the model variables.
- Residual SS: Sum of squares of all the terms not included in the model
- Residual DF: Corrected total DF (number of experimental runs (n) minus 1) minus model DF. Therefore, (n-1)-(p-1) = n-p.
- Residual mean square (MSE): The estimate of process variance, which is MSresidual=SS/DF=SS/n-p.
- Pure error SS: Pure error sum of squares from replicate points.
- LOF SS: Residual SS - pure error SS.
- LOF Prob>F: In this case a small value of this variable means that the LOF is significant. Therefore, a LOF (Prob>F)>0.1 is preferable.

ANOVA output:

- Standard deviation (Std Dev) associated with the experiment: √MSE
- Mean: Average of all the response data.
- Coefficient of variance (C.V.): (Std Dev / Mean)*100.
- Predicted Residual Error Sum of Squares (PRESS): It is an indicator of the accuracy of the model to predict each design point. It is calculated predicting where each point would be in a model which contains all the other points. Then the squared residuals (difference between actual and predicted values) are summed up.
- R-squared (R2): This value indicates the variability of the data around the mean described by the model and it provides a measure of the model accuracy to predict future points. R2 value can vary from 0 to 1 and the closer it is to 1 the better the model is.
- Adjusted R-squared (R2adj): This value adjusts R2 for the number of terms in the model. It decreases if the number of non-significant terms in the model is increased.
- Predicted R-squared (R2pred): This value indicates the variability in new data described by the model. This value and the previous one should be within 0.2 of each other.

- Adequate precision: This value reflects the signal to noise ratio and, therefore, the ratio of the predicted response to its associate error. A value greater than 4 is required to obtain adequate model discrimination.

Adequacy measures are calculated by the software, but can also be calculated by means of Equations (3-15) - (3-18) [137]-[139].

$$\text{Sum of squares-model= } SS_M = \sum_{u=1}^{N}(\hat{y}_u - \overline{y})^2 \quad (3\text{-}12)$$

$$\text{Sum of squares-residuals= } SS_R = \sum_{u=1}^{N}(y_u - \hat{y}_u)^2 \quad (3\text{-}13)$$

$$\text{Sum of squares-total= } SS_T = SS_M + SS_R = \sum_{u=1}^{N}(y_u - \bar{y})^2 \quad (3\text{-}14)$$

$$\text{R-squared= } R^2 = \frac{SS_M}{SS_T} \quad (3\text{-}15)$$

$$\text{Adjusted R-squared} = AdjR^2 = 1 - \left[\left(\frac{SS_R}{df_R}\right) \times \left(\frac{SS_T}{df_R + df_M}\right)\right] \quad (3\text{-}16)$$

$$\text{Predicted R-squared= } PredR^2 = 1 - \left[\frac{\sum_{u=1}^{N}(y_u - \hat{y}_{u-1}}{SS_T}\right] \quad (3\text{-}17)$$

$$Adeq\ precision = \left[\frac{Max(\hat{y}) - Min(\hat{y})}{\sqrt{\frac{p \times MS_R}{N}}}\right] \quad (3\text{-}18)$$

Where: y, $y\hat{}$ are the experimental data and the estimated value respectively.

P: Number of coefficients in the model.

N: Total number of runs.

n_0: Number of centre points.

df: Degree of freedom.

MS: Mean square.

$\hat{y}_{ui-1}$: The predicted output based on the estimated model after removing the current observation.

7. Final Model development

Usually, the full model, Equation (3-4), includes insignificant model terms, ie: that have a p-value greater than the level of significance (α= 0.05), and that need to be eliminated. Elimination can be done manually or automatically. The three automatic methods are: forward selection, backward elimination, and stepwise regression [140]. The resultant model contains only the significant terms and the terms that are necessary to be maintained hierarchically.

8. Post analysis

The final model was tested and checked and was found to be adequate. As a result, predicting the response in the design space using this adequate model was now possible. Important plots such as 3D graphs, contours, perturbation, and interaction plots could now also be produced to demonstrate the factors effect and how they contributed towards the response. The potential of employing the developed model for establishing the optimal solution is discussed in the next chapter.

3.4 Response Surfaces Based Optimization

Typically, as part of the analysis of energy absorbing components, the various responses being investigated need to be optimized simultaneously. However, multi-objective optimization problems can involve incommensurate and conflicting responses. Based on the response surface models, there are different statistical techniques that solve multiple response problems. These include, overlaying the contour plots for each response, constrained optimization problems, and the desirability approach. The desirability method is recommended due to its simplicity, availability in the design-expert software, and because it offers flexibility in weighting and can assign different importance values for individual responses.

3.4.1 Desirability approach

Solving multi-objective optimization problems using the desirability approach consists of a technique that combines multiple responses into a dimension-less measure of performance, called an overall desirability function. In particular, the desirability approach indicates the transforming of each estimated response, Y_i, into a unit-less utility bounded by ($0 < d_i < 1$), where a greater d_i value indicates that response value Y_i is more desirable, i.e.: if $d_i = 0$ this means that the response is completely undesired, while $d_i = 1$ indicates a fully desired response [141]. In the current work using the Design-expert V8 software [138], the shape of the desirability function can be changed for each goal by the weight field "wt_i". Weights are used to give added emphasis to the upper/lower bounds or to emphasize the target value. Weights could be ranged between 0.1 and 10; a weight greater than one gives more emphasis to the goal, while a weight less than one gives less emphasis to the goal. With a weight value of one, the values of di will vary between zero and one in a linear mode. In the desirability objective function (D), each response can be assigned an importance (r) relative to the other responses. Importance varies from the least important value of 1(+), to the most important value of 5(+++++). If varying degrees of importance are assigned to the different responses, the overall objective function is shown in equation (3-19). Where n is the number of responses in the measure, d_i is the target value of the i-th response and ri are user-specified parameters that make possible the assignment of priorities to di [141].

$$D = \left(\prod_{i=1}^{n} d_i^{r_i}\right)^{\frac{1}{\sum r_i}} \qquad (3\text{-}19)$$

- For a maximum value as the required goal, the desirability can be defined by:

$$d_i = \begin{cases} 0 & , \quad Y_i \le Low_i \\ \left(\dfrac{Y_i - Low_i}{High_i - Low_i}\right)^{wt_i} & , \quad Low_i < Y_i < High_i \\ 1 & , \quad Y_i \ge High_i \end{cases} \tag{3-20}$$

- For a minimum value as the required goal, the desirability can be defined by:

$$d_i = \begin{cases} 1 & , \quad Y_I \le Low_i \\ \left(\dfrac{High_i - Y_i}{High_i - Low_i}\right)^{wt_i} & , \quad Low_i < Y_i < High_i \\ 0 & , \quad Y_i \ge High_i \end{cases} \tag{3-21}$$

- For a target value as the required goal, the desirability can be defined by:

$$d_i = \begin{cases} \left(\dfrac{Y_i - Low_i}{T_i - Low_i}\right)^{wt_i} & , \quad Low_i < Y_i < T_i \\ \left(\dfrac{High_i - Y_i}{High_i - Low_i}\right)^{wt_i} & , \quad T_i < Y_i < High_i \\ 0 & , \quad otherwise \end{cases} \tag{3-22}$$

- For a value within range as the required goal, the desirability can be defined by:

$$d_i = \begin{cases} 1 & , \quad Low_i < Y_i < High_i \\ 0 & , \quad otherwise \end{cases} \tag{3-23}$$

3.4.2 Optimization approach in Design-expert V8 software

The optimization function of the Design-expert V8 software searches for a combination of factor levels that simultaneously satisfy the desired requirements (i.e. optimization criteria) from each of the responses and factors (i.e. multiple response

optimization). As mentioned in the previous section, the optimization process involves combining the goals into an overall desirability function (D). The numerical optimization feature in the Design expert V8 software package searches for one or more points in the factors domain that will maximize the desirability function (D). In the graphical optimization with multiple responses, the software defines regions where requirements simultaneously meet the responses, and the software defines regions where requirements simultaneously meet the proposed criteria, superimposing or overlaying critical response contours on a contour plot. This enables a visual search for the best compromise. In the case of performing an MOD study for the energy absorber as described in this thesis, it is recommended to first carry out a numerical optimization; otherwise it might be difficult to uncover a feasible region. Figure 3-7 shows a flow chart of carrying out an MOD study of thin-walled structures that are used as energy absorbers, by using Design expert V8 software.

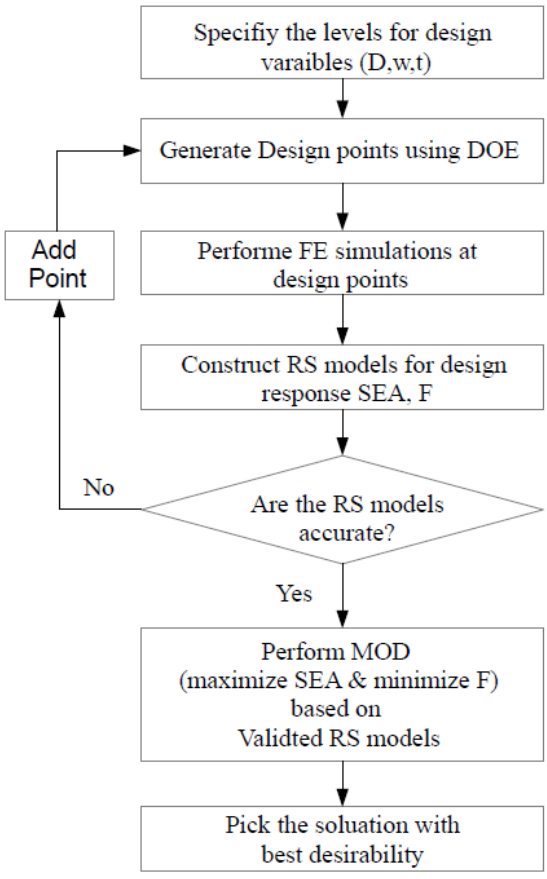

Figure 3-7: Flow charts of performing MOD study.

3.5 Summary

This chapter outlined the most important theories used to analyse the various energy absorbers. The first section provided an account of some of the important topics within the finite element method solution, such as linearity and non-linearity, static and dynamic analysis, material models, and contact methods used in both ANSYS and ANSYS-LSDYNA. This fundamental information can assist in understanding and improving the responses of finite element models of various tubes under lateral loading, as will be presented in Chapter 5. Section 2 and Section 3 of this chapter theoretically explained the response surface methodology and response surface based optimisation. The information provided in these sections will be very useful when employing the response surface methodology (RSM) as a tool for performing the parametric analysis and multi-objective optimisation design (MOD) in Chapter 6. In general, this chapter presented a summary of the theory behind this research. The interested reader can refer to the various quoted references throughout the chapter for further in depth understanding of the underlying theory.

4

Chapter 4

MATERIAL & METHODS

4.1 Experimental Set-Up

4.1.1 Quasi-Static Loading

4.1.1.1 Mechanical Features of the Instron 4204 Series Testing Machine

The Insron Model 4204 testing machine was used to perform the quasi-static experiments on the respective specimens. The loading frame comprises of two vertical lead screws, a moving crosshead and an upper and a lower bearing plate. The maximum capacity of this loading frame is 50 kN. This machine was calibrated to confirm that the obtained results were accurate [the calibration certificate is shown in Appendices A].

4.1.1.2 Load Cell Features.

The loading force is measured by a loading cell which is attached to the moving crosshead of the loading frame. This load cell is comprised of multi strain gauges. The gauges are connected as a Wheatstone bridge, so any unbalance in this bridge is

recorded as voltage. This voltage is then used to indicate the amount of force applied to the samples.

4.1.1.3 Data Acquisition System

A CPU is used as control unit to control movement of the crosshead. This control unit also provides the data acquisition and data readout from the loading frame. Instron 4204 series software is integrated to display the results. Many parameters such as displacement, load, strain and energy can be obtained. Figure 4-1 shows the Instron machine and control unit.

Figure 4-1: Instron Model 4204 with the control unit.

4.1.1.4 Experimental Procedure

A prescribed velocity of 10 mm/min was applied to the moving crosshead of the instrument to ensure that there were no dynamic effects. Many researchers [69]-[71], [83], and [87] used velocities between 0.5 and 15 mm/min in the quasi-static lateral compression tests. The quasi-static test set- up for nested tube sample is shown schematically in Figure 4-2.

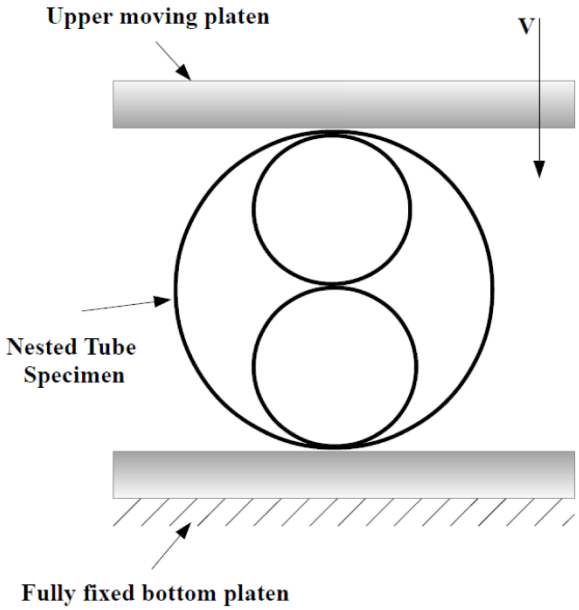

Figure 4-2: Schematic of a nested tubes sample tube under quasi-static load.

4.1.1.5 Experimental set-up of oblique loading

For simplicity and due to the difficulty of modifying the moving crosshead of the instrument, inclined bases designed by the author were integrated with the Instron machine to produce oblique loading. A simple fixture was employed to prevent lateral movement of the tubes under oblique load. This fixture plays an insignificant role in decreasing the effective stroke length. The experimental set-up of the oblique loading case is presented in Figure 4-3.

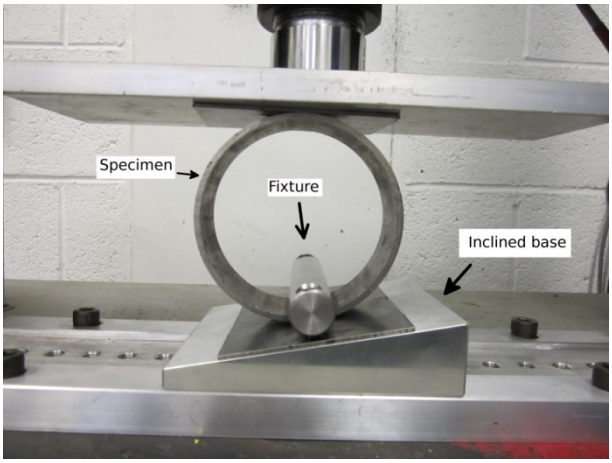

Figure 4-3: Experimental Set-up of oblique loading.

4.1.2 Dynamic Loading

4.1.2.1 Mechanical Features of the Zwick Roell 5HV Series

The Zwick Roell 5HV series (Figure 4-4) was used to conduct the impact testing on the various samples. The load-time response during the impact event was captured by using a Kistler 9091 series piezoelectric force transducer which has a large dynamic range. The transducer has a maximum load capacity of 250 KN and frequency of 160,000 samples per second. The transducer is mounted in the moving carriage and attached to a striker by a lock-unlock mechanism. The maximum drop height is 1.2 meters. The impact mass consists of a striker mass and a carriage mass, and slides vertically along the guide rails. The initial velocity of the striker (impact velocity) was captured by a photo gate arrangement which is comprised of photo diodes passing through a flagged gate. Figure 4-4 displays the Zwick Roell 5HV impact testing machine with explanation of striker mass and sample positions.

4.1.2.2 Data Acquisition System

Rosand IFW (Intelligent Free Wheel) V 1.10 was employed as data acquisition system. This system has a maximum rate of 670 KHz and a total data point capture of 4000. The system obtains the signals from the force transducer. The system software records the force measurements with respect to time. The software is equipped with a filter option, which is based on the second order Butterworth filter. The second order Butterworth filter is implemented in the software as an IIR (infinite impulse response).

4.1.2.3 Experimental Procedure

The samples were fixed in their position by using a simple fixture. The use of this fixture prevented the full displacement stroke to be achieved. The total mass consisted of the striker mass and the carriage mass. The striker was set in motion by selecting the velocity of impact and hence the drop height and the energy absorption were calculated by the machine software. The appropriate drop height was adjusted automatically by the machine by setting the zero position and the velocity of the

striker. For each sample tested, a frequency of 1000Hz and a total of 100 data points were selected to collect the data from the transducer.

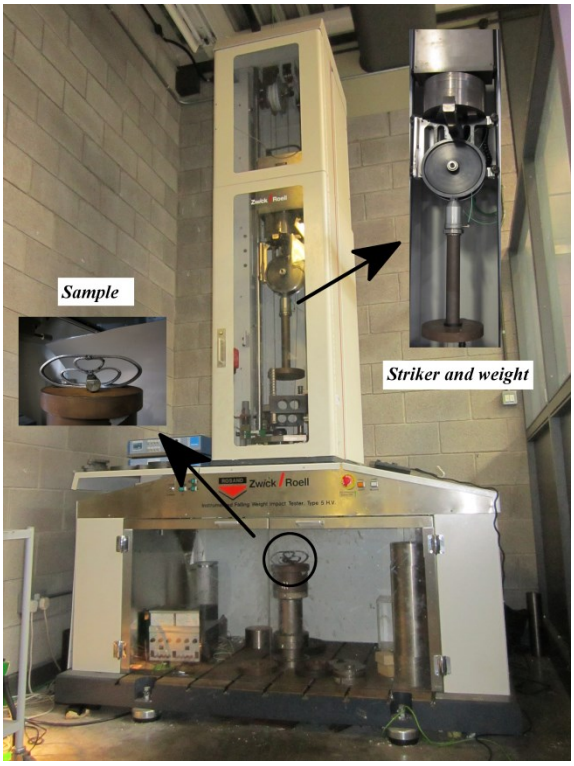

Figure 4-4: Zwick Roell 5HV series used to conduct the impact experiments.

4.2 Material Properties & Samples

4.2.1 Material Properties

Mild steel tubes were used for manufacturing the empty and nested samples. The tubes were drawn over a mandrel (DOM), cold finished and manufactured according to the DIN standards, DIN 2393 ST 37.2. The drawn over a mandrel process is normally used to give the tube more exact dimensions relative to the inside and outside diameters, a smoother finish, and better alignment of the crystal lattice structure. The chemical composition of the steel used in this work is displayed in Table 4-1. Tensile tests were carried out in order to determine the mechanical properties of the tubes as shown in Figure 4-5. The dog bone samples (tensile samples) were prepared by flattening the tube and cutting the specimens. Figure 4-6 displays the true stress-strain curves of the tensile sample. Upon examination of this figure, it can be seen that the stress-strain curve displays unusual behaviour in which

strain softening occurred almost immediately after yielding with no evidence of strain hardening. This phenomenon is due to sample necking which takes place immediately after yielding. This behaviour is termed as tension instability and the cold rolling process might be the reason for this. In addition, the preparation method of the tensile sample might also have an effect on the stress – strain behaviour of the tensile sample. Table 4-2 shows the mechanical properties of the mild steel material derived from the true stress-strain curve and used in the FE modelling. The yield stress is validated according to DIN standards, which state that the yield stress of this material is within the range of 450–525MPa [13, 14]. Furthermore, the yield stress is also within the range suggested by the supplier, which state that the yield stress of this material may nearly be as high as the tensile strength which is equal to 490 [MPa] (See Appendices B). A non-zero value of 1500 MPa was employed to represent the hardening modulus of this material. This value was selected due to the limitation of ANSYS in defining the softening stage in the bilinear material model so, the value was selected to be as low as possible. The same value of hardening modulus was used by [13] and [14] to define the softening stage of the same material.

Table 4-1: Chemical Composition of steel tubes [from company catalogue as seen in Appendices B]

	C % (max)	*Si % (max)*	*Mn % (max)*	*P % (max)*	*S %*
DIN 2393 ST 37.2	0.17	0.35	0.7	0.05	0.05

Table 4-2: Material properties of empty and nested tubes

	Density (kg/m3)	*Young's modulus (GPa)*	*Poisson's ratio*	*Yield strength Rp0.2 (MPa)*	*Tangent modulus(GPa)*
DIN 2393-ST 37.2	7861	200	0.3	470	1.5

Figure 4-5: The tensile test carried out to indicate the mechanical properties of the steel tubes.

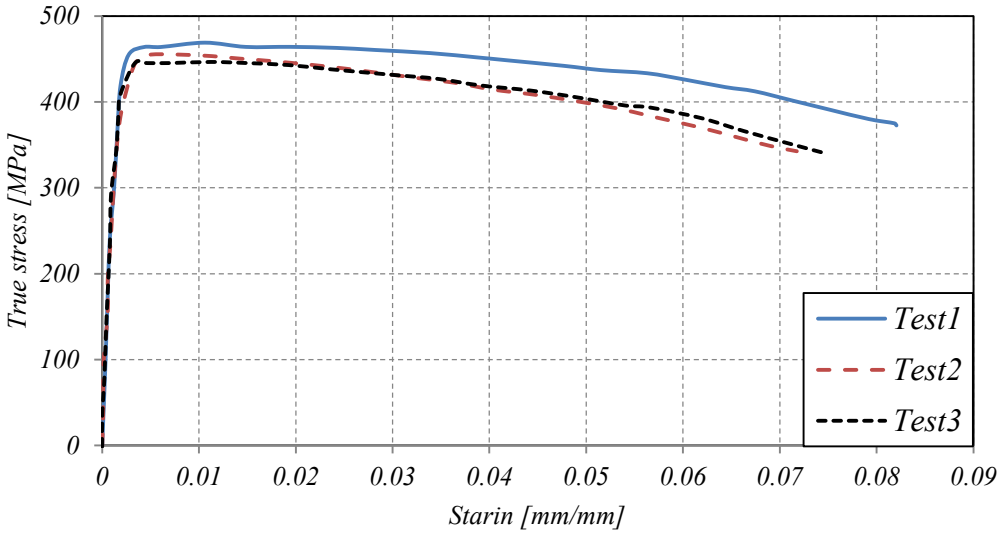

Figure 4-6: True stress–strain curves obtained from three tensile tests.

4.2.2 Samples

Table 4-3 and Table 4-4 summarize the geometry profiles and the dimensions of all samples used in this work.

Table 4-3: Configurations and dimensions of samples used in this work.

Geometry	Dimension
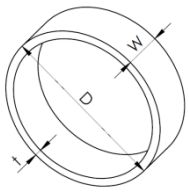	D=101.6[mm] t=3.25[mm] W=20[mm](quasi-static)-W=10 [mm](dynamic).
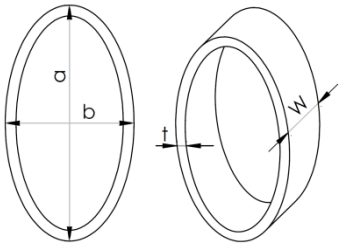	a=100[mm] b/a=0.5 t=5[mm] W=20[mm]
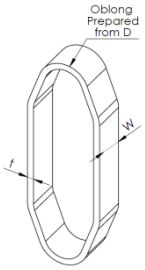	D=101.6[mm] t=3.25[mm] Elongation Distance=40[mm] W=40[mm]
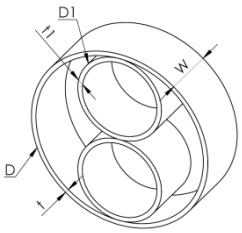	D=127[mm]-t=3.25[mm] D1=63.5[mm]-t1=3.25[mm] W=40[mm](quasi-static)-W=10 [mm] (dynamic)
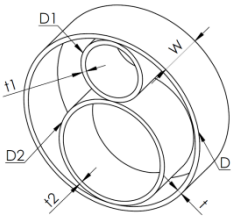	D=127[mm]-t=3.25[mm] D1=41[mm]-t1=3.25[mm] D2=76[mm]-t2=3.25[mm] W=40[mm] (quasi static test)-W=10 [mm] (dynamic test)
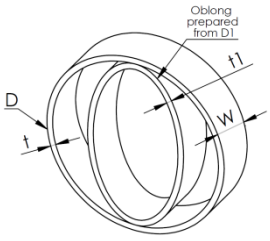	D=101.6[mm]-t=3.25[mm] D1=76[mm]-t1=3.25[mm] W=40[mm](quasi-static)-W=10 [mm](dynamic)

Table 4-4: The geometrical and mass properties of circular tubes with various longitudinal cross sections

Partial section in the 3D model of circular tubes						
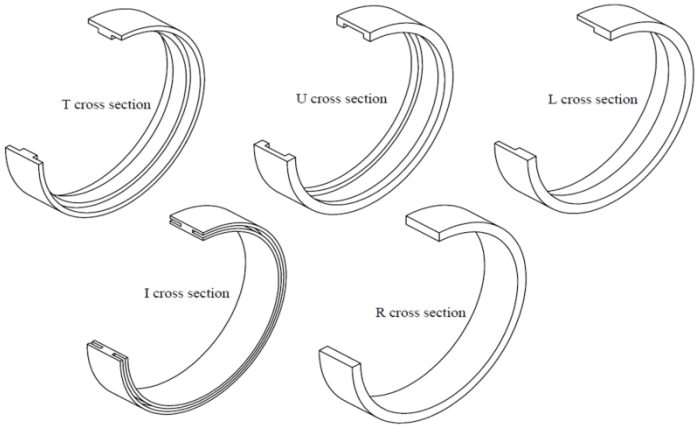						
Cross section shape	*Cross section Symbol*	*mass (gram)*	*cross section area (mm)*	*Area moment of inertia (mm⁴)*	*Outer diameter (mm)*	*Width (mm)*
	T	167.1	70	125.74	100	20
	L	177.5	75	145.92	100	20
	U	167.7	70	125.74	100	20
	R	178.28	75	87.89	100	20
	I	166.2	70.5	145.21	100	20

4.3 Summary

This chapter presented details on the various aspects of experimental set-up under various loading condition. Explanations were given for the mechanical features of instruments, data acquisition systems, and experimental procedures for the quasi-static and dynamic loading conditions. Following the experimental set-up, a detailed description was given of sourcing the material properties of the tubes used in this work. For single and nested tubes, a set of tensile tests was performed on machined dog bone specimens to obtain stress-strain curves and to represent the behaviour of the mild steel material. Furthermore, this chapter also introduced the geometry profiles for various tubes used in this research. The information provided in this chapter about the material properties and experimental set-up can be used for constructing and calibrating the finite element models of various tubes under various loading conditions, as will be presented in the next chapter (Chapter 5).

5

Chapter 5

DEVELOPMENT & VALIDATION OF FINITE ELEMENT (FE) MODELS

Comprehensive finite element (FE) modelling was employed to achieve the aims of this thesis. Various FE models were developed throughout this thesis to simulate the deformation behaviour and energy absorption of single and nested tubes under lateral loading, for both quasi-static and dynamic loading conditions. These FE models were validated using experimental techniques to ensure that they can predict the responses of thin-walled tubes under lateral loading with sufficient accuracy. The validated FE models could then be employed to simulate the responses of the laterally crushed thin-walled tubes, for variations in their geometry parameters such as thickness, diameter, and width. All modelling in this research was performed using 3D CAD design software SolidWorks then exported into the commercial FE package ANSYS. The material properties used in the FE modelling were obtained by performing standard tensile tests.

5.1 Development of finite element models

5.1.1 Quasi - Static loading case

An implicit finite element code (ANSYS) was employed for creating the FE models of various empty and nested thin walled tubes under quasi-static loading. A 3D-structural solid element (solid 45) that had eight nodes with large strain, large deflection, and plasticity capabilities was used to model the various tubes. The various indenters were modelled as rigid bodies and constrained to move vertically along the y-axis. A bilinear isotropic hardening material model was employed to define the material behaviour of the samples. The yield stress and plastic modulus that depict the plastic portion of the stress-strain curve were determined depending on the tensile test as demonstrated in section (4.2.1). The contact algorithm employs a non-linear surface to surface formulation to define contact between various interacting surfaces. An augmented Lagrangian penalty option with a friction coefficient value of 0.2 was employed for all contact pairs. All models were subjected to symmetry boundary conditions in order to reduce simulation solving times. Large strain deformation was included in the finite element model due to the test specimen experiencing significantly high displacement. The loads were defined by applying the predefined displacement on the pilot node, which was also used to gather the reaction force from each node. Figure 5-1 shows the finite element mesh of the half model of single and nested tubes. A mesh convergence study was performed to determine the mesh density. Figure 5-2 shows a force convergence plot of six different mesh densities. It was found that element size of 2 mm was able to produce a converged solution within a reasonable period of time.

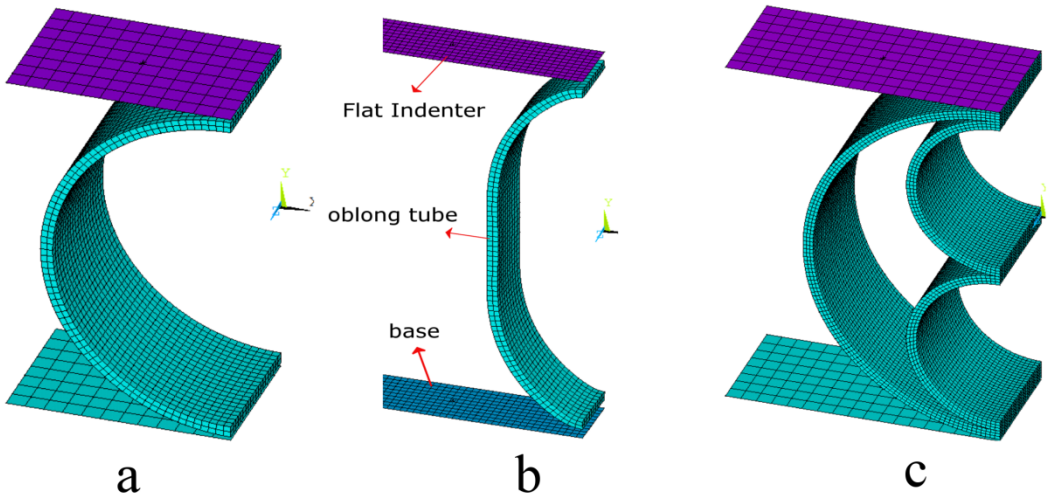

Figure 5-1: FE model of (a) a Circular Tube, (b) an Oblong Tube, (c) Nested Tubes.

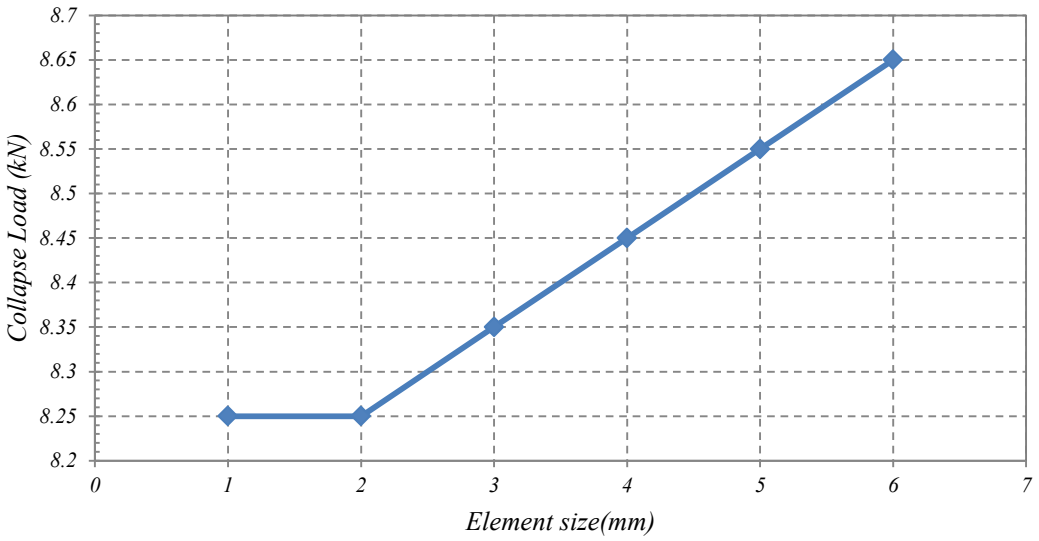

Figure 5-2: Convergence of crushing force versus mesh density for OTFIU system

5.1.2 Dynamic Loading case

The numerical analysis for the impact event was conducted by using the explicit non-linear finite element code (ANSYS-LSDYNA). Basically the finite element model consists of the striker, samples, and the base. The samples were modelled by an explicit structural solid element (solid 164), which consists of eight nodes having translations, velocities, and accelerations in the x, y, and z directions at each node.

The striker was modelled as a rigid body and constrained to move vertically along the y axis. The inertia properties and initial velocity of the striker were provided. The mass defined in the inertia properties of the striker consisted of a carriage mass plus striker mass. The base was also modelled as a rigid entity with all rotations and translations being fixed. An explicit shell element (shell 163) was used to define both striker and base. A fully integrated solid elements formulation was used in order to avoid the undesirable hour glassing phenomenon. A 'Plastic Kinematic Hardening' material model was used to define material characterization of the tubes subjected to dynamic loading. Values of 0.3 and 200 GPa were employed to define Poisson's ratio and Young's modulus respectively. This material model considers strain rate material sensitivity by using the Cowper-Symonds constitutive equation. Values of 6844 and 3.91 were given to D and q respectively. These values were used in previous studies for the axial and lateral crushing of mild steel tubes under dynamic loading [14], [36] , and [41].

5.2 Validation of FE models for various tubes

The numerical results obtained by FE models were validated against the results of the experiments carried out by the author. The validation was performed by comparing the load-displacement response, energy-displacement response, crush load, specific energy absorbing capacity, and the collapse modes. It should be noted the validation process is conducted by comparing the energy absorption parameters only. This was due to the fact that a simple material model was used to develop the FE model for predicting the behaviour of thin walled tubes under lateral loading, but which is very complex in real life.

5.2.1 Circular tubes

Figure 5-3 shows the force-deflection curves and energy-deflection curves for circular tube with an outer diameter of 101.6 mm, a thickness of 3.25 mm, and a width of 40 mm under quasi-static lateral loading. It can clearly be seen that the FE results were in reasonable agreement with the collapse load, followed by a slight over prediction in final stages of the collapse. This over-prediction is due to the material stress-strain curve used in this study exhibiting an unusual 'material' strain

softening phenomenon that is characterised by a negative slope. This type of material behaviour cannot be accounted for in the bilinear material prediction model since it requires that the data points generate a slope greater than zero. Therefore, it is possible that the finite element model's ability to capture the 'material' strain softening phenomenon with sufficient accuracy is limited. Table 5-1 shows the comparison of experimental and predicted values of SEA and F. It can be seen that the percentage errors are within acceptable tolerances. From Table 5-1 and Figure 5-3, it is evident that a good correlation was achieved between the FE and experimental results.

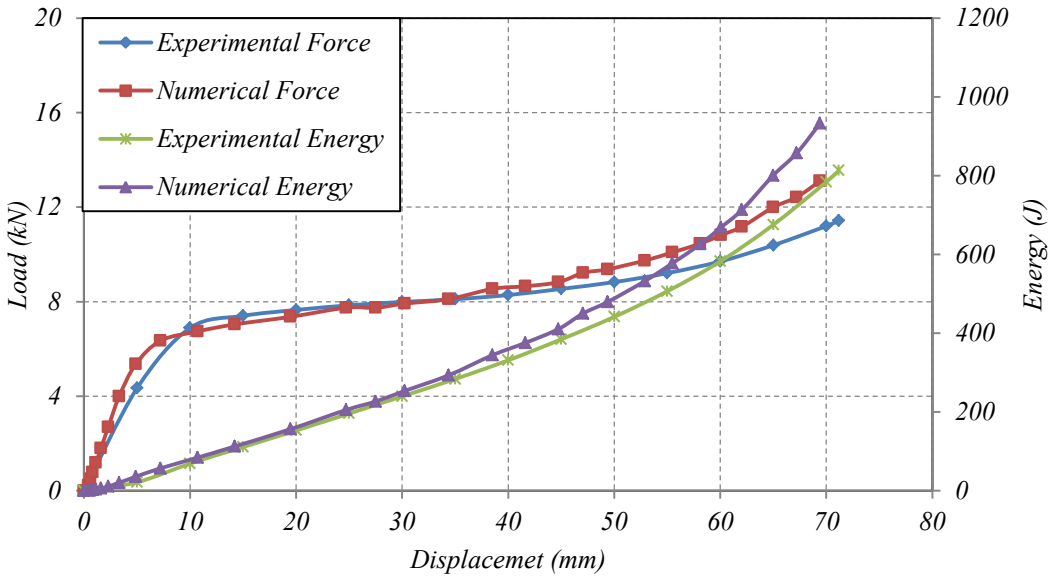

Figure 5-3: Comparison of FE & experimental results for a circular tube.

Table 5-1: Comparison of the FEA results with the Experimental results for a circular tube

	SEA[J/kg]	*F crush[kN]*
Experimental	1761.15	6.8
Numerical	1791	6.3
Error	1.7%	7%

The deformation modes of a circular tube under quasi-static lateral loading predicted by the FE code was in close correlation with that from the experimental testing, as shown in Figure 5-4. In general, the collapse mode of thin-walled tube under quasi-static lateral loading is plastic bending around plastic hinges.

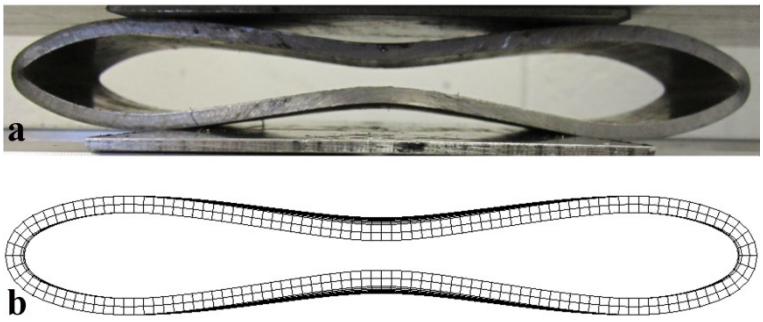

Figure 5-4: Comparison of (a) the experimental and (b) the numerical deformation mode of a circular tube.

Figure 5-5 , Figure 5-7, and Figure 5-9 depict the numerical and experimental comparison of circular tubes with various cross section shapes subjected to quasi-static lateral loading. It can be seen that the predicted results were accurate in terms of collapse load prediction, followed by a slight overestimation in the post-collapse stages. As mention earlier, this over-prediction is due to the softening behavior displayed by the material stress-strain curve, which could not be predicted by the FE model with sufficient accuracy. However, the FE results were very satisfactory and in close agreement with the results obtained from experiments. Also, it can be seen that the predicted final deformed shapes were very similar to those obtained by

experiments, as shown in figures (Figure 5-6, Figure 5-8 and Figure 5-10) and thus proving the validity of FE models.

For dynamic loading, the Figure 5-11 compares load-deflection curves obtained from the experimental testing with the FE simulations. The experimental results were obtained for an impact mass of 31.45 Kg and an impact velocity of V=4.5 m/sec. The slight oscillation in dynamic experimental response noticed at the beginning of collapse is probably due to the elastic effects. However, reasonable agreement between the curves was obtained.

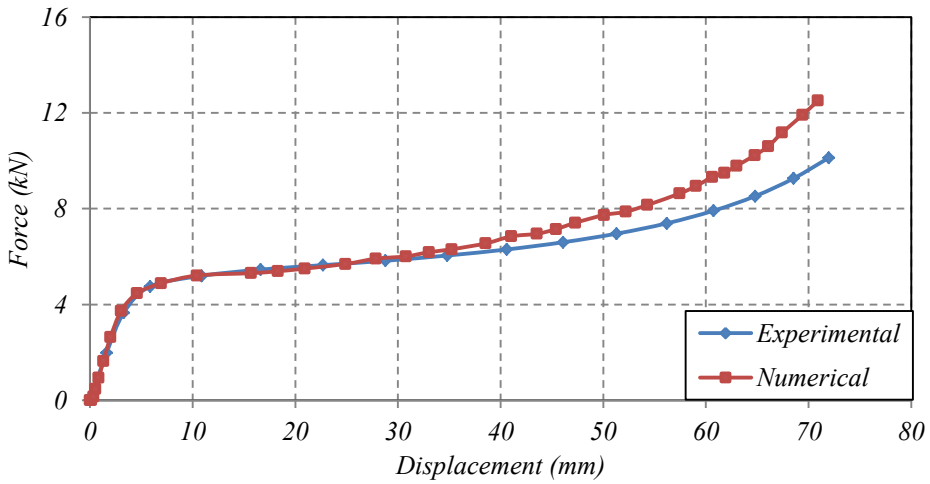

Figure 5-5: Comparison of FE & experimental results for a circular tube with L cross section.

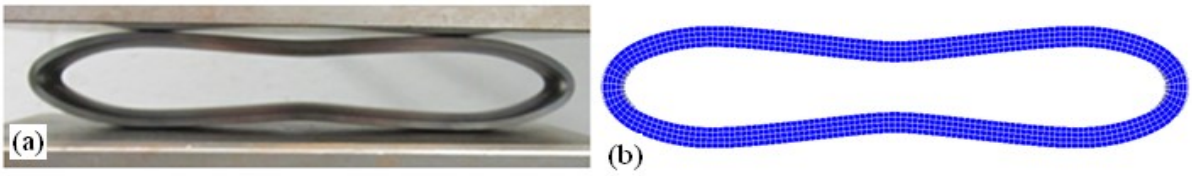

Figure 5-6: Comparison of (a) the experimental and (b) the numerical deformation mode of a circular tube with L cross section.

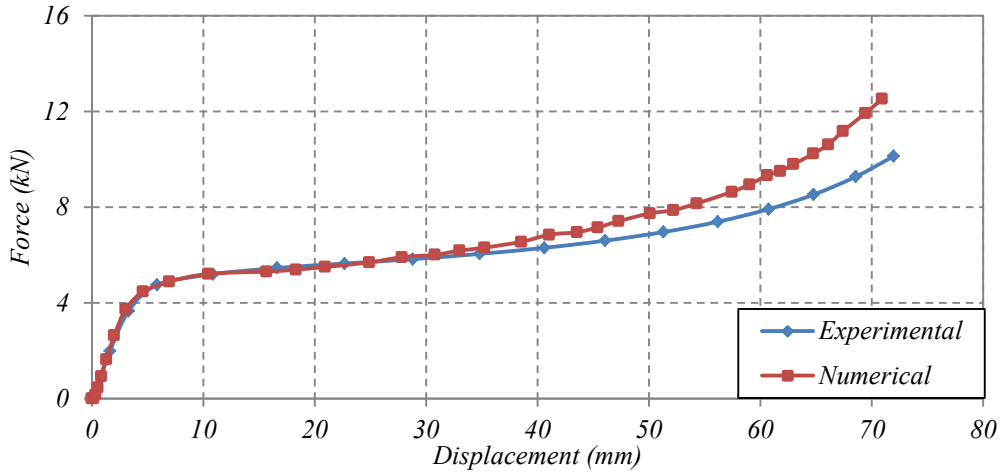

Figure 5-7: Comparison of FE & experimental results for a circular tube with T cross section.

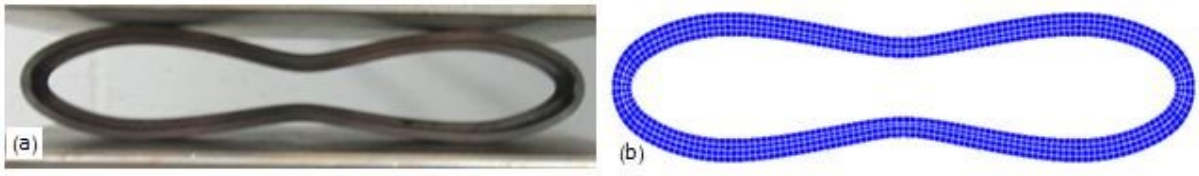

Figure 5-8: Comparison of (a) the experimental and (b) the numerical deformation mode of a circular tube with T cross section.

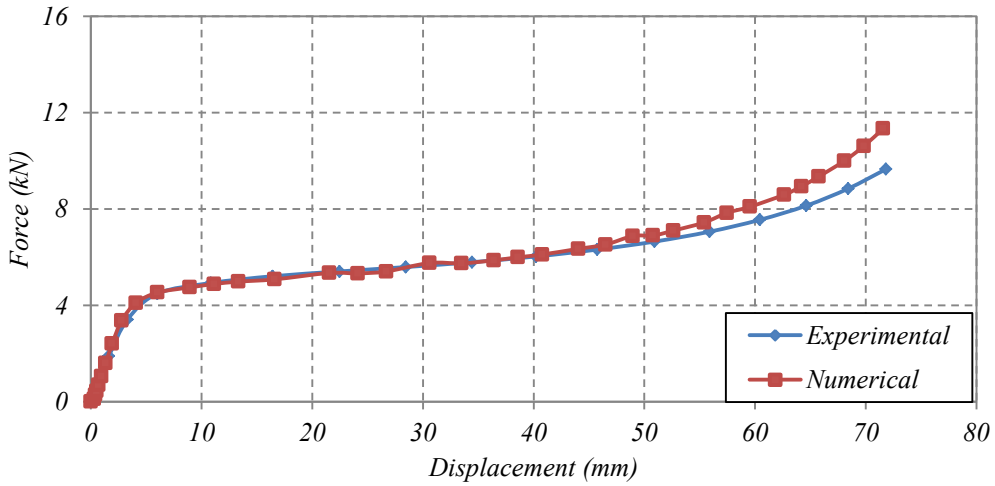

Figure 5-9: Comparison of FE & experimental results for a circular tube with U cross section.

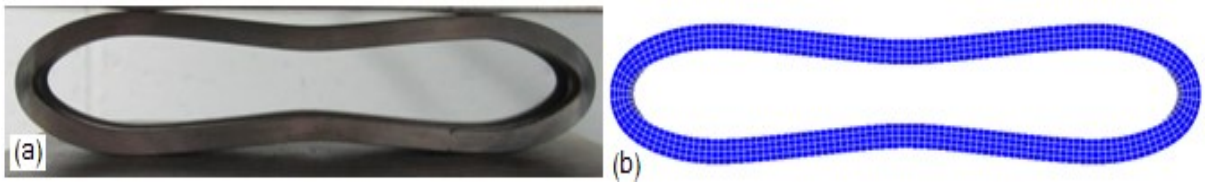

Figure 5-10: Comparison of (a) the experimental and (b) the numerical deformation mode of a circular tube with U cross section.

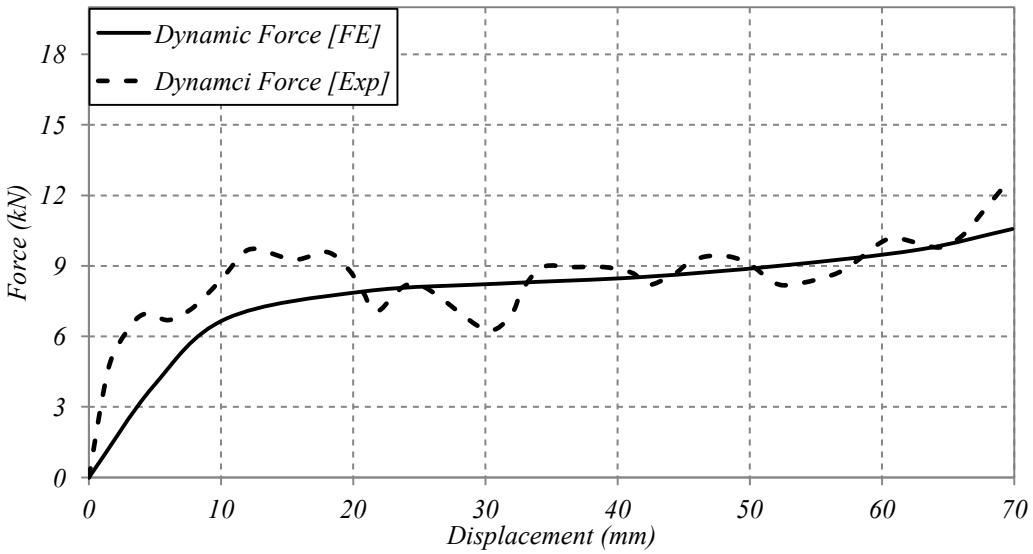

Figure 5-11: Comparison of FE & experimental results for a circular tube system under dynamic loading (V=4.5 m/sec).

5.2.2 Oblong tube

The profile of the oblong specimen was obtained by applying the same load and boundary condition as used in the experiments. A displacement of 40 mm was applied to a circular tube with an outer diameter of 101.6 mm, thickness of 3.25 mm, and width of 40 mm. Figure 5-12 shows the initial and final stages of tensile displacement. This newly formed oblong profile was then used as a finite element model for subsequent analysis.

Figure 5-13 shows the predicted and experimental force-deflection and energy-deflection curves for compression of an oblong tube under a flat indenter. It can be seen that the collapse load is in close agreement. This is indicative of the predicted

model being sufficiently accurate in capturing the position of the localised hinges. However, in the post collapse stages the predicted results tend to underestimate the force-deflection, followed by a slight over-estimation towards the end of the displacement stroke.

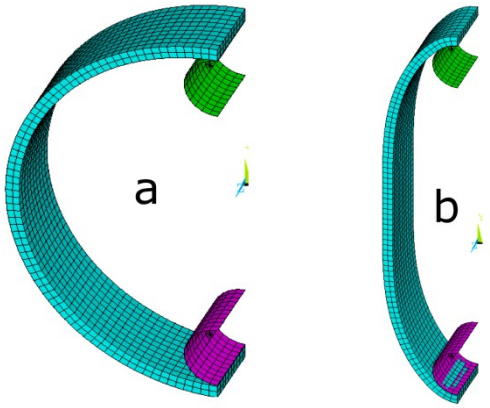

Figure 5-12: (a) Initial and (b) final deformed shape of the FE model.

The slight discrepancy may be due to a number of reasons. Firstly, recall that the oblong tube was prepared by subjecting it to tensile loads as outlined earlier. It is possible that the force deflection response is very sensitive to the final curvature of this profile. A slight difference between the profile used in the experiment, and that predicted by the finite element model, may result in differences during the post collapse stage of loading. In addition to the sensitivity of the oblong tube profile, the material strain softening phenomenon might be the reason for the slight discrepancy, particularly at the final stages of deformation as described in the previous section.

Table 5-2 shows a comparison of the FE results for the OTFIU system with the experimental results. From the comparison showed in Table 5-2 and Figure 5-13, it can be seen that all of the numerical results are in excellent agreement with the experimental results. This agreement indicated that the FE model was valid. The typical deformation mode of an oblong tube under quasi-static lateral loading was also reliably predicted by the FE simulation as displayed in Figure 5-14. The validity of the FE model is evident from this figure (Figure 5-14).

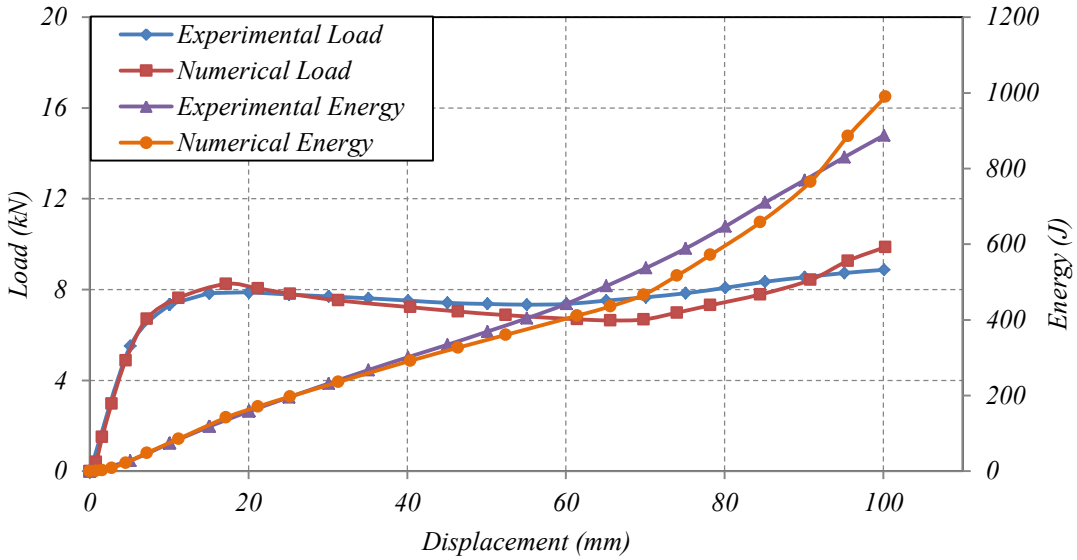

Figure 5-13: Comparison of FE & experimental results for an oblong tub

Table 5-2: Comparison of FE & experimental results for an oblong tube

	SEA (J/kg)	*F crush (kN)*
Experimental	*2326.17*	*8.25*
Numerical	*2256.01*	*8.3*
Error	*3%*	*0.60%*

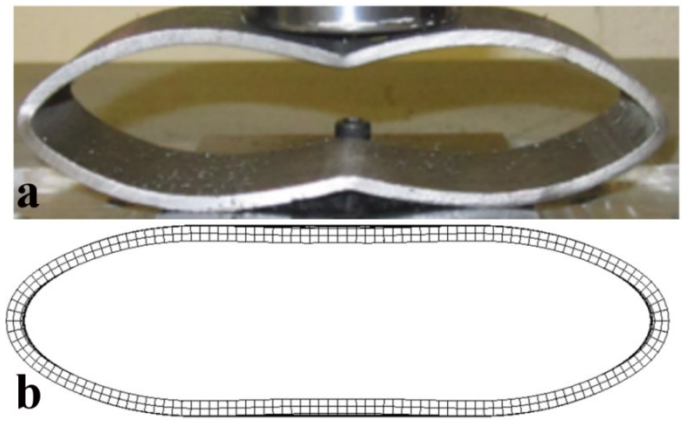

Figure 5-14: Comparison of (a) the experimental, and (b) the numerical deformation mode of an oblong tube.

5.2.3 Nested tube

The Figure 5-15 shows the quasi static load-deflection and energy-deflection curves of the NTSC system. Results showed reasonable agreement between the experimental results and the FE predictions. The Figure 5-16 compares the dynamic load-deflection for the NTSC under dynamic loading. The response in Figure 5-16 corresponds to an impact velocity, *V,* of 4.5 m/s and an impact mass, *M,* of 31.45 kg. As noticed in the quasi-static case, a close correlation was also observed for the dynamic loading case. By comparing the results under quasi-static and dynamic loadings, it can be seen that similar responses were obtained under both loading conditions. This is evidence of the negligible effects of the strain rate sensitivity and inertia at the applied velocity. It is worth noting the ability of the FE model to predict these insignificant effects of dynamic loading on the responses of nested systems.

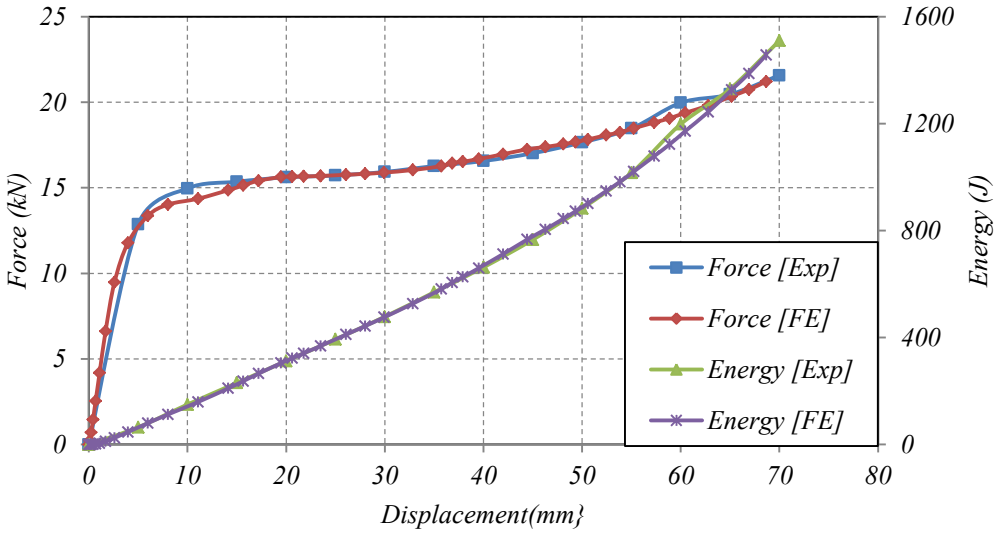

Figure 5-15: Comparison of FE & experimental results for a nested tube system under quasi-static loading.

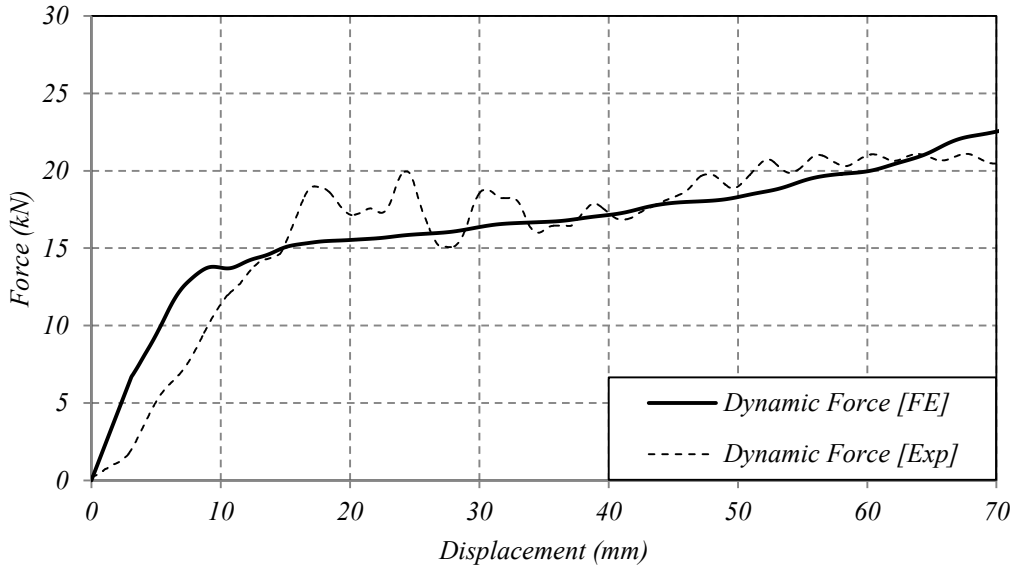

Figure 5-16: Comparison of FE & experimental results for a nested tube system under dynamic loading (V=4.5 m/sec).

Of interest for validating simulation results is the deformation mode predicted by the FE code. The deformation modes predicted by the FE code were compared with those from the experiments, as displayed in Figure 5-17. The prediction given by the FE results for the deformation was excellent. This also supports the validity of the numerical model.

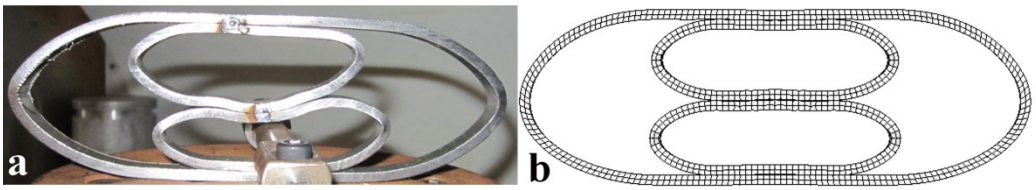

Figure 5-17: Comparison of (a) the experimental and (b) the numerical deformation mode of nested tubes.

Overall, the FE results were in excellent agreement with the experimental results for the lateral collapsing of empty and nested tubes under various loading conditions.

5.3 Summary

This chapter detailed the development and validation of finite element models for the lateral collapse of single and nested tubes under both quasi-static and dynamic loading conditions. The numerical results of finite elements models were validated by using experimental techniques. The results of the models were in good agreement with the experimental results, which means that the models were able to predict the behaviour of various tubes under various loading conditions with sufficient accuracy. The validated numerical models can therefore be used, along with response surface methodology (RSM), to perform parametric analysis on the lateral collapse of various tubes with a variety of geometrical parameters such as thickness diameter and width, as will be demonstrated later in Chapter 6. In addition to parametric analysis, the validated FE model under dynamic loading can be used to predict the behaviour of energy absorbers under high impact velocity which cannot be obtained experimentally, as will be addressed in Chapter 6 and Chapter 7.

6

Chapter 6

RESPONSES OF SINGLE TUBES UNDER LATERAL LOADING

6.1 Circular tubes

Circular tubes crushed laterally have been used by many researchers as energy absorbing components. The energy absorption responses of circular tubes are significantly affected by their geometrical factors. In this chapter, an attempt is made to investigate the effect of these geometrical factors on the responses of circular tubes under lateral loading.

6.1.1 Effect of cross section shape

6.1.1.1 Theoretical Analysis

The collapse load (F) for the lateral compression of a circular tube with rectangular cross section shape was derived by DeRuntz and Hodge [66]

$$F = \frac{2Yt^2W}{D} \qquad (6\text{-}1)$$

Where Y is the yield stress, t, W, and D are the thickness, width, and diameter respectively of the tube, as shown in Figure 6-1

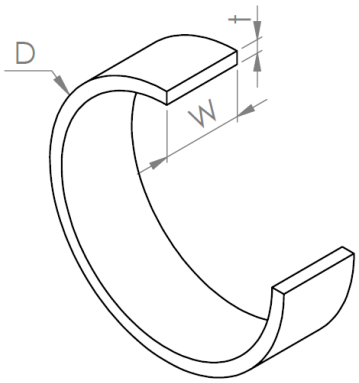

Figure 6-1: Section of a circular tube.

The cross-sectional properties of a rectangular shape are determined by the expressions:

$$I = \frac{t^3 \times W}{12} \qquad (6\text{-}2)$$

$$A = \mathrm{t} \times \mathrm{W} \qquad (6\text{-}3)$$

Where I is the second moment of area (area moment of inertia) around the x-x axis, A is the cross sectional area, t is the thickness of the tube, and W is the width of the tube.

Combining equations (6-1), (6-2) and (6-3), the collapse load is given by

$$F_o = \frac{24YW}{D} \times \frac{I}{A} \qquad (6\text{-}4)$$

It can be seen from equation (6-4) that the collapse load can be controlled by the cross-sectional properties. The cross-sectional shape with the higher I/A ratio can absorb more energy due to its higher collapse load.

Redwood [67] proposed an equation (6-5) in order to include the strain hardening effects in his theoretical prediction for the response of the lateral compression of a circular tube:

$$M = M_p + E_p k \times I \qquad (6\text{-}5)$$

Where I is the second moment of area, E_p is the strain-hardening modulus of the assumed rigid-linear hardening material, k is the average curvature of the deformed length, M is the collapse moment in the post-collapse stage, and M_p is the initial collapse moment.

It is clear from the equation (6-5) that the strain hardening effect is greater in a tube with a higher area moment of inertia.

6.1.1.2 Experimental and numerical responses of circular tubes with different cross sections shapes under lateral loading

Figure 6-2 and Figure 6-3 show the force-deflection and energy-deflection responses of circular tubes with three different cross sectional shapes. The tubes with various shapes of the cross section were machined from tubes with rectangle cross section using a lathe machine. The tubes were crushed laterally between flat plate indenters. The details of tubes geometry and dimensions of the cross sections are as displayed in Table 4-4. Although the circular tubes have different cross sectional shapes, the responses under lateral compression are similar. It was observed that the force increases rapidly up to its characteristic 'collapse' load, followed by strain hardening behaviour in the post collapse stages. The values of the collapse load in the three tubes are somewhat different. The L cross-section offered the higher collapse load comparing to the T and U cross sections. This is due to its higher I/A value. As the tubes with T and U cross sections have the same I/A ratio, their responses are almost the same. It seemed that the post-collapse responses of all tubes were not affected very much by the cross sectional shapes. According to the theoretical analysis, the strain hardening effect should have been increased in the tube with a higher value of the area moment of inertia. But, in this study the effect of the cross sectional shapes was not very clear as the values for I were very similar for all tubes.

Figure 6-4 depicts the initial and final stages of deformation of circular tubes with different cross sections under quasi-static loads. Similar deformation modes are noticed for various tubes.

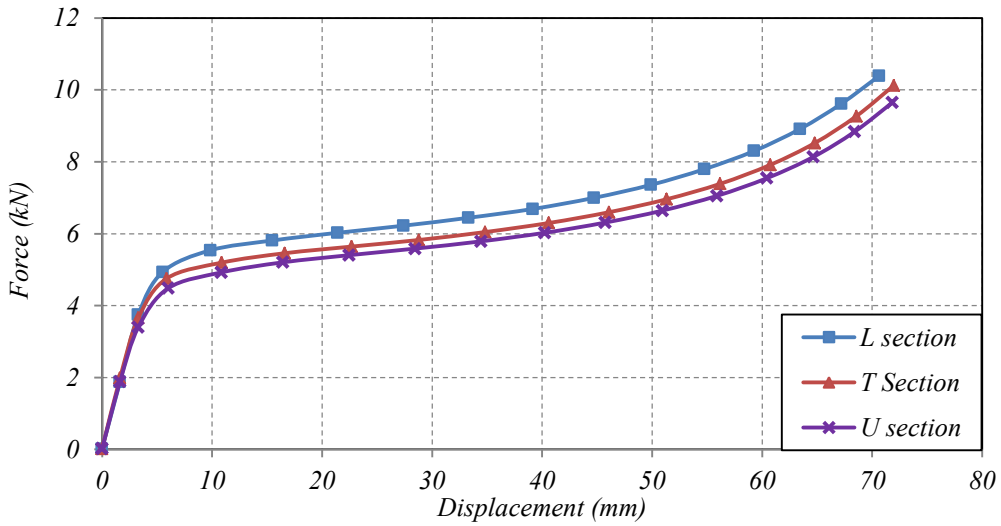

Figure 6-2: The experimental force- deflection responses of L, T, and U cross section circular tubes.

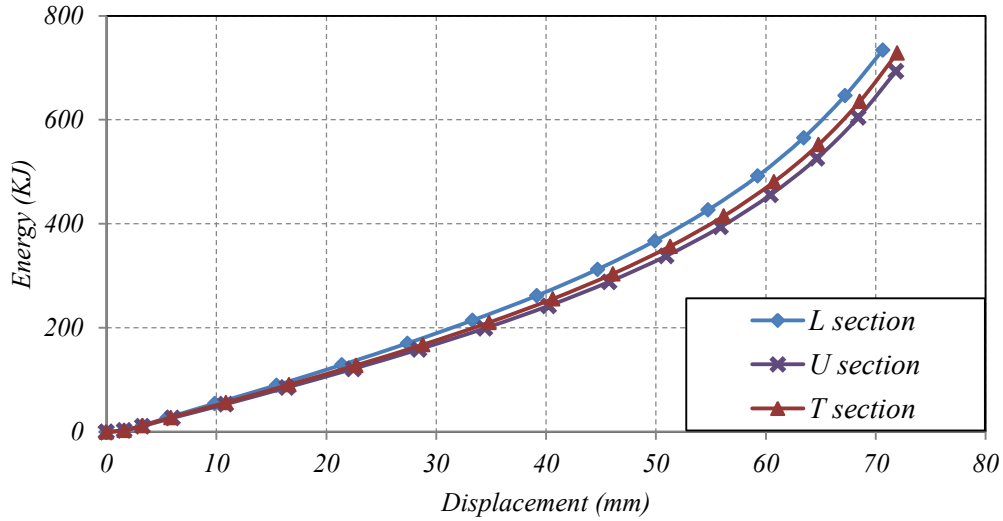

Figure 6-3: The experimental energy- deflection responses of L, T, and U cross section circular tubes.

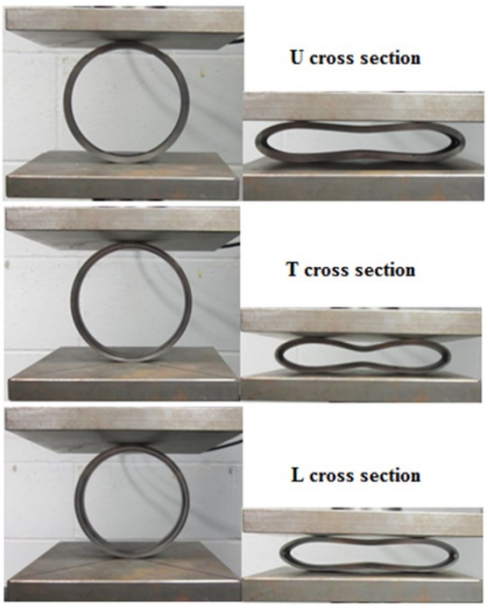

Figure 6-4: Initial and final stages of deflection for circular tubes with different cross sectional shapes under quasi-static loading condition.

Based on the validated FE model as presented in section 5.2.1, another cross sectional shape was investigated numerically, namely the I-section. The I-section was selected because its cross-sectional properties gave the highest second moment of inertia with respect to area. Figure 6-5 plots the load-deflection curves for the lateral compression of tubes with different cross-sectional shapes. As predicted, the I cross-section offered the higher value of collapse load due to its higher value of the area moment of inertia. The effect of the second moment of area in the post-collapse stages was not clear in this study, as their values were very similar. An additional numerical investigation was carried out in order to confirm the results and to allow these to be included in the conclusions of this study. A circular tube with a rectangular cross section was modelled and studied using ANSYS. The dimensions of the cross section were selected in order to produce a lower ratio. It can be seen from Figure 6-5 that the rectangular cross-section offered a lower collapse load. This observation was found to be consistent with the theoretical analysis.

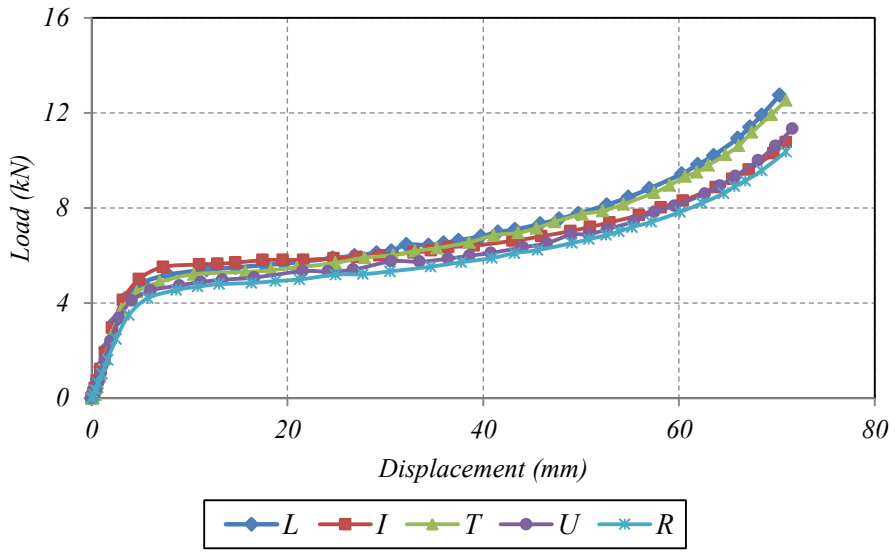

Figure 6-5: The numerical force-deflection responses of L, T, U, I, and R cross sectional circular tubes.

Table 6-1 presents the indicators (SEA, e_g, e_E and W_{eff}) for the various tubes.
It can be seen that all of the tubes have the same value of e_g, as all were compressed up to 70% of the tube diameter. The I-section offered the higher values of efficiencies due to its force-deflection response and its cross sectional properties that provided the higher value of I/A ratio.

Table 6-1: Comparison of effectiveness indicators for CT with various longitudinal cross sections.

	L	*T*	*U*	*I*	*R*
SEA	2754.48	2886.60	2679.87	2892.78	2468.61
e_g	70	70	70	70	70
e_E	40.7	38.5	43	48	46
W_{eff}	1928.13	2020.62	1875.91	2024.95	1728.03

Overall, the range in the dimensions of the longitudinal cross section was limited in the thin-walled short length circular tubes, as it appeared that it was not worth

modifying the cross-sections as it only resulted in very slight variations in responses. Changing the other geometric dimensions such as diameter, thickness, and width had a greater effect. Therefore, the effects of these parameters on the energy absorption responses will be further investigated in the following section. Response surface methodology (RSM) of the design of experiment (DOE) approach was adopted to examine the effect of geometrical parameters (i.e. diameter, thickness, and width) on the energy absorption responses.

6.1.2 Development and validation of Response Surface (RS) models for a CTFIU system

The energy absorption behaviour of the structures under various loading conditions is one of highly nonlinear mechanics problems, for the responses of which it is very complicated to establish mathematical relationships. The surrogate model method, such as RS models, was found to be very effective to relate the energy absorption responses to the different design variables such as geometrical, material and loading parameters. The advantage of employing the (RSM) as an analysis and optimization tool in the field of energy absorption systems is that the energy absorbing behaviour of a structure in a certain design space can be identified through performing a limited number of experiments (numerical simulations) at the sampling design points of the design space. The sampling design points are determined by using one of the many design of experiments (DOE) techniques. The experiments can be by means of physical tests (real test), or numerical simulations based on validated FE model.

In this section, An integration of Finite Element Modelling (FEM) and the Response Surface Method (RSM) for the Design of Experiment (DOE) was utilized to model the relationship between the energy absorption responses (specific energy absorbed (SEA) and collapse load (F)) and the geometrical parameters of the tube (diameter, width, and thickness) within a certain range of these geometrical parameters (specific design space). The statistical software package, Design-Expert 8, was used to create the sampling design points and to apply RSM on the results of the numerical model described and validated earlier in section 5.1.1 and section 5.2.1 respectively. The models developed in this section are useful formulations which relate the SEA and F to the geometrical parameters. These models allow prediction of the energy absorption

responses of laterally crushed tubes, based on their geometry parameters. In addition, the formulations can provide engineering designers with an initial estimate of the energy absorption responses for a thin walled tube of given dimensions. Also, the formulations provide a guide as to which parameters have the most influence on the energy absorption responses. Furthermore, the RS models can be used for structural optimization after verifying their accuracy, as will be shown in section 6.1.4. Figure 6-6 displays the flow chart which explains the steps for constructing the RS models.

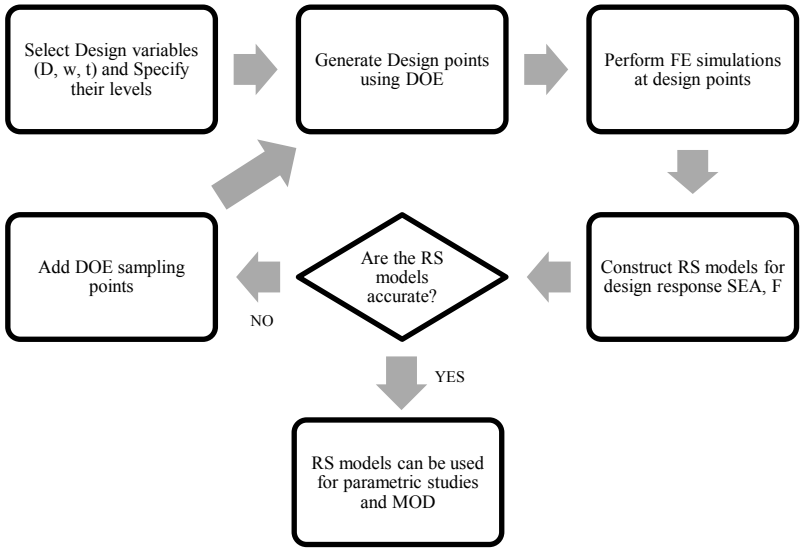

Figure 6-6: Flow chart showing the steps of creating the RS models.

6.1.2.1 Sampling design points

Different methods were offered by Design-Expert to construct the sampling design points such as factorial, Box–Behnken, composite, D-optimal, etc. In this study, the sampling design points were created based on a three level Box–Behnken design with full replication. A presentation of Box–Behnken design and its advantages was introduced in section 3.2. The independent variables used in this design were as follows: tube width (W) ranged between 10 and 60 mm, tube outer diameter (D) between 80 and 130 mm, and tube thickness (t) between 2.5 and 6 mm. Table 6-2 shows the geometrical variables and experimental design values used. The dimensions were chosen to cover the typical range of tube sizes commonly used in crashworthiness applications. The specific energy absorbed (SEA) and collapse load (F) were selected as the design responses. Detailed FE models were created for the

circular tubes representing the sampling design points. Numerical simulations were performed for the different combinations of independent variables determined through design of experiment (DOE). The energy absorption responses (SEA and F) were measured for each combination of geometrical factors. The different combinations of design variables with corresponding design responses are tabulated in Table 6-3.

6.1.2.2 Accuracy evaluation of the RS models

A step-wise regression method was used to fit the polynomial equation (RS model) to the numerical result (obtained from validated FE models) and to identify the relevant model terms. This method (step-wise regression method) is recommended because it eliminates the insignificant model terms automatically from the polynomial equation. The statistical significance of the developed models and each term in the regression equation were inspected using statistical measures to achieve the best fit. From the analysis the measured responses by the Design-expert software, the summary output of best fit indicates that linear and quadratic models are statistically recommended for the specific energy absorption (SEA) and collapse load (F) respectively. The Analysis of variance (ANOVA) methodology was employed by the software to check the adequacy of the developed models. The ANOVA tables summarise the analysis of variance for each response, and show the significant model terms and the adequacy measures. The adequacy measures are the sequential F-test (Model F-value), probability (Model P-value), coefficient of determination R2, Adjusted R2, Predicted R2, and Adequate precision. Detailed explanations and definitions of each of these terms were presented earlier in section 3.2. Table 6-4 displays the analysis of variance (ANOVA) results generated by the Reduced Linear Model of the SEA response. The model F value of 36.59 indicated that the model was significant. A p-value of 0.0001 suggested that there was a low chance that the F value could occur due to noise in this model. The predicted R2 of 0.7463 is in reasonable agreement with the adjusted R2 of 0.8165. The adequate precision was found to be 45.12 indicating an adequate signal. This means that this model can be used to navigate the design space.

Table 6-2: Independent variables and experimental design levels that were used (CTFIU)

Variable	*Code*	*-1*	*0*	*1*
Diameter(mm)	A	80	105	130
Width(mm)	B	10	35	60
Thickness(mm)	C	2.5	4.25	6

Table 6-3: The design matrix (CTFIU).

Exp no	*D(mm)*	*W(mm)*	*t(mm)*	*SEA (J/kg)*	*F (kN)*
1	105	4.25	35	2479.676	9
2	105	4.25	35	2479.676	9
3	130	2.5	35	983.6662	2.6
4	105	4.25	35	2479.676	9
5	105	4.25	35	2479.676	9
6	105	2.5	10	1192.236	0.82
7	80	4.25	60	3567.553	21
8	130	4.25	10	3606.76	1.9
9	105	6	60	3944.481	33
10	130	6	35	2885.621	14
11	105	6	10	3558.28	5.2
12	80	2.5	35	1819.339	4
13	80	4.25	10	3345.156	3.4
14	130	4.25	60	1945.13	12
15	80	6	35	5591.202	24
16	105	4.25	35	2479.676	9
17	105	2.5	60	1277.148	5

The analysis of variance indicated that the following terms are the most significant ones that were associated with the specific energy absorbed:

The first order effect of thickness (t) and diameter (D).

The final mathematical models in terms of actual factors as determined by the design expert software are shown in Table 6-4. The F values of the design variables shown in the ANOVA table (Table 6-4) can be used to indicate the order of the influence of the factors on the resultant SEA. It can be seen that the thickness (t) was the most influential factor with the highest F- value of 61.8.

Table 6-4: Analysis of variance (ANOVA) table for SEA – Reduced Linear Model (CTFIU)

Source	*Sum of Squares*	*Mean Square*	*F Value*	*p-value*
Model	1683.86	841.93	36.59	< 0.0001
A-Diameter	261.67	261.67	11.37	0.0046
C-Thickness	1422.19	1422.19	61.80	< 0.0001
Residual	322.16	23.01		
Cor Total	2006.02			
		Final equation obtained from the mode for SEA		
R-Squared	0.8394	*Sqrt(SEA) =+42.57734-0.22877*Diameter +7.61897* Thickness*		
Adj R-Squared	0.8165			
Pred R-Squared	0.7463			
Adeq Precision	18.909			

The resulting ANOVA table (Table 6-5) for the Quadratic Model of response F was constructed. The model F value of 7096.57 indicates that this model is significant. The p-value of 0.0001 suggests that there is only 0.01% chance that the F value could occur due to noise. The "Pred R-Squared" of 0.9982 is in excellent agreement with the "Adj R-Squared" of 0.9997. High R^2 values suggest that there is a statistically significance correlation between the factors and the response. The

adequate precision ratio was found to be 311.457, which is significantly higher that the significance threshold level of 4. This means that the model had very little noise, therefore it can be used to navigate the design space. The ANOVA table shows p-values less than 0.05 for all model terms. Such low p-values highlight the significance of these factors and their interactions. The most significant terms associated with collapse load (F) were as follow:

1. The first order effect of tube diameter (D), tube thickness (t) and tube width (W).
2. The second order effect of tube thickness (t), tube width (W), and tube diameter (D).
3. The two level of interaction effects between the tube thickness and the tube width (t-w), the diameter and t (D-t), the diameter and width (D-W). Resulting F can be modelled by the final equation produced by the model given in Table 6-5.

Order of factor influence on collapse load (F) can be established through comparing the F-values magnitudes (Table 6-5) as follows: $B>A>C>BC>C^2>AB>AC>A^2>B^2$.

6.1.2.3 Validation of RS models

Figure 6-7 and Figure 6-8 show the relationship between the actual and predicted values of the specific energy absorbed and the collapse force, respectively. These figures indicate that the developed RS models are adequate, as the residuals in the prediction for each response are small since the residuals tend to be close to the diagonal line.

Furthermore, to verify the adequacy of the RS models, a comparison between the numerical, experimental, and predicted responses has been performed. Using the point prediction option in the DOE software, the specific energy absorbed and the collapse load of the validation experiments were predicted using the previously developed models. Table 6-6 summarises the experimental condition, actual values, numerical values, predicted values, and the percentage error. It can be seen that all the percentage errors are within acceptable tolerances, thus indicating that the RS models were valid.

Table 6-5: Analysis of variance (ANOVA) table for F–Quadratic model (CTFIU)

Source	*Sum of Squares*	*Mean Square*	*F-value*	*p-value*
Model	26.68	2.96	7096.57	< 0.0001
A-Diameter	1.22	1.22	2928.97	< 0.0001
B-Width	12.28	12.28	29391.60	< 0.0001
C-Thickness	11.57	11.57	27683.08	< 0.0001
AB	0.15	0.15	354.57	< 0.0001
AC	0.11	0.11	255.13	< 0.0001
BC	1.14	1.14	2724.17	0.0015
A^2	8.317E-003	8.317E-003	19.91	0.0029
B^2	1.492E-003	1.492E-003	3.57	0.1007
C^2	0.22	0.22	520.21	< 0.0001
Residual	2.925E-003	4.178E-004		
Cor Total	26.69			
		Final equation obtained from the model for F		
R-Squared	0.9999	*Sqrt(F)= -0.70896-2.74166E-003*Diameter+ 0.049148*Width+0.69084*Thickness -4.39871E-003*Diameter*Thickness +0.012192*Width*Thickness -2.61188E-004Diameter*Width +7.11119E-005*Diameter^2 -3.63515E-004*Width^2 +6.14765E-003* Thick^2*		
Adj R-Squared	0.9997			
Pred R-Squared	0.9982			
Adeq Precision	311.457			

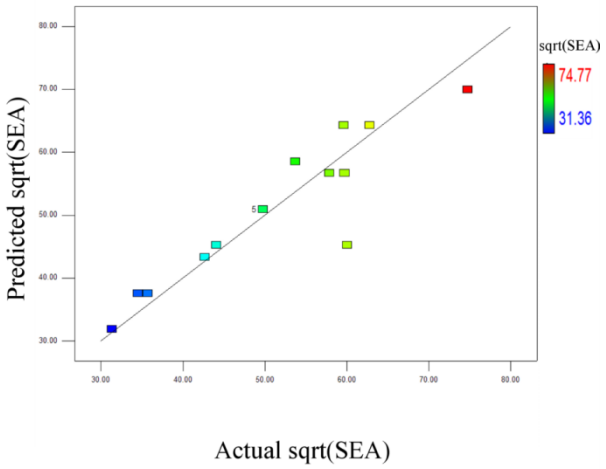

Figure 6-7: Scatter diagram of SEA (CTFIU).

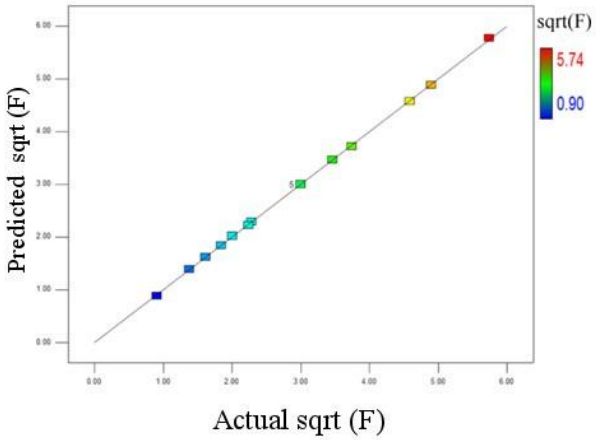

Figure 6-8: Scatter diagram of F (CTFIU).

Table 6-6: Confirmation experiment (CTFIU).

D(mm)	*t (mm)*	*w(mm)*		*SEA (J/kg)*	*F (kN)*
101.6	3.25	40	*Experimental*	1761.15	6.8
			Numerical (FEM)	1791	6.3
			Error (%)	1.7%	0.60%
			Predicted (RSM)	1944.5	6.31
			Error (%)	8.5%	0.15%

The essential design information for thin-walled tubes used as energy absorbing structures can be obtained through performing a parametric study. To this end, the RS models were employed to study the effects of geometrical parameters on the energy absorption responses of circular tubes, as will be presented in the next section.

6.1.3 Parametric study

6.1.3.1 Effect of geometrical factors on SEA response

The perturbation plot of SEA shown in Figure 6-9 indicates that SEA depended mainly on the thickness and the diameter of the tube. The perturbation plot provides the possibility to compare the effect of all of the factors at a particular point in the design space. Due to use of the step-wise regression method, the insignificant effect of the width on the SEA has been eliminated by the software package. Figure 6-10 shows the effect of tube diameter (D) on the SEA. It is seen that the SEA decreases as the tube diameter increase. In spite of increasing the displacement stroke in the larger tubes, the SEA decreased in these tubes. This behaviour is probably due to the deformation mode of circular tube under lateral loading, which is plastic bending around plastic hinges. Because of the strain localization around the plastic hinges, the larger tubes have a smaller relative volume of material subjected to plastic deformation. In addition, the weight of larger tubes is more than that of smaller tubes. Consequently, the energy absorbed per unit mass (SEA) was less in the larger

tubes. A similar effect of the tube diameter on the SEA of circular tubes was noticed by Gupta et al [70].

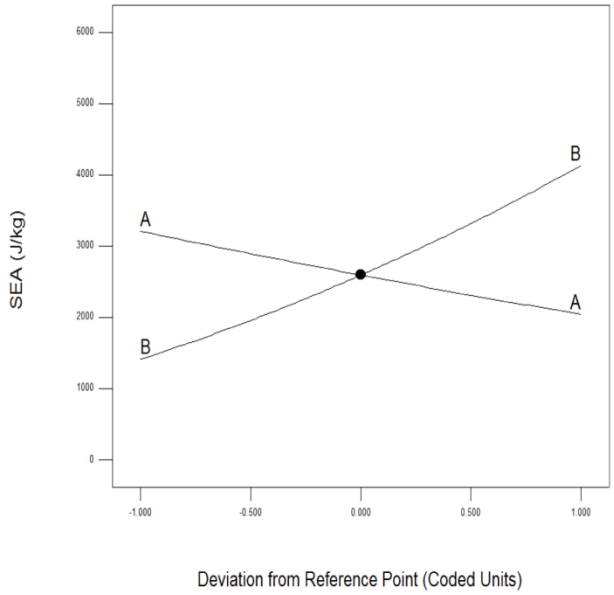

Figure 6-9: Perturbation plot of SEA (CTFIU)

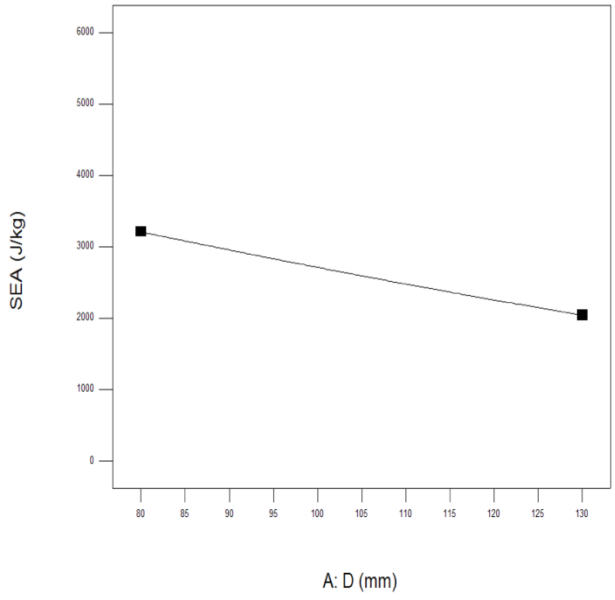

Figure 6-10: Effect of D on SEA (CTFIU)

Figure 6-11 displays the effect of tube thickness on the SEA. It can be seen that the thickness had a significant effect on the SEA and the latter increased as the thickness

increased. This trend is due to thicker tubes having more material available for plastic deformation.

Figure 6-12 shows the variation of the SEA with diameter and thickness, it can be seen that the maximum SEA that could be obtained was with a tube with minimum diameter and maximum thickness.

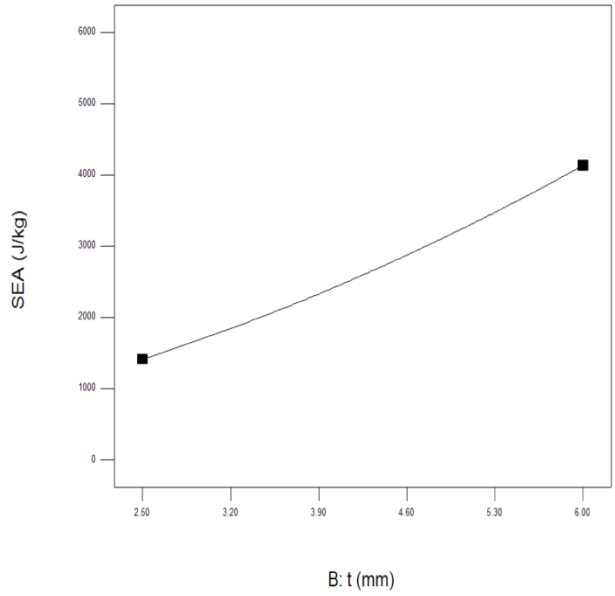

Figure 6-11: Effect of t on SEA (CTFIU).

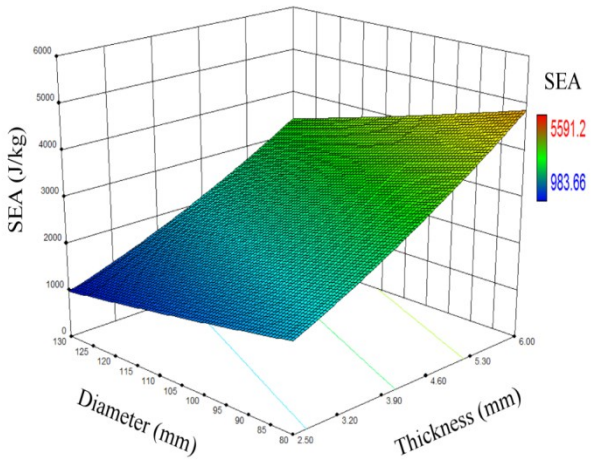

Figure 6-12: Variation of SEA with D & t (CTFIU).

6.1.3.2 Effect of geometrical factors on F response

The effect of tube diameter on crush force is shown in in Figure 6-13 and Figure 6-14. It can be seen that the crush force decreased as the tube diameter increased. Increasing the tube diameter leads to a decrease in the stiffness of the tube structure, so larger tubes have lower reaction forces. A similar phenomenon was observed by [66] and [70]. It is clear from Figure 6-13 and Figure 6-14 that the thinner and shorter tubes were less influenced by tube diameter as the crush force remained reasonably constant. From the same figures, it can be seen that the crush force increased with increasing thickness and width. The rate of increase of crush load with thickness and width, decreased with increasing tube diameter. Figure 6-15 presents the interaction effects of thickness and width on the crush force. It is obvious that the wall thickness had more influence on the crush force as the width increased. Therefore, the wall thickness was more effective for controlling the crush force of wider tubes. In general, the increase in the collapse load with increasing tube thickness and width is due to the greater amount of material across the section of the tube, which effectively increased the lateral stiffness of the tube and hence it required a greater load to initiate the collapse.

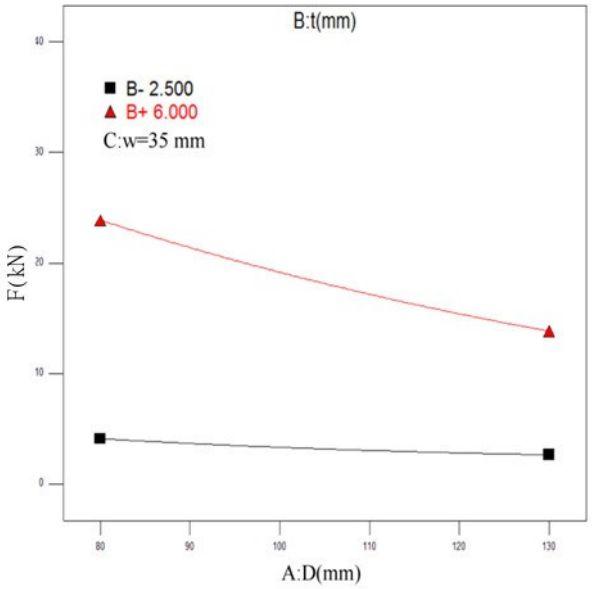

Figure 6-13: Interaction effects of D and t on F (CTFIU).

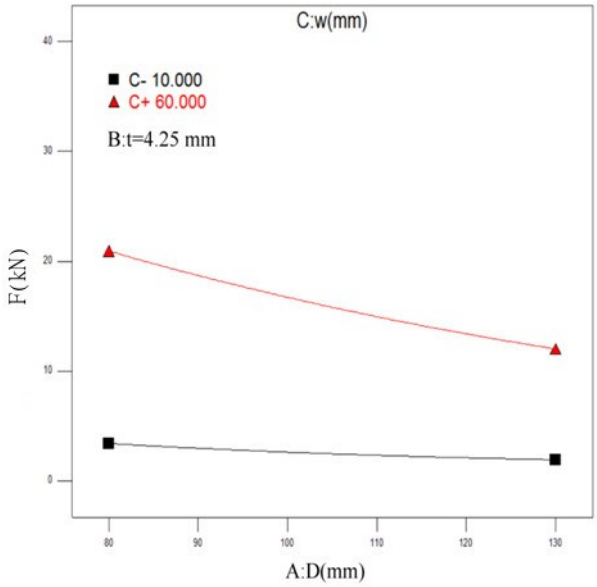

Figure 6-14: Interaction effect D and W on F (CTFIU).

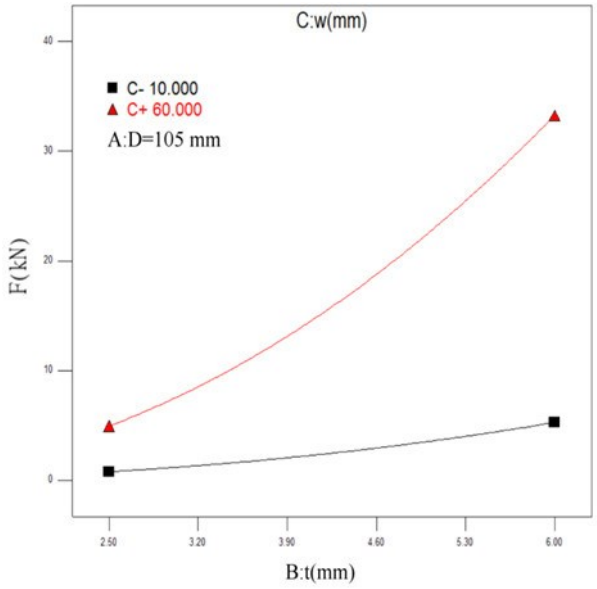

Figure 6-15: Interaction effect of t and W on F (CTFIU).

Figure 6-16 shows the variation of F with thickness and width, indicating that a minimum crush force was obtained in the tubes that had a minimum width and thickness.

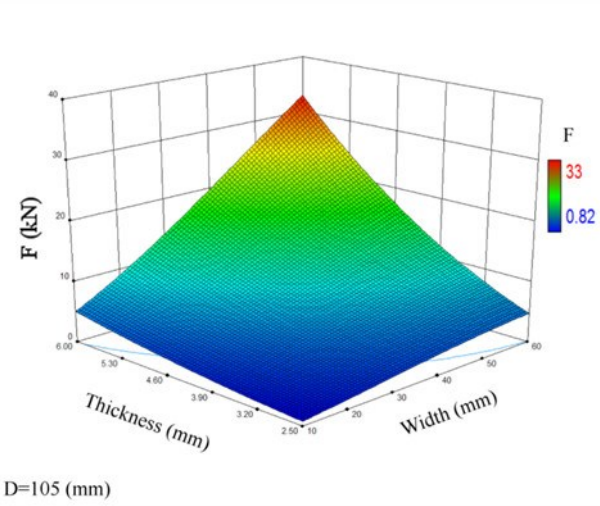

Figure 6-16: Variation of F with W and t (CTFIU).

6.1.4 Multi-objective optimization design (MOD) of the CTFIU system

As an energy absorbing structure, the circular tube should absorb as much energy as possible per unit mass. So the SEA was chosen as the first objective and maximized in the crashworthiness optimization evaluations. A designer of energy absorbing devices should be confident that the absorber doesn't transmit too much force to the other parts of the structure and doesn't cause high decelerations of the occupants in the structure, particularly at the beginning of the impact event. To this end, the collapse load was taken as another objective and was minimized. The multi-objective optimization design (MOD) is aimed at achieving the maximum SEA and to minimize the value of the collapse load (F). Due to the high computational cost of crash simulation, the FE modelling cannot be used directly to solve the MOD problem as it would require hundreds of performance evaluations. The surrogate models such as RS models are used widely in lieu of nonlinear FEA to solve the MOD problem for fast iteration. So, A multi-objective design can be drawn up based on the RS models constructed in section 06.1.2. These RS models describe the effects of geometrical factors on the SEA & F responses of circular tube compressed by flat plates. The Design-Expert software, which employs the desirability approach as an optimization algorithm, was used to solve the MOD problems. A full

description of the desirability approach was introduced earlier in section 3.4. The values of diameter D, thickness t, and width W were set to vary in order to seek the optimal configuration of the tube. As it is important that the energy absorbing components achieve a higher SEA, a value of 10 was assigned to weight the SEA response. Table 6-7 shows the responses and the variables constraints of the optimization criteria.

Table 6-7: The criterion of numerical optimization (CTFIU).

Name	*Goal*	*lower Limit*	*Upper Limit*	*Weight*	*Importance*
D (mm)	is in range	80	130	1	3
t (mm)	is in range	2.5	6	1	3
W (mm)	is in range	10	60	1	3
SEA (J/kg)	maximize	983.67	5591.2	10	5
F (kN)	minimize	0.82	33	1	3

Table 6-8 shows the geometrical values which led to a maximum specific energy absorbing capacity while minimizing the crush force. It can be seen that the greatest desirability was offered by the tube with D=80 mm, t=6 mm, and W=10mm. Therefore, a multi-objective optimization tube design can be obtained if the tube has a minimum width, a minimum diameter, and a maximum thickness. It is interesting to note also that the optimal solution occurred at the extremities of the design variables. A numerical FE simulation was carried out to validate the optimized results obtained by the DOE. The comparisons between the predicted and the numerical results are presented in Table 6-9. The responses and geometry of the optimal configuration are also listed in Table 6-9. It can be seen that the percentage error is within the acceptable range, therefore the optimized results are valid.

Table 6-8: Optimal solutions as obtained by Design-Expert (CTFIU).

Number	*Diameter (mm)*	*Thickness (mm)*	*Width (mm)*	*SEA (J/kg)*	*F (kN)*	*Desirability*
1	80	6.00	10.00	4899	7.6149	0.330528
2	80.0005	6.00	10.41	4899	7.82992	0.329473
3	80	6.00	10.67	4898	7.96334	0.328748
4	80	6.00	11.21	4898	8.25337	0.327339
5	80.0003	6.00	13.15	4899	9.31554	0.322045

Table 6-9: Confirmation experiment of optimal solution (CTFIU).

	SEA[J/kg]	*F[kN]*
Numerical (FE)	5300	7.6
Predicted (RSM)	4899	7.61
Error	8%	0%
Geometry	*Force and Energy Responses of optimal configuration*	
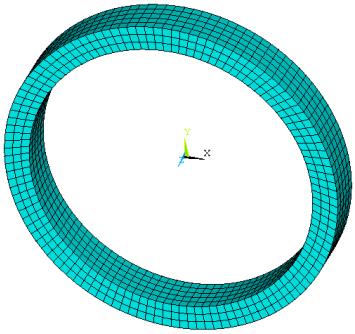	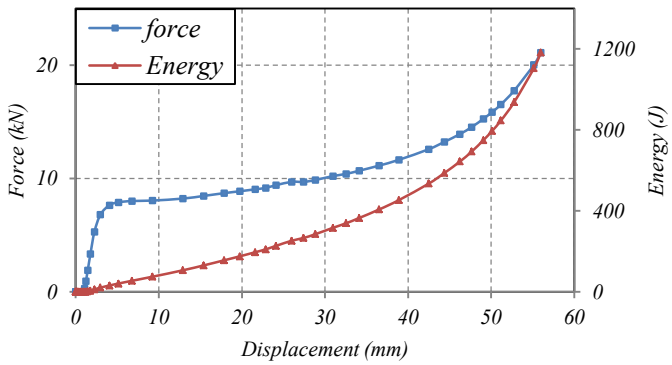	

As a practical implication, the main outcomes of the parametric and optimization studies for design purposes are drawn as follows.

(1) The specific energy absorption capacity (SEA) for the circular tubes can be controlled using the tube thickness and diameter. However, the tube thickness has more influence on this response parameter than the tube diameter.
(2) The collapse load (F) increases with increasing thickness, increasing width, and decreasing diameter. Also, the collapse load can be more effectively controlled using the thickness in wider and smaller tubes
(3) From the optimization study, it was found that smaller, shorter, and thicker circular tubes are preferred for use as energy absorbing components.

In Chapter 1 and Chapter 2, it was identified that a car bumper is one of the potential applications for using the laterally crushed tubes as energy absorption components. In this context (vehicle crashworthiness), the energy absorbers are frequently subjected to a combination of straight and oblique loads. The energy absorption responses of thin walled tubes under lateral oblique loads have received relatively little attention compared to the number of studies conducted on the responses of thin-walled tubes under straight loads. Thus, the energy absorption behaviour of circular tube under lateral oblique loading is of particular interest, and is presented in the next section.

6.1.5 Responses of circular tube under a lateral oblique load

Figure 6-17 shows the force-deflection responses of tubes crushed under oblique lateral loading. It can be seen in all cases that at the early stages of deformation, the crush force increased linearly with the displacement. This stage is called the elastic phase. Following the elastic phase, the force started to increase gradually as the displacement increased. This behaviour is due to the strain hardening characteristic of the steel tubes and geometric change of the circular tubes. By comparing the various cases, it can be seen that the collapse load dropped and the strain hardening characteristic increased with increased load angle. In addition, the stroke length decreased as the load angle increased due to the geometrical restrictions. Figure 6-18, Figure 6-19, and Figure 6-20 show the sequence of collapse of a

circular tube under various loading angles. It can be seen that the tube compressed under a straight load exhibited a symmetric collapse mode about both the vertical and horizontal axes. Non-symmetric collapse modes were observed when the tubes were compressed under an oblique load. Furthermore, it is worth to note that in all cases the mode of collapse was plastic bending with the formation of plastic hinges.

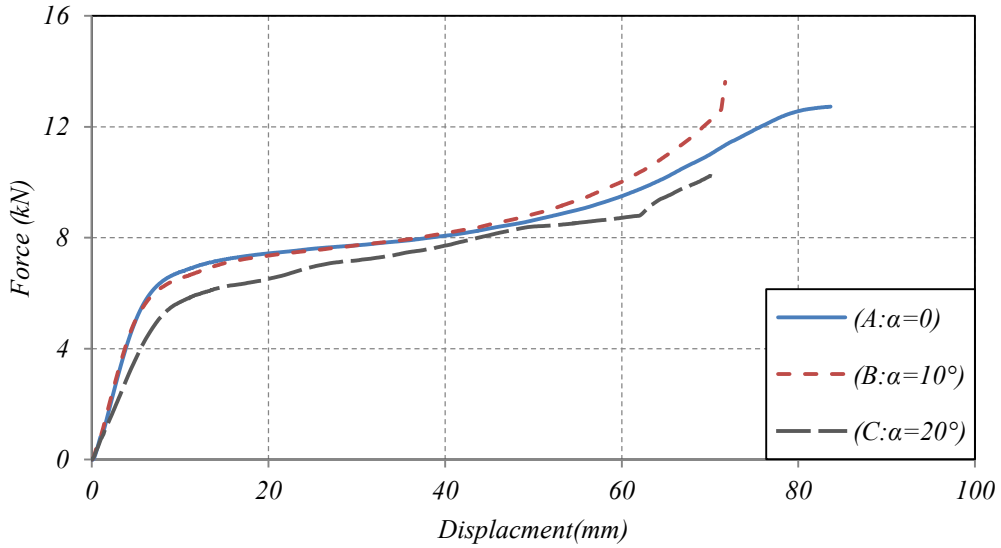

Figure 6-17: Effect of load angle on the Force-Displacement response.

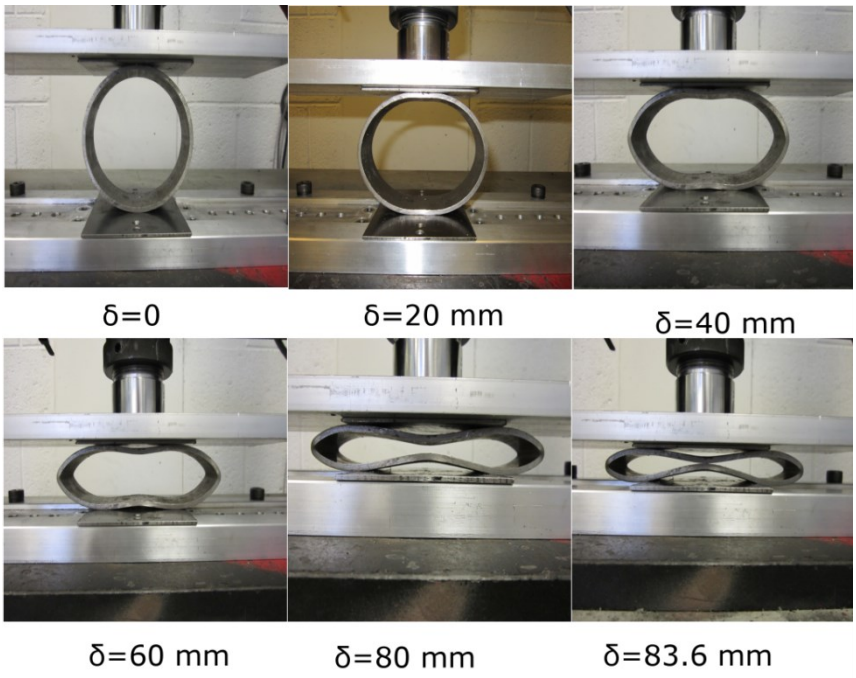

Figure 6-18: Deformation history of a circular tube under quasi-static loading.

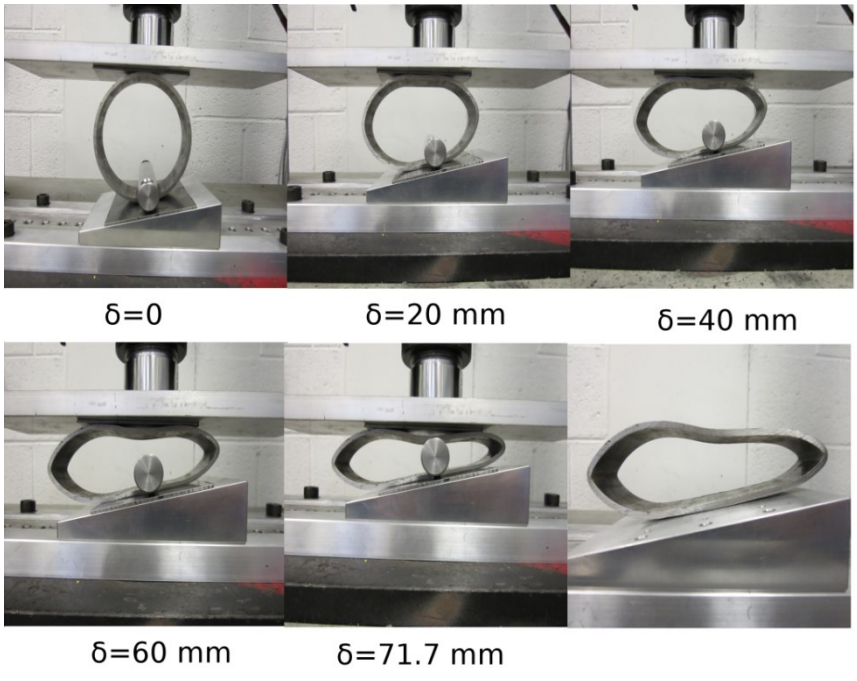

Figure 6-19: Deformation history of a circular tube under quasi-static oblique loading where $\alpha=10^{o}$

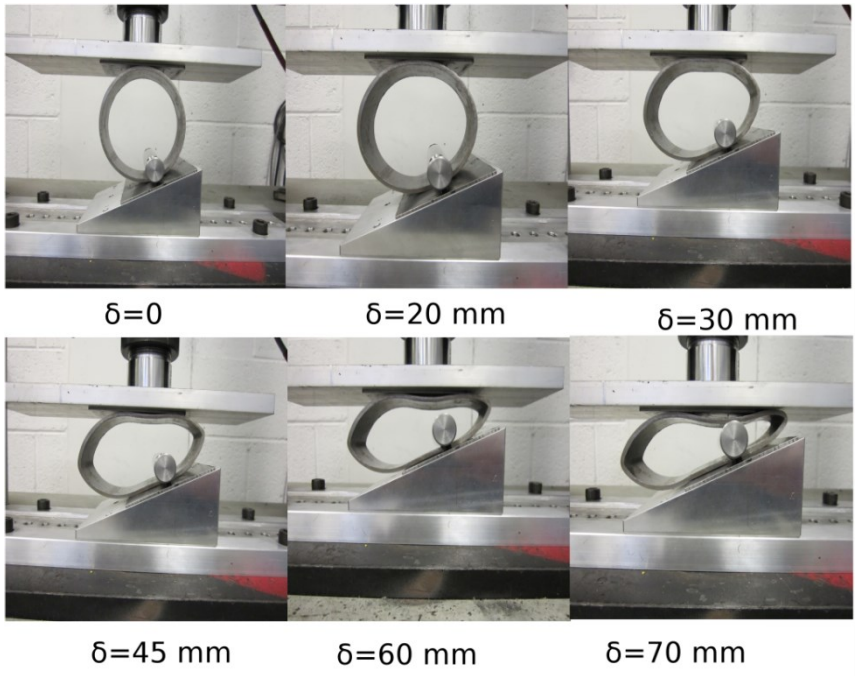

Figure 6-20: Deformation history of a circular tube under quasi static oblique load where $\alpha=20^{o}$

Various indicators that describe the energy absorbing effectiveness of circular tubes under lateral oblique loading are displayed in Table 6-10. It can be seen that tube A (compressed by straight loading) offers higher efficiencies than both tubes B and C (compressed by oblique loading). This is due to a longer crush stroke and a higher energy absorption capacity offered by tube A.

Generally, for many reasons, the designers of energy absorbing structures start their study with conducting quasi-static analysis, as has been shown already. First, the experimental setup for quasi-static loading is relatively simple compared with that for a dynamic loading test. Second, the energy absorption responses and deformation mode of structures under a low impact velocity are very similar to those obtained with quasi-static loading. Third, it is very important to compare the dynamic results against quasi-static results so that the effect of dynamic loading can be determined and quantified. However, in real-world energy absorption applications, the structure is mainly subjected to dynamic loading. Thus the response of circular tubes under lateral impact loading is addressed in the next section.

Table 6-10: Comparison of effectiveness indicators for circular tubes compressed under various load angles (CT).

	SEA (J/kg)	E_g *(%)*	e_E *(%)*	W_{eff} *(J/kg)*
A	2206	82.3	55	1815.2
B	1795.8	70.7	41.8	1269
C	1549.7	68.9	48	1067.7

6.1.6 Dynamic response of a single circular tube

The Figure 6-21 presents the load-deflection results from the quasi-static and dynamic tests. The dynamic test was carried out by using a crush velocity of 4.5 m/s, and the data obtained from the dynamic test was filtered using a Butterworth filter provided in the system software. It can be seen that the quasi-static and dynamic responses were very similar, almost having the same crushing strength. The same observation was reported by Fan et al. [118] for the dynamic response of aluminium

tubes under a velocity of 10 m/s. The slight difference between the dynamic and quasi-static responses noticed at the beginning of collapse is probably due to the elastic effects. The deformation stages of a circular tube under impact loading are displayed in Figure 6-22. It can be seen that the deformation mode is very much the same as that for a typical quasi-static case. The similar responses and deformation modes of the circular tubes under various loading conditions indicated that there are insignificance strain rate and inertial effects for a given applied velocity of the striker.

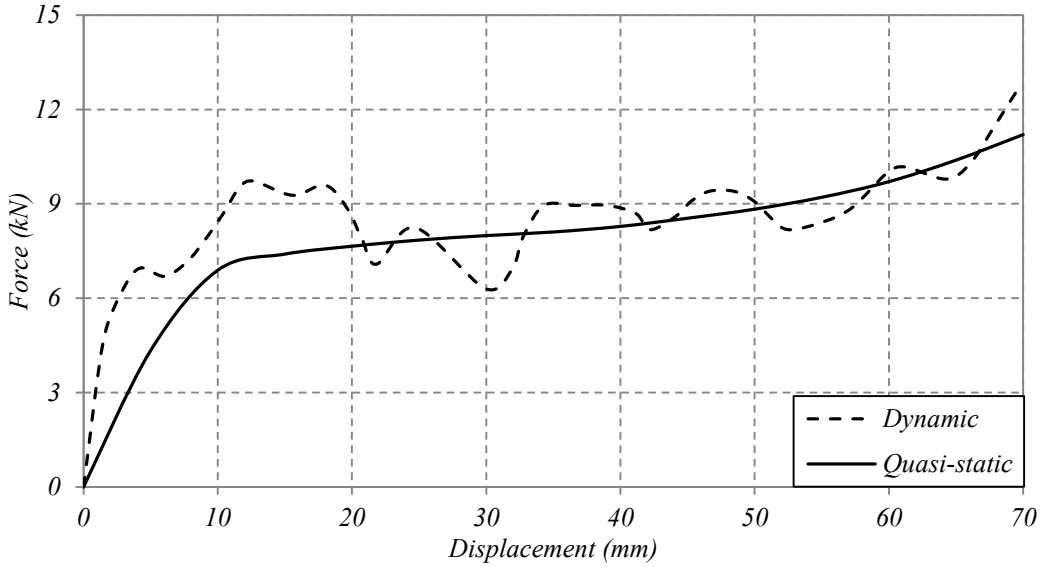

Figure 6-21: Comparison of experimental responses for a circular tube under static and dynamic loading (v=4.5 m/sec).

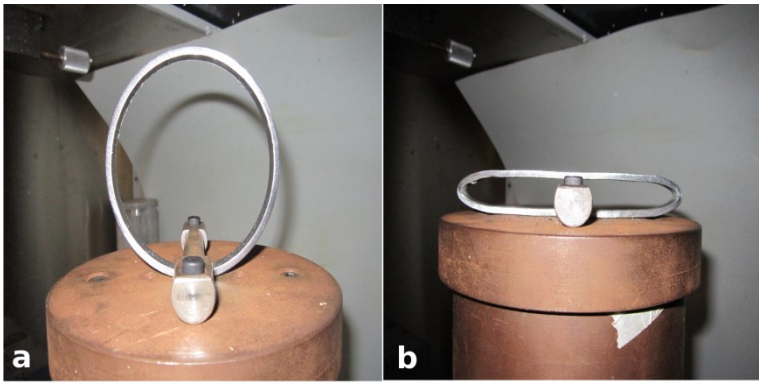

Figure 6-22: Initial and final stages of deflection for a circular tube under dynamic loading (v=4.5 m/sec).

Of interest is to see how the comparison of the dynamic and the quasi-static response of the energy absorbing component changed with the velocity of the impinging mass, using the Dynamic Amplification Factor (DAF). This parameter is important for design purposes as it allows the effect of various parameters on the dynamic response to be quantified with respect to the quasi-static response. Based on the calibrated FE model presented in section 5.2.15.2.1, Figure 6-23 which depicts the effect of impact velocity on DAF factor was created. Examination of this figure shows, that an increase in impact velocity caused an increase in the DAF. This was due to an increase in the total internal plastic energy dissipation with an increase of compression velocity. It is clear from Figure 6-23 that in the range up to a velocity of 30 m/sec, the dynamic effects still did not cause much difference in response of the circular tube, as the DAF magnitude was less than 1.2.

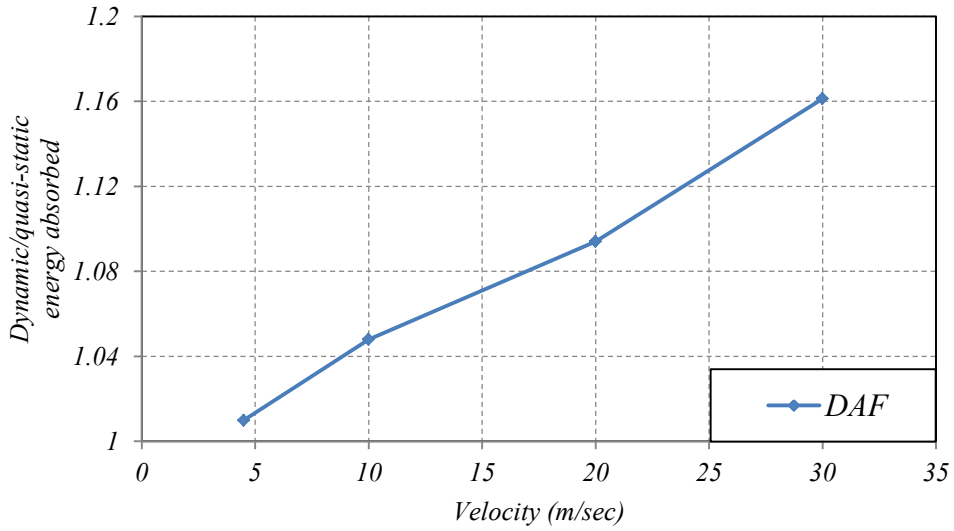

Figure 6-23: Effect of impact velocity on the *DAF*.

The deformed profiles of circular tubes under two different compression velocities are shown in Figure 6-24. It can be seen that the deformed profiles under a compression velocity equal to v=10 m/sec, are very similar to those under a quasi-static loading case. But, for a compression velocity of v=100 m/s, plastic deformation initially occurred around the impact region of the tube (upper part of the tube), with a slight bending deformation in the remaining portion. As the tube was further compressed by the upper plate, large plastic deformation extended to the

whole tube. So it can be seen that the circular tube offered a non-symmetric deformation mode around the horizontal axis under high velocity impact. The same behaviour was reported for aluminium and sandwich tubes by Fan et al. [118]. From Figure 6-24, it can be concluded that the dynamic effects played a key role in increasing the energy absorbed by the tube compressed under high impact velocities through changing the deformation and collapse mechanism.

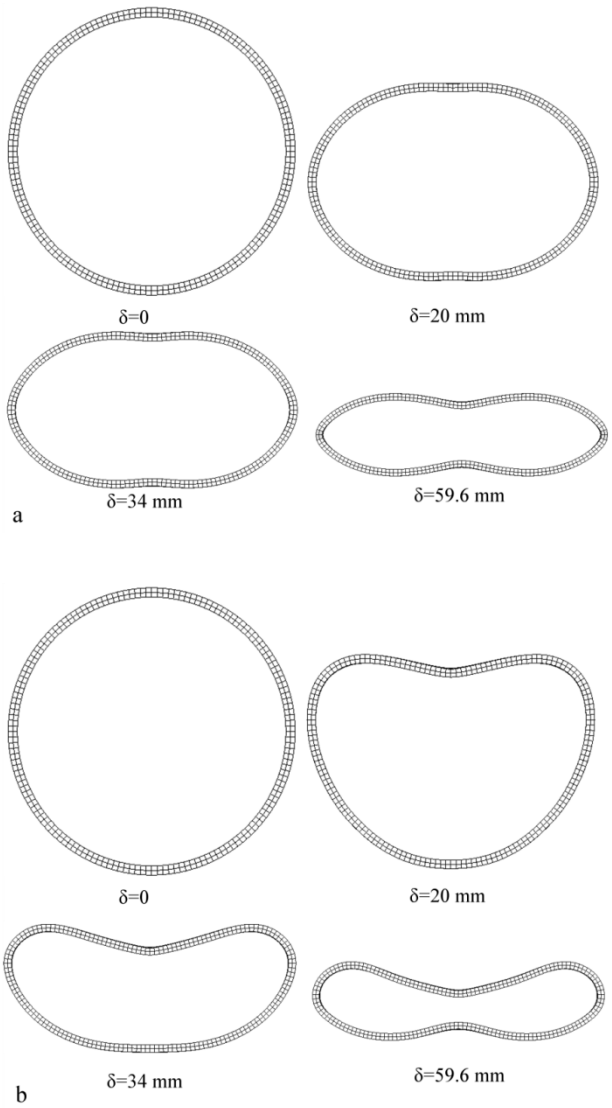

Figure 6-24: Deformed profiles of a circular tube under two different compression velocities a: v=10m/sec, and b: v=100 m/sec.

6.2 Oblong tube

Much of the research on thin-walled tube energy absorbers crushed laterally has focused on those that are circular in cross section. However, the oblong tubes which are a modified form of circular tubes have received less attention. An oblong tube was generated by elongation of a circular tube. External constraints were applied as a means of increasing energy absorption capacity. Three types of indenters, ie: flat plate, cylindrical indenter, and point load, were used to compress the oblong tubes. These tubes were expected to have high energy absorptions performances as they had a greater lateral displacement stroke compared with the circular tubes.

6.2.1 Oblong Tube Specimen Preparation

Using suitable fixtures, an oblong curve profile was generated by subjecting a cylindrical tube to opposing tension forces, as shown in Figure 6-25. A displacement of 40 mm was applied to a circular tube test piece with outer diameter of 101.6 mm, thickness of 3.25 mm and width 0f 40 mm, this value is the maximum extension distance that can be applied to a given circular tube as any further increase in the elongation distance might cause the formation of plastic hinges at the horizontal line of the tube, and hence buckling inwards would occur. This elongation distance value was also used by Olabi et al. [13]. Figure 6-26 shows the force-deflection response of a test piece during the tensile loading phase. The objective is to load the tube plastically so that extra displacement during the compression phase can be achieved. This allows for more energy to be absorbed for the same mass.

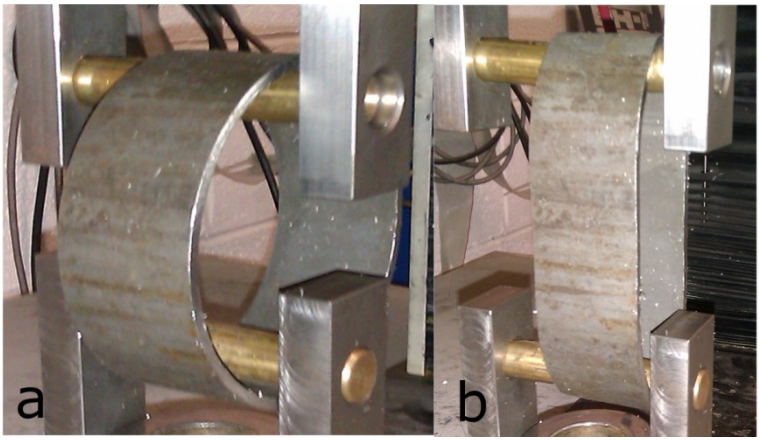

Figure 6-25: Elongation procedure of an oblong tube.

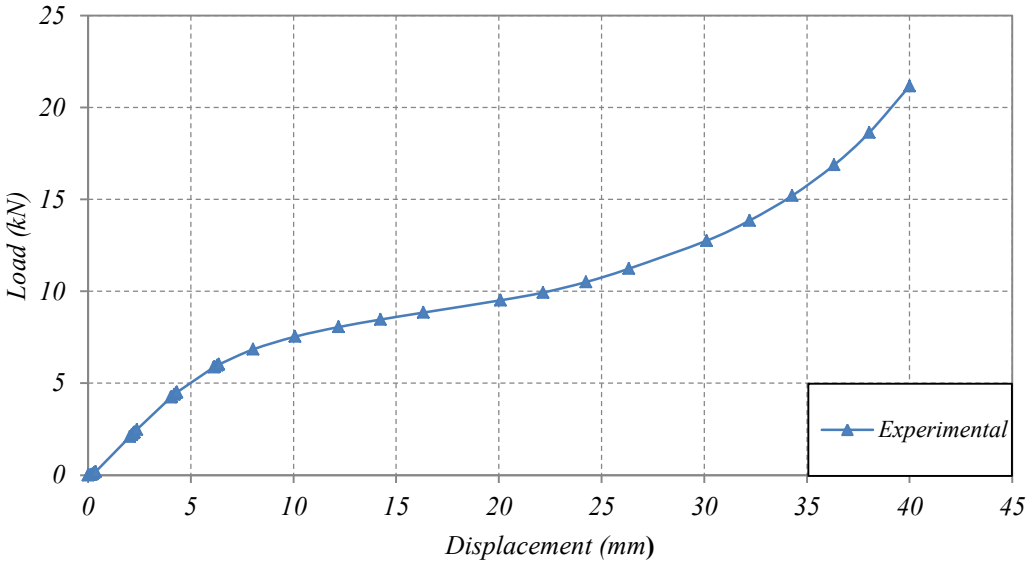

Figure 6-26: Tensile force–deflection response of the test piece during the tensile loading phase.

6.2.2 Experimental results comparison of oblong and circular tubes under lateral loading

To prove the crash resistance advantages of the oblong system, a comparison of the crush behaviour of the oblong and circular tubes has been performed. The force-deflection responses for the circular and oblong tubes under quasi-static loading are shown in Figure 6-27. The tubes were crushed up to 70 % of their original diameter/height to avoid the self-contact of the tube.

It can be clearly seen that the oblong tube has a longer crushing stroke which is around 30 % more than the circular tube. The circular and oblong tubes have almost the same magnitude of the collapse load while the post collapse stage is more stable and almost constant in the oblong tube. The constant force-deflection response of the oblong tube is due to residual stresses created during the forming of the oblong tube specimen. Table 6-11 shows the comparison of oblong and circular tubes in terms of energy absorption capacity and specific energy absorption capacity. It can be seen that the oblong tube can absorb around 35% energy more than the circular tube.

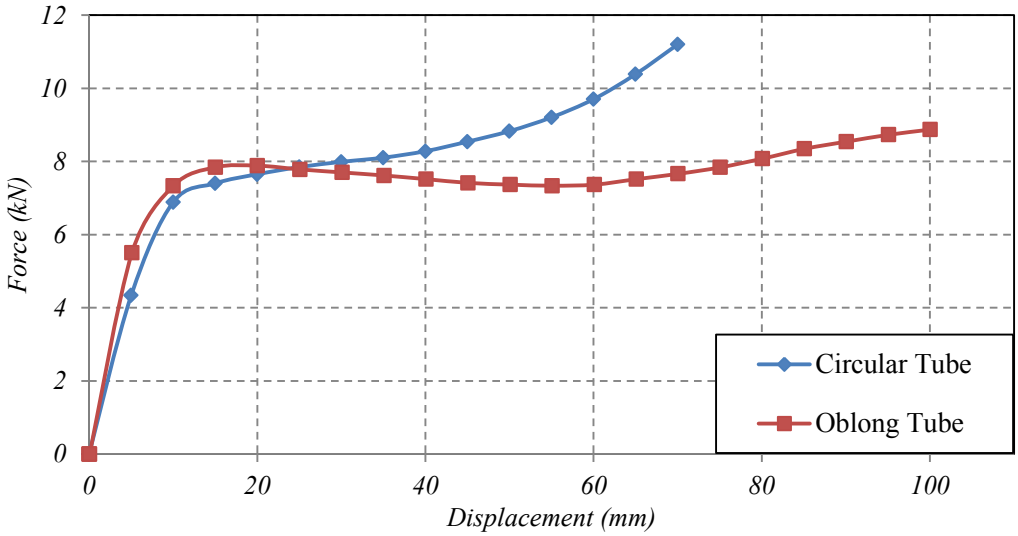

Figure 6-27: Comparison of load-deflection responses of circular and oblong tubes.

Table 6-11: Comparison of E and SEA for circular and oblong tubes

	E (J)	*Mass (kg)*	*SEA (J/kg)*
Oblong	746	0.322	2316.77
Circular	554	0.322	1720.497

Overall, it is clear from the above comparison that the oblong tubes display several key advantages over circular tubes for absorbing energy under lateral loading, as follows:

- Oblong tubes display a more stable and almost constant force-deflection response in the post collapse stages.
- The energy absorption capacity of oblong tubes is greater than that for circular tubes of equivalent mass.

As mentioned early in chapter 2, the energy absorbed by laterally crushed tubes can be enhanced by using external constraints. These external constraints increase the number of plastic hinges generated during the collapse and thus subject the system to greater volumetric deformation. The concept of external constraints was used to further improve the performance of oblong tube under lateral loading, as will be presented in the next section.

6.2.3 Responses of oblong tube compressed by different indenters and exposed to external constraints

6.2.3.1 Flat plate indenter

Figure 6-28 and Figure 6-29 illustrate the force and energy absorption responses and the stages of compression for the OTFIU system. The force increases rapidly up to its characteristic ‘collapse’ load followed by a slight strain softening response. This softening stage is due to the oblong curve profile generated during the preparation/loading phase. The elongation of a circular tube plays a role in generating a larger moment arm from the point of load application to the horizontal hinge points in the post stages of the collapse. As a result less force is required to maintain the deformation. At approximately 60 mm deflection, the force begins to rise. This is due to the points of contact continually moving away from the centre between the upper plate and the oblong structure. This results in a shorter moment arm, which therefore requires a greater force to continue or sustain the deformation process. Since the tube is elongated in the vertical direction, the potential displacement stroke is increased. In order to avoid a system overload that may cause the tube to fracture, the responses of all systems were calculated up to 100 mm (70%

of oblong tube length), as shown in Figure 6-29. It can be noticed from Figure 6-28 that an almost constant crushing force is achievable in the OTFIU system, which is a desirable feature in energy absorbing systems.

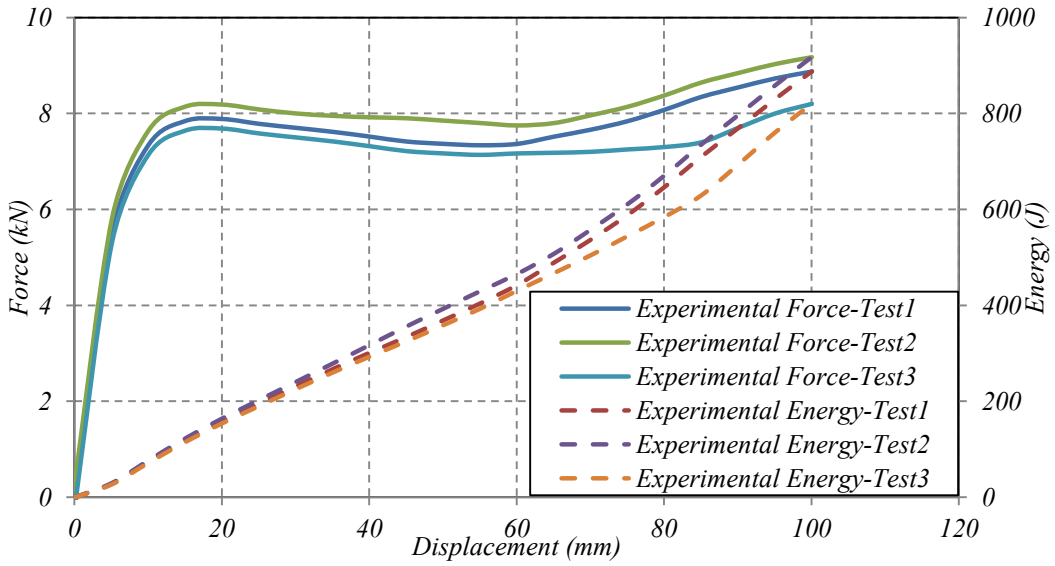

Figure 6-28: Experimental responses of an OTFIU system.

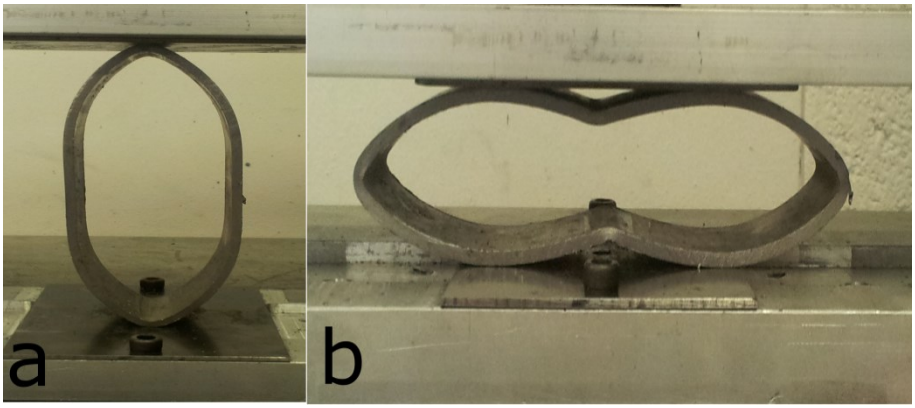

Figure 6-29: (a) Initial and (b) final stages of an OTFIU system

The force and energy responses of the OTFIIC system are presented in Figure 6-30. External inclined constraints at an angle 15 degrees were used to create OTFIIC, as shown in Figure 6-31. It can be seen that similar responses to unconstrained tests were obtained, but with an increase in resulting force being observed in the post

collapse stages. This increase was due to the presence of the constraints resulting in more volume of the material being subjected to deformation, as reported by Reid [143].

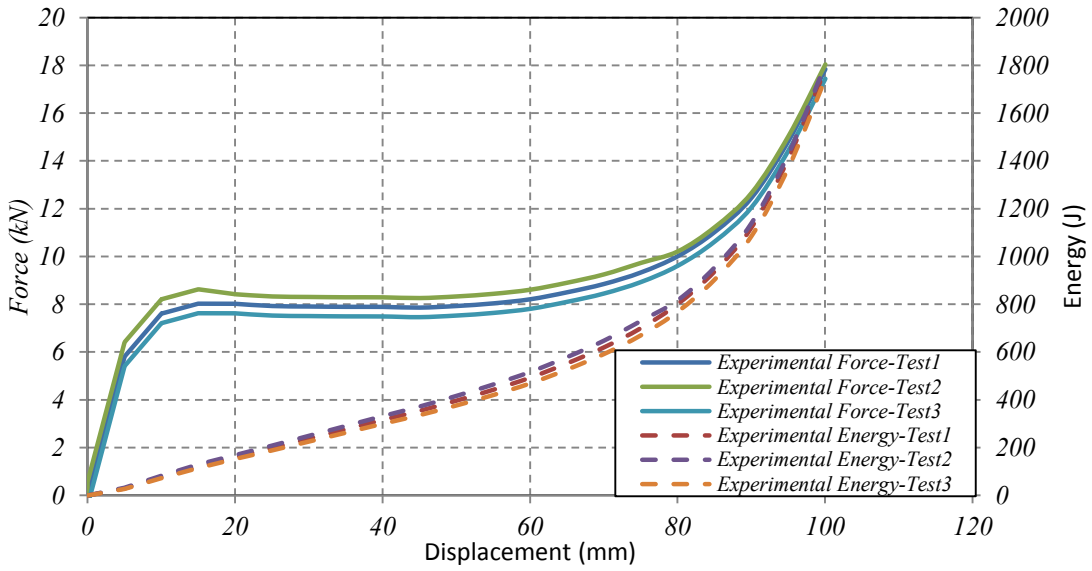

Figure 6-30: Experimental responses of an OTFIIC system.

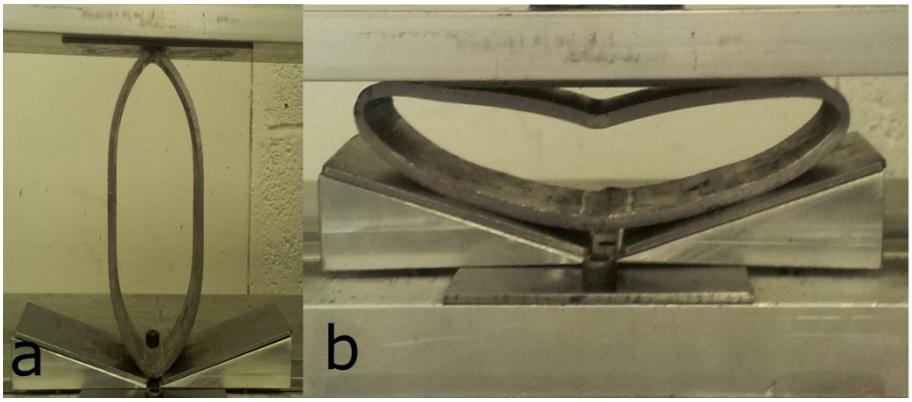

Figure 6-31: (a) Initial and (b) final stages of an OTFIIC system.

Figure 6-32 depicts the crush force and energy absorption for an OTFISC system. A smaller flat indenter is incorporated in this system as there was limited width availability after installing the side constraints, as seen in Figure 6-33. It is possible to choose an indenter equal to the available width. However this brings its own complications in the sense that a very large load would be required to compress the system, which may exceed the limit of the load cell. At approximately 60mm

deflection, the force increases due to the presence of the side constraint preventing the horizontal diameter of the oblong specimen from moving laterally and thus exposing more material to plastic deformation. A similar observation was reported by [72], where side constraints were used during the compression of circular tube. From approximately 70mm, the peak force drops briefly and rises again and then continues dropping. The slight oscillation in force noticed at 70 mm is due to additional plastic hinges being formed between the edge of the indenter and the test piece, as shown in Figure 6-33.

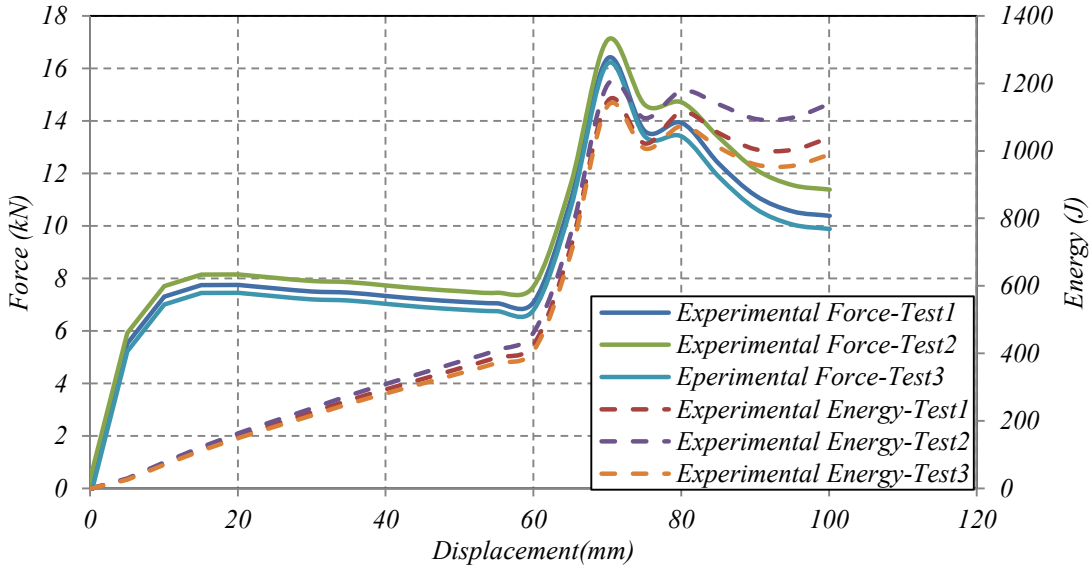

Figure 6-32: Experimental responses of an OTFISC system.

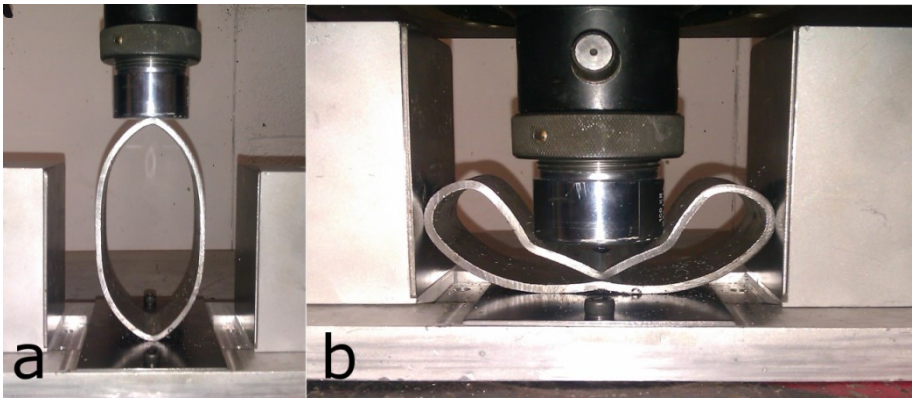

Figure 6-33: (a) Initial and (b) final stages of OTFISC system.

6.2.3.2 Cylindrical indenter

Figure 6-34 displays the force and energy response for an OTCIU system. When the crush force is reached, the system begins to strain soften. This is an unstable deformation characteristic and is due to the moment arm increasing and thus requiring less compressive force to maintain the compression stroke.

Due to the design of the cylindrical indenter, a higher stroke length can be obtained in systems that use this indenter configuration. At approximately 80 mm, more strain softening was noticed due to partial structural failure occurring at the top plastic hinge, as shown in Figure 6-35.

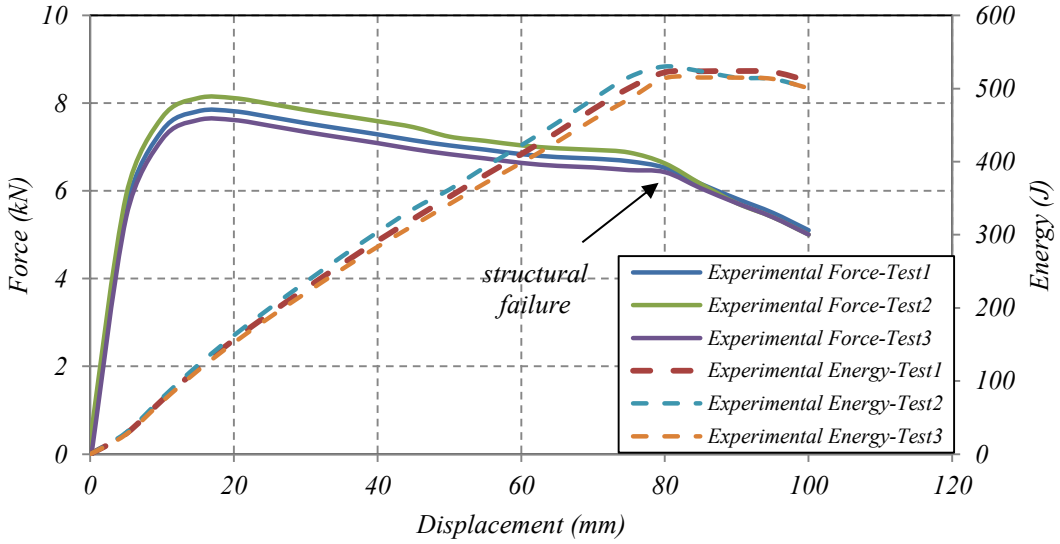

Figure 6-34: Experimental responses of an OTCIU system.

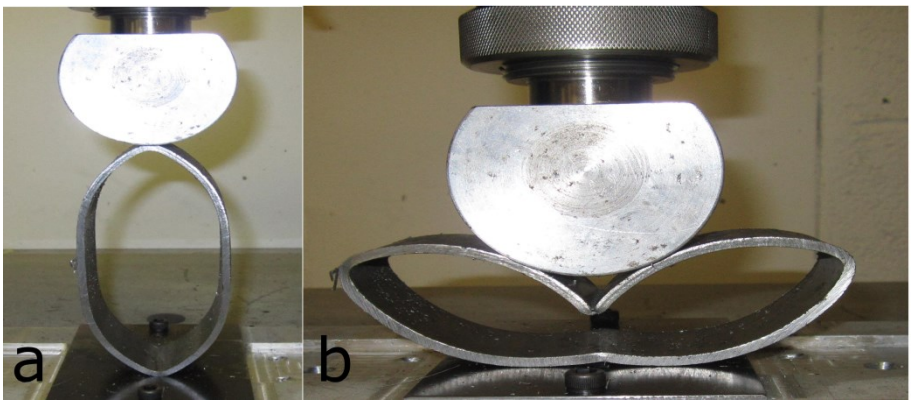

Figure 6-35: Initial and final stages of OTCIU system.

Figure 6-36 and Figure 6-37 illustrate results for an OTCIIC system. A slight increase in the resulting force occurs due to the presence of the inclined constraints. Similar to the OTCIU system, the OTCIIC system exhibits unstable behaviour and partial structural failure (Figure 6-37). The responses of the OTCISC system are presented in Figure 6-38 and Figure 6-39. When contact was established between the test piece and the side constraints, an increase in force was observed due to the prevention of the horizontal diameter of the test piece being deflected, thereby inducing additional plastic hinges. These additional hinges required extra force in order to overcome local plastic deformation. A significant increase in load was noticed towards the end of the displacement stroke for both OTCIIS and OTCISC. This increase was due to the oblong tube conforming to the shape of the cylindrical indenter, as shown in Figure 6-37 and Figure 6-39, and also due to material strain hardening characteristics.

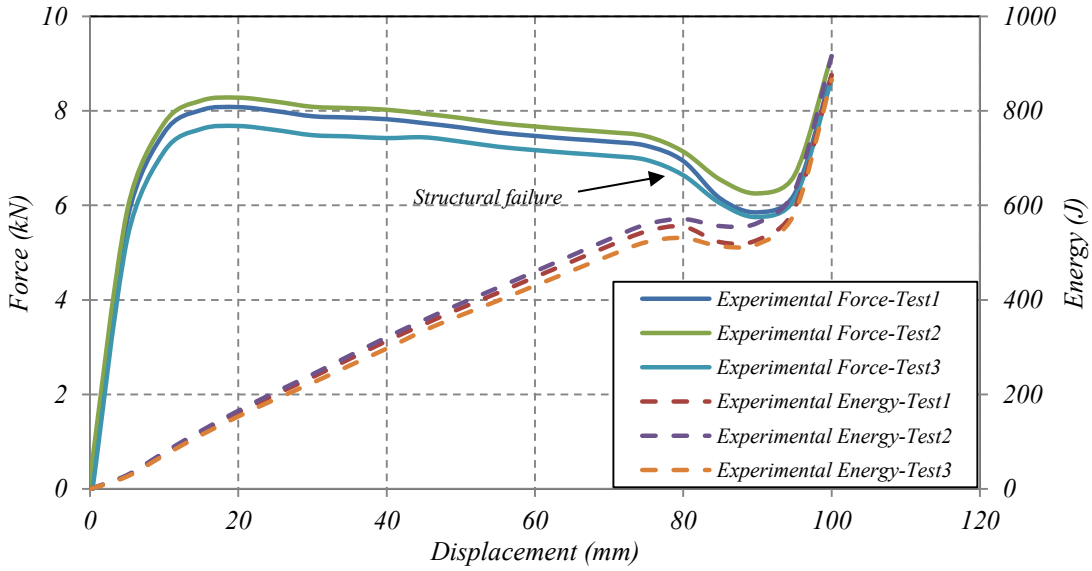

Figure 6-36: Experimental responses of an OTCIIC system.

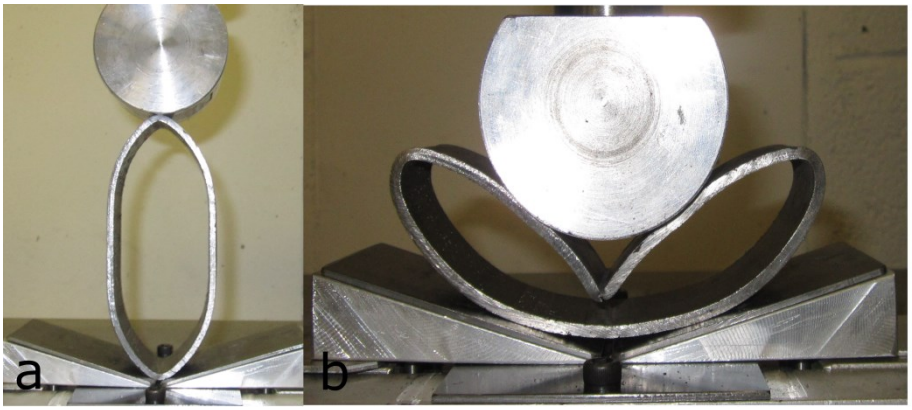

Figure 6-37: Initial and final stages of an OTCIIC system.

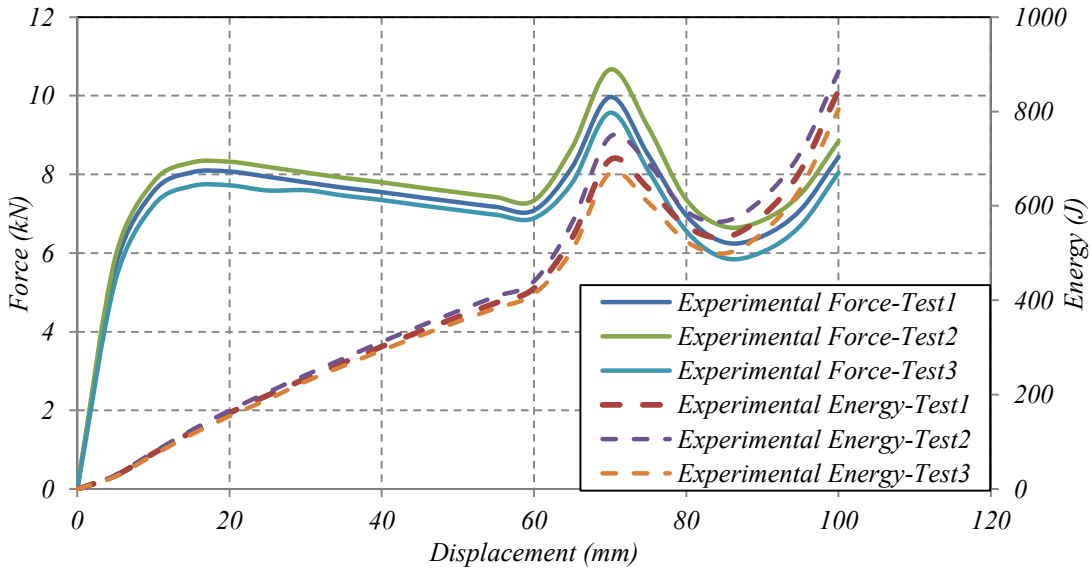

Figure 6-38: Experimental responses of an OTCISC system

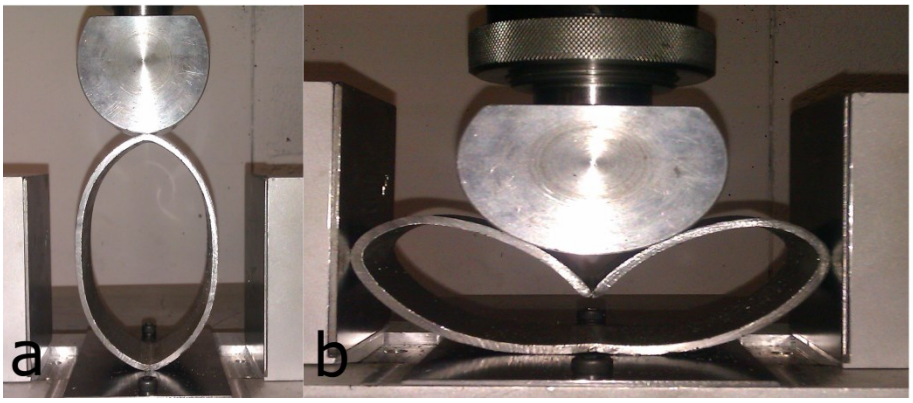

Figure 6-39: Initial and final stages of an OTCISC system.

6.2.3.3 Point indenter

(Figure 6-40, Figure 6-41, Figure 6-42, Figure 6-43, Figure 6-44, and Figure 6-45) illustrate the force and energy response of test specimens being compressed using a point indenter. The responses of these specimens are very similar to those specimens compressed using cylindrical indenters. In all systems (OTPIU-OTPIIC-OTPISC) at approximately 60 mm deflection, complete structural failure occurs due to excessive plastic deformation occurring in a very localised region at the point of load application (Figure 6-46).

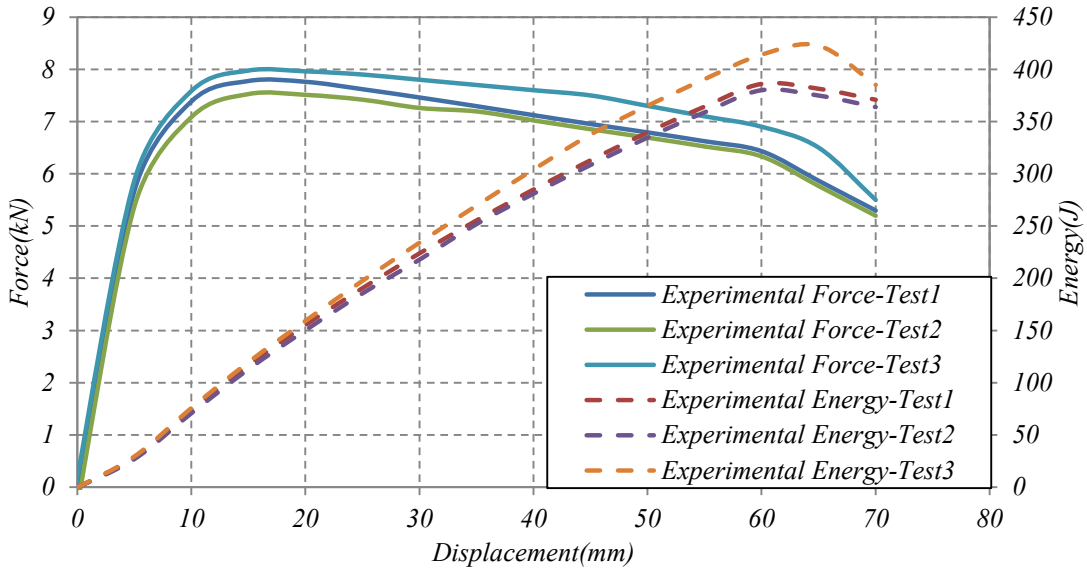

Figure 6-40: Experimental responses of an OTPIU system.

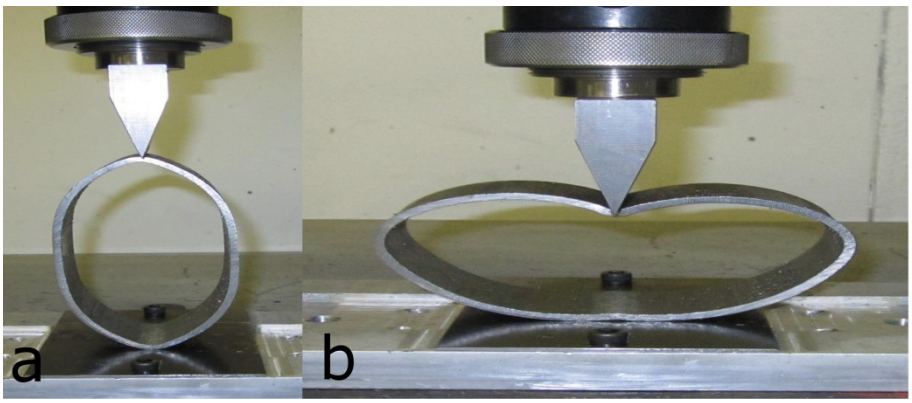

Figure 6-41: (a) Initial and (b) final stages of an OTPIU system.

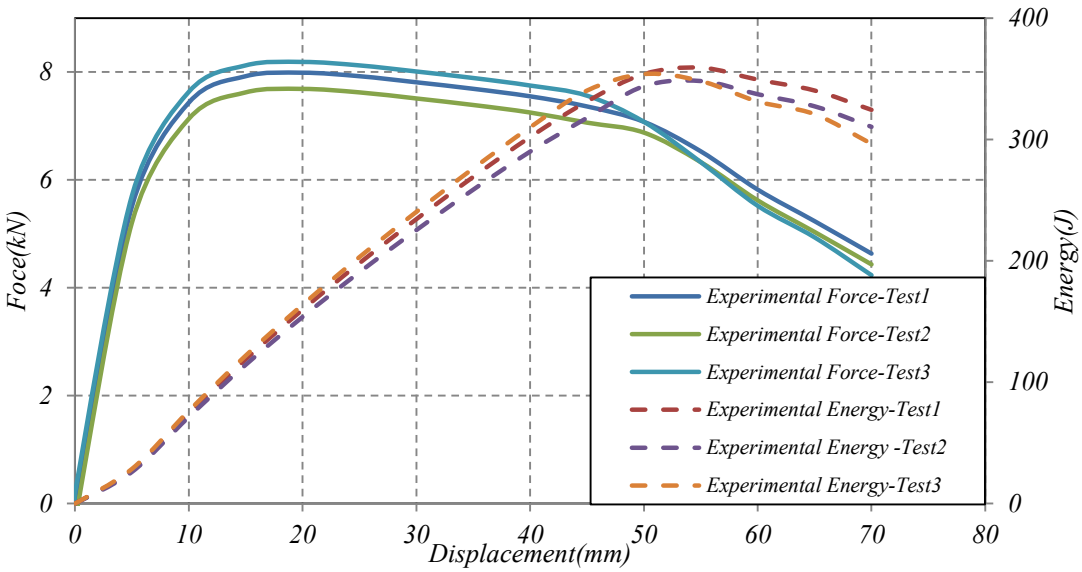

Figure 6-42: Experimental responses of an OTPIIC system.

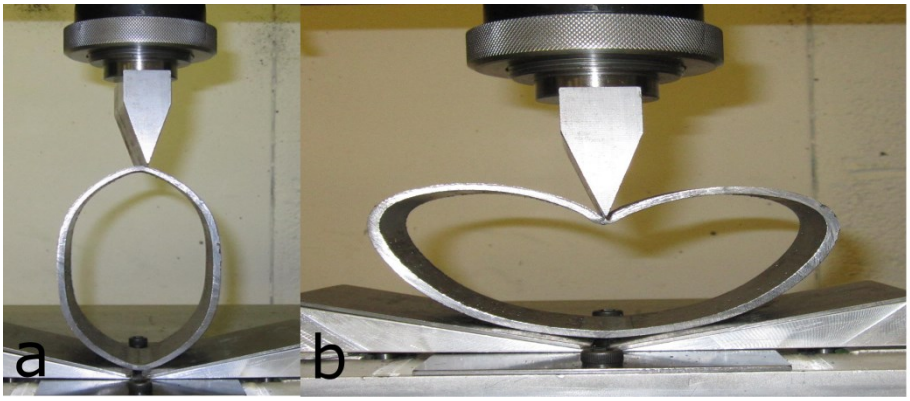

Figure 6-43: Initial and final stages of an OTPIIC system.

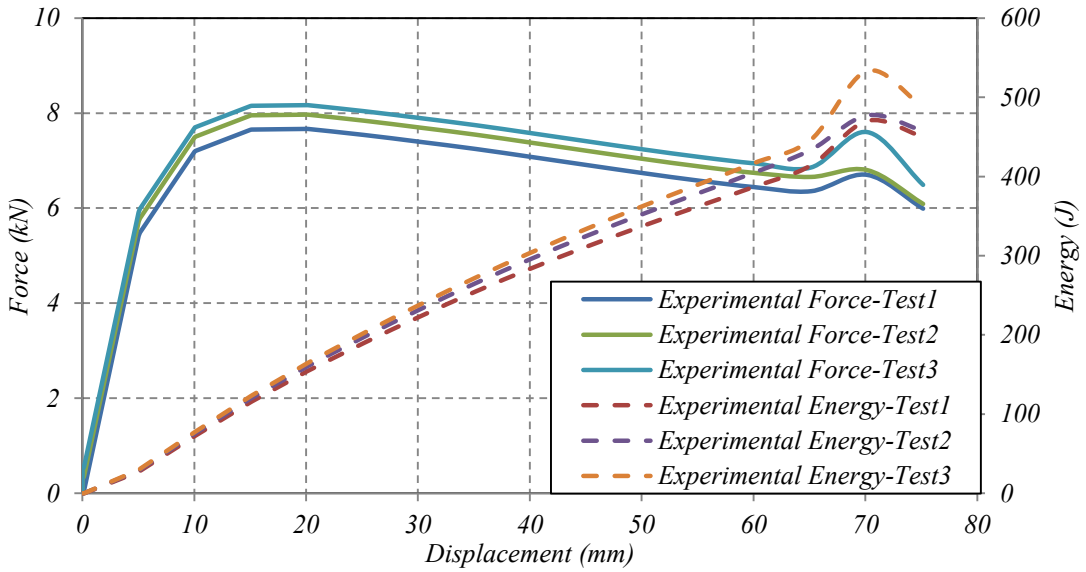

Figure 6-44: Experimental responses of an OTPISC system.

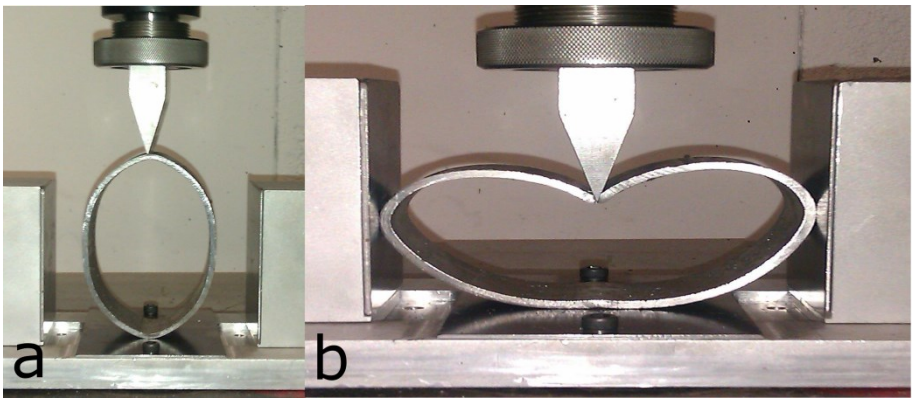

Figure 6-45: Initial and final stages of an OTPISC system.

Figure 6-46: The final collapse profile of specimen with a point load application.

6.2.4 Energy absorption characteristics (OT)

Figure 6-47 presents the various indicators (e_g, e_E , W_{eff}) for all oblong tube systems. The oblong tubes compressed by flat plate indenters (OTFIU-OTFIIC-OTFISC) presented the best efficiencies, while the point indenter systems (OTPIU-OTPIIC-OTPISC) resulted in lower efficiencies. The maximum energy and crush efficiency were obtained from the OTFIU system due to its response characteristics exhibiting a rectangular or constant crushing force throughout its loading phase. The maximum weight effectiveness was obtained by OTFISC due to a larger amount of specific energy absorbed by it.

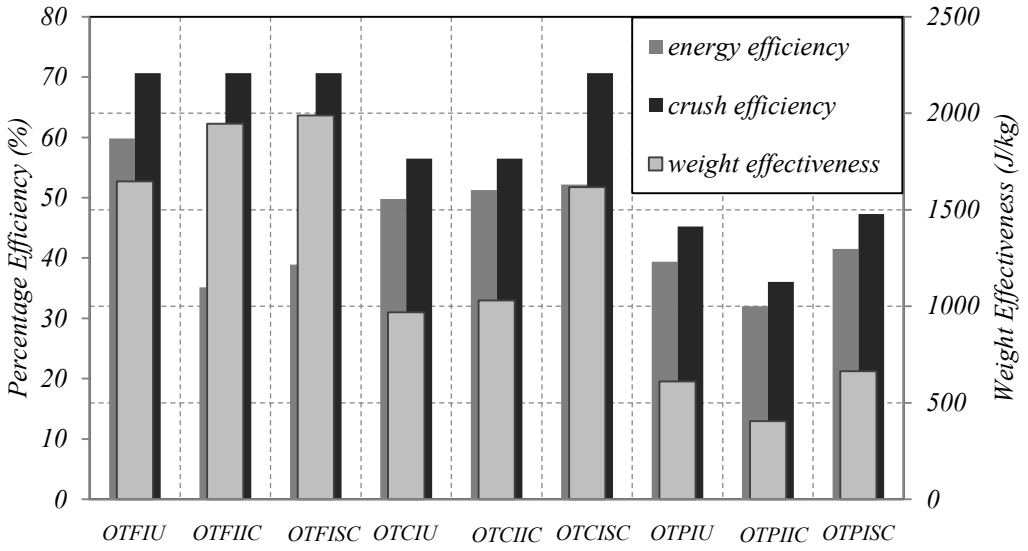

Figure 6-47: Comparison of effectiveness indicators for OT systems.

From the results shown above, it appears that the OTFIU system showed a better performance in terms of (e_g, e_E) under lateral loading, compared with the other systems configurations. Moreover, the OTFIU has the simplest design and an almost optimal force-deflection response. The OTFIU system was thus selected as the best energy absorption system in the oblong tubes category. In the following sections, the influences of important geometric parameters on the crushing response of OTFIU tubes are first examined by means of a parametric study, followed by a multi-objective optimization design (MOD) to further improve its crashworthiness under lateral loading.

6.2.5 Development and validation of response surface (RS) models for an OTFIU system

Using the same procedures that were followed in section 6.1.2, the RS models for energy absorption responses of oblong tubes under lateral loading were created and validated.

6.2.5.1 Sampling design points

An experimental design was created based on a three level Box–Behnken design with full replication. Tube widths (W) ranging between 10 and 60 mm, tube outer diameters (D) between 8 and 130 mm, and tube thicknesses (t) between 2.5 and 6 mm were applied as independent input variables. Table 6-12 shows the specific values used in the experiments. These dimensions were chosen as they covered the typical range of tube sizes commonly used in crashworthiness applications. The specific energy absorbed (SEA) and collapse load (F) were selected as design responses. The oblong tube models were prepared by the elongation method as described earlier. A ratio of 2.54 between the outer diameter of the circular tube and the elongation distance was used to create the oblong tube models. This same ratio was used by [13]. The SEA responses for all models have been calculated up to 70% of the oblong tube length.

Table 6-12: Independent variables and experimental design levels used (OTFIU).

Variable	*code*	*-1*	*0*	*1*
Diameter(mm)	A	80	105	130
Width(mm)	B	10	35	60
Thickness(mm)	C	2.5	4.25	6

Numerical simulations were performed for the different combinations of independent variables provided by the DOE software. The design responses were calculated for each combination of design variables. The different combinations of design variables with corresponding design responses are tabulated in Table 6-13.

Table 6-13: The design matrix (OTFIU).

Exp no	D(mm)	W(mm)	t(mm)	SEA (J/kg)	F (kN)
1	80	35	2.5	2200.901	5.6
2	130	60	4.25	2349.348	16.5
3	105	60	2.5	1761.163	8.16
4	105	60	6	4943.279	50.44
5	130	35	6	3678.03	21.43
6	80	35	6	7504.022	42.42
7	80	60	4.25	4604.727	32.378
8	105	35	4.25	3257.608	13.084
9	80	10	4.25	4321.494	5.07
10	105	35	4.25	3257.608	13.084
11	105	10	6	4577.168	8.1
12	105	35	4.25	3257.608	13.084
13	130	10	4.25	4263.601	2.6
14	105	35	4.25	3257.608	13.084
15	130	35	2.5	1122.162	2.86
16	105	10	2.5	1423.097	1.025
17	105	35	4.25	3257.608	13.084

6.2.5.2 Accuracy evaluation of the RS models

Using the step-wise regression method, first and second order polynomials were suggested by Design-Expert to obtain the RS models of the SEA and F respectively. The Table 6-14 shows the resulting ANOVA table for the Reduced Linear Model of SEA. The model F-value of 45.5 implies that the model is significant. A p-value of 0.0001 suggests that there is only a 0.01% chance that the F-value could occur due to

noise. The adequate precision of 21.38 is higher than the threshold of 4. This indicates that the model had very little noise and can be used to navigate the design space. The "Pred R-Squared" of 0.7851 agrees well with the "Adj R-Squared" of 0.8467. Based on F-values of each term shown in ANOVA table, it can be seen that thickness F-value of 74.35 is higher than Diameter F-value of 16.65 so it can be concluded that the thickness (t) was the most influential factor of the SEA. Due to use of step-wise regression method, the width was eliminated by the software package due to its insignificant effect on the SEA. The most significant terms associated with specific energy absorbed (SEA) were:

The first order effect of thickness (t) and diameter (D).

The final mathematical model of SEA in terms of actual factors as proposed by the design expert software is displayed in Table 6-14.

Table 6-14: Analysis of variance (ANOVA) table for SEA – Linear model (OTFIU).

Source	*Sum of squares*	*Mean Square*	*F Value*	*p-value*
Model	2395.722442	1197.861221	45.50313719	< 0.0001
A-Diameter	438.4345749	438.4345749	16.65480797	0.0011
C-Thickness	1957.287867	1957.287867	74.3514664	< 0.0001
Residual	368.5472723	26.32480517		
Cor Total	2764.269714			
		Final equation obtained from the model for SEA		
R-Squared	0.8667	*Sqrt(SEA)=* *+50.63974* *-0.29612*Diameter* *+8.93808* Thickness*		
Adj R-Squared	0.8467			
Pred R-Squared	0.7851			
Adeq Precision	21.38			

The resulting ANOVA table for the Quadratic Model of collapse load F is displayed in Table 6-15. The Model F-value of 3488.81 implies that the model is highly significant. A p-value of 0.0001 indicates that there is a low chance that the F-value could occur due to noise in this model. The predicted value of R^2 of 0.9969 is in

excellent correlation with an adjusted R2 of 0.9992. A high R^2 of 0.9995 indicates that there is an excellent correlation between the actual and the predicted values. The adequate precision was found to be 45.12, indicating an adequate signal. This means that the model can be used to navigate the design space. The analysis of variance indicated that the following terms are the most significant terms associated with the crush force:

1. The first order effect of tube diameter (D), tube thickness (t) and tube width (W).
2. The second order effect of tube thickness (t) and tube width (W).
3. The two level of interaction effect between the tube thickness and the tube width (t-w).

The F values from the ANOVA table can be used to rank the influence of independent variables interactions on collapse load (F). The order of factor influence on F is as follow: $C>B>A>B^2>C^2>BC$.

The model suggests that collapse load (F) can be modelled by the final equation shown in Table 6-15.

6.2.5.3 Validation of RS models

Figure 6-48 and Figure 6-49 show the relationship between the actual and predicted values of specific energy absorbed and mean force, respectively. These figures indicate that the developed RS models are adequate, because the residuals in the prediction of each response are small since most of SEA and F values lie on the best-fit line of the predicted results. Furthermore, to verify the adequacy of the developed RS models, a comparison between the numerical, experimental, and predicted responses was performed. Using the point prediction option in the DOE software, the specific energy absorbed and collapse load of the validation experiments were predicted using the previous developed models. Table 6-16 presents the experimental condition, the actual values, the numerical values, the predicted values, and the percentages of error. It can be seen that all of the percentage errors are within the acceptable tolerances and this indicate that the RS models are validated.

Table 6-15: Analysis of variance (ANOVA) table for F – Quadratic model (OTFIU).

Source	*Sum of Squares*	*Mean Square*	*F-Value*	*P-Value*
Model	3.15	0.53	3488.81	< 0.0001
A-Diameter	0.17	0.17	1138.04	< 0.0001
B-Width	1.36	1.36	9051.85	< 0.0001
C-Thickness	1.48	1.48	9834.73	< 0.0001
BC	2.85E-03	2.85E-03	18.88	0.0015
B^2	0.1	0.1	682.22	< 0.0001
C^2	0.025	0.025	166.87	< 0.0001
Residual	1.51E-03	1.51E-04		
Cor Total	3.16			
		Final equation obtained from the model for F		
R-Squared	0.9995	*Log10(F)= -0.74264-5.85586E-003*Diameter+0.036580*Width +0.48143*Thickness -6.09578E-004*Width*Thickness -2.49636E-004*Width² -0.025197* Thick²*		
Adj R-Squared	0.9992			
Pred R-Squared	0.9969			
Adeq Precision	214.12			

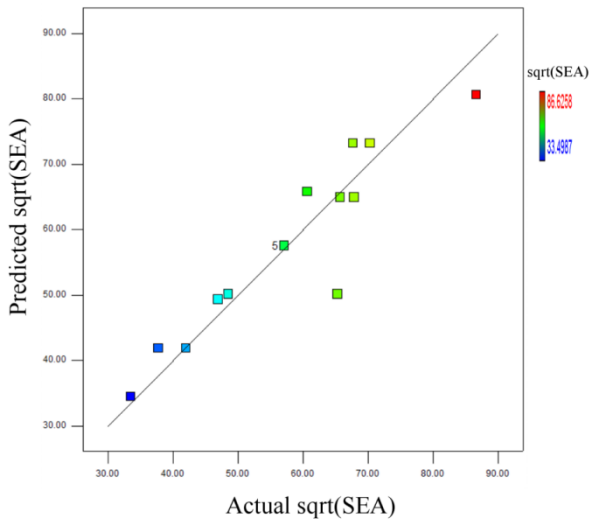

Figure 6-48: Scatter diagram of SEA (OTFIU).

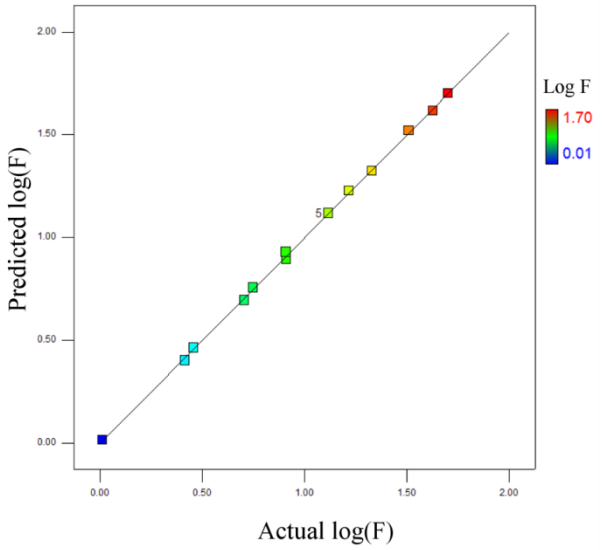

Figure 6-49: Scatter diagram of F (OTFIU).

Table 6-16: Confirmation experiment

D(mm)	*t (mm)*	*w(mm)*		*SEA (J/kg)*	*F (kN)*
101.6	3.25	40	*Experimental*	2326.17	8.25
			Numerical (FEM)	2256.01	8.3
			Error (%)	3%	0.60%
			Predicted (RSM)	2460.431	8.82
			Error (%)	9%	6.2%

6.2.6 Parametric study

6.2.6.1 Effect of geometrical factors on SEA response

The perturbation plot of SEA shown in Figure 6-50 indicates that the SEA depended mainly on the thickness and diameter of the tube. The insignificant effect of the width on the SEA has been eliminated by the software package.

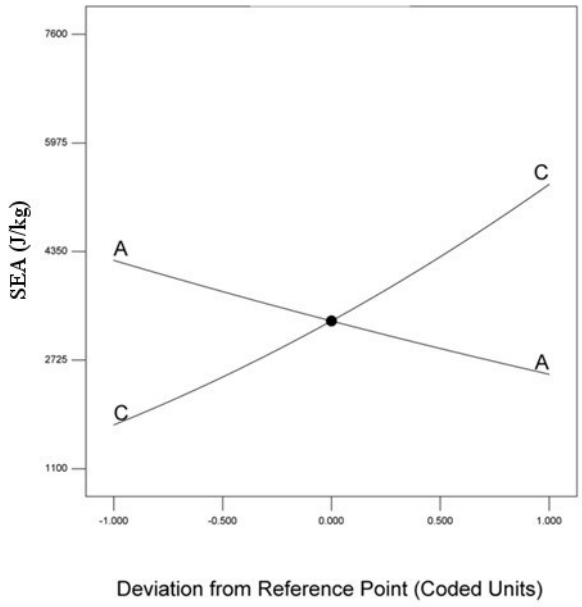

Figure 6-50: Perturbation plot of SEA (OTFIU)

Figure 6-51 shows the effect of tube diameter (D) on SEA. It is seen that SEA decreases as the tube diameter increases. This behaviour was also noticed for circular tubes, as discussed in section 6.1.3.1. This behaviour is probably due to localization of plastic strain around the plastic hinges that reduce the volume of material subjected to plastic deformation in the larger tubes. In addition, the increased weight in the larger tubes made the energy absorbed per unit mass (SEA) lower. Figure 6-52 displays the effect of tube thickness on the SEA. Obviously, it can be noticed that SEA increased as the thickness increased. This phenomena is due to fact that the thicker tubes have more material available for plastic deformation. Figure 6-53 shows the variation of SEA with diameter and thickness, it can be seen that a greater amount of SEA can be absorbed if smaller and thicker tubes were used.

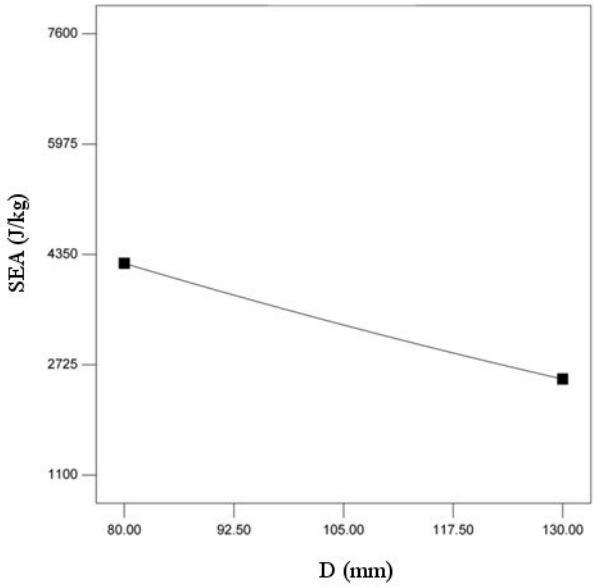

Figure 6-51: Effect of Diameter on SEA (OTFIU)

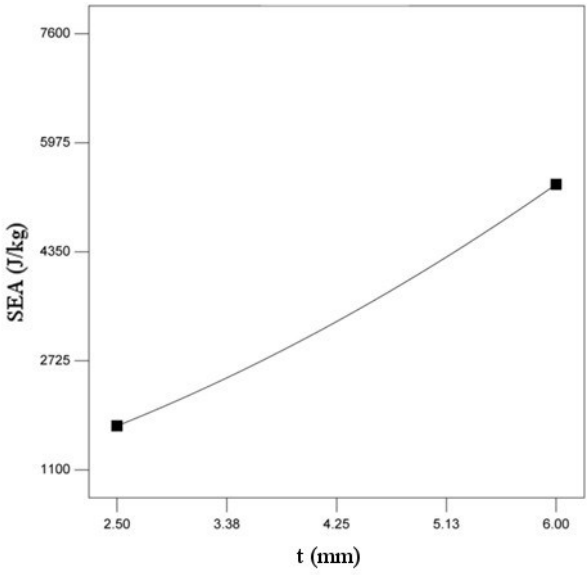

Figure 6-52: Effect of thickness on SEA (OTFIU).

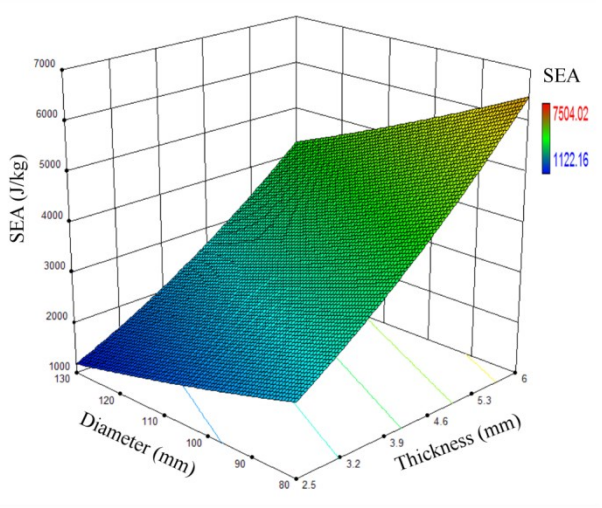

Figure 6-53: Variation of SEA with diameter and thickness (OTFIU).

6.2.6.2 Effect of Geometrical factors on F response

The effect of tube diameter on the crush force is presented in Figure 6-54. It can be noticed that the crush force decreased with increasing of tube diameter. The resistance of larger tubes to lateral collapse is lower than in the case of the smaller tubes, so lower reaction forces can be obtained in the larger tubes. This effect was found to be consistent with the effect of circular tube diameter on its collapse load, as addressed by [66] and [70]. Figure 6-55 shows the interaction effect of width and thickness on the collapse load (F). A two-factor interaction effect occurs when the effect of a first factor on the design response depends on the setting of the second factor. From Figure 6-55, it can be seen that the effect of tube thickness on F depended on the tube width. The effect of thickness on F is more significant in the wider tubes. It can be reported that thicker and longer oblong tubes require a higher load to initiate lateral collapse due to the greater amount of material across the section of the tube. The same observation was reported by [66] for the lateral collapse of circular tubes. Figure 6-56 shows the variation of F with thickness and width. It can be seen that the minimum magnitude of F was obtained when the minimum magnitude of width was chosen.

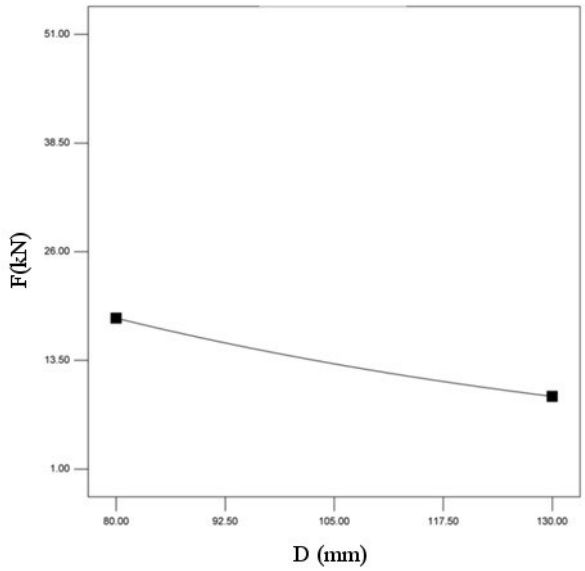

Figure 6-54: Effect of diameter on F (OTFIU).

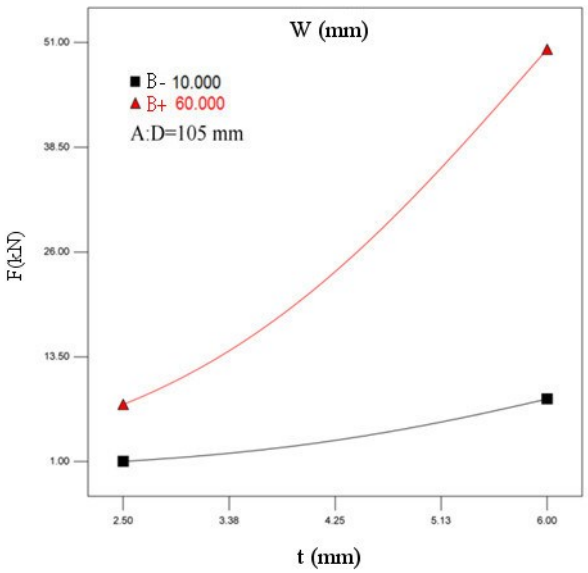

Figure 6-55: Interaction effect of Thickness and width on F (OTFIU)

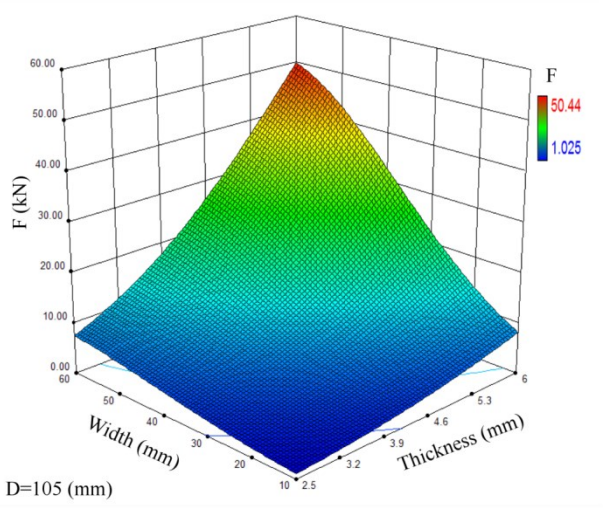

Figure 6-56: Variation of F with thickness and width (OTFIU).

6.2.7 Multi-objective optimization design (MOD) of OTFIU system

In order to find the best oblong tube geometry for crashworthiness applications, the procedure of multi-objective optimization design (MOD) was applied. Tube diameter D, thickness T, and width W were selected as design parameters. In crashworthiness design, the energy-absorption capacity of a thin-walled tube is evaluated by means of the specific energy absorption (SEA), which is the energy absorbed per unit mass of a thin-walled tube. Therefore, the main objective of this optimum design is to maximize the SEA. On the other hand, and based on human safety issues, the collapse load (F) should not exceeds a certain criterion. Thus the collapse load (F) can be set and minimized as another objective function. The RS models constructed in Section 6.2.5 were employed to obtain the MOD. The desirability approach was adopted for solving the MOD problem. Design-expert software was employed to apply the desirability approach and find the optimal solution. The design variable limits and responses objectives of the MOD are listed in Table 6-17.

Table 6-17: The criterion of numerical optimization (OTFIU).

Name	*Goal*	*lower Limit*	*Upper Limit*	*Weight*	*Importance*
D (mm)	is in range	80	130	1	3
t (mm)	is in range	10	60	1	3
W (mm)	is in range	2.5	6	1	3
SEA (J/kg)	maximize	1122.16	7504	10	5
F (kN)	minimize	1.025	50.44	1	3

The Table 6-18 shows the geometrical factors that lead to a maximized SEA and minimized F. The best desirability was achieved when the tube diameter and tube width were set at their minimum limit (80 mm, 10 mm), and the maximum tube thickness (6 mm).

Table 6-18: Optimal solutions as obtained by Design-Expert (OTFIU).

Number	*Diameter(mm*	*Width(mm)*	*Thickness(mm*	*SEA(J/kg)*	*F(kN)*	*Desirability*
1	80	10	6	6492.91	11.88	0.31
2	80	10.27	6	6492.87	12.08	0.309
3	80	10.84	6	6490.09	12.52	0.307
4	80	11.53	6	6492.92	13.08	0.306
5	80	11.81	6	6492.92	13.31	0.306

The model with the optimized configuration was tested numerically to confirm the validity of optimized results. The Table 6-19 shows the comparison between the numerical results and the predicted results. The geometrical shape and the responses of optimal solutions are also displayed in Table 6-19. It can be seen that the numerical results offered by FE (ANSYS) are in reasonable correlation with the predicted results offered by RSM (DOE).

Table 6-19: Confirmation experiment of optimal solution (OTFIU)

	SEA (J/kg)	*F (kN)*
Numerical	6821.4	11.71
Predicted	6492.917	11.81
Error	4.80%	0.85%
Geometry	*Force and Energy Responses of optimal configuration*	
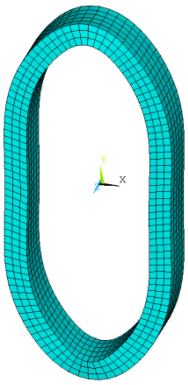	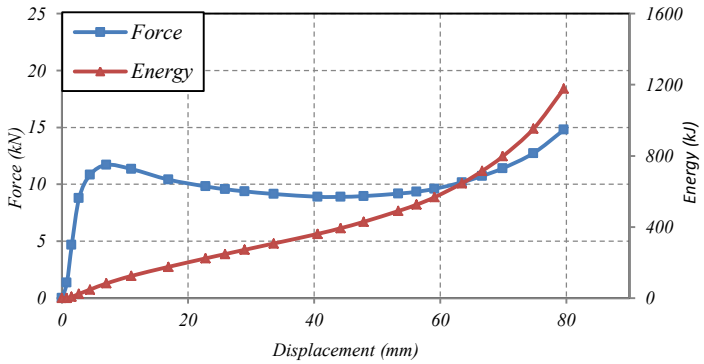	

The following important practical conclusions can be drawn from the parametric and optimization study of OTFIU system:

1- The specific energy absorption capacity (SEA) of oblong tubes under lateral loading increases with increasing thickness and decreasing diameter. The effect of tube width on SEA is insignificant.
2- The collapse load (F) can be controlled by changing the geometrical parameters. It increases with increasing thickness, increasing width, and decreasing diameter. However, the tube diameter is not as effective for controlling F as the tube width and tube thickness.
3- From MOD studies it was found that thicker, shorter, and smaller oblong tubes are more appropriate for crashworthiness applications.

6.3 Elliptical tube

The elliptical tubes crushed laterally were also proposed as energy absorbing components. A set of numerical simulations was carried out to investigate the effect of the elliptical ratio (r) on the responses of elliptical tubes under lateral loading.

6.3.1 Effect of elliptical ratio on the responses of laterally crushed elliptical tubes (ET)

Figure 6-57 shows the elliptical tube geometry. The elliptical ratio (r) is defined as the ratio between horizontal and vertical semi-axes of the elliptical tube and given by:

$$r = \frac{b}{a} \tag{6-6}$$

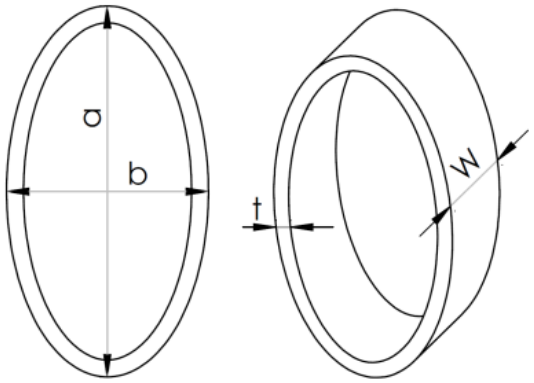

Figure 6-57: Elliptical tube.

Figure 6-58 and Figure 6-59 display the force-displacement and energy-displacement curves for elliptical tubes with different elliptical ratios compressed under quasi-static lateral loadings. Upon examination of Figure 6-58, it can be seen that in the early stages of deformation, the load is increased linearly with the displacement up to the characteristic ‘collapse’ load. This stage is called the elastic phase. It is clear that the elliptical ratio had a significant influence on the value of the collapse load, with the latter increasing as the elliptical ratio decreased. After the elastic phase, and

based on the value of the elliptical ratio, the elliptical tubes might experience strain hardening behaviour or the strain softening phenomenon. Tubes with an elliptical ratio of more than r=0.75 exhibited a softening behaviour in the post collapse stages. This behaviour is due to the radius of the curvature of the ellipse at the top and bottom of the vertical hinge line having increased. Therefore the contact between the flat plate indenter and the elliptical tube can be approximated as a 'point' load application, as reported by Shim and Stronge [62]. This resulted in a greater moment arm from the point of load application to the horizontal hinge points for each tube. And because of this less force was needed to maintain the deformation, and hence a strain - softening stage occurred. For elliptical tubes with a ratio of less than r=0.75, a strain hardening behaviour was recorded. This trend might be due to the radius of curvature of the elliptical tube having decreased at the top and bottom of the vertical hinge points. Therefore, upon initial contact, one line of contact was established between flat plate indenter and the elliptical tube, however as deformation proceeded, this contact line split in two and moved away from the centreline, causing the moment arm to reduce about the horizontal hinge points. Therefore, as a consequence, a greater force was needed to sustain the deformation. This behaviour is termed geometrical strain – hardening, as demonstrated by Reddy and Reid [68]. The elliptical tube with an elliptical ratio of r=0.75 offered an intermediate response between strain hardening and strain softening in which an almost perfectly plastic response was noted. At approximately 55 mm of deflection, a significant increase in load was noticed towards the end of the displacement stroke for all elliptical tubes due to the material strain hardening phenomenon. Table 6-20 presents the various energy absorption indicators for elliptical tube systems (ET). Both energy and specific energy increased with decreasing elliptical ratio. All tubes had the same value of crush efficiency because the same displacement was applied to all tubes. The tubes that had lower elliptical ratios exhibited higher efficiencies and weight effectiveness than the tubes that had higher elliptical ratios, due to the greater amount of energy that was absorbed by these tubes. However as discussed earlier in this section, the lower elliptical ratio might have caused strain softening behaviour in the post collapse stages so that the designer should be careful in choosing the appropriate elliptical ratio.

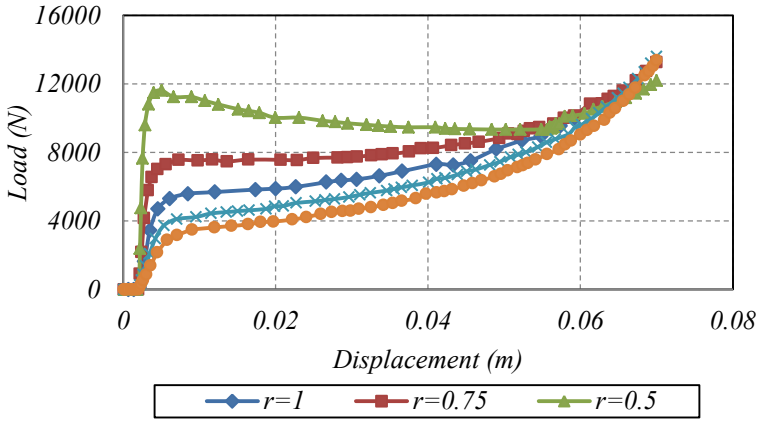

Figure 6-58: Load-displacement responses for elliptical tubes with various elliptical ratios.

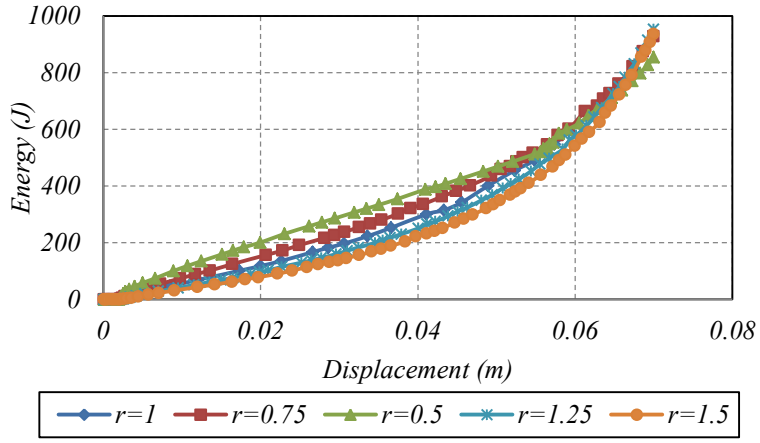

Figure 6-59: Energy-displacement response for elliptical tubes with various elliptical ratios.

Table 6-20: Comparison of effectiveness indicators for ET systems.

r	*E*	*SEA(J/kg)*	e_σ *(%)*	e_E *(%)*	W_{eff} *(J/kg)*
0.5	685.94	4122	70%	56%	2885
0.75	581.17	2836.5	70%	44%	1985
1	478.36	2039	70%	35%	1427
1.25	448.97	1685	70%	33%	1179.5
1.5	398.82	1334	70%	30%	934

6.4 Summary

This chapter investigated the responses and energy absorption characteristics of short length single tubes under lateral loading. Three configurations were analysed and named as circular, oblong, and elliptical tubes. In the first section of this chapter, the responses of circular tubes under quasi-static and dynamic loading conditions were addressed. The effect of cross section shape on the responses of circular tubes was investigated experimentally and numerically. The response surface method (RSM) for design of experiments (DOE) was used in conjunction with the finite element modelling (FEM) studied in (Chapter 5) to explore the effects of the other geometrical factors such as thickness (t), diameter (D), and width (W) on the responses of the circular tube. The specific energy absorption capacity (SEA) and the collapse load (F) of the circular tube were modelled as functions of geometrical parameters. Based on the developed models of the SEA and F, the approach of multi-objective optimization design was applied to find the optimal configuration of the circular tube. The responses of circular tubes under lateral oblique loads were also examined in this section. In the second section of this chapter, the responses of oblong tubes under lateral loadings were introduced. The oblong tubes were subjected to lateral compression by various indenters and exposed to various external constraints. The RSM was employed along with FEM to attain a thorough investigation of the effects of geometrical parameters on the responses of oblong tubes under lateral loading. The multi-objective optimisation design was also carried out to seek the optimal configuration of oblong tubes. The last section of this chapter detailed the responses of elliptical tubes under lateral loading. Based on the validated finite element model, the effect of the elliptical ratio (r) on the load and energy responses of elliptical tubes were presented and discussed.

7

Chapter 7

RESPONSES OF NESTED TUBES UNDER LATERAL LOADING

7.1 Introduction:

In order to increase the energy absorbing capacity of single empty tubes, nested tube systems using internally stacked groups of circular tubes have been proposed in the past. Nested tubes systems are of particular importance for applications that are restricted in terms of space and with a limited crush zone. In the present study, three different configurations were analysed, all of which have deformable tubes arranged so that they deformed synchronously upon loading, in order to achieve the desirable force-deflection response.

7.2 Responses of nested systems under quasi-static loading conditions

7.2.1 Analysis of the NTCO system

The Figure 7-1 shows the force and energy responses of the NTCO system, and The Figure 7-2 shows the deformation history of NTCO system. Originally, this system consisted of two different circular tubes with a gap between them. This gap allowed

the two components to deform sequentially as loading proceeded, hence it caused a non-monotonic rise in force throughout the deformation stroke. In previous studies carried out by Olabi et al. [13] and [14], two cylindrical spacers were inserted between the gaps of the tubes to eliminate a non-monotonic increase in force as contact was establish between the tubes. In this system (NTCO), the gap between the tubes was eliminated by elongation of the internal tube which changed its profile to oblong. Using oblong tubes instead of circular tubes had two aims: firstly, to eliminate the non-monotonic increase in force, and secondly, to reduce mass as in other systems the cylindrical spacers used to fill the gap increased the mass of the system. Upon examination of the force-deflection response of the NTCO (Figure 7-1), it can be seen that the force increased linearly up to its characteristic 'collapse' load, followed by a slight strain hardening behaviour in the post collapse stages. The strain hardening behaviour of this system at the early stages of plastic deformation seemed to be negligible. This phenomenon is due to the use of a combination of two different profiles (ie: circular & oblong) that have contrary hardening behaviours. At approximately 50 mm deflection, the force started to rise again. This is due to the 'bottoming out' of the oblong tube. This can be avoided by simply applying a slightly shorter displacement stroke. It was noticed that the force response up to 50 mm deflection was almost rectangular in shape, which is a very desirable feature in energy absorption systems. As a result of obtaining this rectangular shaped response, the corresponding energy absorption response was almost linear for the entire deflection stroke. The deformation history of the NTCO is presented in Figure 7-2 . Upon observation of the collapse mode history (Figure 7-2), it can be seen that the system exhibits a symmetrical mode of collapse at all stages and the two components of the system deformed simultaneously.

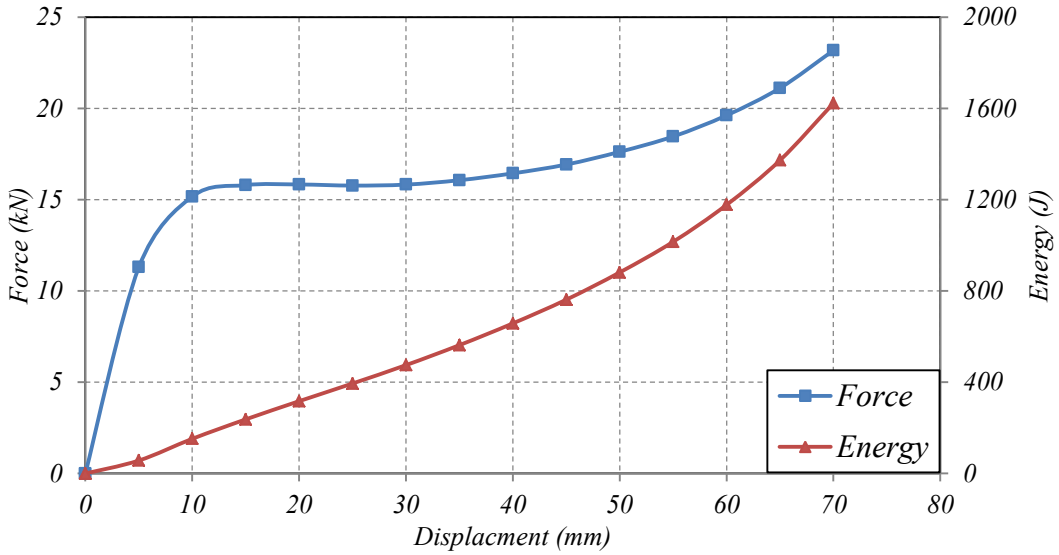

Figure 7-1: Experimental force and energy responses of a NTCO system.

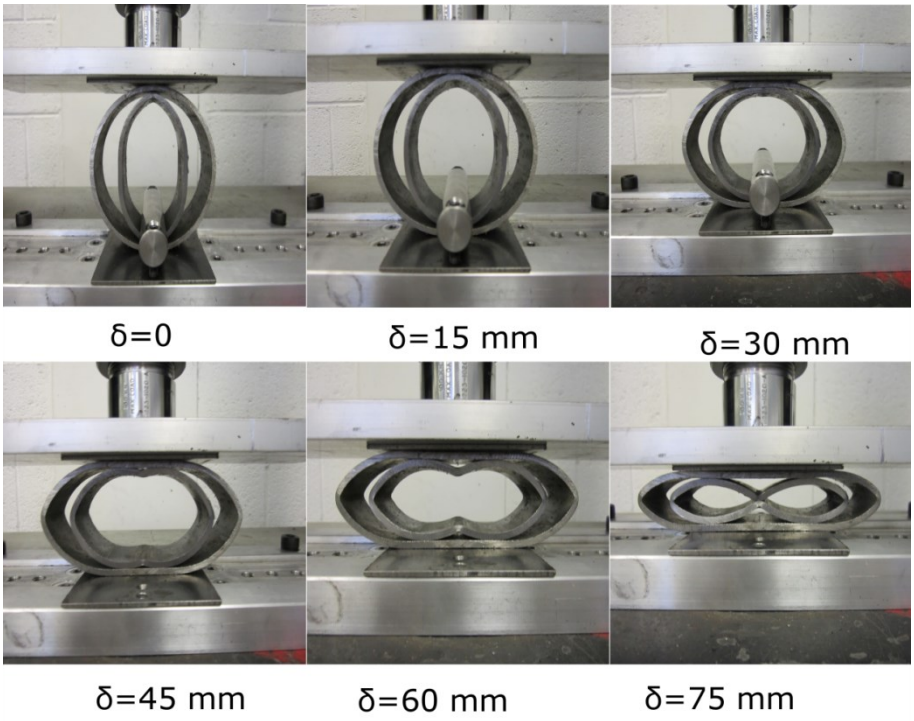

Figure 7-2: Deformation history of a NTCO system.

7.2.2 Analysis of the NTDC system

The NTDC system consists of two small tubes placed inside one large tube; the internal tubes have different diameters and the same thicknesses. The energy and force responses of the NTDC system are depicted in Figure 7-3, with the various stages of deformation of a typical sample shown in Figure 7-4. In the range up to 70 mm deflection, the force response of the NTDC had a rectangular shape. The small tube was not deformed at this stage and worked as a cylindrical indenter for compression of the other internal tube. This rectangle response is due to a combination of strain hardening of the outer tube which was compressed by a flat plate indenter, and strain softening of the internal large tube which was compressed by the small internal tube. Once the large tube collapsed and was completely destroyed (at approximately 70 mm deflection), the small internal tube started to deform causing an increase in the force values of up to 27.5 [kN], following which the whole system start to strain harden up to the end of the compression process. The test was stopped at a deflection of 90 mm, due to the significant increase in the load might cause harm to the testing instrument. From the various stages of the deformation profile of the NTDC presented in Figure 7-4, it can be seen that the system exhibits an asymmetry collapse around the horizontal axis, while it collapses symmetrically around the vertical axis. The asymmetrical collapse mode is due to the fact that two components of the system (the large tubes) deformed simultaneously at the beginning of the collapse, while the smaller tubes deformed at the very end of compression process.

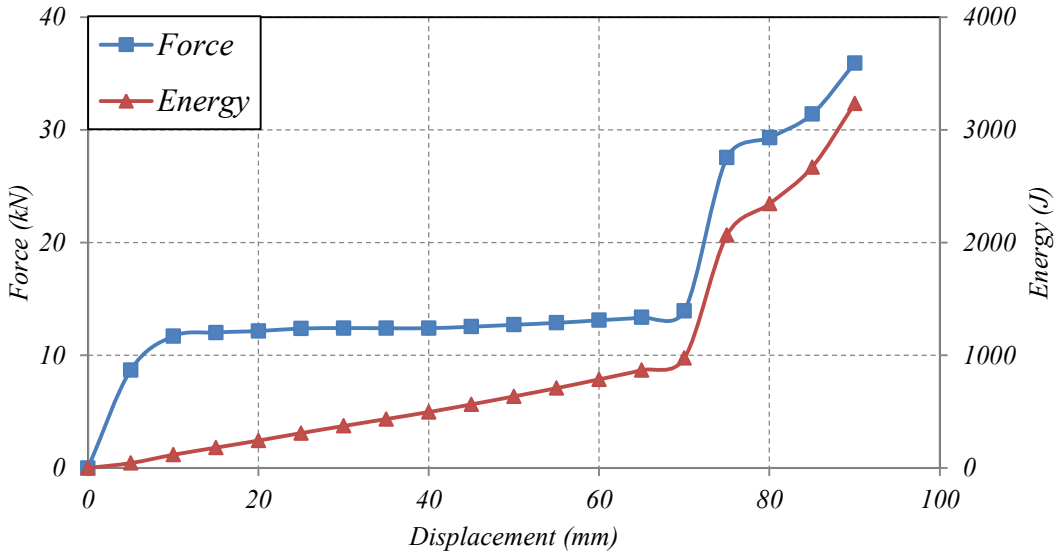

Figure 7-3: Experimental force and energy responses of the NTDC system.

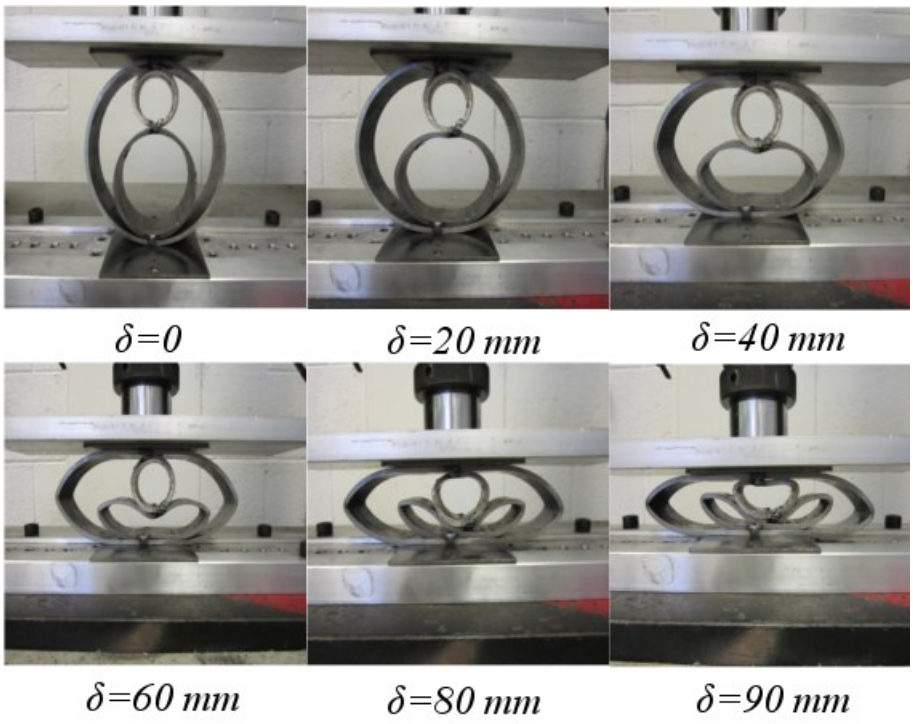

Figure 7-4: Deformation history of the NTDC system.

7.2.3 Analysis of the NTSC system

Generally, for an effective energy absorbing structure, the system components need to deform simultaneously. To apply this concept, the different sized circular tubes of the NTDC were replaced by same sized tubes. The internal tubes had the same

thicknesses and same diameter and were manufactured from the same material. Theoretically, when a compression load is applied to the NTSC system, the three components (outer large tube & internal small tubes) should deform at the same time. The Figure 7-5 displays the experimental responses of the NCST system along with the various stages of deformation in Figure 7-6. Upon examination of Figure 7-6, it can be seen that a symmetrical collapse mode was not achieved, and neither was the simultaneous deformation of the three components. One possible reason for this phenomenon may be the difficulty of getting two tubes that are exactly the same for the internal components. It was therefore concluded that the NTSC system was more sensitive to geometrical imperfections, with any small difference between the internal tubes resulting in the collapse of one tube before the other. From the force response of the NTSC shown in Figure 7-5, the strain hardening rate is higher than that noticed in the NTDC, as the internal tubes are of the same size. A slight rise in force was noticed at a deflection of 55 mm. This rise was due to the collapse of the second internal tube and the self-contact of the first internal tube. At approximately 75 mm of deflection, the system starts to experience a significant increase in force up to the end of the compression process. This increase is due to the material strain hardening that occurred in the three tubes, which led to a greater overall force required to compress the system.

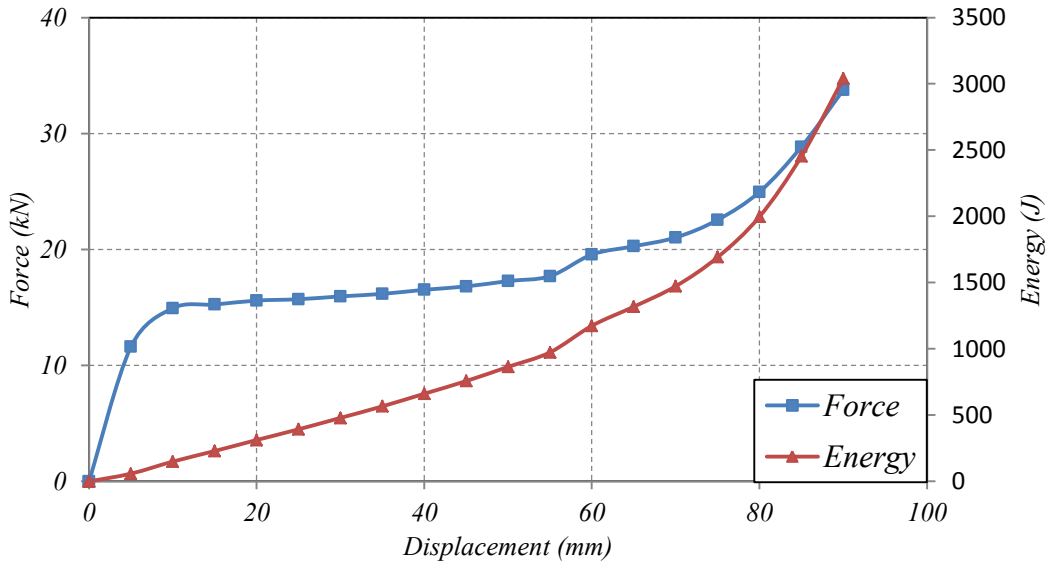

Figure 7-5: Experimental force and energy responses of the NTSC system.

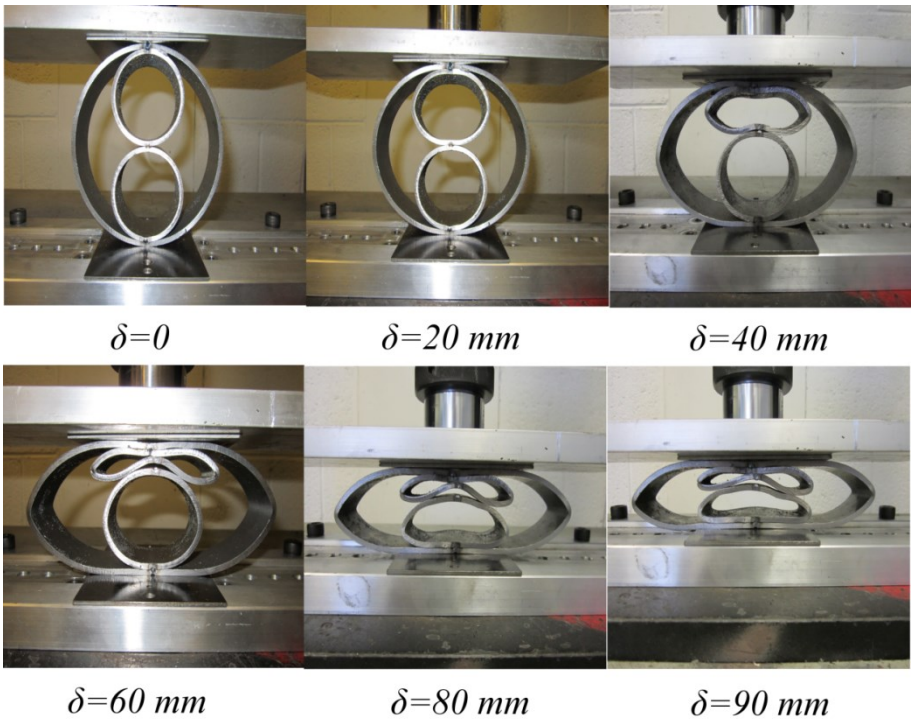

Figure 7-6: Deformation history of the NTSC system.

7.3 Responses of nested systems under dynamic loading conditions

7.3.1 Evaluation of the NTCO

The dynamic load-deflection response of NTCO was very close to its quasi-static counterpart, as can be seen in Figure 7-7. This indicates the insignificant role of strain rate and inertial effects on the dynamic response of the system under the given applied velocity of the striker. The initial and final deformed stages of the NTCO system under dynamic loading are plotted in Figure 7-8. From this figure, it can be observed that the final deformed profile of the system under the quasi static and dynamic loading conditions are very similar. In general, the energy dissipated by the lateral collapse of the thin walled components is localised around the plastic hinges which were formed during the collapse. Taking into account the similar deformation

modes of NTCO under various loading conditions, the amount of dissipated energy by the NTCO under both conditions was similar.

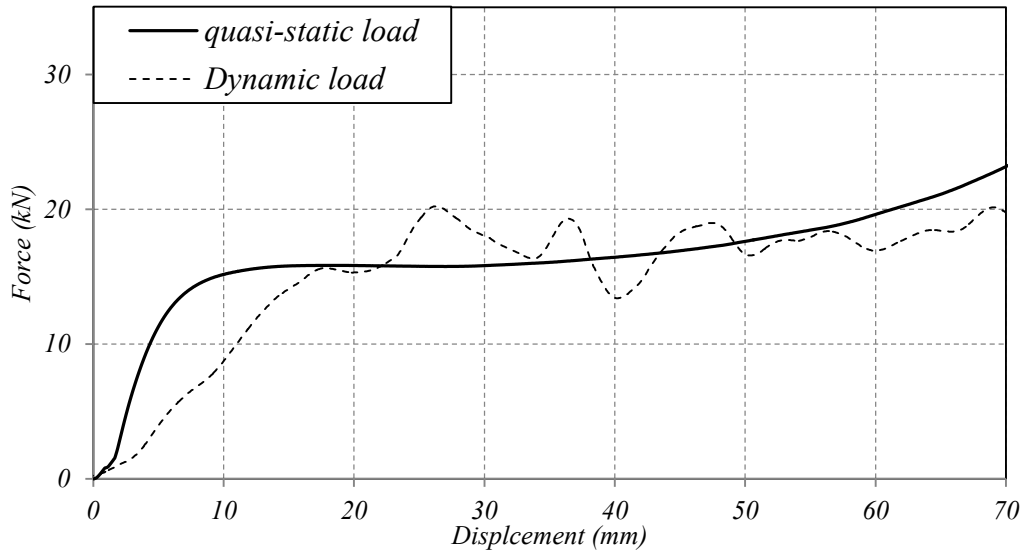

Figure 7-7: Comparison of load-displacement curves of the NTCO system for quasi-static and dynamic crushing (v=4.5 m/sec).

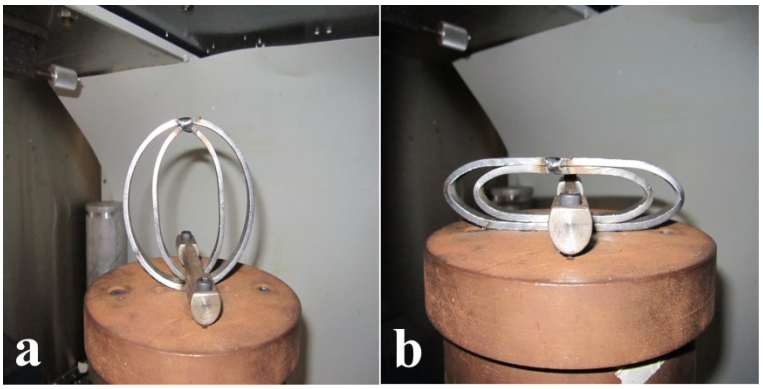

Figure 7-8: a- initial, and b- final stages of NTCO under dynamic loading.

Figure 7-9 shows the collapse stages of the NTCO system under two different impact velocities. It can be seen that for test velocity v=4.5 m/sec, the collapse modes are very similar to the modes under quasi-static loading. But for high impact velocity v=100 m/sec, the effect of system inertia becomes more significant, as the system start to deform close to the impact region with a slight deformation noticed in the bottom regions. As the compression proceeds, more plastic deformation was transferred to the other parts of the system. More information about the effect of

inertia and impact velocities on the responses of nested systems is presented in section 7.3.3.

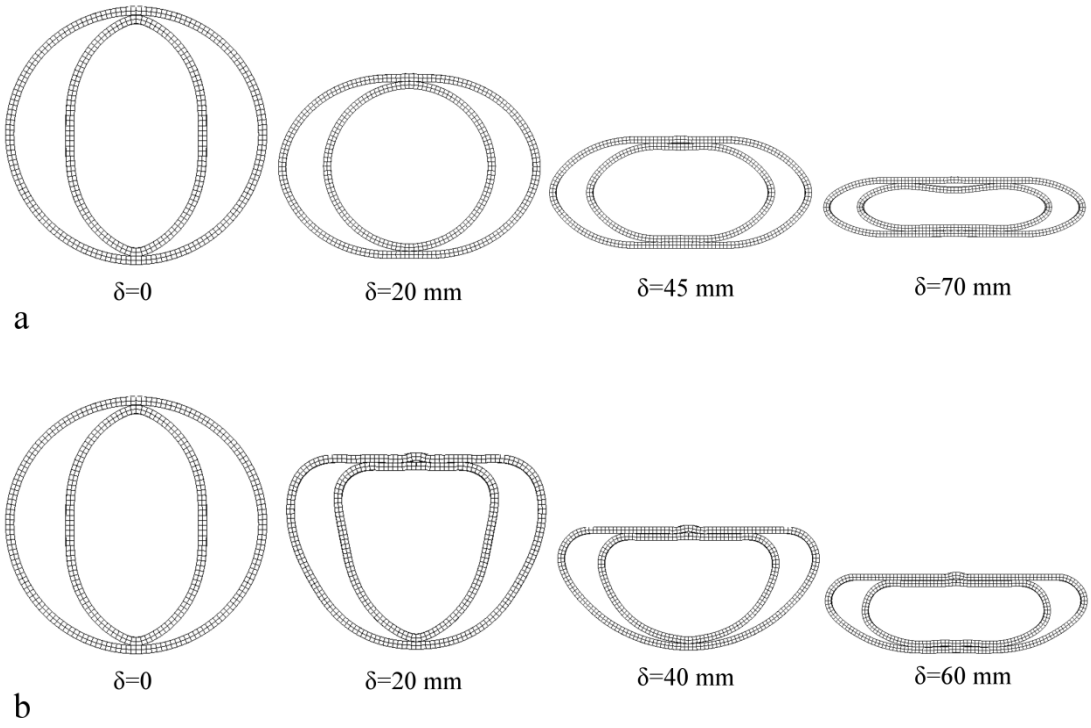

Figure 7-9: Deformed profiles of the NCOT system under two different compression velocity a: v=10m/sec, and b: v=100 m/sec.

7.3.2 Evaluation of the NTDC

The quasi-static and dynamic force deflection response of NTDC is presented in Figure 7-10. Due to the presence of the clamping bar in the dynamic test, the full collapse of the large inner tube was not achieved. At approximately 49 mm of deflection, the small inner tube started to collapse causing a rise in the dynamic force. Apart from the geometrical difference between the quasi-static and dynamic tests due to the need for clamping the absorbing system, the crushing strengths of the systems under both loading conditions were very similar. This is evidence of the insignificant role of the dynamic effects on the system response under test impact velocity. Also, as evidence of the negligible role of the inertia effects for the given test velocity (v=4.5 m/sec), the deformation profile of the system was plotted in

Figure 7-11. It can be seen that the final deformation profile of the system under dynamic loading is very similar to that of quasi-static loading, particularly if the symmetric collapse mode of the large outer tube is taken into consideration.

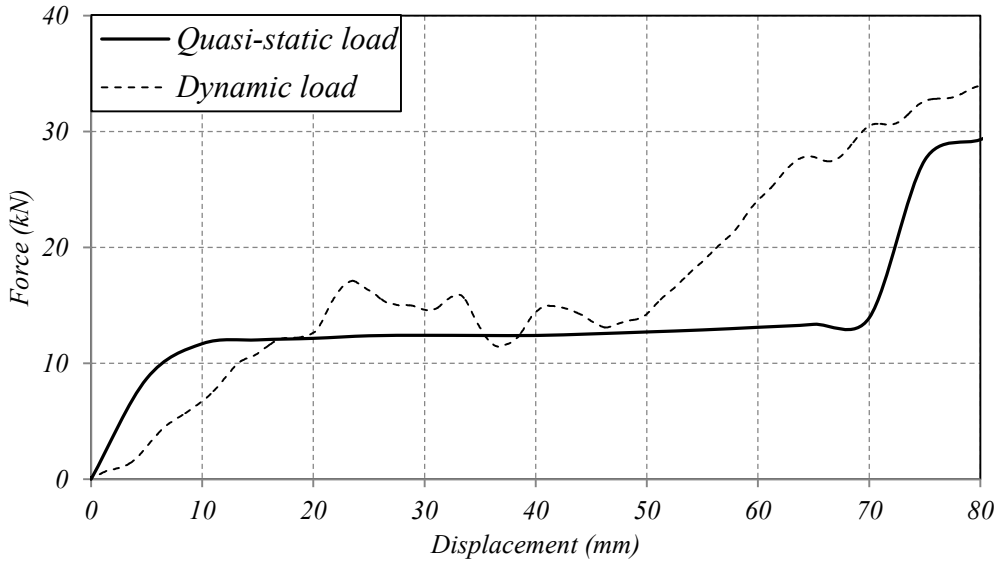

Figure 7-10: Comparison of load-displacement curves for the NTDC system for quasi-static and dynamic crushing (v=4.5 m/sec)

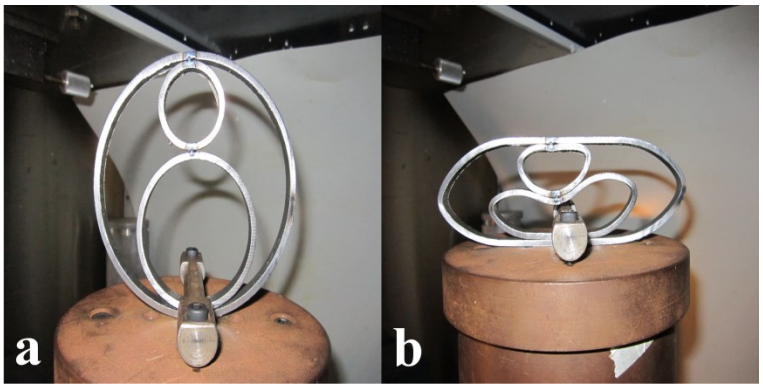

Figure 7-11: a- initial, and b- final stages of the NTDC under dynamic loading

The inertia effect of the dynamic loading becomes more important and significant in the event of high impact velocity. The Figure 7-12 shows the deformation history of NTDC under high and low impact velocities as indicated by the FE simulation. This figure demonstrates how the plastic deformation of the system under high impact velocity took place around the impact region, thus causing the energy to be

dissipated in the components close to the impact (i.e.: the upper small tube). For a low impact velocity, the deformed profiles seem to be the same as those for quasi static loading. It should also be noted that in spite of the stiffness of the small tube being higher than the lower internal tube, it was deformed before the large tube when the system was subjected to high impact velocity. So it can be concluded that system inertia is the dominated factor in the case of high impact velocity.

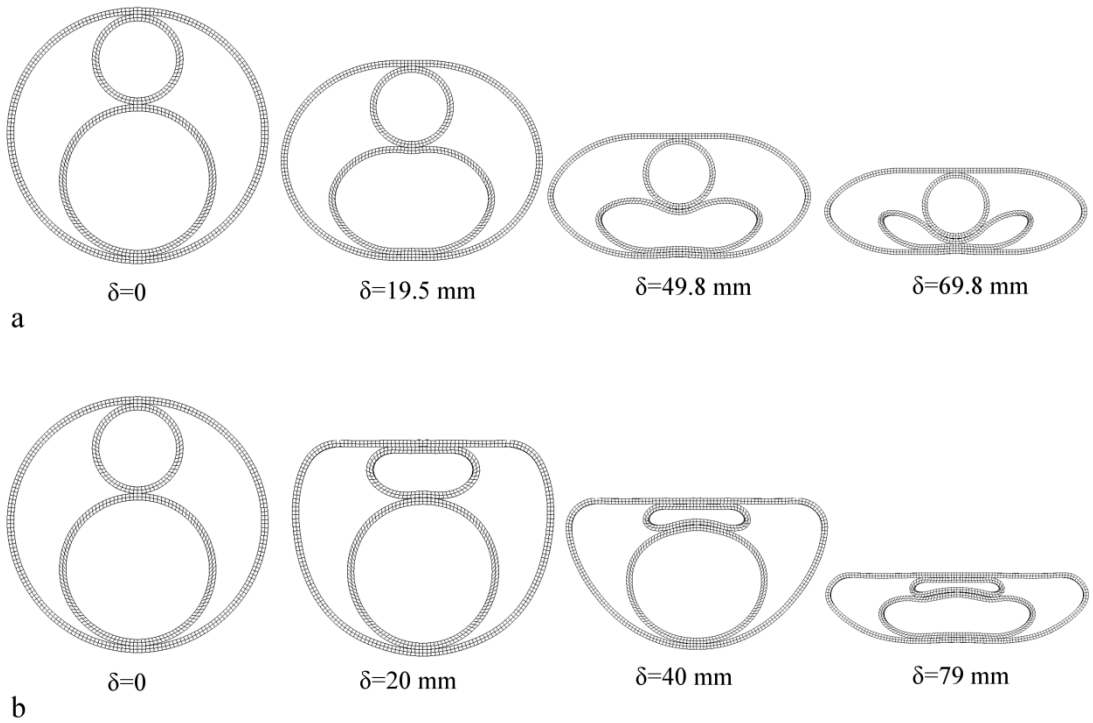

Figure 7-12: Deformation profiles of the NTDC system under two different compression velocity a- v=10m/sec, and b- v=100 m/sec

7.3.3 Evaluation of the NTSC

The load-deflection curves of the NTSC system under quasi-static and dynamic loading conditions are shown in Figure 7-13. The dynamic results are for an impact velocity of 4.5 m/s. The initial and final stages of the deformation under impact loading are presented in Figure 7-14. From Figure 7-13, it can be seen that the dynamic force-displacement response is very similar to its quasi-static counterparts. The close responses of the NTSC under quasi-static and dynamic loadings demonstrate that the strain rate and inertial effects for the given applied velocity of the striker are almost negligible.

Upon examination of the deformed profiles of the NTSC (Figure 7-14), it can be clearly seen that the three components of the system have been crushed simultaneously and an almost symmetrical collapse mode was obtained.

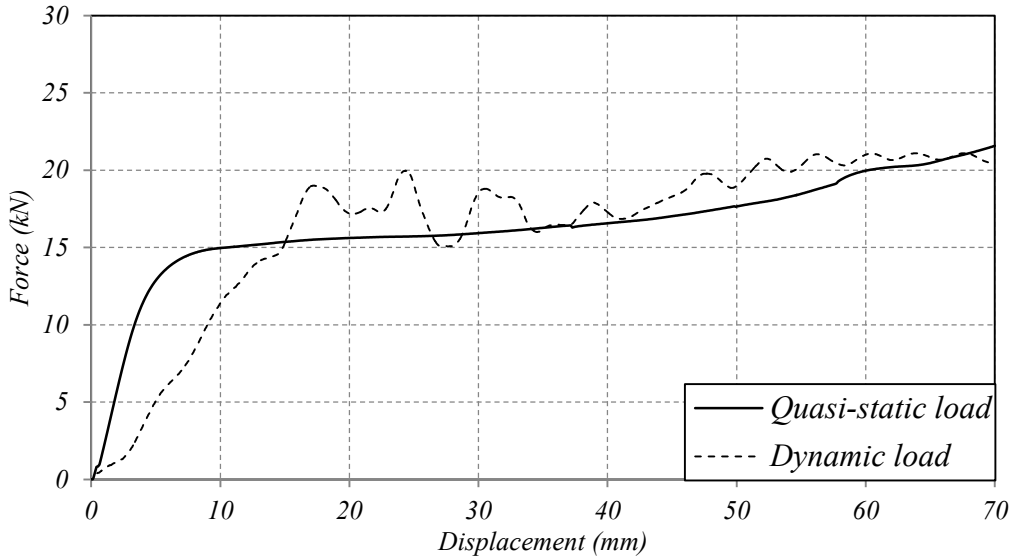

Figure 7-13: Comparison of the quasi-static and dynamic crushing load-displacement curves for the NTSC system (v=4.5 m/sec).

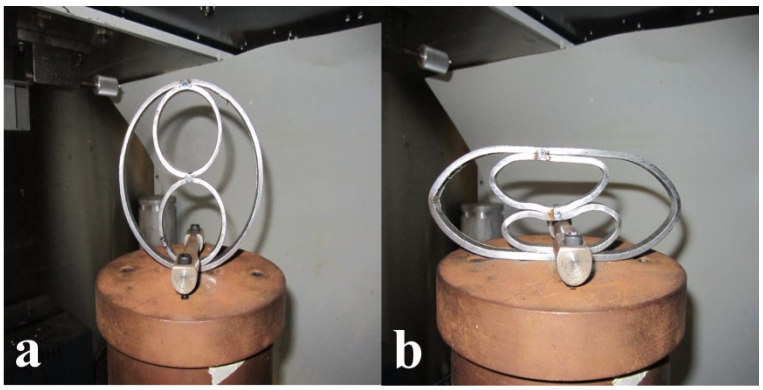

Figure 7-14: a- initial, and b- final stages of NTSC under dynamic loading.

Figure 7-15 illustrates the effect of the impact velocity on the energy absorbed by the NTSC system. This figure plots the energy-deflection responses of the NTSC under different impact velocities. It can be seen that the absorbed energy increased as the impact velocity increased. It also shows that when the impact velocity was less than

a certain value, the energy absorbed by the structure was not significantly affected by the velocity. This is due to fact that the deformation mode of low impact velocity remains the same as that in the quasi-static case, with a little more plastic deformation localised around the "plastic hinges". For a high impact velocity (v=100 m/sec), a notable increase in energy absorption was recorded. This behaviour might be due to the inertia effect that changed the collapse mode of the NTSC system, as the plastic deformation started in the impact region and then gradually propagated to the whole of the system. The Figure 7-16 shows the collapse sequence of the NTSC system under two different impact velocities. A typical deformation mode was offered by the system under low impact velocity (v=4.5 m/sec). While for v=100 m/sec, the plastic deformation initially occurred near the impact region of the system (upper part of the system), with a little bending deformation in the rest of the system. As the system was further compressed by the upper plate, further plastic deformation extended to the whole system. To assess the energy dissipation characteristics of the NTSC system, the energy dissipated by each component of NTSC system was plotted in Figure 7-17. Upon examination of this figure, it can be seen that the lower small tube did not contribute to the energy dissipation process until the crushing of the upper tube at approximately 40 mm of deflection. This is evidence of the inertia effect with a localised deformation near to the impact region at the beginning of the impact event.

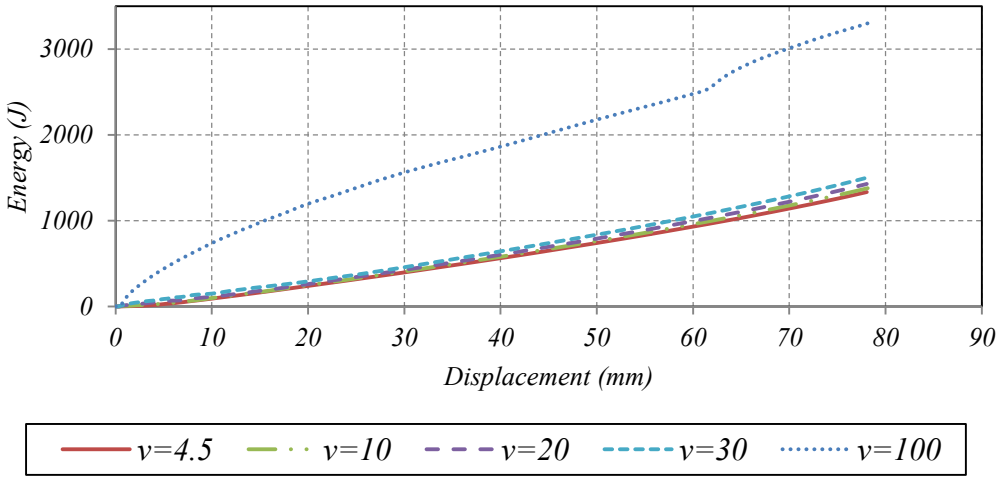

Figure 7-15: Energy-deflection responses of the NTSC system under different impact velocities.

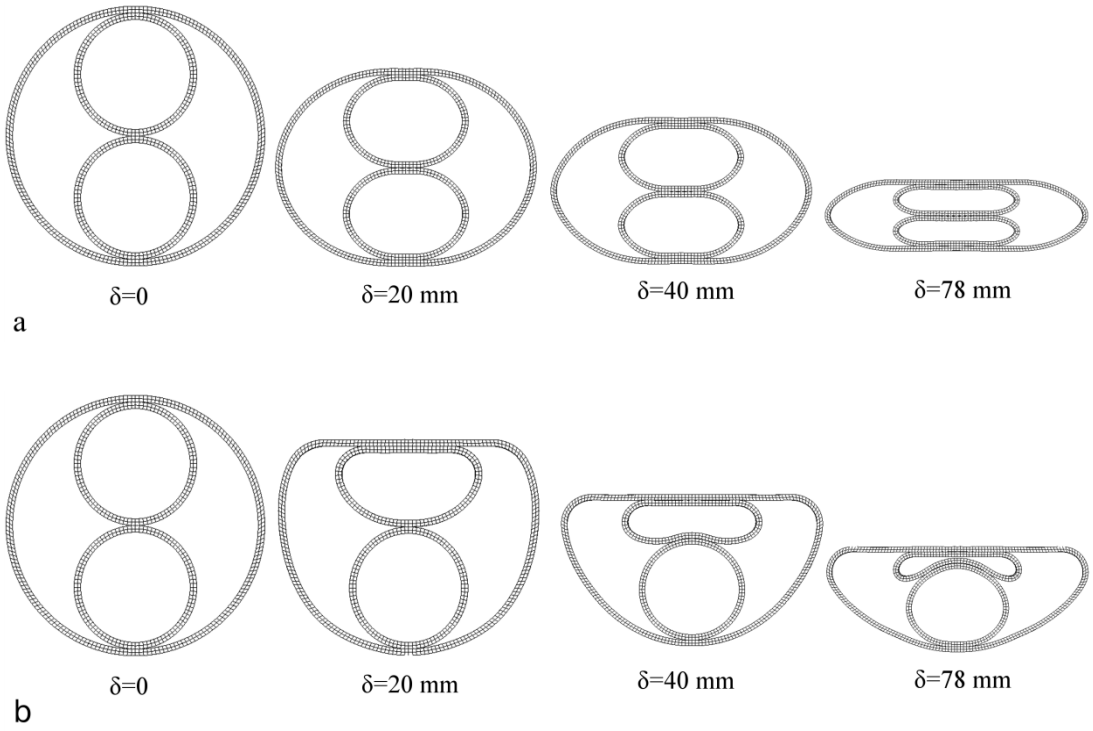

Figure 7-16: Deformation profiles of the NTSC system under two different impact velocity, a: v=10 m/sec, and b: v=100 m/sec.

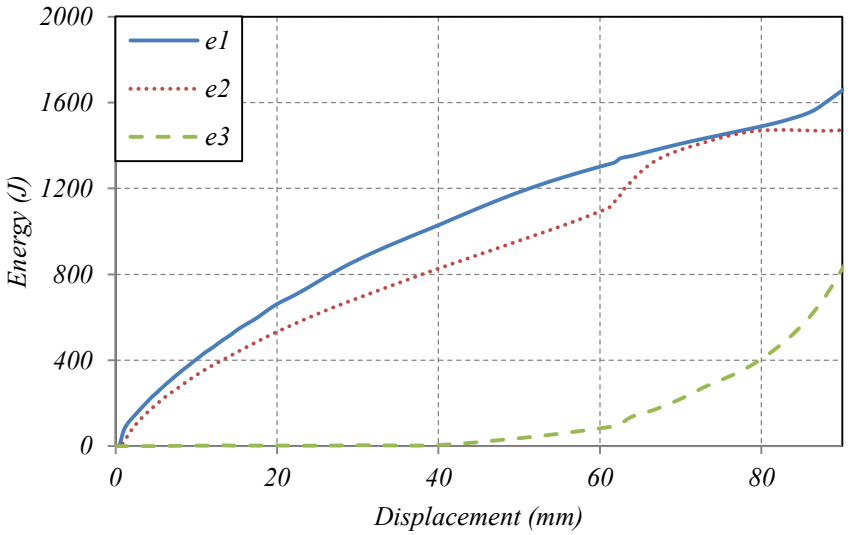

Figure 7-17: Energy-displacement responses for each component of the NTSC system under an impact velocity of 100 m/sec where e_1 is the energy absorbed by main tube, e_2 is energy absorbed by upper tube and e_3 is the energy absorbed by the lower tube.

7.4 Summary

This chapter presented the experimental and numerical analysis of various nested systems subjected to lateral quasi-static and dynamic loading. Three configurations of nested tube systems were analysed in this chapter. This chapter was divided into two main sections. In the first section a detailed description was given on the lateral collapse of nested tubes under quasi-static conditions. In the second section the responses of nested systems under lateral dynamic loading were presented and discussed. Furthermore, the effect of impact velocity on the dynamic responses of these systems was also examined numerically by using the validated finite element models presented in Chapter 5.

8

Chapter 8

DISCUSSION & CONCLUSION

8.1 Discussion

This research addressed the design and analysis of metallic tubes subjected to lateral compression. The laterally compressed tubes have received less research attention in comparison with axially compressed tubes. The ultimate goal of this research was to generate the design guidelines for the thin-walled empty and nested tubes crushed laterally under quasi-static and dynamic loading, and to employ these components in the crashworthiness applications and energy absorption systems such as crush boxes behind car bumpers (Figure 1-3). Two different configurations of energy absorbing mechanisms were studied in this thesis. The first type was a single tube. The main configuration studied in the category of single tubes was the circular tubes. The lateral collapse of circular tubes was investigated by many researchers [66], [68], [69], [70], and [87]. All studies showed that the collapse mode of circular tubes was plastic bending at plastic hinges. From the structural mechanic studies, it is well known that the value of fully plastic bending moment depends on the shape of cross section [15]. To this end, the effect of longitudinal cross section shape on the responses of circular tubes was presented in section 6.1.1. Five different shapes for

the cross section were analysed experimentally and numerically. The circular tube with a cross section I in the longitudinal direction offered the maximum value of specific energy absorbed (SEA) and best efficiencies. This was due to cross section I having the greatest magnitude of the $\frac{I}{A}$ ratio which made the collapse load (F) of the tube with cross section I higher than the other tubes, as was displayed in equation (6-4). However, the shape of the longitudinal cross section was found to have a slight effect on the responses of short length circular tubes crushed laterally as the dimensions of the longitudinal cross section were very limited. The effect of other geometry parameters such as diameter, thickness, and width on the responses of circular tubes was studied through applying RSM. The validated finite element model of the circular tube studied in sections 5.1.1 and 5.2.1 was integrated with the Response Surface Methodology (RSM) for the Design of Experiment (DOE) to study the effects of these parameters on the responses of circular tubes and to construct models for the specific energy absorption capacity (SEA) and collapse load (F). These models were used to perform the parametric studies and to find the optimal configuration of the circular tube energy absorber. The SEA of circular tubes under lateral loading increased with increasing the thickness. This was due to the fact that thicker tubes have more material for plastic deformation. Conversely, the SEA was found to be lower in a larger tube (tubes with greater diameter). This was due to localization of plastic strain around the plastic hinges that reduce the volume of material subjected to plastic deformation in the larger tubes. In addition, the increased weight in the larger tubes made the SEA lower. The crush force (F) was found to be greater in the thicker and wider tubes. This was due to the greater amount of material across the section of the tube, which effectively increased the lateral stiffness of the tube and hence it required a greater load to initiate the collapse. Also, it was found that the crush force was greater in the smaller tubes. This behaviour is due to smaller tubes having shorter moment arm from the point of load application to the horizontal hinge points. Therefore, a greater magnitude of force was required to initiate the collapse in the smaller tubes. Thinner and shorter circular tubes were less influenced by changing the tube diameter compared to longer and thicker tubes. As previously mentioned in this section, the developed models of SEA and F were used to perform the multi-objective optimization design

to seek the optimal configuration of energy absorbers as presented in section 6.1.4. The multi-objective optimization design (MOD) of the energy absorption structures were presented by many researchers [98], [120]-[129]. As a general rule in the crashworthiness design of energy absorbing structures, the structure with good crashworthiness is able to absorb as high energy as possible, with relatively as low crushing force as possible. So the SEA was selected as the first objective and maximized, while the collapse load (F) was taken as another objective and minimized. Actually, minimizing the collapse load in the crashworthiness design was based on the human safety issue as the large collapse load often leads to a high deceleration and may cause serious injury or even death of passengers inside the survival space. Also, minimizing the collapse force ensures that the absorber doesn't transmit too much force to the other parts of the protected structure. The design variables (the geometrical parameters) varied between upper and lower limits. The optimum configuration of the circular tube under lateral loading was found to have a minimum width, a minimum diameter, and a maximum thickness. So, it can be concluded that the circular tubes with smaller width (W) and diameter (D), and higher thickness (t) are more suitable for use as energy absorbing components. In the context of vehicle crashworthiness, the energy absorber is rarely subject to pure axial (straight) or pure bending load, rather it is subjected to combination of axial (straight) and non-axial or oblique loads. Therefore, the responses of circular tubes under oblique lateral loadings were studied in section 6.1.5. It was found that the collapse load and energy absorption decreased as the load angle increased for a given tube. Also, it was found that tube compressed by straight loading had higher efficiencies than both tubes compressed by oblique loading. This was due to a longer crush stroke and a higher energy absorption capacity (E) offered by this tube. Circular tubes crushed laterally under an oblique loading exhibited plastic bending collapse mode at all angles as shown in figures (Figure 6-18, Figure 6-19, and Figure 6-20). This feature can be considered an advantage for the lateral collapse procedure over the axial collapse of thin-walled members as the lateral collapse did not exhibit undesirable collapse modes. On the other hand, the undesirable collapse mode, termed global bending (Euler), was observed during the axial collapse of thin-walled members under an oblique load [9] and [102]. The Euler deformation mode is

generally unstable and can cause extreme reduction in the energy absorption capacity of a tube. The responses of circular tubes under lateral dynamic loading were presented in section 6.1.6. The responses of circular tube crushed under a low impact velocity were very similar to their quasi-static counterparts. This was due to insignificant effects of strain rate and inertia under low impact velocity (v=4.5 m/sec). The circular tube crushed under a high impact velocity (v=100 m/sec) was involved in an asymmetry collapse mode. This was due to inertia effects which had a significant effect on the response and the deformation mode of circular tubes under high impact velocity.

The second configuration of the single energy absorbing structures studied in this thesis was the oblong tube. The oblong tube was formed by elongating the standard circular tube plastically in the diametric direction as presented in section 6.2.1. To prove the effectiveness of the new modified form (oblong tube) as an energy absorbing device, a comparison of the crush behaviour of the oblong and circular tubes was performed in section 6.2.2. It was found that oblong tube showed more stable and almost constant force-deflection response in the post collapse stage. In addition, the energy absorption capacity of oblong tubes is greater than that for circular tubes of equivalent mass. The deformation mode of the oblong tubes was found to be as same as that of circular tubes (i.e, plastic bending at plastic hinges). Due to strain localisation around the plastic hinges, the concept of using external to increase the volume of material reaching plasticity was applied in section 6.2.3. Since the geometry profile of the rigid object impinging on the energy absorber in the real application does not has a standard profile and may neither be a flat rigid surface nor a point shaped indenter, but an intermediate condition between these, the oblong tubes were experimentally compressed using three forms of indenters named as flat plate, cylindrical, and point load indenters. It was found that the systems compressed by cylindrical and point indenters produced unstable deformation characteristics due to strain-softening phenomena noticed in the post-collapse stage of the load-displacement curves. Smaller crush and energy efficiencies were obtained from these systems (systems compressed by cylindrical and point-load indenters) because of the tendency for complete fracture to occur at the point of applied load. Performance characteristics as outlined in section 2.3 were used to

evaluate the various oblong tube systems. The maximum efficiencies were obtained from the OTFIU system because of its ideal response, while the maximum value of weight effectiveness was recorded in the case of the OTFISC system because of the greater amount of specific energy that it absorbed. Thus, the OTFIU system was selected as the best energy absorption system in the oblong tubes category due to its simple design, ideal force-deflection response, and maximum efficiencies. The design information for such oblong tubes (OTFIU) as energy absorbers can be generated through performing a parametric study. To this end, the response surface methodology (RSM) for the design of experiments (DOE) was employed along with finite element modelling (FEM), as outlined in section 6.2.6, to explore the effects of geometrical parameters on the responses of circular tubes and to construct models for the specific energy absorption capacity (SEA) and collapse load (F) as functions of geometrical parameters such as thickness (t), diameter (D), and width (W). The FE model of the oblong tube was constructed and experimentally calibrated as displayed in section 5.2.2. It was found that the tube geometry had significant effects on the responses of the OTFIU system. It was noted that the smaller and thicker tubes had higher SEA and F. Tube width was found to have an insignificant effect on SEA. Increasing tube width led to an increase of crush force. Based on the RS models of the SEA and F for the OTFIU system, the approach of multi-objective optimization design was applied to find the optimal configuration of the oblong tube. It was found that the optimal design for the OTFIU could be achieved if tube diameter and tube width were set at their minimum limit and tube thickness was set at a maximum.

The elliptical tubes were the third and final configuration in the category of single tube energy absorbers. The effects of the elliptical ratio (r) on the load and energy responses of elliptical tubes were introduced in section 6.3.1. It was found that the elliptical ratio had a great influence on the responses and collapse of elliptical tubes. The collapse load was found to be greater in the tubes with a smaller elliptical ratio. This behaviour is due to elliptical tubes with a smaller elliptical ratio having a shorter moment arm from the point of load application to the horizontal hinge points. Therefore a greater magnitude of force is required to initiate the collapse in these tubes. The greater collapse load in the tubes with a lower elliptical ratio made the energy absorbed by these tubes also greater. The post-collapse stages of the load-

displacement curves were also affected by changing the elliptical ratio. It was noticed that for tubes with an elliptical ratio higher than r=0.75, the force-deflection response exhibited strain hardening behaviour in the post collapse stages. While elliptical tubes with an elliptical ratio of lower than r=0.75, a strain softening behaviour was observed.The appropriate selection of the elliptical ratio can result in a rectangle force-deflection, which is very desirable in energy absorbing systems (for example an elliptical tube with r=0.75). In addition, it was found that the energy efficiency and work effectiveness were higher in the tubes with a lower elliptical ratio. This was due to a greater magnitude of energy absorbed by these tubes (ie: tubes with lower elliptical ratio).

The second type of energy absorbing structures studied and analysed in this thesis were nested tube systems (NTS). The nested systems were in the form of short internally stacked tubes. The NTS are of particular importance for applications that are restricted in terms of space and with a limited crush zone. The nested systems were proposed as energy absorbers in previous studies carried out by [13] and [14]. An attempt was made by them to optimise the response of nested system by inserting two cylindrical rods between the gaps of the tubes to provide the synchronous deformation for the members of the nested system and to eliminate a non-monotonic increase in the collapse force. Three different configurations of the nested tubes systems named NTOC, NTSC, and NTDC were analysed in the current study. Each configuration had deformable tubes which were arranged in particular ways so that they deformed synchronously upon loading in order to achieve the desirable force-deflection response. The responses of the nested tubes systems under quasi-static lateral loading were presented in section 7.2. It was found that the nested tube systems NTCO and NTSC exhibited *monotonically increasing* force-deflection responses due to synchronous deformation of all components. The NTSC system was very sensitive to geometrical imperfection as any slight difference between the geometries of internal tubes led to *non-monotonic increase* of the force-deflection response. A non-monotonic increase in the collapse force was noticed in the collapse of NTDC system. This behaviour is due to sequential deformation for the internal tubes of NTDC system. The responses of the nested systems under dynamic loading were displayed in section 7.3. It was found that the magnitude of response from the

dynamic cases was similar to their quasi-static counterparts under an experimental velocity of v=4.5 m/sec. This behaviour can be considered as an indicator of the non-significance of strain rate and inertial effects of the applied velocity of the striker. Since the dynamic loading instrument had a limited velocity of 4.5 m/sec, the validated FE model detailed in sections 5.1.2 and 5.2.3 was employed to investigate the responses of nested tube systems under higher impact velocities. Non-symmetrical collapse mode was noticed for all systems in the case of high velocity of the striker as shown in figures (Figure 7-9, Figure 7-12, and Figure 7-16). This is due to inertia effects that cause localised plastic deformation around the impact region. The effect of impact velocity on the dynamic responses of the nested systems was also investigated as shown in Figure 7-15. It was found that the nested tube systems absorbed more energy under high impact velocities. This trend may be due to the inertia effect increased plastic deformation around the plastic hinges. Also, it was found that at certain velocities, the nested tube systems dissipated the same amount of energy which indicates that the responses were not significantly affected by impact velocity. But when the impact velocity was raised above a certain level, the absorbed energy did increase with an increase of impact velocity due to inertia effects. This is evidence of the presence of a critical impact velocity, where under this velocity the dynamic effects on the responses of nested system can be neglected. Further investigation is required to establish the value of this critical velocity. The same behaviour was also noticed by [118] for dynamic response of the single circular tube.

For comparative purposes, the energy absorption characteristics of the main systems analysed in this thesis were calculated and tabulated in Table 8-1. Each of these systems was compressed up to 70 % of their original diameter/height to avoid the tube self-contact which leads to inefficient energy absorption process. Upon examination of the response characteristics in Table 8-1, it can be seen that the OTFIU exhibited the highest specific energy absorption capacity (SEA) followed by the NTSC, NTCO, CTFIU, and the NTDC system respectively. Due to higher SEA offered by the OTFIU, the use of oblong tube systems as energy absorbing structures are recommended for applications where weight reduction is important such as

moving structures (vehicles). In terms of energy efficiency, the OTFIU experienced the highest efficiency of approximately 60%, whereas the CTFIU and NTCO showed values of 47.9% and 48.7% respectively, with the nested tubes systems NTSC and NTDC showing the lowest values of e_E. Table 8-1 also illustrates the energy absorbed per unit crush length (E_{cl}) of five energy absorbers, where the NTCO shows the greatest E_{cl} followed by the NTSC, NTDC, OTFIU and the CTFIU respectively. It can be seen that the nested tubes systems have the higher values of E_{cl} , therefore use of nested tubes energy absorbers are highly recommended for applications where the available crush zone is limited.

Table 8-1: The various performance characteristics of the main systems analysed in this thesis.

	Geometry	*E (J)*	*Mass (kg)*	*SEA (J/kg)*	e_g *(%)*	e_E *(%)*	W_{eff} *(J/kg)*	E_{cl} *(J/mm)*
OTFIU	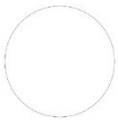	746	0.322	2316.77	70	59.4	1621.7	7.46
CTFIU		554	0.322	1720.5	70	48.7	1204.35	11.2
NTCO	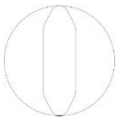	1141	0.6	1882.7	70	47.9	1317.9	27
NTSC	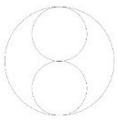	1648.4	0.843	1955.4	70	38	1368.7	21.7
NTDC	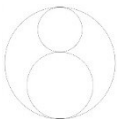	1385.8	0.829	1671.65	70	30.3	1170.15	15.3

8.2 Conclusion

The main aim of this thesis is to generate design information on the energy absorption responses of structural components under quasi static and dynamic lateral loading, in order to enhance their applicability as crashworthiness components and as energy absorbing devices. In order to achieve this objective, two types of systems were investigated, ie: empty tubes and nested tubes systems. The influence of the variations of geometric parameters on the force and energy responses of these systems was examined in detail to evaluate the energy absorbing capacity of all the systems under investigation. The main conclusions of this thesis can be summarized as follow:

- Design information on laterally crushed structural components was generated, by investigating the main and interaction effects of geometric parameters on the response of the proposed energy absorbing systems.
- Validated finite element (FE) models of various systems are cost-effective means of performing parametric studies of energy absorbing systems, as they negate real experiments.
- The response surface (RS) models constructed as part of this thesis can be used as mathematical models of the absorbed specific energy and collapse load as functions of the geometric parameters.
- Moreover, the multi objective optimization design (MOD) of the various systems of this research provided the optimal configuration for the various tubes. These optimal configurations resulted in the desired responses of thin walled tubes as energy absorbing devices.
- Absorption of impact energy through the lateral collapse of thin-walled structural components, as outlined in this thesis, has an advantage over the axial collapse of energy absorbing devices. This is because the dominant collapse mode of thin-walled members under lateral collapse is the bending mode, which results in a smoother force-deflection response. On the other hand, undesirable collapse modes such as global bending and Euler buckling have been reported for axial collapse by many researchers. In addition, the energy absorbed through lateral collapse can be easily enhanced and

controlled by introducing external constraints and using different indenters to compress the system.

- Finally it can be concluded that a positive outcome was achieved for the objectives of the thesis and can thereby contribute to the literature in the field of energy absorbers.

8.3 Future work

From the results outlined in this thesis, the following recommendations for future work are suggested:

- Further investigation is recommended of the use of thin-walled components crushed laterally as supplementary energy absorbing devices in Vehicle Frontal Protection System (VFPS). A primary study was carried out by the author as outlined in Appendices C. The aim of this primary study was to demonstrate the utilization of such energy absorbers in real engineering applications.
- Inclusion in the parametric studies and RS models developed in this thesis of loading parameters such as velocity, and material parameters such as density, is recommended for further investigation.
- It was mention in section 2.4.3, studies on the collapse behaviour and energy absorption response of foam-filled tubes under lateral loading were less reported in the literature. Therefore, the author recommends that further studies be conducted in the field of lateral collapse of sandwich tubes as follows.
  - Enhancing the energy absorption performance of laterally crushed sandwich tubes by employing external constraints as displayed in Appendices D.
  - Performing MOD study to construct the optimal configuration of sandwich tube systems under lateral loading.
  - Enhancing the energy absorption performance of laterally crushed systems by using nested sandwich tube system, (Appendices E), is also recommended for future work.

- The use of non-metallic foams such as polyurethane, polystyrene, polyethylene, etc., as foam cores in sandwich tube systems is recommended for future investigation.
- Investigation of the impact and energy absorption responses of sandwich tube systems with different geometric shapes of the outer and inner layers, like those displayed in Appendix E, is also suggested for future work.
- Finally, filling the sandwich tube system with a compound material such as foams of two different densities should also prove to be interesting in future work.

REFERENCES

[1] Calladine, C.and English, R., (1984), "Strain-rate and inertia effects in the collapse of two types of energy-absorbing structure", *Int.J.Mech.Sci.,* Vol.26 pp. 689-701.

[2] Zhang, T.and Yu, T., (1989), "A note on a 'velocity sensitive'energy-absorbing structure", *Int.J.Impact Eng.,* Vol.8 (1), pp. 43-51.

[3] Tam, L.and Calladine, C., (1991), "Inertia and strain-rate effects in a simple plate-structure under impact loading", *Int.J.Impact Eng.,* Vol.11 (3), pp. 349-377.

[4] Ahmad, Z. , (2009), "Impact and energy absorption of empty and foam-filled conical tubes", Queensland University of Technology,.

[5] Su, X., Yu, T.and Reid, S., (1995), "Inertia-sensitive impact energy-absorbing structures Part I: Effects of inertia and elasticity", *Int.J.Impact Eng.,* Vol.16 (4), pp. 651-672.

[6] Hanssen, A.G., Langseth, M.and Hopperstad, O.S., (2000), "Static and dynamic crushing of circular aluminium extrusions with aluminium foam filler", *Int.J.Impact Eng.,* Vol.24 (5), pp. 475-507.

[7] Karagiozova, D.and Alves, M., (2004), "Transition from progressive buckling to global bending of circular shells under axial impact—Part I: Experimental and numerical observations", *Int.J.Solids Structures,* Vol.41 (5), pp. 1565-1580.

[8] Reid, S.and Reddy, T., (1986), "Static and dynamic crushing of tapered sheet metal tubes of rectangular cross-section", *Int.J.Mech.Sci.,* Vol.28 (9), pp. 623-637.

[9] Nagel, G. , (2005), "Impact and energy absorption of straight and tapered rectangular tubes", Queensland University of Technology, Brisbane,.

[10] Harrigan, J., Reid, S.and Peng, C., (1999), "Inertia effects in impact energy absorbing materials and structures", *Int.J.Impact Eng.,* Vol.22 (9-10), pp. 955-979.

[11] Jones, N., (2011)*, Structural impact,* , Cambridge University Press,.

[12] Su, X., Yu, T.and Reid, S., (1995), "Inertia-sensitive impact energy-absorbing structures part II: Effect of strain rate", *Int.J.Impact Eng.,* Vol.16 (4), pp. 673-689.

[13] Olabi, A., et al., (2008), "Optimised design of nested oblong tube energy absorbers under lateral impact loading", *Int.J.Impact Eng.,* Vol.35 (1), pp. 10-26.

[14] Olabi, A., et al., (2008), "Optimised design of nested circular tube energy absorbers under lateral impact loading", *Int.J.Mech.Sci.,* Vol.50 (1), pp. 104-116.

[15] Lu, G. and Yu, T., (2003)*, Energy absorption of structures and materials,* , Woodhead Publishing,.

[16] Du Bois, P., et al., (2004), "Vehicle crashworthiness and occupant protection", *American Iron and Steel Institute, Southfield, 330p,* .

[17] Bisagni, C. (2002), "Crashworthiness of helicopter subfloor structures", *Int.J.Impact Eng.,* Vol.27 (10), pp. 1067-1082.

[18] Xue, P., Qiao, C.and Yu, T., (2010), "Crashworthiness study of a keel beam structure", *Int.J.Mech.Sci.,* Vol.52 (5), pp. 672-679.

[19] Marsolek, J.and Reimerdes, H., (2004), "Energy absorption of metallic cylindrical shells with induced non-axisymmetric folding patterns", *Int.J.Impact Eng.,* Vol.30 (8), pp. 1209-1223.

[20] Wang, L., et al., (2008), "An impact dynamics analysis on a new crashworthy device against ship–bridge collision", *Int.J.Impact Eng.,* Vol.35 (8), pp. 895-904.

[21] Ahmad, Z.and Thambiratnam, D., (2009), "Application of foam-filled conical tubes in enhancing the crashworthiness performance of vehicle protective structures", *International Journal of Crashworthiness,* Vol.14 (4), pp. 349-363.

[22] Clark, B., Thambiratnam, D.and Perera, N., (2008), "Enhancing the impact energy absorption in roll over protective structures", *International Journal of Crashworthiness,* Vol.13 (2), pp. 167-183.

[23] Dundulis, G., et al., (2009), "Static analytical and experimental research of shock absorber to safeguard the nuclear fuel assemblies", *Nucl.Eng.Des.,* Vol.239 (1), pp. 1-8.

[24] Thornton, P., Mahmood, H.and Magee, C., (1983), "Energy absorption by structural collapse.Chapter 4 Structural Crashworthiness. Editors: N. Jones and T. Wierzbicki", *Structural crashworthiness,* pp. 96–117.

[25] Olabi, A., Morris, E.and Hashmi, M., (2007), "Metallic tube type energy absorbers: A synopsis", *Thin-Walled Structures,* Vol.45 (7-8), pp. 706-726.

[26] Alghamdi, A.A.A. (2001), "Collapsible impact energy absorbers: an overview", *Thin-Walled Structures,* Vol.39 (2), pp. 189-213.

[27] Abramowicz, W. (2003), "Thin-walled structures as impact energy absorbers", *Thin-walled structures,* Vol.41 (2), pp. 91-107.

[28] Reid, S. (1993), "Plastic deformation mechanisms in axially compressed metal tubes used as impact energy absorbers", *Int.J.Mech.Sci.,* Vol.35 (12), pp. 1035-1052.

[29] Guillow, S., Lu, G.and Grzebieta, R., (2001), "Quasi-static axial compression of thin-walled circular aluminium tubes", *Int.J.Mech.Sci.,* Vol.43 (9), pp. 2103-2123.

[30] Wang, B.and Lu, G., (2002), "Mushrooming of circular tubes under dynamic axial loading", *Thin-walled structures,* Vol.40 (2), pp. 167-182.

[31] Hsu, S.and Jones, N., (2004), "Quasi-static and dynamic axial crushing of thin-walled circular stainless steel, mild steel and aluminium alloy tubes", *International journal of crashworthiness,* Vol.9 (2), pp. 195-217.

[32] Zeinoddini, M., Parke, G.and Harding, J., (2002), "Axially pre-loaded steel tubes subjected to lateral impacts: an experimental study", *Int.J.Impact Eng.,* Vol.27 (6), pp. 669-690.

[33] Langseth, M., Hopperstad, O.and Berstad, T., (1999), "Crashworthiness of aluminium extrusions: validation of numerical simulation, effect of mass ratio and impact velocity", *Int.J.Impact Eng.,* Vol.22 (9-10), pp. 829-854.

[34] Rossi, A., Fawaz, Z.and Behdinan, K., (2005), "Numerical simulation of the axial collapse of thin-walled polygonal section tubes", *Thin-walled structures,* Vol.43 (10), pp. 1646-1661.

[35] Nagel, G.and Thambiratnam, D., (2004), "A numerical study on the impact response and energy absorption of tapered thin-walled tubes", *Int.J.Mech.Sci.,* Vol.46 (2), pp. 201-216.

[36] Nagel, G.and Thambiratnam, D., (2005), "Computer simulation and energy absorption of tapered thin-walled rectangular tubes", *Thin-walled structures,* Vol.43 (8), pp. 1225-1242.

[37] Nagel, G.and Thambiratnam, D., (2004), "Dynamic simulation and energy absorption of tapered tubes under impact loading", *International Journal of Crashworthiness,* Vol.9 (4), pp. 389-399.

[38] Nagel, G. and DP Thambiratnam 2002, "Energy absorption and performance of a vehicle impact protection system", "Energy absorption and performance of a vehicle impact protection system", *Proceeding of the seventh international conference on structures under shock and impact, Montreal, Canada, May,*Vol.27, 29.

[39] Gupta, N.and Gupta, S., (1993), "Effect of annealing, size and cut-outs on axial collapse behaviour of circular tubes", *Int.J.Mech.Sci.,* Vol.35 (7), pp. 597-613.

[40] Zhang, X.and Zhang, H., (2013), "Energy absorption of multi-cell stub columns under axial compression", *Thin-Walled Structures,* Vol.68 pp. 156-163.

[41] Colokoglu, A.and Reddy, T., (1996), "Strain rate and inertial effects in free external inversion of tubes", *International Journal of Crashworthiness,* Vol.1 (1), pp. 93-106.

[42] Webb, D., Webster, J.and Kormi, K., (2001), "Finite element simulation of energy absorption devices under axial static compressive and impact loading", *International Journal of Crashworthiness,* Vol.6 (3), pp. 399-424.

[43] Kinkead, A. (1983), "Analysis for inversion load and energy absorption of a circular tube", *The Journal of Strain Analysis for Engineering Design,* Vol.18 (3), pp. 177-188.

[44] Reid, S.and Harrigan, J., (1998), "Transient effects in the quasi-static and dynamic internal inversion and nosing of metal tubes", *Int.J.Mech.Sci.,* Vol.40 (2-3), pp. 263-280.

[45] Miscow F, P.and Al-Qureshi, H., (1997), "Mechanics of static and dynamic inversion processes", *Int.J.Mech.Sci.,* Vol.39 (2), pp. 147-161.

[46] Reddy, T.and Reid, S., (1986), "Axial splitting of circular metal tubes", *Int.J.Mech.Sci.,* Vol.28 (2), pp. 111-131.

[47] Lu, G., et al., (1994), "An experimental study on tearing energy in splitting square metal tubes", *Int.J.Mech.Sci.,* Vol.36 (12), pp. 1087-1097.

[48] Jiang, P., Wang, W.and Zhang, G., (2006), "Size effects in the axial tearing of circular tubes during quasi-static and impact loadings", *Int.J.Impact Eng.,* Vol.32 (12), pp. 2048-2065.

[49] Stronge, W., Yu, T.and Johnson, W., (1983), "Long stroke energy dissipation in splitting tubes", *Int.J.Mech.Sci.,* Vol.25 (9-10), pp. 637-647.

[50] Huang, X., Lu, G.and Yu, T.X., (2002), "Energy absorption in splitting square metal tubes", *Thin-walled structures,* Vol.40 (2), pp. 153-165.

[51] Huang, X., Lu, G.and Yu, T.X., (2002), "On the axial splitting and curling of circular metal tubes", *Int.J.Mech.Sci.,* Vol.44 (11), pp. 2369-2391.

[52] Sowerby, R., Johnson, W.and Samanta, S., (1968), "The diametral compression of circular rings by point loads", *Int.J.Mech.Sci.,* Vol.10 (5), pp. 369-370.

[53] Jing, Y.Y.and Barton, D.C., (1998), "The response of square cross-section tubes under lateral impact loading", *International Journal of Crashworthiness,* Vol.3 (4), pp. 359-378.

[54] Thomas, S., Reid, S.and Johnson, W., (1976), "Large deformations of thin-walled circular tubes under transverse loading--I:: An experimental survey of the bending of simply supported tubes under a central load", *Int.J.Mech.Sci.,* Vol.18 (6), pp. 325-326, in3-in6, 327-333.

[55] Watson, A., et al., (1976), "Large deformations of thin-walled circular tubes under transverse loading--II: Experimental study of the crushing of circular tubes by

centrally applied opposed wedge-shaped indenters", *Int.J.Mech.Sci.,* Vol.18 (7-8), pp. 387-388, IN11-IN14, 389-397.

[56] Watson, A., Reid, S.and Johnson, W., (1976), "Large deformations of thin-walled circular tubes under transverse loading—III: Further experiments on the bending of simply supported tubes", *Int.J.Mech.Sci.,* Vol.18 (9), pp. 501-502.

[57] Zhao, Y.P., Holmes, A.and Fang, J., (1996), "The load carrying capacities of circular rings with arc-shaped supports", *Int.J.Pressure Vessels Piping,* Vol.67 (1), pp. 7-10.

[58] Zhao, Y.P.and Fang, J., (1995), "Experimental investigation into the dynamic behavior of circular rings with arc-shaped supports", *Int.J.Pressure Vessels Piping,* Vol.62 (1), pp. 83-85.

[59] Reid, S.and Bell, W., (1982), "Influence of strain hardening on the deformation of thin rings subjected to opposed concentrated loads", *Int.J.Solids Structures,* Vol.18 (8), pp. 643-658.

[60] Lu, G. (1993), "A study of the crushing of tubes by two indenters", *Int.J.Mech.Sci.,* Vol.35 (3-4), pp. 267-278.

[61] Liu, K., et al., (2005), "Dynamic behavior of ring systems subjected to pulse loading", *Int.J.Impact Eng.,* Vol.31 (10), pp. 1209-1222.

[62] Shim, V.P.W.and Stronge, W., (1986), "Lateral crushing of thin-walled tubes between cylindrical indenters", *Int.J.Mech.Sci.,* Vol.28 (10), pp. 683-707.

[63] Kardaras, C.and Lu, G., (2000), "Finite element analysis of thin walled tubes under point loads subjected to large plastic deformation", *Key Eng Mat,* Vol.177 pp. 733-738.

[64] Wierzbicki, T.and Suh, M., (1988), "Indentation of tubes under combined loading", *Int.J.Mech.Sci.,* Vol.30 (3-4), pp. 229-248.

[65] Ghosh, S., et al., (1981), "On thin rings and short tubes subjected to centrally opposed concentrated loads", *Int.J.Mech.Sci.,* Vol.23 (4), pp. 183-194.

[66] DeRuntz Jr, J.A.and Hodge Jr, P., (1963), "Crushing of a tube between rigid plates", *Journal of Applied Mechanics,* Vol.30 pp. 391.

[67] Redwood , R. (1964), "Discussion of ‘‘An investigation into the energyabsorbing properties of metal tubes loaded in the transversedirection’’", *Journal of Applied Mechanics,* Vol.31 pp. 357-8.

[68] Reid, S.and Reddy, T.Y., (1978), "Effect of strain hardening on the lateral compression of tubes between rigid plates", *Int.J.Solids Structures,* Vol.14 (3), pp. 213-225.

[69] Reddy, T.Y.and Reid, S., (1980), "Phenomena associated with the crushing of metal tubes between rigid plates", *Int.J.Solids Structures,* Vol.16 (6), pp. 545-562.

[70] Gupta, N., Sekhon, G.and Gupta, P., (2005), "Study of lateral compression of round metallic tubes", *Thin-walled structures,* Vol.43 (6), pp. 895-922.

[71] Avalle, M.and Goglio, L., (1997), "Static lateral compression of aluminium tubes: strain gauge measurements and discussion of theoretical models", *The Journal of Strain Analysis for Engineering Design,* Vol.32 (5), pp. 335-343.

[72] Yella Reddy, T.and Reid, S., (1979), "Lateral compression of tubes and tube-systems with side constraints", *Int.J.Mech.Sci.,* Vol.21 (3), pp. 187-199.

[73] S Reid, T. R. 1979, "Large deformation behaviour of thick rings under lateral compression", "Large deformation behaviour of thick rings under lateral compression", *In: Proceedings Symposium on Large Deformations,*.

[74] Yella Reddy, T.and Reid, S., (1979), "On obtaining material properties from the ring compression test", *Nucl.Eng.Des.,* Vol.52 (2), pp. 257-263.

[75] Reid, S. and T. Y. Reddy 1980, "Effects of strain rate on the dynamic lateral compression of tubes", "Effects of strain rate on the dynamic lateral compression of tubes", *Proc. 2 nd Conf. Mechanical Properties of Materials at High Rates of Strain, Oxford, England, Mar. 1979,* 288-298.

[76] Reid, S., Drew, S.and Carney III, J., (1983), "Energy absorbing capacities of braced metal tubes", *Int.J.Mech.Sci.,* Vol.25 (9-10), pp. 649-667.

[77] Leu, D.K. (1999), "Finite-element simulation of the lateral compression of aluminium tube between rigid plates", *Int.J.Mech.Sci.,* Vol.41 (6), pp. 621-638.

[78] Gupta, N.and Ray, P., (1998), "Collapse of thin-walled empty and filled square tubes under lateral loading between rigid plates", *International Journal of Crashworthiness,* Vol.3 (3), pp. 265-285.

[79] Sherbourne, A.and Lu, F., (1993), "Strain hardening in the moving hinge method", *Int.J.Solids Structures,* Vol.30 (24), pp. 3475-3489.

[80] Wu, L.and Carney, J.F., (1997), "Initial collapse of braced elliptical tubes under lateral compression", *Int.J.Mech.Sci.,* Vol.39 (9), pp. 1023-1036.

[81] Wu, L.and Carney, J.F., (1998), "Experimental analyses of collapse behaviors of braced elliptical tubes under lateral compression", *Int.J.Mech.Sci.,* Vol.40 (8), pp. 761-777.

[82] Shrive, N., Andrews, K.and England, G., (1984), "The impact energy dissipation of cylindrical systems", *Structural impact and crashworthiness,* Vol.2 pp. 544-554.

[83] Johnson, W., Reid, S.and Reddy, T.Y., (1977), "The compression of crossed layers of thin tubes", *Int.J.Mech.Sci.,* Vol.19 (7), pp. 423-428, IN3-IN4, 429-437.

[84] Reid, S., T. Reddy and C. Austin 1980, "Dynamic deformation of tube and ring systems", "Dynamic deformation of tube and ring systems", *Proceedings of the 5th Symposium on Engineering Applications of Mechanics,* 301-305.

[85] Reid, S.and Reddy, T.Y., (1983), "Experimental investigation of inertia effects in one-dimensional metal ring systems subjected to end impact--I. Fixed-ended systems", *Int.J.Impact Eng.,* Vol.1 (1), pp. 85-106.

[86] Reddy, T.Y., Reid, S.and Barr, R., (1991), "Experimental investigation of inertia effects in one-dimensional metal ring systems subjected to end impact--II. Free-ended systems", *Int.J.Impact Eng.,* Vol.11 (4), pp. 463-480.

[87] Morris, E., Olabi, A.and Hashmi, M., (2007), "Lateral crushing of circular and non-circular tube systems under quasi-static conditions", *Journal of Materials Processing Tech.,* Vol.191 (1-3), pp. 132-135.

[88] Morris, E., Olabi, A.and Hashmi, M., (2006), "Analysis of nested tube type energy absorbers with different indenters and exterior constraints", *Thin-Walled Structures,* Vol.44 (8), pp. 872-885.

[89] Taher, S., et al., (2006), "A new composite energy absorbing system for aircraft and helicopter", *Composite structures,* Vol.75 (1), pp. 14-23.

[90] MEGUID, S. (2004), "Crush behavior of metallic foams for passenger car design", *International journal of automotive technology,* Vol.5 (1), pp. 47-53.

[91] Børvik, T., et al., (2003), "Empty and foam-filled circular aluminium tubes subjected to axial and oblique quasistatic loading", *International journal of crashworthiness,* Vol.8 (5), pp. 481-494.

[92] Kavi, H., Toksoy, A.K.and Guden, M., (2006), "Predicting energy absorption in a foam-filled thin-walled aluminum tube based on experimentally determined strengthening coefficient", *Mater Des,* Vol.27 (4), pp. 263-269.

[93] Toksoy, A.and Güden, M., (2005), "The strengthening effect of polystyrene foam filling in aluminum thin-walled cylindrical tubes", *Thin-walled structures,* Vol.43 (2), pp. 333-350.

[94] Yan, W., et al., (2007), "Crushing simulation of foam-filled aluminium tubes", *Materials transactions,* Vol.48 (7), pp. 1901-1906.

[95] Hanssen, A.G., Langseth, M.and Hopperstad, O.S., (2000), "Static and dynamic crushing of square aluminium extrusions with aluminium foam filler", *Int.J.Impact Eng.,* Vol.24 (4), pp. 347-383.

[96] Santosa, S.P., et al., (2000), "Experimental and numerical studies of foam-filled sections", *Int.J.Impact Eng.,* Vol.24 (5), pp. 509-534.

[97] Seitzberger, M., et al., (2000), "Experimental studies on the quasi-static axial crushing of steel columns filled with aluminium foam", *Int.J.Solids Structures,* Vol.37 (30), pp. 4125-4147.

[98] Zarei, H.and Kröger, M., (2008), "Optimization of the foam-filled aluminum tubes for crush box application", *Thin-Walled Structures,* Vol.46 (2), pp. 214-221.

[99] Gupta, N.and Velmurugan, R., (1999), "Axial compression of empty and foam filled composite conical shells", *J.Composite Mater.,* Vol.33 (6), pp. 567-591.

[100] Ahmad, Z.and Thambiratnam, D., (2009), "Crushing response of foam-filled conical tubes under quasi-static axial loading", *Materials and Design,* Vol.30 (7), pp. 2393-2403.

[101] Ahmad, Z.and Thambiratnam, D.P., (2009), "Dynamic computer simulation and energy absorption of foam-filled conical tubes under axial impact loading", *Comput.Struct.,* Vol.87 (3), pp. 186-197.

[102] Ahmad, Z., Thambiratnam, D.and Tan, A., (2010), "Dynamic energy absorption characteristics of foam-filled conical tubes under oblique impact loading", *Int.J.Impact Eng.,* Vol.37 (5), pp. 475-488.

[103] Mirfendereski, L., Salimi, M.and Ziaei-Rad, S., (2008), "Parametric study and numerical analysis of empty and foam-filled thin-walled tubes under static and dynamic loadings", *Int.J.Mech.Sci.,* Vol.50 (6), pp. 1042-1057.

[104] Chen, W. (2001), "Experimental and numerical study on bending collapse of aluminum foam-filled hat profiles", *Int.J.Solids Structures,* Vol.38 (44), pp. 7919-7944.

[105] Song, H., et al., (2005), "Partition energy absorption of axially crushed aluminum foam-filled hat sections", *Int.J.Solids Structures,* Vol.42 (9), pp. 2575-2600.

[106] Thornton, P. (1980), "Energy absorption by foam filled structures", .

[107] Lampinen, B. and Jeryan, R., (1982)*, Effectiveness of polyurethane foam in energy absorbing structures,* , Society of Automotive Engineers,.

[108] Banhart, J. (2001), "Manufacture, characterisation and application of cellular metals and metal foams", *Progress in materials science,* Vol.46 (6), pp. 559-632.

[109] Reyes, A., et al., (2004), "Modeling of material failure in foam-based components", *Int.J.Impact Eng.,* Vol.30 (7), pp. 805-834.

[110] Hanssen, A., Hopperstad, O.and Langseth, M., (2001), "Design of aluminium foam-filled crash boxes of square and circular cross-sections", *International Journal of Crashworthiness,* Vol.6 (2), pp. 177-188.

[111] Asavavisithchai, S., Slater, D.and Kennedy, A., (2004), "Effect of tube length on the bucking mode and energy absorption of Al foam-filled tubes", *J.Mater.Sci.,* Vol.39 (24), pp. 7395-7396.

[112] Seitzberger, M., et al., (1997), "Crushing of axially compressed steel tubes filled with aluminium foam", *Acta Mech.,* Vol.125 (1), pp. 93-105.

[113] Reid, S., Reddy, T.and Gray, M., (1986), "Static and dynamic axial crushing of foam-filled sheet metal tubes", *Int.J.Mech.Sci.,* Vol.28 (5), pp. 295-322.

[114] Zhang, X.and Cheng, G., (2007), "A comparative study of energy absorption characteristics of foam-filled and multi-cell square columns", *Int.J.Impact Eng.,* Vol.34 (11), pp. 1739-1752.

[115] Reyes, A., Hopperstad, O.and Langseth, M., (2004), "Aluminum foam-filled extrusions subjected to oblique loading: experimental and numerical study", *Int.J.Solids Structures,* Vol.41 (5), pp. 1645-1675.

[116] Shahbeyk, S., Vafai, A.and Petrinic, N., (2005), "Axial crushing of metal foam-filled square columns: Foam density distribution and impactor inclination effects", *Thin-walled structures,* Vol.43 (12), pp. 1818-1830.

[117] Fan, Z., Shen, J.and Lu, G., (2011), "Investigation of Lateral Crushing of Sandwich Tubes", *Procedia Engineering,* Vol.14 pp. 442-449.

[118] Fan, Z., et al., (2012), "Dynamic lateral crushing of empty and sandwich tubes", *Int.J.Impact Eng.,* .

[119] Burton, R.and Craig, J., (1963), "An investigation into the energy absorbing properties of metal tubes loaded in the transverse direction", *BSc (Eng) Report, University of Bristol, England,* .

[120] Hou, S., et al., (2007), "Design optimization of regular hexagonal thin-walled columns with crashworthiness criteria", *Finite Elements Anal.Des.,* Vol.43 (6), pp. 555-565.

[121] Hou, S., et al., (2008), "Multiobjective optimization of multi-cell sections for the crashworthiness design", *Int.J.Impact Eng.,* Vol.35 (11), pp. 1355-1367.

[122] Hou, S., et al., (2009), "Crashworthiness design for foam filled thin-wall structures", *Mater Des,* Vol.30 (6), pp. 2024-2032.

[123] Liu, Y. (2008), "Crashworthiness design of multi-corner thin-walled columns", *Thin-Walled Structures,* Vol.46 (12), pp. 1329-1337.

[124] Liu, Y. (2008), "Optimum design of straight thin-walled box section beams for crashworthiness analysis", *Finite Elements Anal.Des.,* Vol.44 (3), pp. 139-147.

[125] Zarei, H.and Kröger, M., (2008), "Optimum honeycomb filled crash absorber design", *Mater Des,* Vol.29 (1), pp. 193-204.

[126] Yin, H., et al., (2011), "Crushing analysis and multiobjective crashworthiness optimization of honeycomb-filled single and bitubular polygonal tubes", *Mater Des,* Vol.32 (8), pp. 4449-4460.

[127] Zarei, H.and Kröger, M., (2008), "Bending behavior of empty and foam-filled beams: Structural optimization", *Int.J.Impact Eng.,* Vol.35 (6), pp. 521-529.

[128] Zhang, Z., Liu, S.and Tang, Z., (2009), "Design optimization of cross-sectional configuration of rib-reinforced thin-walled beam", *Thin-walled structures,* Vol.47 (8), pp. 868-878.

[129] Qi, C., Yang, S.and Dong, F., (2012), "Crushing analysis and multiobjective crashworthiness optimization of tapered square tubes under oblique impact loading", *Thin-Walled Structures,* Vol.59 pp. 103-119.

[130] El-Hage, H., Mallick, P.and Zamani, N., (2005), "A numerical study on the quasi-static axial crush characteristics of square aluminum tubes with chamfering and other triggering mechanisms", *International Journal of Crashworthiness,* Vol.10 (2), pp. 183-196.

[131] Meguid, S., et al., (2007), "Solution stability in the dynamic collapse of square aluminium columns", *Int.J.Impact Eng.,* Vol.34 (2), pp. 348-359.

[132] ANSYS® Academic Research, Release 14.0, Help System, Theory Reference for the Mechanical APDL and Mechanical Applications, ANSYS, Inc. 2009 http://orange.engr.ucdavis.edu/Documentation12.0/120/ans_thry.pdf.

[133] ANSYS® Academic Research, Release 14.0, Help System, ANSYS LS-DYNA User's Guide, ANSYS, Inc. 2009 http://orange.engr.ucdavis.edu/Documentation12.1/121/ans_lsd.pdf.

[134] Box, G.E.and Behnken, D., (1960), "Some new three level designs for the study of quantitative variables", *Technometrics,* Vol.2 (4), pp. 455-475.

[135] Croarkin, C.and Tobias, P., (2006), "Nist/sematech e-handbook of statistical methods", *NIST/SEMATECH, July.Available online: http://www.itl.nist.gov/div898/handbook,* .

[136] Benyounis, K. , (2006), "Prediction and optimization of residual stresses, weld-bead profile and mechanical properties of laser welded components", Dublin City University,.

[137] Montgomery, D.C., (2008)*, Design and analysis of experiments,* , Wiley,.

[138] Stat-Ease Inc. 'Design-Expert software V8 user's guide',Technical Manual, Stat Ease, Inc., Minneapolis, MN,2010.

[139] Khuri, A.I. and Cornell, J.A., (1996)*, Response surfaces: designs and analyses,* , CRC PressI Llc,.

[140] Chatterjee, S. and Hadi, A.S., (2006)*, Regression analysis by example,* , Wiley-Interscience,.

[141] Myers, R.H. and Anderson-Cook, C.M., (2009)*, Response surface methodology: process and product optimization using designed experiments,* , John Wiley & Sons,.

[142] Shen, J., et al., (2012), "Short sandwich tubes subjected to internal explosive loading", *Eng.Struct.,* .

[143] Reid, S. (1983), "Laterally compressed metal tubes as impact energy absorbers", *Structural crashworthiness,* Vol.3 (1),.

[144] Antony, J., (2003)*, Design of experiments for engineers and scientists,* , Butterworth-Heinemann,.

APPENDICES

Appendices A

Certificate of calibration of Instron 4204

CERTIFICATE OF CALIBRATION

ISSUED BY ZWICK TESTING MACHINES LIMITED

DATE OF ISSUE 12 March 2012
CERTIFICATE NUMBER 1203-0436

UKAS CALIBRATION

0167

Zwick / Roell

Zwick Testing Machines Ltd.
Southern Avenue, Leominster, Herefordshire, HR6 0QH.

Tel: +44 (0) 1568 Sales 615201, Service 613516
Fax: +44 (0) 1568 Sales 612626, Service 619929

APPROVED SIGNATORY

C. C. Stanley,
P. J. Morris,
M. C. Marchbank.

FOR	Dublin City University		
LOCATION	School of Mechanical Engineering, Glasnevin, Dublin 9.		
DESCRIPTION	A 50 kN testing machine having one range and using the Integral, Serial No. H0046 as display.		
MACHINE TYPE	Instron 4204	**SERIAL NO.**	H0046
YEAR OF MANUFACTURE	N/a		
LOAD CELL CAPACITY	50 kN	**SERIAL NO.**	49520
DATE OF VERIFICATION	08 March 2012		

CLASSIFICATION:

The above testing machine has been verified in tension and compression for increasing forces only, to BS EN ISO 7500-1 : 2004 using verification equipment calibrated to BS EN ISO 376 .

The machine complied with the requirements of the Standard for the following classification and ranges:

These results are as found

50 kN Range	**Class 2.0**	**Tension**	**50 kN down to 2 kN**
50 kN Range	**Class 2.0**	**Compression**	**50 kN down to 10 kN**
50 kN Range	**Class 3.0**	**Compression**	**50 kN down to 2 kN**

Certified.....

The reported expanded uncertainty is based on a standard uncertainty multiplied by a coverage factor k=2, providing a level of confidence of approximately 95%. The uncertainty evaluation has been carried out in accordance with UKAS requirements.

CERTIFICATE OF CALIBRATION

CERTIFICATE NUMBER
1203-0436

UKAS ACCREDITED CALIBRATION LABORATORY No.: 0167

VERIFICATION EQUIPMENT

The following equipment calibrated to BS EN ISO 376 was used to effect the verification:

100 kN Tension and Compression load cell	Serial No. 074830065	Certificate No. 2648	Dated 13 April 2010

The class of the verification equipment was equal to or better than the class to which this testing machine has been verified.

NOTE. The expiry date of the above certificates of calibration for the proving device is 26 months from the above given dates.

METHOD

When using the proving device, from 50 kN down to 2 kN, the indicated force method was used to effect the verification.

Three verification tests were made on each range.

No accessories were fitted.

MEASUREMENTS

1. The testing machine satisified the requirements of BS EN ISO 7500-1 : 2004 in respect to the relative error of accuracy, repeatability, zero and resolution (see Table 2 of the standard).

2. The ambient temperature at the time of verification was 16.2°C

NOTE

Clause 9 of BS EN ISO 7500-1 states that: The time between two verifications is dependant on the type of testing machine, the standard of maintenance and amount of use. Unless otherwise specified, it is recommended that the verification shall be carried out at intervals not exceeding 12 months.

The machine shall in any case be reverified if it has been dismantled for moving or subjected to major repair or adjustment

CERTIFICATE OF CALIBRATION

UKAS ACCREDITED CALIBRATION LABORATORY N0: 0167

CERTIFICATE NUMBER
1203-0436

Table of Results - Tension

Verification Devices

Nominal	Relative Error %	Uncertainty%
2.000 kN	1.00	0.29
5.000 kN	1.90	0.24
10.000 kN	1.64	0.22
20.000 kN	1.87	0.22
30.000 kN	1.98	0.22
40.000 kN	1.95	0.22
50.000 kN	1.89	0.22

NOTE

The relative error quoted is the difference between the true value expected from the verification device(s) at the force loading values indicated by the machine in column 1 and the mean of three readings taken from the device(s) at those points. The uncertainty calculation made at each force reading is indicated in column 3.
The uncertainties stated above refer to the values obtained during verification and make no allowances for factors such as long term drift, temperature and alignment effects - the influences of such factors should be taken into account by the user of the testing machine

The reported expanded uncertainty is based on a standard uncertainty multiplied by a coverage factor k=2, providing a level of confidence of approximately 95%. The uncertainty evaluation has been carried out in accordance with UKAS requirements.

CERTIFICATE OF CALIBRATION

UKAS ACCREDITED CALIBRATION LABORATORY N0: 0167

CERTIFICATE NUMBER
1203-0436

Table of Results - Compression

Verification Devices

Nominal	Relative Error %	Uncertainty%
2.000 kN	1.95	0.23
5.000 kN	2.19	0.22
10.000 kN	1.86	0.23
20.000 kN	1.93	0.22
30.000 kN	1.97	0.23
40.000 kN	1.96	0.22
50.000 kN	1.99	0.22

NOTE

The relative error quoted is the difference between the true value expected from the verification device(s) at the force loading values indicated by the machine in column 1 and the mean of three readings taken from the device(s) at those points.
The uncertainty calculation made at each force reading is indicated in column 3.
The uncertainties stated above refer to the values obtained during verification and make no allowances for factors such as long term drift, temperature and alignment effects - the influences of such factors should be taken into account by the user of the testing machine

The reported expanded uncertainty is based on a standard uncertainty multiplied by a coverage factor k=2, providing a level of confidence of approximately 95%. The uncertainty evaluation has been carried out in accordance with UKAS requirements.

Appendices B

Material properties from company catalogue

IMPACT IRELAND ‹METALS› LTD
Engineering Steels Stockists

CHEMICAL COMPOSITION (LADLE ANALYSIS)

Specification	C	Si		Mn		P	S
	Max %	min%	max%	min%	max%	max%	max%
EN 10305-1 E235 +C	0.17		0.35		1.20	0.025	0.025
DIN 2393 ST37-2 BK (Precision welded)	0.17		0.30		0.70	0.050	0.050
BS 6323 PT4 CFS3 BK	0.20		0.35		0.90	0.050	0.050

MECHANICAL PROPERTIES AT ROOM TEMPERATURE

Specification	Tensile strenght Rm MPa	Upper yield Strength Re MPa	Elongation Min
EN 10305-1 E235 +C	480 min	see note*	6%
DIN 2393 ST37-2 BK (Precision welded)	490 min	see note*	6%
BS 6323 PT4 CFS3 BK	450 min	360 min	6%

Notes:
* Depending on the degree of cold work in the finishing pass the yield strength may nearly be as high as the tensile strength. for calculation purposes thefollowing relationships are recommended . for delivery condition `C` : ReH ≥ 0.8 Rm.

COLD FINISHED SEAMLESS

MECHANICAL

TOLERANCES ON OUTSIDE DIAMETER	DIN 2393 PRECISION WELDED (CEW) mm	EN10305-1 E235 +c mm
Up to 30mm	±0.08	±0.08
30-40mm	±0.15	±0.15
40-50mm	±0.20	±0.20
50-60mm	±0.20	±0.25
60-70mm	±0.25	±0.30
70-80mm	±0.30	±0.35
80-90mm	±0.35	±0.40
90-100mm	±0.40	±0.45
100-110mm	±0.45	±0.50
110-120mm	±0.45	±0.50
120-130mm	±0.50	±0.70
130-140mm	±0.70	±0.70
140-150mm	±0.80	±0.80
150-160mm		±0.80
160-170mm		±0.90
170-180mm		±0.90
180-190mm		±1.00
190-200mm		±1.00
200-220mm		±1.20
220-240mm		±1.20
240-260mm		±1.30

Wall Thickness	±7.5% (min 0.1mm)

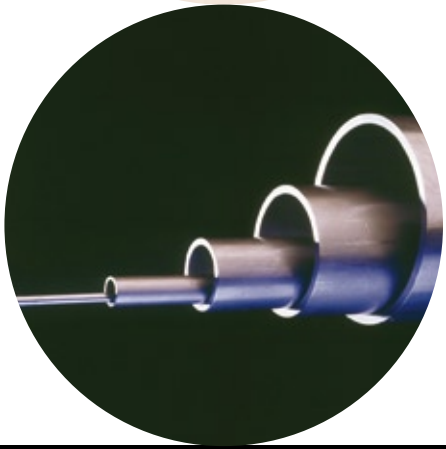

nqa.
ISO 9001
Registered
Certificate No. 4665

Appendices C

VFPS Application

Various configurations of thin-walled tubes crushed laterally can be used as crash boxes in Vehicle Frontal Protection Systems (VFPS), as shown in Figure A-1 .

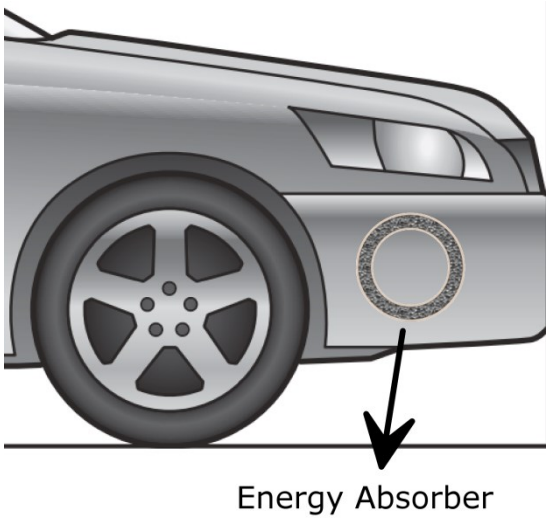

Figure A-1: Application of lateral crushed thin walled tubes in VFPS system [Car photo www.automobiles.honda.com [Accessed April 2013]].

Figure A-2 shows the components and assembly of the VFPS system. Welding is used to join all bumper components. The vehicle longitudinal axis indicates the orientation of the system when it is installed on a vehicle. Two energy absorbers are located at each end of a channel that acts to transfer an applied load to each absorber. Each absorber itself is a thin-walled circular tube.

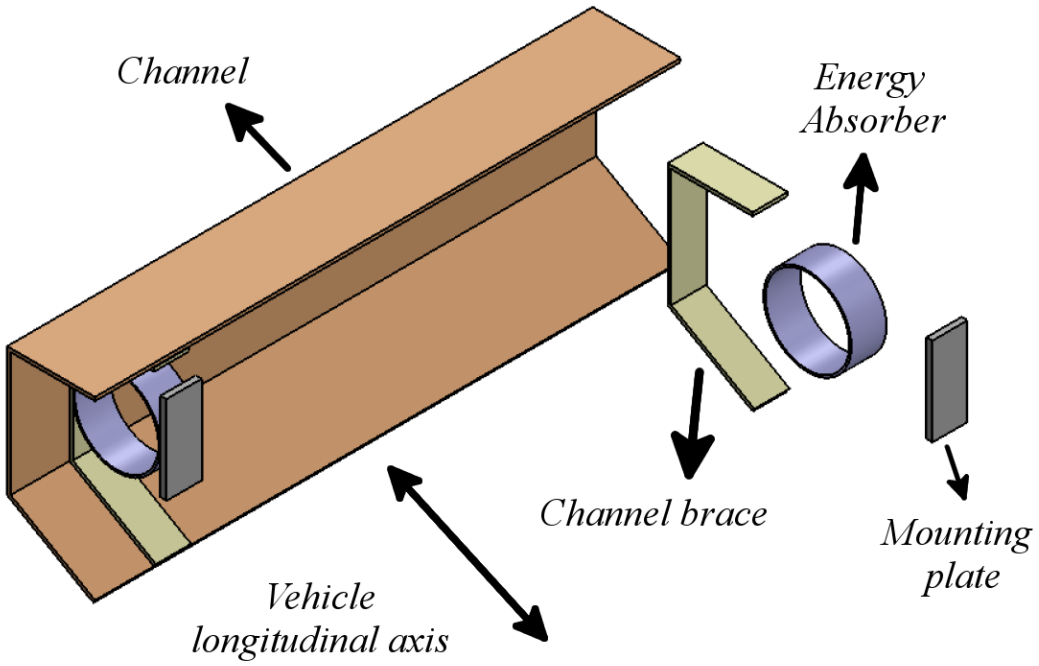

Figure A-2: A VFPS system consisting of single circular tube crushed laterally

The deformation of a VFPS system under working load is presented in Figure A-3.

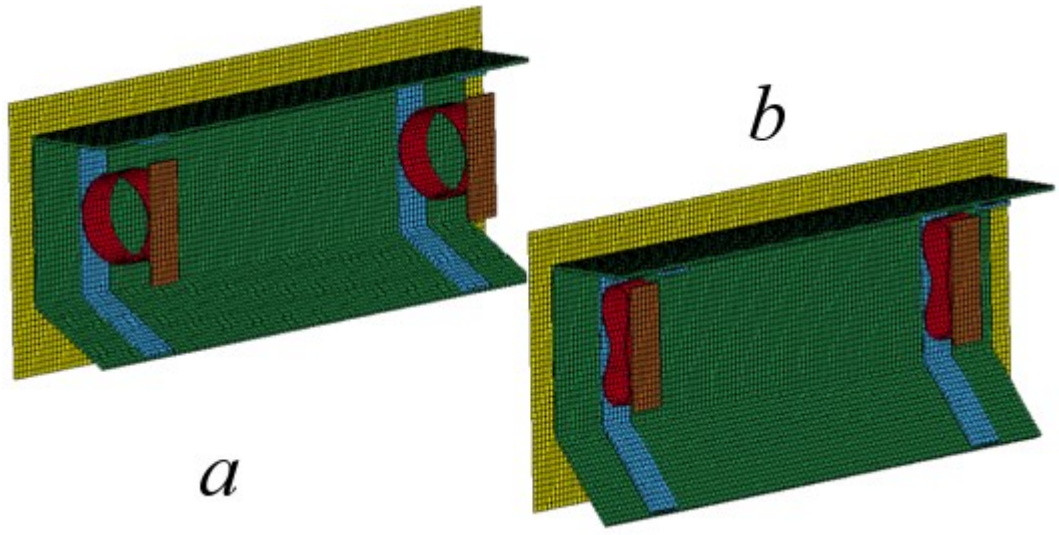

Figure A-3: a- Initial and b- final stages of VFPS system

Appendices D

Sandwich tube systems with external constraints

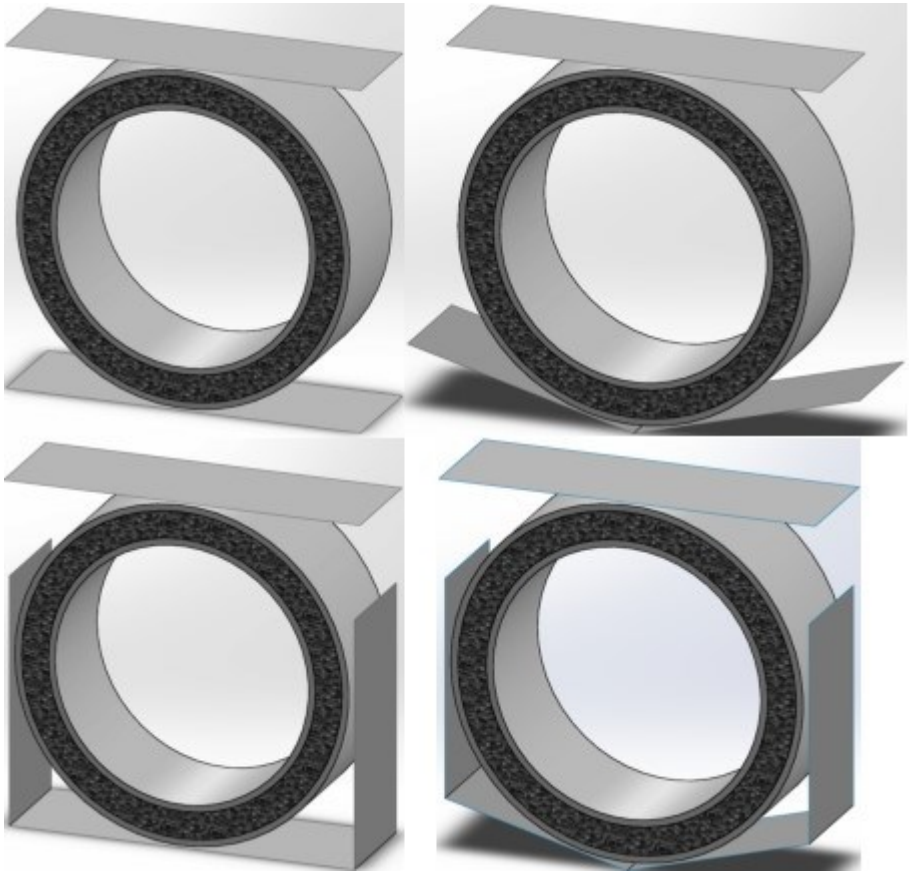

Appendices E

Various configurations of sandwich tube systems

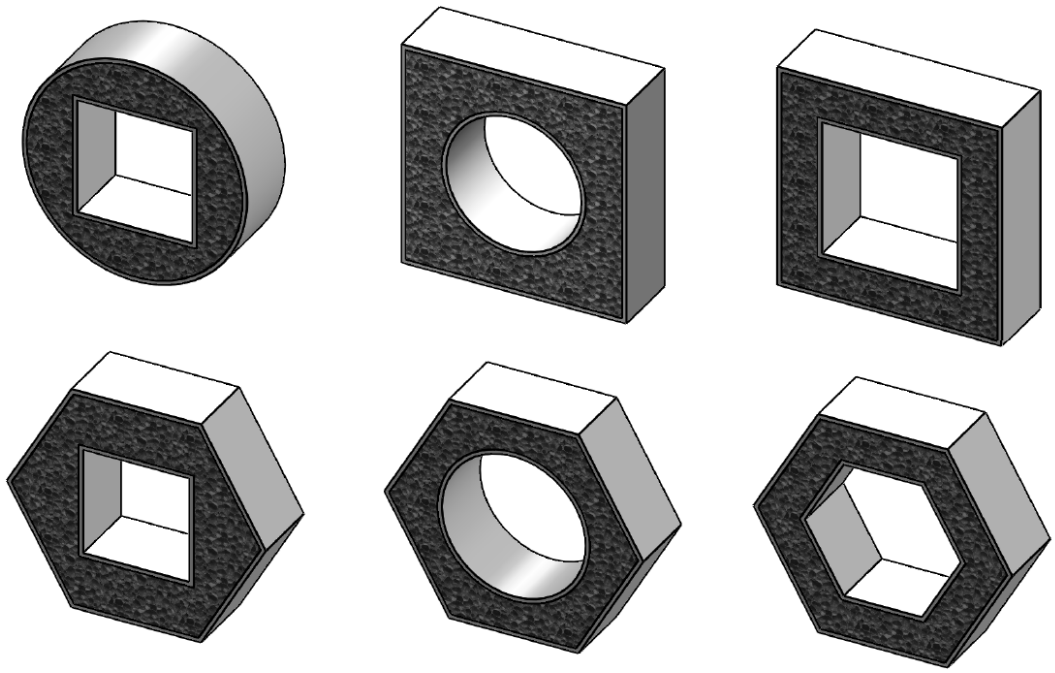

Appendices F

Publication

Book Chapter:

Ahmad Baroutaji and Abdul Ghani Olabi. "Analysis of the Effect of the Elliptical Ratio in Tubular Energy Absorbers Under Quasi-Static Conditions." In Materials with Complex Behaviour II, pp. 323-336. Springer Berlin Heidelberg, 2012.

Peer Review Journal:

A.Baroutaji, A.G.Olabi, "Lateral collapse of short-length sandwich tube compressed by different indenters and exposed to external constraints". Materialwissenschaft und Werkstofftechnik 45.5 (2014).

A.Baroutaji, E.Morris, A.G.Olabi," Quasi-static response and multiobjective crashworthiness optimization of oblong tube under lateral loading."International Journal of Thin Walled Structures, 82, pp.262-277 (2014).

A.Baroutaji, A.G.Olabi, " Quasi-static and Dynamic Analysis of nested tubes energy absorbers under lateral loading" 2014, Submitted for review to the International Journal of Solid and Structures.

A.Baroutaji, A.G.Olabi, "Crushing analysis and multiobjective crashworthiness optimization of circular tubes under lateral loading" 2014, Submitted for review to the International Journal of Thin-Walled Structures.

A.Baroutaji, A.G.Olabi, "Crushing analysis and multiobjective crashworthiness optimization of sandwich tubes under lateral loading", 2014, Submitted for review to the International Journal of Impact Engineering.